SINI VARGHESE C. “ EVALUATION ON THE INHIBITIVE EFFECT OF HETEROCYCLIC DERIVATIVES AND POLYAMINO COMPOUNDS ON THE CORROSION OF CARBON STEEL AND COPPER IN ACID MEDIA.” THESIS. RESEARCH AND POSTGRADUATE DEPARTMENT OF CHEMISTRY, ST. THOMAS’ COLLEGE (AUTONOMOUS), UNIVERSITY OF CALICUT, 2019.

PART II

CORROSION INHIBITION STUDIES

CHAPTER 1

INTRODUCTION AND REVIEW

The origin of the word corrode is from the Latin word *corrodere* which means*"to gnaw to pieces"*. Corrosion results in gradual destruction of metals as it reacts with the environmental agents. It can also be considered as the exact reverse of extractive metallurgy. If we take the example of iron which is produced from haematite, corrodes and form rust which have exactly same composition of haematite. Large number of definitions exists for corrosion which all has a common factor citing the interaction of materials with the environment which can also be applied to polymers, ceramics, composites, semiconductors etc. Other than the usual metals and alloys which gets mentioned regularly.[1] Encyclopædia Britannica defines Corrosion as "wearing away due to chemical reactions, mainly oxidation (see oxidation-reduction, oxide), occurs whenever a gas or liquid chemically attacks an exposed surface, often a metal, and is accelerated by warm temperatures and by acids and salts."

The historical references to the corrosion start from the works of Plato who lived from 427 B. C. – 347 B. C. He defined rust as earthy component separating out of metal. Later the great Roman Philosopher Gaius Secundus Pliny (23 A. D. – 79 A. D.) also recorded the existence of rust as ferrumcorrumpitur which meant spoiled iron. Herodotus who lived in 5th century B. C. also suggested that corrosion of iron can be fought by using tin[2]. Georgius Agricola in De naturafossilium described iron rust (lat. ferrugo or rubigo) as a secretion of

metallic iron and iron can be protected against corrosion by employing various wrappings, such as red lead, white lead, gypsum, bitumen or tar[3].

Corrosion of metals usually happens via electrochemical oxidation reactions in presence of moist, air or water environments and hence, corrosion can be considered as a diffusion-controlled process[4]. Iron ore haematite after metallurgical process yield steel which upon corrosion with the environment results in the formation of iron oxide Fe_2O_3.

Different types of corrosion are termed by the nature of its occurrence. Atmospheric corrosion, galvanic corrosion, crevice corrosion, pitting, microbial corrosion are some major ones.

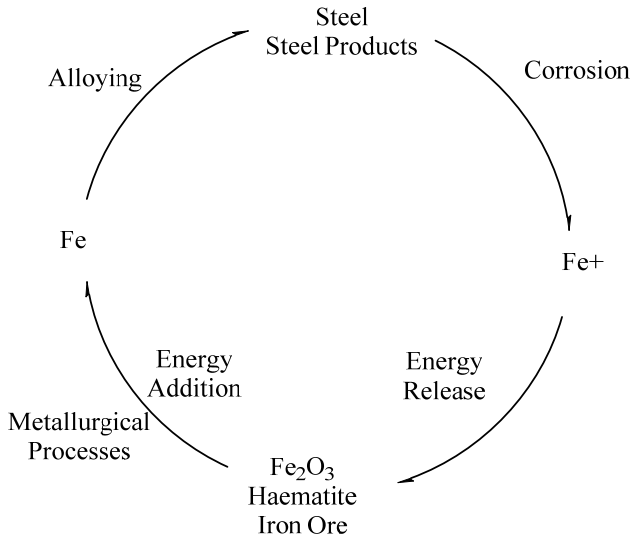

Corrosion: Consequences

Corrosion is an important threat to be addressed in the sense that it can cause much aggravated damage by structural degradation of metals as the refined metal is converted to its corresponding ore's chemical composition. It is responsible for the malfunctioning and failure of various structures and systems.

The adverse effects are related to cost of materials, their reduced reliability and performance and environmental impact.

The corrosion in daily lives has direct as well as indirect impact on us. The direct impact includes corrosion of our belongings made up of metals and the indirect impact is from the cost of corrosion protection by the suppliers and producers of goods levied on us. We can see effect of corrosion on metal tools, furniture, automobiles and many household items. We usually use paints for the prevention of corrosion.

The structural damage occurring due to the corrosion can sometimes be catastrophic. A concrete reinforcement bar can corrode under the concrete and hence can go undetected but can collapse buildings or bridges, which cost lives. A pipeline carrying explosive material can cause fire and explosions if leaks, occur due to corrosion. Similarly, toxic materials containers can corrode and release toxic material to the environment. Very recently there are reports of seized Endosulfan containers kept in custody were leaking due to corrosion in Kerala. Similarly, nuclear wastes were also reported leaking from their containers from different parts of the world. A corroded water pipeline can lose precious water as well as take in waste materials which can give serious health issues. Ultimately it is the depletion of resources we are dealing with.

Economic impact of corrosion

In 2013 the global cost of corrosion was estimated around 2.5 trillion USD approximate value which is the 3.5% of GDP of the world and 15 to 35% of this can be saved through proper corrosion control measures and management. The

economic impact from corrosion is from various requirements, which results in the increase of cost of production and consequent economic loss[3]. Few aspects of economic impact of corrosion are shown below.

- Replacement of equipment damaged due to corrosion
- Design and control of corrosion so that extra materials are used to compensate the loss
- Preventive measures which is to be taken on a regular basis like painting
- Forced or preventive shut down of equipment as a result of corrosion failure
- Product contamination
- Precious product loss due to leakage
- Collateral damage

Causative factors for corrosion

The mode of fight against any threat is to find out the nature and mechanism of attack. Fighting corrosion also follows the same track. Find out what the causative factors are? Understand the underlying mechanism of corrosion and block it. The Romans had trouble with the corrosion of iron and their philosopher Pliny thought about the causative factor and since there was no experimental method, he arrived at a metaphysical conclusion that rusting of iron is a sort of punishment as the metal showed itself as a tool for wars and weaponry. And because of this, religious ceremonies were conducted for corrosion prevention even though he was sceptical about it.

Corrosion can be defined as the deterioration of a metal which occurs as a result of its interaction with its environment. Environment in this case can be defined as the surroundings existing in contact with the substance under consideration. The major factors considered are the physical state, chemical composition and temperature of the substance. There are some additional factors to be considered which is like flow rate in case of pipelines, velocity if it is dynamic, mechanical load and stress. The corrosion of a material can only be discussed relating to its environment, because the corrodent usually is from the environment.

It is interesting to see that there are desirable corrosions too. Nickel in caustic environments, lead in water and aluminium in air – these examples are desirable corrosions. As they make a protective coating or corrosion is useful here.

In the modern world, corrosion occurs due to many factors. The potential culprits being: air and humidity, fresh / distilled / salt and marine water, natural / urban / marine and industrial atmospheres, steam and gases (like chlorine, ammonia, hydrogen sulfide, sulfur dioxide and oxides of nitrogen), fuel gases, acids, alkalies, soils, animal secretions etc.[5]

Chemistry of corrosion

Corrosion happens through a series of electrochemical or redox reactions and thus is an electrochemical process. The primary requirements for wet corrosion are a metal surface, atmospheric or dissolved oxygen and an electrolyte (water). The metal undergoes an oxidation reaction acting as an anode forming

positively charged metal ions and free electrons. The metal being hydrated dissolves and thus goes in to the solution resulting in a pit or the solid compound gets deposited on the surface which results a crust.

Wet corrosion of iron is represented in the following chemical equations as an example:

$$Fe^{2+}_{(aq)} + 2OH^{-}_{(aq)} \longrightarrow Fe(OH)_{2\,(s)}$$

$$4Fe(OH)_{2(s)} + O_{2(g)} + 2H_2O_{(l)} \longrightarrow 4Fe(OH)_{3(s)}$$

The anodic half-cell reaction for dissolution of metal M is

$$M \rightarrow M^{n+} + ne^-$$

For corrosion to proceed, the electrons produced in the above half reaction taking place at the anode are consumed by a reaction at the cathode. The cathodic reactions in acidic and basic media are as follows:

$$O_2 + 4e^- + 4H^+ \rightarrow 2H_2O \text{ (acidic medium)}$$

$$O_2 + 4e^- + 2H_2O \rightarrow 4OH^- \text{ (basic medium)}$$

$$2H^+ + 2e^- \rightarrow H_2 \text{ (acidic medium)}$$

$$2H_2O + 2e^- \rightarrow H_2 + 2OH^- \text{ (in basic medium)}$$

These electrochemical reactions involve the reduction of oxygen and evolution of hydrogen.

Other than wet corrosion involving water or its vapour as electrolytic medium, corrosion also occurs in dry conditions and are termed as dry corrosion. It usually occurs due to corrosive vapours and high temperature[6].

Dry corrosion occurs by the direct attack of atmospheric gases without any moisture or liquid. It is a uniform corrosion.The gases such as oxygen, halogen,

hydrogen sulphide, sulphur dioxide and nitrogen etc attack the suface of metal and accumulate the corrosion products at the site of attack. This type of corrosion is highly temperature depended, at high temperature the dry corrosion rate is very high compared to the normal temperature. The rate of corrosion also varied with the nature of metal. When oxygen comes in contact with metal surface, it will form an oxide layer on the surface of the metal. This metal oxide layer prevent the further attack of oxygen

Different types of corrosion

Corrosion classification is widely done as three depending upon the factors: Nature of the corrodent, mechanism of corrosion and appearance of the corroded metal[7].

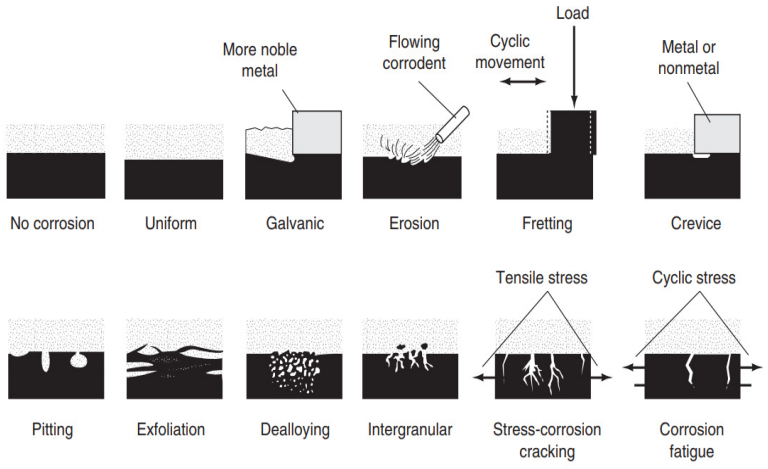

- **Uniform corrosion:** This form of corrosion refers to a general attack on the entire metal area which is exposed in a corrosive environment without a localized attack. Hence, there is no deep penetration. Some examples are the corrosion of iron in sulphuric acid solution and corrosion of steel in

atmosphere. This is usually compensated with a corrosion allowance during design of equipment.

- **Fretting**: Fretting corrosion occurs on metallic contact between two surfaces and are initiated by miniscule movements at small sites of surface protrusions known as asperities. This mechanical abrasion due to small movement can create high temperature in which the metal can react with air or moisture to form corresponding oxides. Vertical and subsurface cracks can also form due to this and can increase the damage.[7]
- **Galvanic corrosion**: In a corrosive electrolyte, if two metals with different electrochemical potentials come into contact, there is a formation of a localised galvanic cell and hence the corrosion caused by this means is called galvanic corrosion. For example, if copper and iron having potentials +0.334V and -0.440V respectively is joined, then there will be galvanic corrosion. The force that drives this corrosion is the potential difference between these metals and was described by Luigi Galvani and hence the name. The components of a galvanic cell are anode, cathode, electrolyte and a metallic electron conducting path. In the above example copper, having a more positive potential act as a cathode and iron as anode, moist atmosphere act as an electrolyte and the metallic surface conducts electrons. It can be reduced by selecting closer metals in galvanic series. Inhibitors can be employed in aqueous systems. Sacrificial anodes can also be used[8] to reduce this type of corrosion.

- **Erosion**: Corrosion by erosion is a combination of corrosion and erosion, as corrosion is caused by a moving fluid or corrodent. The combination of the mechanical effect of the moving liquid along with the corrosive action is the major factor in this type of corrosion. It can be tackled by selecting an appropriate material, controlling velocity of the fluid, reduction of turbulence by the structural streamlining of the pipeline and the usage of inhibitors[9].
- **Crevice corrosion**: Crevice corrosion is a localised corrosion which occurs in a crevice, either metal-metal or a metal-non-metal system. Inside a crevice the mass flow is restricted or stagnant which can enrich the amount of dissolved oxygen (forming a differential aeration cell) and corrosive electrolytes (leading to the formation of a concentration cell) resulting corrosion and hence also called Concentration cell corrosion[10].
- **Pitting**: Pitting is an extremely localised form of corrosion which results in the formation of holes or pits. Usually the passive films occurring naturally due to uniform corrosion can provide a protecting barrier for the metallic surface. However, due to some local defects these passive films can rupture and corrosion will start and usually will form pits. The pits will act as anode and the surface metal as cathode which in turn results much higher rate of corrosion in localised pits making holes. It is more destructive as it cannot be predicted and leads to unexpected failures.[11]
- **Exfoliation corrosion**: It is usually found in aluminium alloys and is a form of intergranular corrosion. The micro structured or extruded alloys

undergo corrosion along grain boundaries and the corrosion products build up leading to a lifting or lamellar leafing up of the effect. Structural integrity of the component is affected by this corrosion.[12, 13]

- **Dealloying**: Selective corrosion of one of the metals in a solid solution or alloy is called dealloying as it unbecomes an alloy. Some common ones of this type are graphitic corrosion, decobaltification, dezincification, denickelification and decarburization. The corrosion of a particular element is due to the difference in the electrode potentials of each metal resulting in the attack of electrolyte on the more active metal[14].
- **Intergranular corrosion**: Intergranular attack is a form of corrosion where the metal crystallites undergo corrosion at their boundaries than interior. This happens due to the higher concentration of one metal creating anodic and cathodic sites in the same locality[15].
- **Stress corrosion cracking**: As the name says it occurs as a combined effect of both tensile stress and a corrosive medium making small cracks in the material and thereby inducing a structural damage. The major accelerating factors are the electrolytic reactions in the crack, surface diffusions, bulk absorptions and chemical reactions.
- **Corrosion fatigue**: It is the result of alternating or cyclic stress forces and a corrosive environment combined action on a material. This fatigue may lead to the rupture of a passive film which would protect the metallic surface and the corrosion is accelerated in the cracked part.

Prevention of corrosion

Corrosion is the consequence of the reactions between a metallic surface and the surrounding environment. So, to control the corrosion, it is to stop these reactions; which can be done in two ways- either completely isolating the metal surface so that no corrodents reach the surface and the second one is to control or suppress the electrochemical reactions.[16] The first method is achieved by barriers and coatings of different materials. The second method is achieved by manipulating the electrochemical redox reactions. The barrier protection is limited to a brief discussion as this thesis deals with inhibition of cathodic and anodic reactions using organic inhibitors.

Corrosion control by barriers and coatings

Coatings isolate the underlying metal from the corrosive media by creating an impermeable barrier to corrodents. Barrier protection methods can be divided broadly into two as metallic and nonmetallic (which includes organic and inorganic coatings).

Metallic coatings utilize the greater corrosion resistance of the noble metal which is coated on an active metal surface (plating). Eg: coating of metallic tin on the steel. A more electrochemically active metal can be applied, so that the coating undergo corrosion preferentially, protecting the substrate (cathodic protection). Eg: galvanized iron, in which zinc is coated and the corrosion happens on the zinc surface. The most common methods for applying metallic

coatings is hot dipping, electrodeposition, flame spraying, cladding and vapor deposition[17].

Nonmetallic coatings are utilized to protect the metal from the corrosive environment. A barrier layer is formed in order to stifle corrosion which is non-permeable to most corrodents. The organic coatings can be infused with corrosion inhibitors. The main agents for organic barrier protection are paints, varnishes, lacquers, polymers etc. They can be easily applied on metallic surface by spraying, diffusion or chemical conversion[18].

Electrochemical corrosion control

Electrochemical corrosion control is achieved by, manipulating anode and cathode reactions so that the desired metal surface of importance is not corroded as a result of corrosion cell reactions.

It can be done mainly by cathodic protection in which corrosion current is suppressed and hence the corrosion cell and corrosion current is disrupted so as to prevent loss of electrons and hence the ionization. This can be achieved by two methods depending upon the source of the protection current.

a) Impressed - current: A power source is employed to push the current to the structure from inert anodes.
b) Sacrificial anode system: An active metal anode like zinc or magnesium is connected to the system that the sacrificial anode gets corroded making the structure safe from corrosion.

Corrosion control by inhibitors

Just like the chemicals accelerating corrosion process, there are some others which can inhibit corrosion. They can affect anodic and cathodic process in a considerable manner so that the corrosion process as becomes retarded and the corrosion cell is disrupted. Such substances are termed as corrosion inhibitors. Some inhibitors are specific to anodic or cathodic sites whereas some others can form adsorbed protective films on the metal surface. Some examples are very effective in very small amounts and this can also be considered as a retarding catalyst as well. Inhibitors include organic[19] and inorganic[20] species as well. Inorganic inhibitors include nitrites, silicates, phosphates and homologues of chromium in group six in the periodic table.

Evidences of inhibitor usage are found since the early XIX century. Those days, they were employed to protect metals in processes of acid picking, aggressive water, acidified oil wells and cooling systems. During 1950's and 1960's, significant advances came in the corrosion inhibitor development and research as the application of electrochemistry was employed to evaluate corrosion inhibitors[21]. In the 1950s, the adsorption and oxidation inhibitors were developed and precipitation inhibitors were developed later. The focus of inhibitor investigation shifted from finding new inhibitors to elucidation of inhibition mechanism lately by the advent of electrochemical experiments, data processing and surface analysis techniques since 1960s. Quantum chemical calculations,[22] linear free energy relationship and hard and soft acid- base principle were invoked for the discussion of the mechanism for corrosion

inhibition. Recently green inhibitors are also an interest in corrosion inhibition study[23].

The usual inhibition mechanisms are as given below but in most cases a combination of two or more of them, generally occurs.

- The chemisorption of the inhibitor on the surface of the metal and thereby forming a thin film.
- Formation of protective film by combination of inhibitor ions and metallic surface.
- Formation of oxide film on the metallic surface
- Formation of complex by the inhibitor reacting with the potential corrosive component in the aqueous media.

Corrosion control by inhibitors can be employed for a variety of applications in the industrial and commercial fields like refinery units, cooling systems, pipelines, oil and gas production units, chemicals, boilers and water processing, pigments, paints, lubricants etc.

According to corrosion mechanism the corrosion inhibitors are classified into anodic inhibitors, cathodic inhibitors and mixed inhibitors

Anodic inhibitor

Anodic inhibitors are also called passivation inhibitors. They reduce the anodic oxidation, by forming a passive oxide layer on the surface of metal thereby control the rate of corrosion. They form the protective layer on the surface of metal in the presence and absence of oxygen, former is non oxidizing type and

later is oxidizing type. Chromates, nitrites, nitrates, tungstate and molybdate are examples for anodic inhibitors.

Cathodic inhibitors

The cathodic inhibitor retard the cathodic reactions, they decrease the the rate of reduction occurs at cathodic site. By using cathodic inhibitors the corrosion potential will shift more towards cathode. The precipitation may takes place on cathodic site which also reduce the rate of corrosion. The cathodic inhibitors acted on the surface of metal in 3 different way i) as cathodic poison ii) as cathodic precipitates iii) as oxygen scavengers. Bicarbonates, polyphosphates, suiphites, metal ions like calcium, zinc etc are used as cathodic inhibitors

Mixed inhibitors

The inhibitors which affect anodic as well as cathodic process of corrosion are mixed type inhibitor. Mainly organic compounds act as mixed inhibitors. Triazoles, thiourea, quinolines and amines etc are used as mixed corrosion inhibitors.

The major classification of corrosion inhibitors are as inorganic and organic corrosion inhibitors, depending on the nature of inhibitors. The crystalline salts of sodium chromate, phosphate, or molybdate etc are used as inorganic inhibitors. The anions present in the compounds will prevent the metal disintegration.

Organic inhibitors

Organic inhibitors usually have O, N, and S hetero atoms. They also have electron density and higher basicity. These hetero atoms act as the active centers

for the adsorption of the inhibitor atoms on the metal surface. Usually the sequence O < N < S < P is followed by the inhibition efficiency. A detailed study of the usage of organic compounds containing oxygen, sulphur, and nitrogen to inhibit corrosion attack on steel has been studied in detail. It is proven that most organic inhibitors adsorb on the designated metal surface by displacement of water molecules and thereby forming barrier which is compact. Electron density transfer from the inhibitor to the metal is facilitated by the availability of nonbonded (lone pair) and p-electrons in inhibitor molecules. The formation of coordinate, covalent bond was involving electron transfer mechanism to the metal surface from inhibitor is usually described.[24]

The factors determining the strength of the chemisorption bond are the polarizability of the group and the electron density on the donor atom of the functional group. Inhibition is improved when an H atom, attached to the C in the ring, is replaced by a substituent group (–NH_2, –CHO, –NO_2 or –COOH). At the point of attachment, the electron density at the metal surface changes and results in retarding the cathodic or anodic reactions. Electrons furnished at the anode are consumed at the cathode and hence corrosion is retarded.

The examination of straight chain amines having carbons between three and fourteen gives a fact that inhibition increases with the number of carbons in the chain to about 10, but, with higher members, there is no significant change in the ability to inhibit corrosion[25]. This result is attributed to the fact that solubility decreases in aqueous solution when the length of the hydrocarbon chain increases. However, it can be overcome by the presence of a hydrophilic functional group in

the molecule which would increase the solubility of the inhibitors in aqueous media.

Chemical structure and physicochemical properties of the compound including functional groups, p-orbital character, electron density at the donor atom and the electronic structure of the molecule affects the efficiency of an organic inhibitor. The inhibition of corrosion by an organic corrosion inhibitor can be due to

- The adsorption on anodic and/or cathodic sites by the molecules or its ions,
- increased cathodic and/or anodic over voltage,
- protective barrier film formation

The action of inhibitors is usually affected by

- chain length,
- the molecule size,
- bonding, aromatic/conjugate,
- bonding strength to the substrate,
- ability of cross-linking,
- solubility in the environment.

Against acid attack, the inhibitors form one or several molecular layer barriers. This is often facilitated by chemical and/or physical adsorption and induces a variation in the net charge of the adsorbed substance and charge transfer between phases.

Heterocyclic compounds containing sulphur and/or nitrogen with various substituents are considered as effective corrosion inhibitors. Thiophene, pyrrole and hydrazine derivatives posses affinity to inhibit metallic corrosion in acid media. Many formulations of primers and anticorrosive coatings make use of these components but came under severe criticism due to the toxicity of these organic components. As a solution to these, alternate organic compounds with polar functionality containing nitrogen, sulphur, and/or oxygen along with a conjugated system were developed as potential anticorrosion alternatives. Their inhibition characteristics are attributed to the ability to get adsorbed on the metallic surface by virtue of the polar reacting group, which acts as an anchor. The adsorbed layer or film thus formed acts as a barrier that separates the metal from the corrodent. Efficiency of inhibition can be attributed to the mechanical, structural, and chemical characteristics of the adsorption layers formed under particular conditions[23].

A literature review on the organic compounds used for corrosion inhibition is done in Part I of this thesis. In this part the survey on previous articles focuses on the corrosion aspects and corrosion study of organic compounds on steel and copper, including the experimental as well as theoretical studies.

Review on organic inhibitors on steel in acidic media

Aljourani et. al., studied the corrosion inhibition of benzimidazole and its two derivatives (2-mercaptobenzimidazole and 2-methylbenzimidazole) for mild steel in 1M HCl solution. Investigations were done on the adsorption and

inhibition efficiency of these compounds. The mechanism of adsorption was evaluated by calculation of the thermodynamic parameters in the presence and absence of the inhibitors. Tafel polarization analysis was conducted for the compounds and corrosion potential, cathodic and anodic Tafel slopes and corrosion current were calculated via extrapolation of the Tafel plot. The calculated surface coverage and inhibition efficiency from these values indicate the adsorption of inhibitors on the metallic surface and blocking of the active reaction sites. The efficiency of inhibition can be increased by increasing the concentration of the inhibitor. The EIS (Electrochemical impedance analysis) Nyquist plots inferred from the analysis showed a depressed semicircle and the values for double layer capacitance and inhibition efficiency is calculated from the plot which is correlated to the results from Tafel studies. The adsorption characteristics of these compounds followed Langmuir adsorption isotherm. The calculated ΔG^0_{ads}values indicated physisorption of the inhibitor molecules to the metallic surface. The efficiency of these compounds decreased with increasing temperature which confirms physical nature of adsorption which is further confirmed by thermodynamic parameters[26].

El-Lateef conducted detailed computational and experimental studies on the corrosion inhibition effect of imines such as sodium 3-[([1-carboxy-3-(methylthio)propyl] imino)methyl]-4-hydroxybenzenesulfonate and sodium 3-([(1-carboxy-2-phenylethyl) imino] methyl)-4-hydroxybenzenesulfonate on mild steel in HCl. The Nyquist and Tafel plots show that the later compound possesses better corrosion inhibition of 95.8% in 1.0mM concentration. The adsorption of

the compound on metal surface seems to obey Langmuir adsorption isotherm. SEM micrographs were taken in order to confirm the protection of the surface by the inhibitors. Quantum chemical calculations also were conducted and the quantum chemical indices such as dipole moment(μ), E_{HOMO}, E_{LUMO}, energy gap (ΔE), chemical hardness (η), electronic chemical potential (*pi*), softness (σ), susceptibility (χ) and electrophilicity (ω) were calculated in order to get an insight about the mode of action of the inhibitors[27].

Hosseini et. al., evaluated the protection efficiency of three imines N,N'-ethylen-bis (salicylidenimine), N,N'-isopropylen-bis (salicylidenimine) and N,N'-ortho-phenylen (acetyl acetone imine,(2-hydroxy benzophenone imine) for mild steel in 0.5M H_2SO_4. They employed Tafel polarization analysis and EIS spectra for the electrochemical analysis and found that all the three compounds acted as good corrosion inhibitors for mild steel by mixed anodic and cathodic type inhibition. It was found that the adsorption follows Langmuir adsorption isotherm and also, the surface area covered by the inhibitor is influenced directly by inhibitor concentration. The calculated free energy values indicated the physisorption of the inhibitor on the metallic surface[28].

Elemike et. al., conducted corrosion inhibition studies of (E)-4-(((4-propylphenyl) imino)methyl)phenol and (E)-4-((2-tolylimino)methyl)phenol by potentiodynamic polarization studies and DFT quantum chemical computational studies. Crystal structures of the compounds were also examined to obtain the geometry and spatial arrangement of the molecules. The analysis of the experimental results concluded the formation of hydrophobic films on the metallic

surface by both the compounds and thereby protecting the surface from corrodents. The mechanism of inhibition as inferred from the potentiodynamic polarization studies had more cathodic nature. ΔG^0_{ads} values suggest that the adsorption is a combination of physisorption and chemisorption which followed Langmuir adsorption isotherm. The Fukui and FMO indices of the molecules were computationally calculated in order to probe the reactivity of the molecules and pointed the reactivity difference of existence of delocalized π- electron cloud on the aromatic ring systems[29]. They also conducted a similar study of two more phenolic imines 4-(((4-ethylphenyl)imino)methyl)phenol and (E)-4-((naphthalen-2-ylimino) methyl) phenol for the assessment of corrosion inhibition potentials on 1M HCl on mild steel surface. The electrochemical analysis revealed the elevated charge transfer resistance which indicates the adsorption of the molecules on the surface contributed to the inhibitory performance. The calculated thermodynamic parameter indicate the chemisorption of the ethylphenyl derivative whereas the naphthalen derivative adsorbed via both chemical and physical means. The study concluded that the performance of the inhibitors were due to the presence of nitrogen and oxygen donors as well as the π electrons and the alkyl chain which enhanced the adsorption of molecules on the surface[30].

Badr et. al., assessed the adsorption and corrosion inhibition performance of three cationic surfactant imines on mild steel in 1.0M HCl. The synthesized cationic amphipathic inhibitors N-(2-(3,4-dimethoxybenzylideneamino)ethyl)-N,Ndimethyloctan-1-ammoniumbromide, N-(2-(3,4-dimethoxy benzylidene amino)ethyl)-N,N-dimethyldodecan-1-ammonium bromide and N-(2-(3,4-

dimethoxy benzylideneamino)ethyl)-N,N-dimethyl hexadecan-1-ammonium bromide were subjected to various experimental analysis including potentiodynamic polarization studies and EIS spectroscopy. The computational analysis included the calculation of various parameters including the atomic bond distances, Mulliken population analysis, NBO analysis, analysis of Fukui function, HOMO – LUMO analysis, electronegativity and global electrophilicity, molecular volume, dipole moment, electron transfer and back donation, and Molecular dynamic simulation. Experimental results indicated the potential inhibitory effects of the synthesized compounds. Tafel plots show the mixed inhibitory character and the thermodynamic parameters calculated indicated the chemisorption of the molecule on the surface which followed the Langmuir adsorption isotherm. Electrochemical Impedance analysis points towards the increase in charge transfer resistance and reduced double layer capacitance attributed to the adsorption of cationic surfactant inhibitor molecules on the surface[31].

Dutta et. al., evaluated corrosion inhibition properties of 2-pyridyl-N-(2'-methylamino phenyl) methyleneimine, 2-pyridyl-N-(2'-methylthiophenyl) methyleneimine and 2-pyridyl-N-(20-methoxyphenyl) methyleneimine with an objective to evaluate the effect of the presence of heteroatom and the stereochemical conformation of inhibitors in corrosion inhibition. The studies employing potentiodynamic polarization analysis and EIS spectroscopy and several computed parameters indicate that the effect of hetero atom is not the explicit parameter in determining the extend of adsorption and hence the

corrosion. The inhibitors were acting by mixed type inhibition mechanism and thermodynamic parameters calculated from experiments suggested that the predominance of chemisorption over physisorption in adsorption mechanisms. The adsorption is also confirmed by comparing the IR spectra of free and adsorbed molecules. The computational data point out that the geometry of adsorbed molecules and their electron donation as well as back donation are the major factors to improve the inhibitory action of the molecules[32].

Behpour et. al., investigated the corrosion inhibition characteristics of mild steel by the imines 2-([(2-sulfanylphenyl)imino]methyl)]phenol, 2-([(2)-1-(4-methylphenyl) methylidene] amin)-1-benznethiol and 2-[(2-sulfanylphen-yl)ethanimidoyl)]phenol by gravimetric, electrochemical and theoretical studies. The first two compounds proved as potent mixed type inhibitors with 99% efficiency on corrosion of mild steel in 15% HCl. The inhibitors' efficiency increased with increase in concentration which proved that the inhibitive action is due to the adsorption of these molecules on the surface which follows Langmuir adsorption isotherm. Thermodynamic adsorption parameters and electrochemical parameters were calculated from adsorption isotherm and electrochemical experiments respectively, to find correlation with theoretical values. The comparative analysis of the molecules shine light on the involvement of coordination through phenolic OH as well as azomethine group and the presence of electronegative donor atom and aromatic π electron system in the inhibition mechanism[33].

Keleş et. al., studied the inhibition ability of an imine and its cobalt complex on low carbon steel in HCl using Tafel potentiodynamic polarization, EIS spectroscopy and surface analysis using SEM and EDS methods. The organic imine and the complex used were 2-(phenylthio) phenyl-1-(o-tolyl)methanimine and its cobalt complex bis(acetate)(2-(phenylthio)phenyl-1-(o-tolyl)methanimine) cobalt(II) respectively. The studies proved that the cobalt complex shows higher inhibition efficiency (97.8%) than imine (97.6%) and for both analytes the inhibition efficiency depends upon the concentration, temperature and time of exposure. The imine exhibited an anodic controlled mixed type inhibition whereas the cobalt complex exhibited a cathodic type inhibition. ΔG^0_{ads} values indicated that the adsorption is not purely chemisorption but a resultant of both donor-acceptor and electrostatic interactions. EDS also confirmed the existence of a stable film on the metallic surface[34].

Recently Vikneshvaran et. al., conducted studies on three L-Tryptophan based halide-substituted chiral Schiff bases namely, 2-((5-chloro-2-hydroxybenzylidene)amino)-3-(1H-indol-3-yl)propanoic acid, 2-((5-bromo-2-hydroxybenzylidene)amino)-3-(1H-indol-3-yl) propanoic acid and 2-((2-hydroxy-5-iodobenzylidene)amino)-3-(1H-indol-3-yl)propanoic acid on their inhibition characteristics on carbon steel in 1 M HCl acid environment. The results showed a mixed type inhibition with the inhibition of anodic dissolution of metal and evolution of cathodic hydrogen along with oxygen reduction. The adsorption of the molecules obeyed Langmuir adsorption and formed a protecting film on the metallic surface from corrosive attack. UV spectra was analyzed in order to find

the metal inhibitor interactions which was confirmed by quantum mechanical calculations[35].

Yurt et. al., examined the corrosion inhibition behavior of some Schiff bases containing heteroaromatic compounds namely 2-((1E)-2-aza-2-pyrimidine-2-ylvinyl) thiophene, 2-((1Z)-1-aza-2-(2-pyridyl)vinyl)pyrimidine, 2-((1E)-2-aza-2-(1,3-thiazol-2-yl)vinyl)thiophene,2-((1Z)-1-aza-2-(2thienyl)vinyl)benzothiazole via potentiodynamic polarisation and ac impedance studies. The polarization studies indicated anodic inhibition and the electrochemical investigations were utilized for the calculation of various thermodynamic corrosion parameters[36].

Amin et. al., employed weight loss, polarization, EIS, PZC, EDX and SEM studies for the examination of the inhibition effect of succinic acid on low carbon steel corrosion in aerated non-stirred 1.0M HCl solutions with pH ranging from 2 to 8. Surface analysis using SEM and EDX confirmed the existence of an adsorbed protective film on the surface of the metal. The polarization curves indicated anodic type inhibition and potential at zero charge is determined from capacitance versus voltage plots and found that the metallic surface is positively charged in the examined pH range. The protection film is formed by an electrostatic adsorption mechanism which retards the H^+ reduction and inhibits the metal dissolution significantly. An increase in inhibition efficiency was observed with concentration, pH and immersion time[37].

Olivares et. al., studied corrosion inhibition effect of decylamides of α-aminoacids on carbon steel in 1.0M HCl medium. The tyrosine and glycine derivatives exhibited 90% protection efficiencies where valine and alanine

exhibited 80%, according to gravimetric and electrochemical techniques. The tyrosine derivatives were found to be anodic inhibitors and the later one cathodic as indicated by the potentiodynamic polarization curves. The thermodynamic parameters were calculated and the adsorption obeyed Flory-Huggins isotherm. The parameters such as active sites, equilibrium constant, enthalpy and change in free energy gave insight to the adsorption and binding of the molecules to the surface and XPS spectra confirmed the interaction of N, C and O atoms to the metallic surface for the formation of a protective film which was continuous in nature. The observed order of efficiency is attributed to the modified molecular structure on binding where as the decrease in efficiency with temperature is attributed to the change in nature of interactions of the inhibitor molecule and surface[38].

Machnikova et. al., determined the corrosion inhibition efficiency of furan derivatives, 2-methylfuran, furfuryl alcohol and furfurylamine on carbon steel in 1M HCl by gravimetric and electrochemical methods. The electrochemical polarization analysis revealed, mixed type inhibition of all derivatives which block both anodic and cathodic processes. The Langmuir adsorption isotherm was applicable for the chemisorption of these compounds on the metallic surface which was indicated by the calculated Gibbs energy values. The experimental results were further verified by correlating with the theoretical results obtained from quantum chemical calculations which employed PM3, AM1, MNDO and MINDO/3 semi-empirical self-consistence field methods. From the analysis it was concluded that the existence of higher number of lone pairs and π-electrons

enhance the interaction of the molecule with the surface and hence the inhibition efficiency. Low values of E_{LUMO}, energy gap and total energy as well as high values of E_{HOMO} accounts the increased inhibition efficiency[39].

Benali et. al., investigated the inhibition of carbon steel corrosion by 2-mercapto-1-methylimidazole in 1M $HClO_4$ with respect to concentration of the inhibitor and temperature of the medium by gravimetric and electrochemical methods. The compound showed mixed type inhibition property as evident from the potentiodynamic polarization studies and is independent of the temperature but increased with concentration of the inhibitor. The impedance analysis indicated the formation of a protective film via adsorption of the inhibitor molecules which was according to Langmuir adsorption isotherm. XPS analysis of the surface is also conducted for the confirmation of the chemisorption of the inhibitor molecule on the surface. Quantum mechanical calculations for HOMO and LUMO energy levels and molecular orbital densities were conducted. It was proposed that the adsorption is due to the donor acceptor interactions between the unpaired electrons of hetero atom and active centers of the metal. Sulphur atom in the molecule possesses higher HOMO density which is evident from theoretical calculations and hence considered to be the most active donor[40].

Tourabi et. al., employed EIS spectroscopic and potentiodynamic polarization techniques for the study of the inhibition of carbon steel in normal HCl pickling solutions by 3,5-bis(2-thienylmethyl)-4-amino-1,2,4-triazole. The compound showed obviously mixed type inhibition as indicated by the polarization curves. The inhibition efficiency increased with increasing

concentration and the adsorption of the inhibitor obeyed Langmuir adsorption isotherm. The calculated Gibbs free energy indicated the chemisorption of the molecule. XPS analysis also was conducted which confirmed the existence of a protective adsorbed film on the metallic surface.[41]

Abdallah et. al., studied the inhibitory effect of aminopyrimidine derivatives such as 2-aminopyrimidine, 2,4-diamino pyrimidine, 2,4-diamino-6-hydroxy-pyrimidine, and 2,4,6-triaminopyrimidine on the corrosion of 1018 carbon steel in 0.05M HNO_3 solution by gravimetric and electrochemical polarization techniques[42].

Copper corrosion

Copper is a coinage metal which is often considered as noble owing to its fulfilled electronic configuration. It is used for the fabrication of electronic devices, integrated circuits, wires, roofing and plumbing etc. and also for preparing alloys like brass and bronze. It is soft and is malleable and ductile having very high thermal and electrical conductivity[43]. The inherent property of corrosion exists for all metals except noble metals like Gold, Platinum and Iridium. In the presence of humidic and acidic environment, metals undergo the slow deterioration.

Normally copper is not very susceptible to corrosion. Its corrosion is almost negligible in unpolluted air, water and deaerated non-oxidising acids. But it undergoes rapid dissolution in presence of strong oxidants. There are two types of copper corrosion namely uniform and non-uniform corrosion. Uniform corrosion can be considered when a uniform layer of corrosion products formed

on the surface of the metal. Non-uniform corrosion is due to the development of isolated corrosion cells and this can be seen at different spots.

High corrosion rates are expected for metals in acid solution and in many industries, they are used. Main industrial procedures involving copper are dissolution of copper in acids and electroplating for claddings. Nitric acid is used as corrosive medium for dissolution of copper metal as the oxidising power of nitric acid is high when compared to sulphuric and other acids. From the surface of the metal, copper is dissolved in to the solution bulk as Cu^{2+}. On reacting with nitric acid there is no formation of passive film for the protection of the metal from corrosive media and hence the dissolution of metal will be more dominant.

The electrochemical reactions responsible for the corrosion of copper in nitric acid are:

Anodic reaction: $Cu \rightarrow Cu^{2+} + 2e$

Cathodic reaction: $NO_3^- + 3H^+ + 2e \rightarrow HNO_2 + H_2O$

$NO_3^- + 4H^+ + 3e \rightarrow NO + 2H_2O$

$O_2 + 4H^+ + 4e \rightarrow 2H_2O$

At anode the diffusion of Cu(II) species controls the dissolution of copper from the outer metallic surface to the bulk solution and, at the cathode, nitrate ions are readily reduced to nitrous acid or nitric oxide. Moreover the dissolved oxygen in aerated solutions can also get reduced on the copper surface.

The corrosion of copper in various corrosive media has been investigated by various research groups. Corrosion in acidic media like HNO_3, H_3PO_4 as well as in aqueous NaCl is also studied. Organic corrosion inhibitors are also

employed for the corrosion inhibition studies on copper in acid media. Most of the corrosion inhibitors contain heteroatoms with unpaired electrons and some of them had π-systems to contribute to electron donation.

Review on organic inhibitors on copper in acidic media

Cubillos et. al., investigated the corrosion behavior of copper in 0.1M NaCl under the influence of inhibitor, 8-aminoquinoline by open circuit potential measurements, potentiodynamic polarization measurements and EIS spectra along with surface analysis using AFM. The inhibitory action was anodic upto 10^{-3}M concentration and then it inhibited both anodic and cathodic currents there by stifling the corrosion current density. The theoretical studies on the same experiments were conducted and geometric, energetic, frontier orbital and total electronic density was calculated to provide insights on the corrosion of copper in NaCl and found that the chloride ion has a significant role in copper corrosion[43].

Ogretir et. al., conducted quantum chemical theoretical studies on the effect of pyridine derivatives on the corrosion of copper and compared with experimental values and found very good agreement. The methods adopted were AM1, PM3, MINDO/3 and MNDO semi empirical SCF molecular orbital method. The values examined were total energy, ionization potential, E_{HOMO}, E_{LUMO}, ΔE, dipole moment, corrosion rate and percentage of inhibition efficiency of neutral species and protonated species[44].

Lashgart et. al., conduted theoretical and experimental studies on the corrosion inhibition properties of 3-mercapto-1,2,4-triazole, benzotriazole, thiophene, and tetra hydro-thiophene towards copper in phosphoric acid medium.

Cluster/polarized continuum and gravimetric approaches, second-order Møller-Plesset perturbation and density functional theories were invoked for the theoretical analysis and calculation of electronic chemical potential. Molecular softness, and extent of charge transfer were determined for inhibitor molecules at the metal/solution interface which provided good correlation between theoretical and experimental values. The mechanism of metal-inhibitor interactions were analysed and various active centres on the moecule were analysed[45].

Khaled et. al., conducted corrosion studies of copper in 1M HNO_3 using some benzotriazole derivatives such as N-(2-thiazolyl)-1H-benzotriazole-1-carbothioamide, M-(furan-2-ylmethyl)-1H-benzotriazole-1-carbithioamide and N-benzyl-1H-benzotriazole-1-carbothioamide by the weight loss, ac impedance and polarization studies. From these studies it was evident that the corrosion rate depends on the varying concentration of the inhibitor. The three inhibitor molecules acted as mixed type inhibitor and they obeyed Langmuir adsorption isotherm. Using density functional theory, theoretical studies were conducted especially through the Fukui indices for explaining inhibition performance[46].

Karthik et. al., examined the corrosion of copper in 0.5M HNO_3 in the presence of Levetiracetam. The maximum inhibition efficiency obtained was 94.99% at 300 ppm. Kinetic and thermodynamic parameters were calculated and it was found that the adsorption obeyed Langmuir adsorption isotherm on the copper surface in nitric acid. The compound acted as mixed type inhibitor. The DFT method was used for the theoretical calculation and surface morphological

studies were done using SEM and AFM. All the results from different methods were supporting to each other[47].

Zarrouk et. al., investigated the inhibitory behavior of a traizole derivative 3-amino-1,2,4-triazole for the copper corrosion in 2.0M HNO_3 using weight loss method, EIS and polarization studies. Maximum inhibition efficiency of 82.2% was obtained for 10^{-2}M concentration and the compound acted as mixed type inhibitor, obeying Langmuir adsorption isotherm. The quantum chemical calculations were done by using DFT at the B3LYP/6-31G* to evaluate the correlation between the inhibition action and the molecular structure of the investigated compound[48].

Nasser et. al., selected 3.0M HNO_3 as the aggressive medium inorder to invesigate copper corrosion in the presence of benzyl phenyl sulphide. The compound showed marked inhibition efficiency on copper corrosion on evaluation with weight loss, EIS, polarization and hydrogen permeation studies. The Temkin adsorption isotherm was obeyed by benzyl phenyl sulphide on copper. Surface morphological analysis was conducted by atomic force microscopy and surface roughness were also calculated[49].

Khan et. al., studied the inhibition of copper corrosion using benzotriazole. 3.5% of NaCl solution under the flow test conditions was used as the aggressive solution and this study revealed that the benzotriazole acted as a protective cage for copper. The surface studies were conducted by SEM and AFM analysis which verified the mechanism of interaction of the inhibitor as surface adsorption which followed Langmuir adsorption isotherm on copper surface[50].

Sherif et. al., examined copper corrosion in 0.5M HCl in the presence of 2-amino-5-ethylthio-1,3,4-thiadiazole by weight loss studies and electrochemical studies and found that the rate of corrosion decreased in the presence of above inhibitor by reducing cathodic, anodic, and corrosion currents. The compound was showing strong adsorption on the surface of metal which was verified by SEM and energy dispersive X-ray (EDX)[51].

Elmorsi et. al., used cyclic voltammetry and uv-visible spectroscopy for the analysis of the mechanism of protective layer formation on the metal in electrolyte solution and copper complex formed on the surface by potentiodynamic polarization method for getting corrosion parameters, using two classes of inhibitors namely phenylazo-pyrazolones and bromobenzyl-carboxy-1,2,3 triazoles in 0.5M H_2SO_4. The effect of temperature on corrosion was also investigated[52].

Raphael et. al., synthesized two heterocyclic compounds which were water-soluble (E)-2-(1-(pyridine-3-yl)ethyldene)hydrazine carbothioamide (3APTSC) and (E)-3-(1-(2-phenyl hydrazono)ethyl) pyridine (3APPH) and compared the inhibition efficiency of both compounds in 0.1 M HNO_3 for copper metal. The 3APPH exhibited a higher efficiency of inhibition than the other. Both compounds obeyed Langmuir adsorption isotherm and acted as an inhibitor of mixed type. Quantum chemical studies were also conducted for calculation of HOMO and LUMO energy, energy difference (AE), electronegativity, chemical hardness, potential for ionization and number of transferred electrons[53].

Scope and objectives of the present investigation

In many industries, metal corrosion is now becoming an emerging problem. Metal protection against corrosion, especially steel and copper, is a challenge for many industries. Researchers and scientists are always looking for new, effective, non-toxic and durable inhibitors of corrosion. Although research on the corrosion inhibition efficiencies of organic molecules on steel corrosion has been reported extensively, very few articles have been published on copper corrosion behavior. The main inhibitors of corrosion are organic molecules, which contain hetero-atoms such as nitrogen, oxygen and sulfur, etc. If C= N linkage, electron cloud on aromatic ring and hetero atoms are present in the compounds, they would act as an excellent corrosion inhibitor. The corrosion inhibition power on steel and copper corrosion of many heterocyclic molecules, particularly derived from pyridine and indole, is to be revealed.

In the present study it is put forward to investigate the corrosion inhibition studies of eleven heterocyclic imines derived from pyridine carbaldehyde and 3-formylindole on carbon steel and copper in three different acids, such as hydrochloric acid, sulphuric acid and nitric acid. The methods used for these studies are weight loss study, electrochemical studies such as electrochemical impedance spectroscopy and potentiodynamic polarization studies. The mechanism of corrosion is to be revealed by plotting different adsorption isotherms, from this adsorption equilibrium constant and free energy of adsorption is to be calculated.

It is also proposed to conduct temperature study to evaluate the effect of temperature on corrosion inhibition efficiency of the molecule. To understand the morphological difference of metal surface, it is planned to perform surface analysis. The quantum mechanical study is used to find out the energy parameters like HOMO, LUMO and energy gap between HOMO and LUMO. It is also proposed to correlate the inhibition efficiency of the molecules experimentally and theoretically.

CHAPTER 2

MATERIALS AND METHODS

Corrosion inhibition studies were carried out by weight loss measurements as recommended by ASTM method[54]. Potentiodynamic polarization studies and electrochemical impedance measurements are the electrochemical experiments used for the verification of the inhibition behaviour of the heterocyclic imines. This chapter explains the materials and the methods used for the investigation of corrosion inhibition studies on synthesised imines.

Metal specimens

Carbon steel specimens of approximate composition C: 0.55%; Mn: 0.08%; P: 0.04%; S: 0.012%; Si: 0.02% and rest Fe (determined by EDAX method) for the weight loss studies were prepared in accordance with ASTM[54] (American Society for Testing and Materials G31-72, ASTM "Standard Practices for Laboratory Immersion Corrosion Testing of Metals") standards. An approximate dimension of 1.0 x 1.0 x 0.155cm were used for metal specimens which were abraded by different grade emery papers such as 100, 200, 400, 600, 800, 1000, 1500 and 2000. Vernier callipers and screw gauge were used to determine the area of these metal specimens and was washed with ethanol, acetone and with distilled water. It is then dried and weighed with electronic balance (0.0001g accuracy). The inhibitor solutions with different concentrations were taken in stoppered bottles to immerse metal specimens in hanging position, using fishing lines.

Aggressive solutions

Heterocyclic imines were synthesized as described in Part I. Stock solution of the imines having concentration 1.0mM were prepared in 1.0M HCl, 0.5M H_2SO_4 and 0.1M HNO_3 (Merck) solution. Different concentration of heterocyclic imine solutions of concentrations 0.2 to 1.0mM were prepared by the serial dilution of the stock solutions of imines with respective acid solutions. A total volume of 50ml and 100ml solutions were used for weight loss and electrochemical studies respectively.

Weight loss studies

ASTM standards were applied for weight loss measurements and the weight loss occurred for the metal specimens were measured for 24 hours. Without adding an inhibitor, a blank was also conducted. Duplicate experiments were carried out and its average values were derived to ensure the reproducibility. From the weight loss measurements, the corrosion rate (mmy^{-1}) and percentage of inhibition efficiency were calculated. The relation between rate of corrosion and inhibition efficiency with respect to weight loss of the metal specimen were shown in equations 1 and 2 respectively.

$$\text{Rate of corrosion } W = \frac{K \times \text{Wt. loss in grams}}{\text{Area in sq.cm} \times \text{time in hrs} \times \text{density}} \quad (1)$$

where 'K' = 87600, a factor used to convert cm/hour into mm/year, the density of Cu = 8.76g/cc and density of CS specimen = 7.88g/cc.

Inhibition efficiency (η) or percentage of inhibition is given by

$$\eta = \frac{W - W'}{W} \times 100 \quad (2)$$

where W & W' corresponds to corrosion rate of the CS/Cu specimen in the absence and presence of the inhibitor respectively[55].

Adsorption studies

Even though corrosion inhibition mechanism on the metal surfaces in organic inhibitor molecules is not fully revealed, the researchers strongly believe that the corrosion inhibition on the metal surface is a result of adsorption by the molecules and this adsorption can be chemical, physical, or both. For the determination of corrosion inhibition mechanism, adsorption isotherm studies are quite inevitable. Langmiur, El-Awady, Flory-Huggin, Freundlich, Temkin, and Frumkin adsorption isotherms[56] are the most commonly used ones. Using the equations mentioned below, all these isotherms were tried for determining the best fit adsorption model[57-60]. By using the value of correlation coefficient (R^2) the best fit isotherm were selected for predicting the mechanism of adsoption

Freundlich adsorption isotherm $\theta = K_{ads}\, C$ (3)

Temkin adsorption isotherm $e^{f\theta} = K_{ads}\, C$ (4)

Langmiur adsorption isotherm $\frac{C}{\theta} = \frac{1}{K_{ads}} + C$ (5)

El-Awady adsorption isotherm $\log(\theta/1-\theta) = \log K + y\log C$ (6)

Flory-Huggin adsorption isotherm $\log(\theta/C) = \log K + x(1-\theta)$ (7)

Frumkin adsorption isotherm $\frac{\theta}{1-\theta}\exp(f\theta) = K_{ads}\, C$ (8)

where C corresponds to concentration of the inhibitor, f is the molecular interaction parameter, θ is the fractional surface coverage and K_{ads} is the adsorption equilibrium constant. The one which got the highest value of correlation coefficient (R^2) is the most adequate one among the different

isotherms tried and is accepted for interpreting the adsorption mechanism.The adsorption equilibrium constant K_{ads} is related to the standard free energy of adsorption ΔG^0_{ads}, by

$$\Delta G^0_{ads} = -RT \ln(55.5\ K_{ads}) \quad (9)$$

where 55.5 is the molar concentration of water, T is the temperature in Kelvin and R is the universal gas constant. From the different adsorption isotherms tried, K_{ads} and hence ΔG^0_{ads} were determined.

Temperature studies

For the investigation of different thermodynamic parameters including enthalpy of corrosion (ΔH^*), activation energy (E_a), entropy of corrosion (ΔS^*), and Arrhenius parameter (A), the gravimetric corrosion inhibition studies were carried out in the temperature range 30- 60°C. By the well-known Arrhenius equation, the rate of corrosion is related to the energy of activation.

$$K = A \exp(-E_a /RT) \quad (10)$$

where K is the rate constant, E_a is the activation energy, T is the temperature in Kelvin scale, R is the universal gas constant and A is pre-exponential or Arrhenius factor. A plot of logK Vs 1000/T will be a straight line with its slope $-E_a/2.303R$ and intercept log A from the above equation. The enthalpy and entropy of activation (ΔH^*, ΔS^*) were calculated from the transition state theory[61].

$$K= (RT/Nh) \exp(\Delta S^*/R) \exp(\Delta H^*/RT) \quad (11)$$

Here, N is the Avogadro number and h is the Planks constant. The equation can be rewritten in the form y = mx +c to obtain

$$\log K/T = \log R/Nh + \Delta S/2.303R - \Delta H/2.303RT \quad (12)$$

The slope of the above equation is $-\Delta H/2.303R$, from which enthalpy of activation can be calculated. Entropy of activation can be calculated from the intercept of the above equation i.e,

$$\log R/Nh + \Delta S/2.303R \quad (13)$$

Electrochemical studies

An electrochemical phenomenon which occur at large number of miniature cells on the metallic surface is called to be the metallic corrosion. With appreciable certainty, the investigation of corrosion rate can be employed with the electrochemical methods since corrosion is an electrochemical process. The advances in the computer technology and electrochemistry gave a key advantage in the origin of fast and accurate potentiostats which are suitable for the investigation of corrosion rate. It also helps the researcher to determine corrosion rate with sensitivity and also to evaluate rate controlling mechanisms. The electrochemical methods are faster and the resulting yield agrees with the conventional ones compared to the time-consuming conventional weight loss studies for the determination of corrosion rates.

From the mixed potential theory, theoretical basis for the investigation of electrochemical corrosion is derived[62]. This theory shows that on the corroding surface of the metal, the total rate of all the oxidation reactions (anodic) is equal to the total rates of all the reduction reactions (cathodic). The open circuit potential (OCP) or corrosion potential which is denoted by E_{corr} is the mixed corrosion potential developed at this moment. The corrosion current density, i_{corr}

is the current density at E_{corr} and is a measure of the rate of corrosion. Electrochemical Impedance Spectroscopy and the polarization studies are the widely used for electrochemical investigations.

A three-electrode assembly is used to perform the EIS measurements including saturated calomel electrode (SCE) as a reference electrode, platinum electrode (area $1cm^2$) as counter electrode and a working electrode which is the metal specimens with an exposed area of $1cm^2$. An Ivium compactstat-e electrochemical system is used to carry out EIS experiments. Electrolyte used is the acid solution without stirring and deaereation and the metal specimen's working area was exposed to the electrolyte for 1 h prior to the measurement. A constant potential (OCP) is applied for performing EIS measurements with amplitude of 10 mV as excitation signal in the frequency range from 1 KHz to 100 mHz.

Electrochemical impedance spectroscopy (EIS) studies

When polarization measurements are unable to provide exact values of current densities electrochemical impedance technique were better employed. This can also provide kinetic and mechanistic information for electrochemical systems and hence used very extensively for the study of corrosion[63].

Equivalent electrical circuits are used for the examination of electrochemical systems. A simple electrochemical system is be represented by the equivalent circuit as depicted in Figure 2.1, where R_{ct} is the charge transfer resistance, R_s is the solution resistance, and C_{dl} is the double layer capacitance arising due to the charged surface of the metal specimen and the charged layer of

opposite polarity from the ions in the corrodent / electrolytic solution. Electrochemical reaction rates can be calculated from R_{ct}.

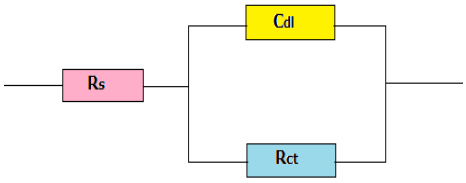

Figure 2.1 Equivalent circuit model

Information about the mechanism of film formation can be obtained from capacitance measurements. By considering the electrical double layer between the charged metal surface and the solution as a capacitor, during the electrochemical measurements, decrease in C_{dl} may be explained. Electrical capacity decreases on the adsorption of the inhibitor on the electrode surface due to their displacement of the water molecules and other ions which were originally adsorbed on the surface. The formation of a protective layer on the electrode surface is indicated by this decrease in capacitance with increasing inhibitor concentration.

In order to make sure that a given electrochemical system fits a particular equivalent-circuit model, EIS measurement is employed and the values of various components of the equivalent circuit are determined. The experimental manifestation of the above is done by applying an ac excitation over a wide range of frequencies and the determination of the response of the electrochemical system towards the same. An ac voltage or an ac current can be applied as an excitation and the corresponding response, which will be an ac current or an ac voltage is measured, and impedance of the system can be calculated[64]. The tendency to resist (or impede) the flow of an alternating electrical current in a

circuit is called its impedance, Z. The real (resistance) and imaginary (capacitance) components of the impedance response of the circuit is measured by the EIS instrument. Impedance is represented by a complex number with real $Z'(\omega)$ and imaginary $Z''(\omega)$ components, as given in the equation 14.

$$Z(\omega) = Z'(\omega) + jZ''(\omega) \quad (14)$$

The impedance data can be plotted in a variety of formats and for revealing certain characteristics of a given test system, different plots are used and the important plots are Nyquist plot, Bode plot and simple impedance plot.

Nyquist plot

In this particular form which is named as Cole-Cole plot or a complex impedance plane diagram, at each excitation frequency, the imaginary component of impedance *(Z'')* is plotted against the real component of impedance (Z')[65]. R_s is the solution resistance which is the uncompensated resistance between the working electrode and reference electrode, R_{ct} is the charge transfer resistance at the solution/electrode interface known as polarization resistance. The only source of the impedance of the system at high frequencies is the ohmic resistance R_s (solution resistance). At the far left end of the semicircle, the frequency reaches its high limit, where the semicircle intercepts the x-axis. Similarly, at the right end of the semicircle, frequency reaches its low limit (Figure 2.2). From R_{ct} the inhibition efficiency of a molecule on the metallic surface can be calculated by equation,

$$\eta_{EIS}\% = \frac{R_{ct} - R'_{ct}}{R_{ct}} X100 \quad (15)$$

where R_{ct} and R'_{ct} are the charge transfer resistances of working electrode with and without inhibitor, respectively[66].

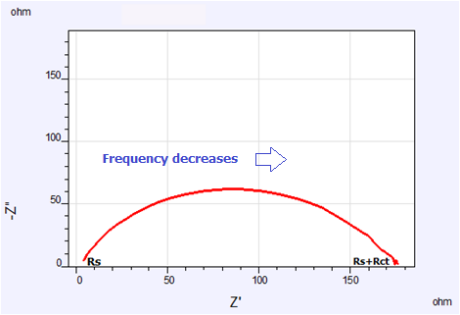

Figure 2.2 Nyquist plot

Bode plot

In this plot, the phase angle θ, of the resultant wave form is plotted as a function of frequency and is used for the calculation of the absolute impedance Z by the equation

$$|Z| = \sqrt{Z'^2 + Z''^2} \quad (16)$$

The Nyquist plot can alternatively be replaced by the Bode plot in order to avoid comparatively long measurement times associated with low frequency. The curve of this impedance plot which represents log|Z| versus log frequency (impedance plot) provides the value of R_s and R_{ct}. At intermediate frequency, this curve has a break point which lies on a straight line with a slope -1. The value of C_{dl} is given by extrapolating this straight line to the y-axis at f = 1 or logf = 0

$$|Z| = \frac{1}{C_{dl}} \quad (17)$$

A peak corresponding to f θ^{max} is observed in the plot of θ against log f which represents the maximum phase shift and C_{dl} can be evaluated from this. The frequency break points attributed to each step is shown by the Bode and

impedance plots when compared to the Nyquist plot. A combined Bode and impedance plot is shown in the Figure 2.3.

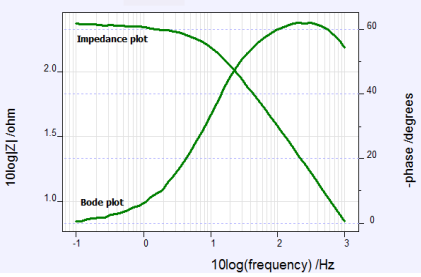

Figure 2.3 Bode and impedance plots

Potentiodynamic polarization studies

Tafel extrapolation and linear polarization studies were considered as the conventional DC polarization techniques. The polarization method is carried out by changing the potential of the working electrode and monitoring the produced current as a function of potential or time.

Linear polarization technique

Similar to the Butler-Volmer equation for reversible reactions, a relation describes the experimental polarization response of a metal (I_{app})[67].

$$I = I_{corr}\left[e\left(\frac{\eta}{\beta a}\right) - e\left(\frac{\eta}{\beta b}\right)\right] \quad (18)$$

where I is the net current density across the metal electrolyte interface, η is the over potential ($E_{measured}$-E_{corr}), I_{corr} is the corrosion current density (Acm^{-2}), βa and βc are the anodic and cathodic constants depending on the reaction mechanism and are given by

$$\beta a = \frac{RT}{(1-\propto)nF} \quad (19) \qquad \beta c = -\frac{RT}{\propto nF} \quad (20)$$

The slowest step in the electrochemical corrosion process is assumed to be the one in equation 8 and is the charge transfer process at the metal-solution interface. It means that the charge transfer process is the key factor that controls the corrosion rate. In the experimental way the relationship is observed in the absence of competing redox reactions between the potential and the applied electrochemical current density for a corroding electrode. This relationship is applicable in the presence of single charge transfer controlled cathodic and anodic reactions and applied to the corrosion potential and corroding electrode, thereby providing the basis for the electrochemical polarization technique.

The practical and theoretical demonstration showing potentials are very close to $E_{corr,}$ +/- 10mV resembles that the linear polarization technique and the applied current density is linear in function of the electrode potential (Figure 2.4).

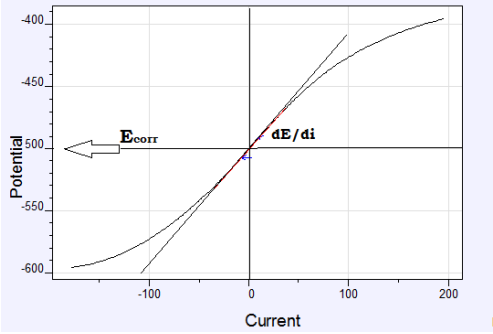

Figure 2.4 Linear polarization plot

This technique is also called as polarization resistance method since the slope, $\frac{\Delta E}{\Delta I}$ has the unit of resistance (R_p). In order to obtain Stern and Geary equation 11, the equation 8 can be mathematically linearized and this equation 11 relates i_{corr} to the inverse of the slope[68].

$$I_{corr} = \left[\frac{b_a b_b}{2.303(b_a b_b)}\right]\frac{\Delta I}{\Delta E} = \frac{B}{R_p} \qquad (21)$$

where b_a and b_b are the anodic and cathodic Tafel slopes, respectively. For the measurement of corrosion rate as current density (I_{corr}), equation 11 can be used and the provided B and R_p are known. This kind of polarization technique lend way for the corrosion inhibition studies due to the fact that polarization resistance (R_p) can be increased with the inhibitor concentration. As the inhibitor molecules gets adsorbed on corroding metal surface, the rate of charge transfer process gets decreased thereby increasing the polarization resistance or minimizing the rate of corrosion. The values of the corrodents polarization resistance is obtained using the slope analysis of the linear polarization curves with the avail of corrosion potential of blank as well as different concentrations of the inhibitor.

There are many corrosion analysis softwares in which the most commercial one have the capability to fit data to this equation and have performed the electrochemical studies using Ivium compactstat-e electrochemical system in the present course of investigation. The software 'Ivium soft", after linear polarization analysis, can directly give the value of R_p and the evaluated polarization resistance can be used to calculate inhibition efficiency using the relationship

$$\eta_{R_p}\% = \frac{R'_p - R_p}{R'_p} X100 \qquad (22)$$

Where R'_p and R_p are the polarization resistance in the presence and absence of inhibitor respectively.

Tafel extrapolation technique

The relationship between the logarithm of current density and the applied potential can be obtained from Tafel equation and this equation can be obtained empirically by Tafel which can be deduced from equation 8 easily. The current density for a simple activation-controlled transport process of dissolution of metal (anodic process), is given by Tafels law: [69,70].

$$I = I_{corr}\, e^{\left(\frac{\eta_a}{\beta_a}\right)} \tag{23}$$

According to the above equation, the corrosion rate of the reaction depends upon the potential and the equation must satisfy $\left(\frac{\eta_a}{\beta_a}\right) \gg 1$ for being the anodic segment in the polarization curve. On taking logarithm of the above equation

$$\eta_a = -\beta_a \ln I_{corr} + \beta_a \ln I_{corr} \tag{24}$$

Converting into logarithm to base 10 and defining the anodic Tafel constants a and b, then

$$\eta_a = a_a + b_a \log I_a \tag{25}$$

where $a_a = -2.303\beta_a \log I_{corr}$ and $b_a = 2.303\beta_a \log I_a$

Similarly, for cathodic process where $\left(\frac{\eta_b}{\beta c}\right) \ll 1$

$$I = -I_{corr}\, e^{\left(-\frac{\eta_c}{\beta c}\right)} \tag{26}$$

$$\text{Then } \eta_c = a_c - b_c \log I_c \tag{27}$$

where $a_c = -2.303\beta_c \log I_{corr}$ and $b_c = 2.303\beta_c \log I_c$

According to equations 25 and 27, the straight-line plot of electrode potential versus the logarithm of current density is called Tafel line. The

mechanism of the electrode process is deduced from the slope of Tafel plot 'b' and the rate constant of reaction is obtained by the intercept 'a' at $\eta = 0$

I_{corr} can be measured by extrapolating the linear segments from the potential-current density plot. The cathodic potential-current density curve is measured over a potential ranging from E_{corr} to E_c, by the metal specimens acting as cathode (Figure 2.5). Similarly, by making specimen to behave as anode, the anodic potential - current density to the noble direction can also be measured. The linear segments obtained from the measurement of both anodic and cathodic potential-current density curves is referred to as Tafel regions. Extrapolating the linear segment of anodic and cathodic curve, both Tafel lines intersect at the point of coordinates (E_{corr}, log I_{corr}). These helps in the estimation of the corrosion current density and the percentage inhibition efficiency is estimated using the corrosion current densities by,

$$\eta_{pol}\% = \frac{I_{corr} - I'_{corr}}{I_{corr}} X100 \qquad (28)$$

where I_{corr} and I'_{corr} are uninhibited and inhibited corrosion current densities, respectively.

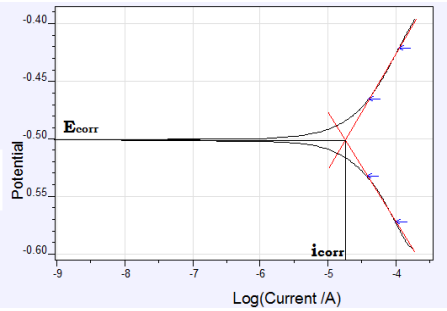

Figure 2.5 Tafel plot

Ivium compactstat-e electrochemical system is used for recording anodic and cathodic potentiodynamic polarization curves in the present Tafel polarization

studies of CS and copper specimens in 1.0M HCl with and without inhibitor with 1cm^2 as the exposed area of the carbon steel specimen in the corrodent. Polarization plots with the electrode potential ranging from -250 to +250 mV Vs corrosion potential (E_{corr}), were obtained at a scan rate of 1mV sec^{-1}.

Electrochemical noise studies

Electrochemical noise (ECN) is the measurement of potential and current fluctuations occurred due to the discrete events associated with corrosion process. ECN also helps to predict the amount of localized pitting corrosion[71,72]. Electrochemical noise (ECN) measurements were performed using a three-electrode cell system, which consists of two carbon steel electrodes of 1 cm^2 area used as working electrode and counter electrode and SCE as reference electrode[73,74]. All ECN analyses were performed for a period of 1200 sec using Ivium compactstat-e-electrochemical system controlled by iviumsoft software.

Noise is considered as a non-deterministic process. Generally deterministic processes are periodic in nature and can be mathematically defined. Fluctuations of corrosion current values are random and evaluated by probability or statistics rather than algebraic equation. Figure 2.6 represents the plot of noise current Vs time, and the noise current values give the idea about the corrosion protective power of sample. Figure 2.7 represents the pitting index curve of the sample and the amplitude of the curve indicates the resisting capacity of imines against pitting corrosion. The data analysis of electrochemical noise study is mainly done by time domain and frequency domain analysis.

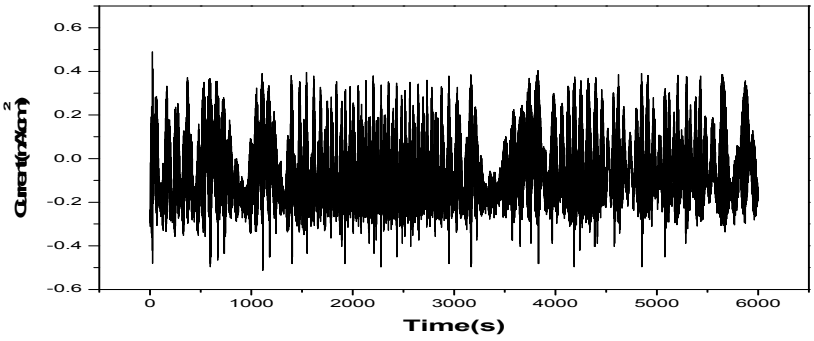

Figure 2.6 Noise current Vs time plot

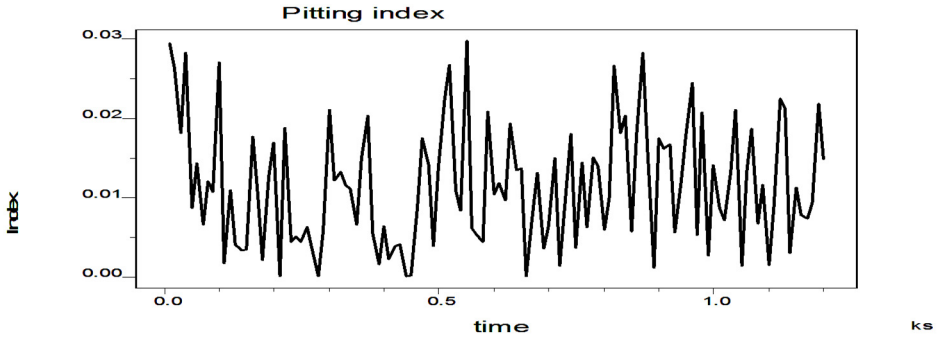

Figure 2.7 Pitting index curve

Time domain analysis

The simplest qualitative approach to data analysis is a visual assessment of the noise data. With uncoated (bare) metals can provide mechanistic information about corrosion type, i.e the shape and the frequency of occurrence of current and potential transients is examined to be an indication of corrosion pit formation and its repassivation/propagation. The noise data obtained from coated metal in not showing these transients of potential and current. Using the time domain analysis the pitting index of corrosion can be calculated.

Frequency domain Analysis

In order to get the mechanistic information of corrosion on conducting ECN on a number of coating systems, it is significant to analysis the ECN data in

time domain as well as frequency domain. The time domain data can be transferred to frequency domain using the Fast Fourier transform (FFT) or Maximum Entropy Method (MEM) algorithms.

According to the frequency-domain analysis is a waveform of any complexity can be taken as the sum of numerous sinusoidal waveforms of suitable amplitude, relative phase and periodicity[75-77]. The frequency domain analysis of noise measurement gave the PSD (Power Spectral Density) of systems, which is represented in the Figure 2.8. The Power Spectral Density (PSD) plot may be used to calculate the spectral noise resistance. It can be applied to the different fields of science and technology.

Power spectra

The estimate of the power present at various frequencies results in plots of the power spectra density (PSD) as a function of frequency. The units of PSD for potential and current are V2/Hz and A2/Hz, respectively. There are two primary methods used in the corrosion field: Fourier transform and maximum entropy.

Fast Fourier Transform

Fast Fourier Transform (FFT) is a faster calculation method of the complex Fourier series by machine; its mathematical properties are familiar to be fully analogous to the traditional Discrete Fourier Transform (DFT). The Fourier transform method computes the combination of sine waves needed to obtain the observed signal. The fast Fourier transform (FFT) algorithm is usually used, where the PSD is determined as the amplitude squared of the sine waves, divided by the frequency separation. To minimize artificial noise in the spectrum, trend

removal and windowing are applied to the time record prior to computing the spectrum and the results from several spectra are then averaged. Two drawbacks of FFT analysis are aliasing and leakage. Aliasing is an error generated in all spectral analysis methods by the reduction of sampling rate. Leakage is resulting mainly because of the assumption that the Fourier Transform is a periodic process.

Maximum entropy method

Among the spectral analysis methods, the Fourier Transform analysis is a basic method[78]. Since the Fourier analysis is become accurate and good resolution obtains only at long length records, the Burg's maximum entropy method was developed to improve the resolution for short length records. This is said to be achieved by extrapolation of the auto-correlation function in such a way that the entropy of the corresponding probability density function is maximized in each step of the extrapolation. The method makes no assumption of the data outside the time interval specified and is thus least committing to the unavailable data. Burg's method is data dependent that is why it is nonlinear data, reliable method and has many applications in different fields of science and technology. Mathematically, the MEM ensures that the fewest possible assumptions are made about unmeasured data by choosing the spectrum which is the most random or has the maximum entropy for the process under investigation, and is consistent with known data.

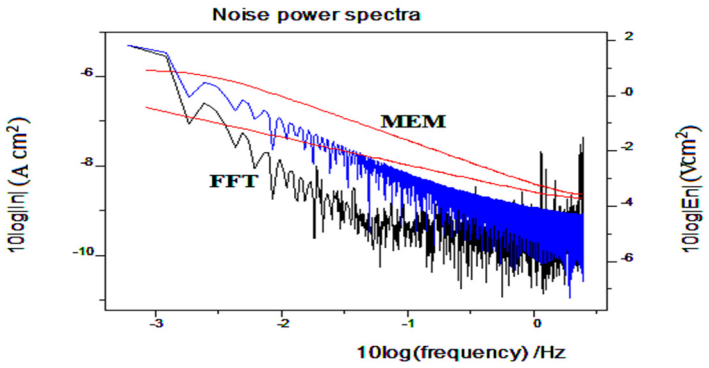

Figure 2.8: PSD plot

Surface morphological studies

Scanning electron microscopic studies were conducted using Joel JSM-6390 LV/JED-2300 model microscope for the investigations of the surface modifications on the metal specimens during the process of corrosion and corrosion inhibition. The SEM images of metal corrosion in the presence and absence of inhibitor can reveal the difference in surface morphology. A comparison of the SEM images of well-polished bare metal specimen, metal specimen corroded in acid solution (blank, treated for 24h) and specimens exposed to the inhibitor solution (treated for 24h) were compared to establish inhibitory action.

Quantum mechanical studies

The corrosion inhibition efficiency of various heterocyclic imines can be correlated with the frontier molecular orbital energies. The donor-acceptor interaction (HSAB concept) between the filled molecular orbitals of the inhibitor molecules and the vacant orbitals of metal atoms (CS/Cu) on the surface has an important role in the prevention of mechanism of metal disintegration. High value

of E_{HOMO}, the lowest value of E_{LUMO} and energy difference between HOMO and LUMO E_{LUMO}-E_{HOMO} (ΔE) are the important quantum mechanical parameters of inhibitors which help them to bind on the metal surface strongly[79,80]. Quantum mechanical calculations were done using DFT method by GAMMESS-2018 software. A combination of Beck's three parameter exchange functional and Lee–Yang–Parr nonlocal correlation functional (B3LYP) was employed in DFT calculations[81]. Approximate HSAB parameters like electro negativity (χ) and chemical hardness (η) of the imines in solution phase were calculated[82] by the following equations 29 and 30.

$$\chi \approx -1/2\ (E_{HOMO} + E_{LUMO}) \quad (29)$$

$$\eta \approx 1/2\ (E_{HOMO} - E_{LUMO}) \quad (30)$$

Quantum mechanical parameters assist for the calculation of number of electrons transferred (ΔN) from donor to acceptor molecules. As an approximation, the chemical hardness of metal is assumed as zero and the approximate electro negativity of bulk Fe is taken as 7ev and for Cu is 4.48eV[83], equation 31 gives the approximate quantity of electron transferred from the imine molecule to the metal atoms.

$$\Delta N = \frac{\chi_{Cu/Fe} - \chi_{inhib}}{2(\eta_{Cu/Fe} + \eta_{inhib})} \quad (31)$$

CHAPTER 3

CORROSION INHIBITION STUDIES OF HETEROCYCLIC IMINES ON CARBON STEEL IN 1.0M HCl

This chapter deals with the study of corrosion inhibition behaviour of eleven heterocyclic imines in which seven imines are derived from pyridine carbaldehyde such as pyridine-2-carbaldehyde oxime (2PCOX), pyridine-3-carbaldehyde oxime (3PCOX), pyridine-2-carbaldehyde-4-aminobenzoic acid (2PC4ABA), pyridine-2-carbaldehyde-3-aminobenzoic acid (2PC3ABA), pyridine-2-carbaldehyde-2-aminobenzoic acid (2PC2ABA), pyridine-3-carbaldehyde-3-aminobenzoic acid (3PC3ABA), pyridine-2-carbaldehyde-2-aminophenol (2PC2AP) and the rest are 3-formylindole phenylhydrazone (3FIPH), 3-formylindole semicarbazone (3FISC), 3-formylindole thiosemicarbazone (3FITSC) and 3-formylindole-1,2-diaminocyclohexane (3FIDACH) which are 3-formylindole derivatives. The aggressive solution used for corrosion inhibition studies on CS was 1.0M HCl. The weight loss studies, electrochemical impedance spectroscopic studies, potentiodynamic polarization studies, quantum mechanical studies, surface morphological studies and adsorption studies were the various analyses used for the evaluation of corrosion inhibition behaviour of the synthesized imines. This chapter is divided into two sections; in which section I deals with the corrosion inhibition studies of heterocyclic imines derived from pyridine carbaldehyde and section II describes detailed investigations on anticorrosive properties of imines which are 3-formyl indole carbaldehyde derivatives in 1.0M HCl.

SECTION I

CORROSION INHIBITION STUDIES OF HETEROCYCLIC IMINES DERIVED FROM PYRIDINE CARBALDEHYDE ON CARBON STEEL IN 1.0M HCl

The corrosion inhibition properties of seven heterocyclic imines derived from pyridine carbaldehyde such as 2PCOX, 3PCOX, 2PC4ABA, 2PC3ABA, 2PC2ABA, 3PC3ABA, and 2PC2AP on carbon steel in 1.0M HCl at various concentrations, (0.2mM to 1.0mM) were discussed in this section.

Weight loss studies

Weight loss studies of CS in the presence and absence of imines were done by dipping CS metal specimens in 1.0M HCl solution for 24h at different concentrations of the inhibitor ranging from 0.2mM to 1.0mM. The variation of corrosion rate of CS in mmy^{-1} is given in the Table 2.1 and Figure 2.9.

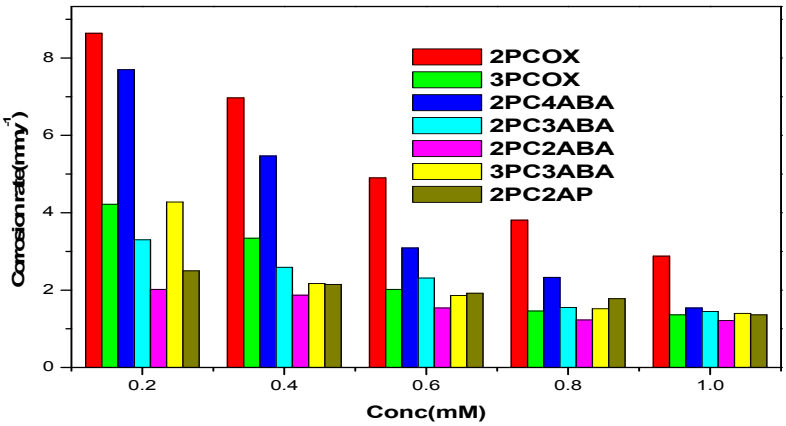

Figure 2.9 Variation of corrosion rate of heterocyclic imines of pyridine carbaldehyde on CS in 1.0M HCl

It was evident from the figure and table that the corrosion rate of CS in HCl was considerably decreased in the presence of imines. A corrosion rate of

9.19mmy^{-1} was showed by blank specimen that is carbon steel specimen immersed in 1.0M HCl solution without any inhibitor. On comparing the corrosion rates of different imines it is understandable that the carbon steel specimen in HCl solution in the presence of imines except 2PCOX exhibited appreciably low values of corrosion rate. The decrease in the corrosion rate with the increase in concentration of imines suggests that the metal dissolution process is considerably prevented by the heterocyclic imine molecules. Figure 2.9 compares the corrosion rates of carbon steel specimens in the presence of varying concentrations of imines. Relatively very low corrosion rate was exhibited by the presence of 2PC2ABA. 3PCOX, 3PC3ABA and 2PC2AP also lowered the metal dissolution of CS considerably in 1.0M HCl. This behaviour of the molecules can be attributed to the strong adsorptive capacity on metal surface.

Table 2.1 Corrosion rate of CS in the presence and absence of heterocyclic imines of pyridine carbaldehyde in 1.0M HCl

Conc	Corrosion rate (mmy^{-1})						
(mM)	**2PCOX**	**3PCOX**	**2PC4ABA**	**2PC3ABA**	**2PC2ABA**	**3PC3ABA**	**2PC2AP**
0	9.19	9.19	9.19	9.19	9.19	9.19	9.19
0.2	8.64	4.22	7.70	3.30	2.02	4.28	2.50
0.4	6.97	3.34	5.47	2.59	1.87	2.17	2.15
0.6	4.90	2.02	3.09	2.31	1.54	1.86	1.92
0.8	3.81	1.46	2.33	1.55	1.23	1.52	1.78
1.0	2.88	1.36	1.54	1.45	1.21	1.40	1.36

Table 2.2 displayed the corrosion inhibition efficiencies of imines on carbon steel in 1.0M HCl medium. Figure 2.10 compares the inhibition efficiencies of imines at various concentrations on CS. It is clear from the data that all imines exhibited marked corrosion inhibition efficiencies against the

metallic corrosion in 1.0M HCl. The inhibition efficiencies were increased with the imine concentrations. At 1.0mM concentration, the heterocyclic imines showed the inhibition efficiencies, as 2PC2ABA - 86.83%, 2PC2AP - 85.16%, 3PCOX - 85.17%, 3PC3ABA - 84.77% 2PC3ABA - 84.22%, 2PC4ABA - 83.20% and 2PCOX - 68.64%. From the data it is evident that all imines showed comparable inhibition efficiency at higher concentration, while at lower concentration it was quite different. Among the oximes 2PCOX and 3PCOX, former one exhibited lesser inhibition efficiency than latter on CS surface in acidic medium at all concentrations.

Table 2.2 Corrosion inhibition efficiencies of heterocyclic imines of pyridine carbaldehyde on CS in 1.0M HCl

Conc (mM)	Inhibition efficiency (%)						
	2PCOX	**3PCOX**	**2PC4ABA**	**2PC3ABA**	**2PC2ABA**	**3PC3ABA**	**2PC2AP**
0.2	5.96	54.03	16.27	63.99	77.95	53.39	72.78
0.4	24.11	63.61	40.52	71.99	79.65	76.34	76.61
0.6	46.67	77.94	66.40	74.87	83.24	79.72	79.12
0.8	58.53	84.06	74.69	83.04	86.52	83.45	80.61
1.0	68.64	85.17	83.20	84.22	86.83	84.77	85.16

All imines other than 2PCOX showed inhibition efficiency of about 85% on CS at 1.0mM concentration. The compounds 2PC2ABA and 2PC2AP showed 77.95% and 72.78% of inhibition efficiency at minimum concentration 0.2mM respectively. The enhanced efficiency of these molecules can be correlated with its molecular structure. Even though the molecule lost its planarity as per the optimized geometry, the imines showed appreciable efficiency. The presence of two aromatic ring systems; one from the aldehyde part and other from amino part

together with azomethine linkage and the nitrogen atom of the pyridine moiety make the molecule so electron rich which assist the molecule to adhere on the surface of metal atoms of carbon steel. This is very useful for the strong binding of the inhibitor on the metal surface and thereby reducing the metal dissolution. In the case of oximes 2PCOX and 3PCOX, hydrogen bond plays an important role in determining the inhibition efficiency and it is well explained in the mechanism of inhibition given below.

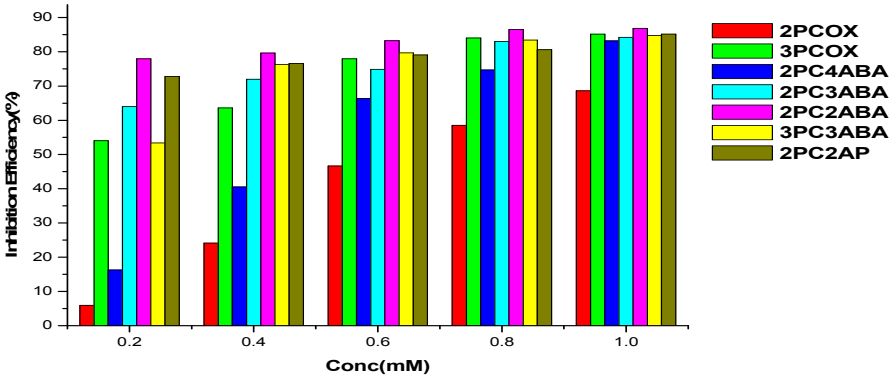

Figure 2.10 Variation of inhibition efficiencies (η_W%) of heterocyclic imines of pyridine carbaldehyde on CS in 1.0M HCl

The lower corrosion inhibition efficiency of 2PCOX compared to that of 3PCOX can be explained as follows. On close examination of the structures of the molecules, one can predict the possibility of formation of hydrogen bonds. 2PCOX prefer to make intra molecular hydrogen bond while 3PCOX molecules largely aggregate by inter molecular hydrogen bonds. It is familiar that the surface interaction by the molecules on the metal is the main factor responsible for the mitigation of the rate of corrosion. If 2PCOX form intra molecular hydrogen bonds, it can be assumed that the molecules interact the metal surface independently i.e., there is no molecular interaction between the adsorbed

molecules. Protons have thus an ample opportunity to attack on the metal surface as depicted in the Figure 2.10a. If we consider the intermolecular hydrogen bond in 3PCOX molecules, we can assume that molecular layers adsorbed on the iron surface appreciably. The exposed area of the metal towards the corroding medium will be significantly reduced due to this phenomenon the Figure 2.10b. Thus the rate of corrosion is appreciably lowered due to the capacity of 3PCOX to make inter molecular hydrogen bonds.

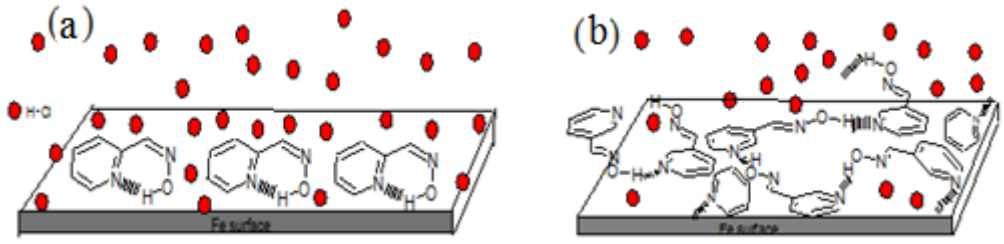

Figure 2.11 (a) Interaction of 2PCOX on carbon steel in 1.0M HCl,
(b) Interaction of 3PCOX on carbon steel in 1.0M HCl

In general, the surface of the metal is positively charged in acid media[84]. In the case of HCl, the Cl^- ions specially adsorbed on the surface of metal creates an excess of negative charge on the metal surface[85]. This will favour the adsorption of protonated imines on the surface of the metal and consequently decrease the dissolution of Fe to Fe^{2+}. On analyzing the structure of imines, several possibilities of inhibitor–metal interaction can be identified. The unshared pair of electrons present on two N atoms is of key importance in making the coordinate bond with the metal. The π-electron cloud of the aromatic rings and the azomethine linkage also take part in the inhibition mechanism[86,87]. Furthermore, the double bonds in the inhibitor molecule permit the back donation of metal d

electrons to the π* orbital and this type of interaction cannot occur with amines[88]. That is why the parent amine exhibits lower inhibition efficiency than that of the heterocyclic imines.

Comparison between the inhibition efficiency of imines and its parent amines

To compare the inhibition efficiencies of imines and their parent amines, weight loss studies of parent amines were performed at concentrations 0.2mM, 0.6mM, and 1.0mM. Table 2.3 and Figure 2.12 show and compare corrosion inhibition efficiencies of imines and their parent amines on CS in 1.0M HCl. The parent amines such as 2-aminobenzoic acid (2ABA), 3-aminobenzoic acid (3ABA), 4-aminobenzoic acid (4ABA), and 2-aminophenol (2AP) showed low corrosion inhibition efficiency on CS in 1.0M HCl compared to its corresponding imine derivatives.

It is evident from the table that all the imines exhibited very high inhibition efficiencies than their respective parent amines. This studies confirmed that the azomethine linkage (C=N) present in the imines, play an important role in the corrosion inhibition mechanism.

2ABA and 4ABA showed negative values of corrosion inhibition efficiency on CS. Negative values of corrosion inhibition efficiency indicate that these parent amines increase the rate of corrosion of carbon steel than the uninhibited solution (blank) in hydrochloric acid medium, i.e., they were behaving as corrosion accelerators for carbon steel in acidic media. This may be due to the strong tendency of 2ABA and 4ABA molecules to combine with the Fe^{2+} ions produced as a result of metal dissolution in acidic media. This

coordinating tendency of these amino compounds with the Fe^{2+} ions is higher than the tendency to adsorb on the metal surface, and hence these amines exhibited the corrosion accelerating behaviour.

Table 2.3 Corrosion inhibition efficiencies of heterocyclic imines of pyridine carbaldehyde and their parent amines on CS in 1.0M HCl.

	Inhibition efficiency (%)								
Conc (mM)	2ABA	2PC2ABA	3ABA	2PC3ABA	3PC3ABA	4ABA	2PC4ABA	2AP	2PC2AP
0.2	-46.8	77.9	6.8	63.9	53.4	-19.6	16.3	12.8	72.8
0.6	-40.5	83.2	18.5	74.8	79.7	-11.4	66.4	20.9	79.1
1.0	-38.9	86.8	28.4	84.2	84.8	-8.4	83.2	31.5	85.2

3ABA and 2AP exhibited low positive values of η_w%. This may be due to the interaction of aromatic rings with the surface metal atom. From the above studies it is established that the C=N linkage in the synthesized molecules is the principal factor in decreasing the corrosion rate of metal in acidic medium, thereby exhibiting higher degree of corrosion inhibition property.

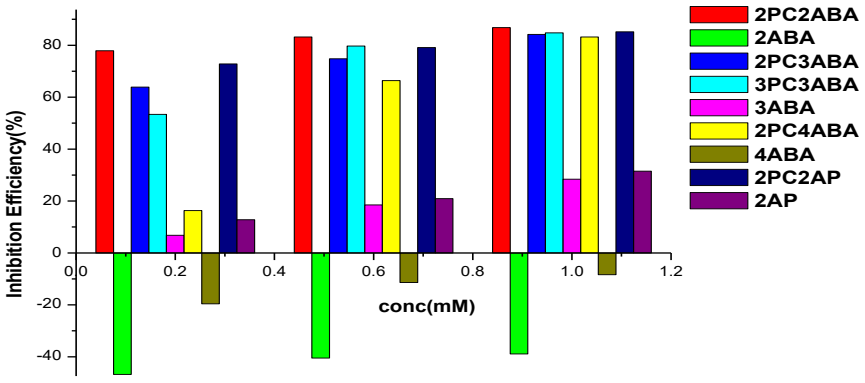

Figure 2.12 Comparison of corrosion inhibition efficiencies of heterocyclic imines of pyridine carbaldehyde and their parent amines on CS in 1.0M HCl.

Adsorption studies

The corrosion inhibition activity of compounds on the surface of metal specimens is due to the adsorption of the compounds. Using the adsorption isotherms, the mechanism of adsorption and the surface behaviour of organic molecules can be found out. Different adsorption isotherms considered are Langmuir, Temkin, Frumkin, El-Awady, Flory-Huggin and Freundlich isotherms. For the evaluation of thermodynamic parameters, with the help of the correlation coefficient (R^2) the best-fit isotherm is selected. Using this adsorption isotherm, adsorption equilibrium constant K_{ads} and standard free energy of adsorption ΔG^0_{ads} can be calculated.

Table 2.4 Adsorption isotherms and regression coefficients of heterocyclic imines of pyridine carbaldehyde on CS in 1.0M HCl

Isotherm	Regression coefficient (R^2)						
	2PCOX	3PCOX	2PC4ABA	2PC3ABA	2PC2ABA	3PC3ABA	2PC2AP
Langmiur	0.555	0.999	0.001	0.954	0.999	0.996	0.997
Freundlich	0.975	0.922	0.936	0.954	0.962	0.730	0.975
Temkin	0.980	0.965	0.987	0.961	0.899	0.898	0.933
Frumkin	0.973	0.990	0.992	0.543	0.013	0.016	0.760
El-Awady	0.996	0.956	0.994	0.934	0.857	0.938	0.891
Flory-Huggin	0.547	0.913	0.000004	0.902	0.898	0.883	0.858

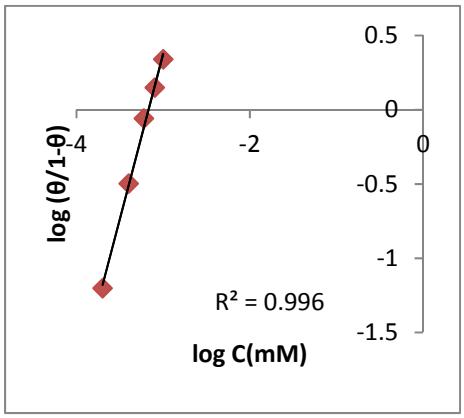

Figure 2.13 El-Awady isotherm for 2PCOX on CS in 1.0M HCl.

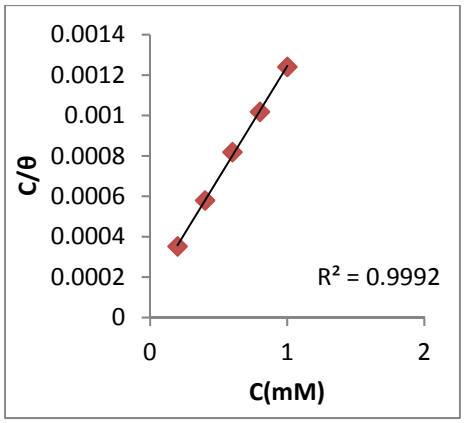

Figure 2.14 Langmuir isotherm for 3PCOX on CS in 1.0M HCl

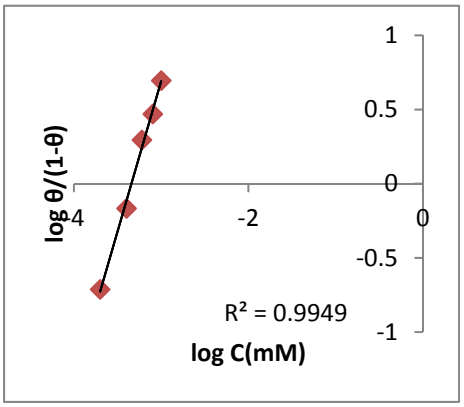

Figure 2.15 El-Awady isotherm for 2PC4ABA on CS in 1.0M HCl.

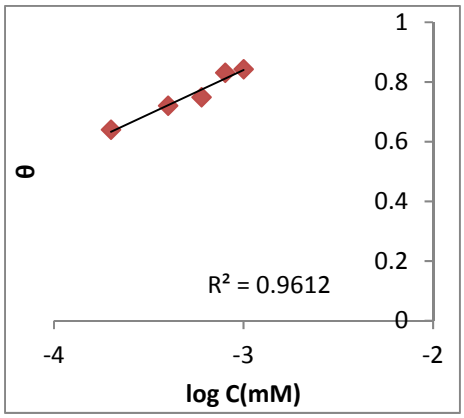

Figure 2.16 Temkin isotherm for 2PC3ABA on CS in 1.0M HCl.

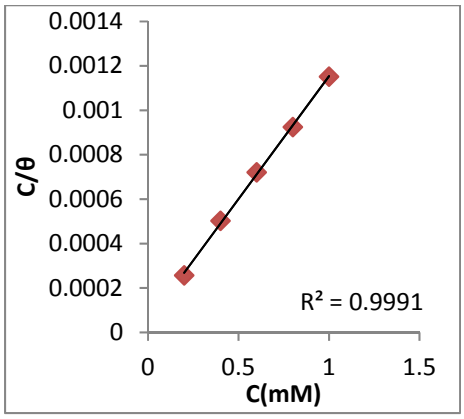

Figure 2.17 Langmuir isotherm for 2PC2ABA on CS in 1.0M HCl

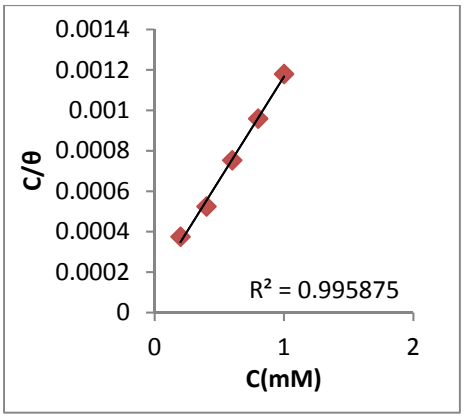

Figure 2.18 Langmuir isotherm for 3PC3ABA on CS in 1.0M HCl.

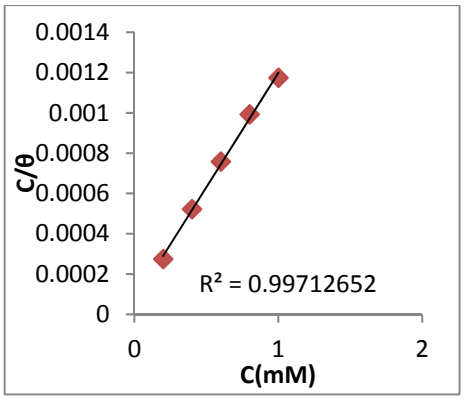

Figure 2.19 Langmuir isotherm for 2PC2AP on CS in 1.0M HCl.

Table 2.4 contains the adsorption isotherm for heterocyclic imines on carbon steel in 1.0M HCl. Among the isotherms discussed above, the best account of the adsorption behaviour of imines 3PCOX, 2PC2ABA, 3PC3ABA and 2PC2AP on carbon steel specimens in 1.0M HCl was Langmuir adsorption isotherm. 2PCOX and 2PC4ABA obeyed El-Awady, while 2PC3ABA satisfied Temkin adsorption isotherm. Figure 2.13 to 2.19 represents the adsorption isotherm plots of the different inhibitor molecules.

Table 2.5 explores adsorption parameters obtained from weight loss measurements of CS specimens in 1.0M HCl. The ΔG^0_{ads} values for all heterocyclic imines on CS showed negative values indicating the spontaneity of the process. The value of ΔG^0_{ads} up to -20kJmol^{-1} is an indication of the electrostatic interaction between the charged molecule and the charged surface of the metal (physisorption), while ΔG^0_{ads} value more negative than -40kJmol^{-1} implies that inhibitor molecules are adsorbed strongly on the metal surface through co-ordinate type bond (chemisorption)[89,90]. In the present investigation, 2PCOX and 2PC4ABA showed ΔG^0_{ads} -28.32 kJ/mol and -29.30 kJ/mol

respectively, and the other compounds have values in between -30.29 kJ/mol and -34.99 kJ/mol for CS specimens, suggesting that the adsorption of molecules involve both electrostatic adsorption and chemisorption. The free energy of adsorptions for the imines 2PC2ABA and 2PC2AP were relatively higher than that of other imines proposing that these imines strongly adsorbed on the surface of CS by forming a monolayer on the metal surface through chemical interaction.

Table 2.5 Adsorption parameters of heterocyclic imines of pyridine carbaldehyde on CS in 1.0M HCl

Adsorption Parameter	2PCOX	3PCOX	2PC4ABA	2PC3ABA	2PC2ABA	3PC3ABA	2PC2AP
K_{ads}	1477	5000	2193	7142	21276	7092	15720
ΔG^0_{ads} (kJ/mol)	-28.32	-31.40	-29.30	-32.26	-34.99	-32.24	-34.23

Temperature studies

The effect of temperature on the inhibition efficiency of the heterocyclic imines was analyzed by weight loss method in the range of 30-60°C. The energy of activation for corrosion in the presence and absence of inhibitor was evaluated by the following Arrhenius equation.

$$K = A \exp\left(\frac{-Ea}{RT}\right)$$

where K is the corrosion rate, E_a is the activation energy, A is the frequency factor, T is the temperature and R is the gas constant. Arrhenius plots were acquired by plotting log K versus 1000/T for the imines and are given in the Figures 2.20 to 2.26. The value of regression coefficients obtained for straight

lines are very near to unity reveals that the corrosion process on CS in HCl medium can be attributed by simple kinetic model.

Enthalpy and entropy of activation (ΔH*, ΔS*) were evaluated by the transition state theory, which is represented by the equation [91],

$$K = \left(\frac{RT}{Nh}\right) \exp\left(\frac{\Delta S^*}{R}\right) \exp\left(\frac{-\Delta H^*}{RT}\right)$$

where N is the Avogadro number and h is the Planck's constant. While in the plot of log(K/T) Vs 1000/T, straight lines are obtained for the corrosion of CS in 1.0M HCl with and without heterocyclic imines (Figures 2.20 to 2.26)

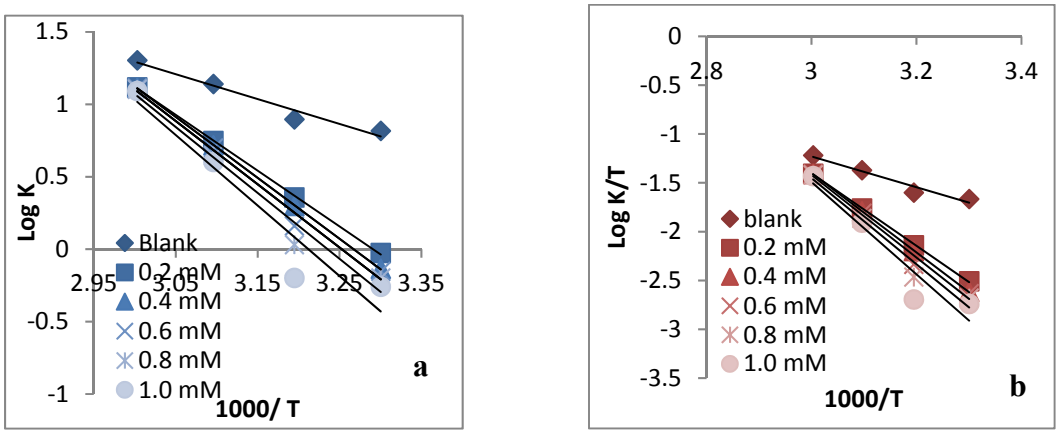

Figure 2.20 a) Arrhenius plots and **b)** log (K/T) Vs 1000/T plots for the corrosion of CS in the presence and absence of 2PCOX in 1.0M HCl.

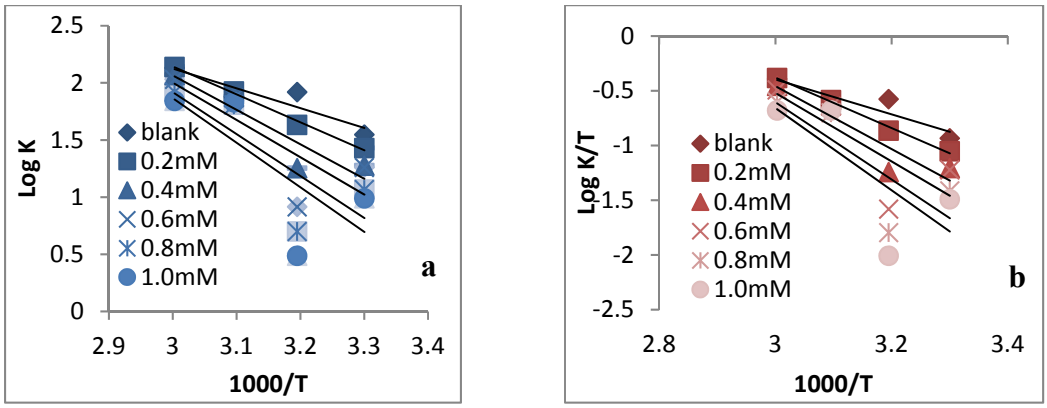

Figure 2.21 a) Arrhenius plots and **b)** log (K/T) Vs 1000/T plots for the corrosion of CS in the presence and absence of 3PCOX in 1.0M HCl

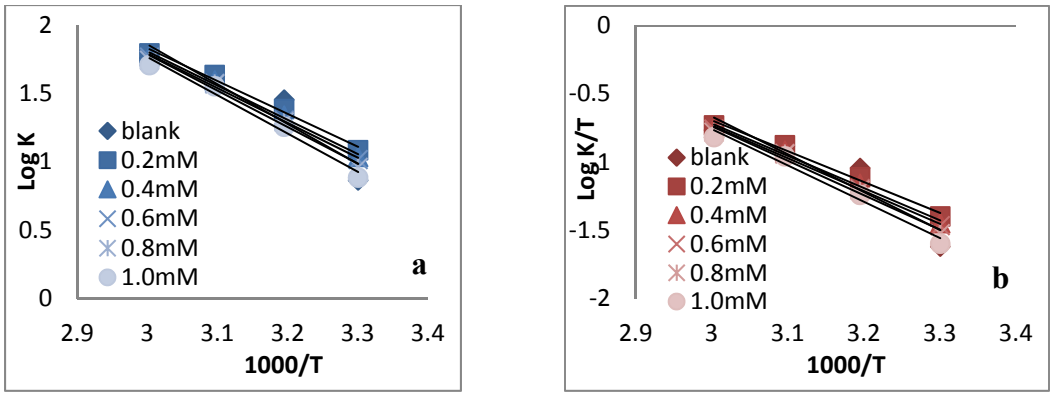

Figure 2.22 a) Arrhenius plots and **b)** log (K/T) Vs 1000/T plots for the corrosion of CS in the presence and absence of 2PC4ABA in 1.0M HCl

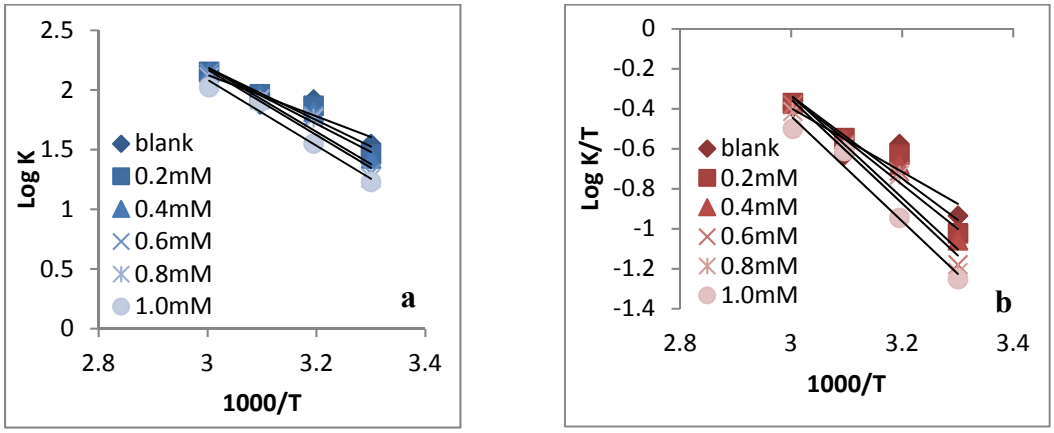

Figure 2.23 a) Arrhenius plots and **b)** log (K/T) Vs 1000/T plots for the corrosion of CS in the presence and absence of 2PC3ABA in 1.0M HCl.

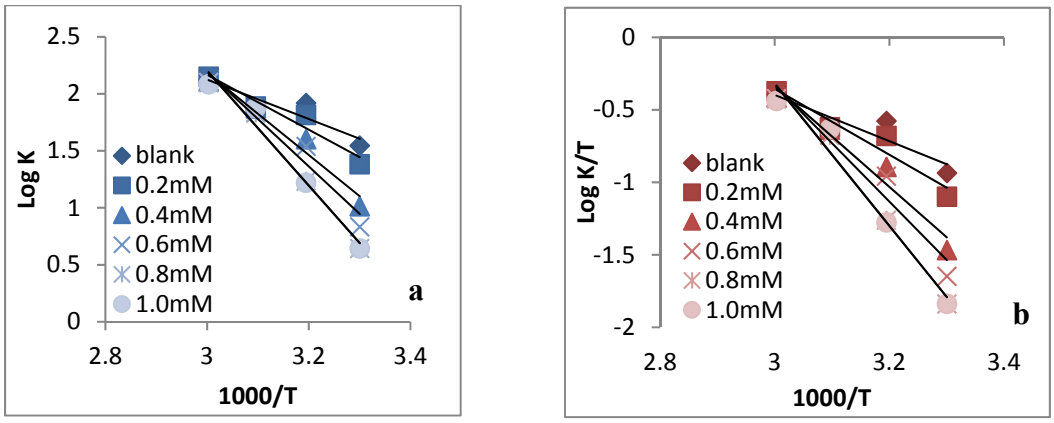

Figure 2.24 a) Arrhenius plots and **b)** log (K/T) Vs 1000/T plots for the corrosion of CS in the presence and absence of 2PC2ABAin 1.0M HCl.

Table 2.6 Thermodynamic parameters of corrosion of CS in the presence and absence of heterocyclic imines of pyridine carbaldehyde in 1.0M HCl.

Imines	Conc (mM)	Ea (kJ/mol^{-1})	A	ΔH* (kJ/mol^{-1})	ΔS* ($Jmol^{-1}K^{-1)}$)
	Blank	32.86	$2.76x10^{6}$	30.21	-100.88
2PCOX	0.2	50.04	$1.34x10^{9}$	50.03	-22.80
	0.4	50.91	$1.61x10^{9}$	50.89	-21.27
	0.6	57.49	$1.66x10^{10}$	57.47	-18.9
	0.8	58.45	$2.15x10^{10}$	58.48	-4.96
	1.0	58.84	$2.48x10^{10}$	58.89	-3.23
3PCOX	0.2	58.59	$3.09x10^{10}$	54.19	-20.26
	0.4	59.62	$3.89x10^{10}$	56.98	-12.62
	0.6	77.12	$2.69x10^{13}$	74.48	-41.76
	0.8	79.96	$7.08x10^{13}$	77.32	-49.61
	1.0	82.87	$2.13x10^{14}$	78.68	-54.02
2PC4ABA	0.2	40.1	$3.36x10^{7}$	40.09	-53.46
	0.4	53.41	$3.93x10^{9}$	53.4	-13.88
	0.6	60.75	$5.25x10^{10}$	60.75	7.68
	0.8	65.65	$2.63x10^{11}$	65.64	21.08
	1.0	79.07	$3.31x10^{13}$	79.06	61.29
2PC3ABA	0.2	46.07	$3.23x10^{8}$	47.1	-34.65
	0.4	47.11	$3.98x10^{8}$	52.86	-32.91
	0.6	52.87	$2.81x10^{9}$	54.76	-16.67
	0.8	54.76	$4.92x10^{9}$	65.57	-12.00
	1	65.59	$2.40x10^{11}$	68.54	20.32
2PC2ABA	0.2	73.73	$4.68x10^{12}$	71.10	-11.14
	0.4	80.50	$5.37x10^{13}$	77.90	8.99
	0.6	83.61	$1.58x10^{14}$	81.01	17.99
	0.8	87.02	$5.01x10^{14}$	84.41	27.57
	1.0	93.17	$4.27x10^{15}$	90.50	45.38
3PC3ABA	0.2	39.83	$3.10x10^{7}$	39.82	-53.92
	0.4	38.96	$1.8x10^{7}$	38.96	-58.51
	0.6	50.47	$1.13x10^{9}$	50.5	-24.24
	0.8	55.13	$5.68x10^{9}$	55.12	-10.82
	1.0	66.37	$2.88x10^{11}$	66.36	21.85
2PC2AP	0.2	69.48	$1.82x10^{12}$	65.31	-23.87
	0.4	69.59	$1.70x10^{12}$	66.96	-19.53
	0.6	88.08	$1.44x10^{15}$	85.45	36.38
	0.8	89.99	$1.55x10^{15}$	85.74	36.95
	1.0	88.38	$3.98x10^{15}$	88.70	44.99

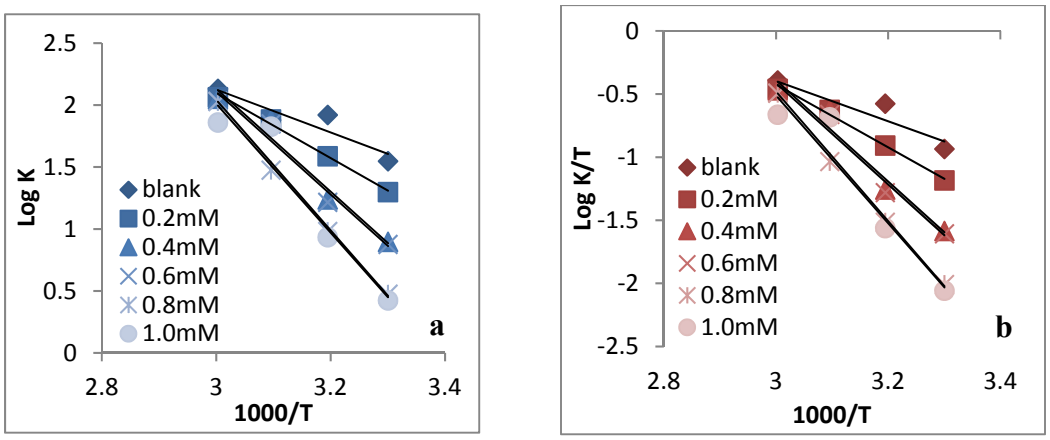

Figure 2.25 a) Arrhenius plots and **b)** log (K/T) Vs 1000/T plots for the corrosion of CS in the presence and absence of 3PC3ABA in 1.0M HCl.

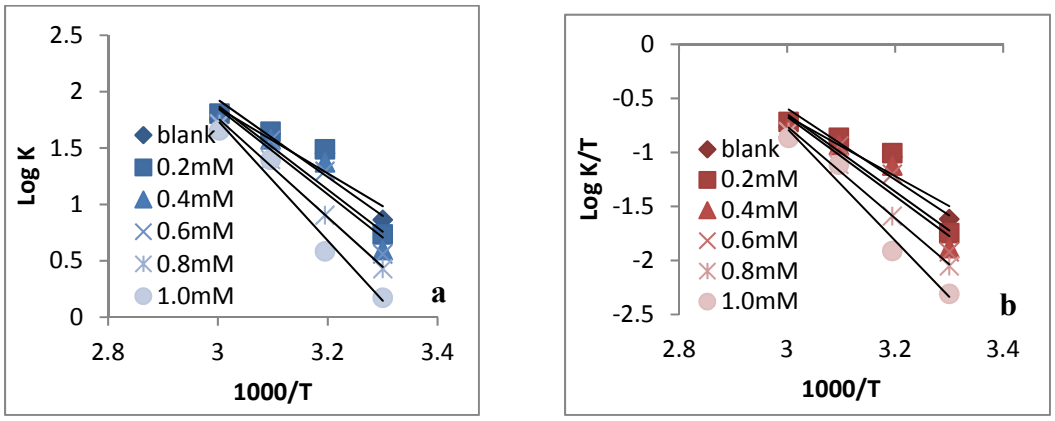

Figure 2.26 a) Arrhenius plots and **b)** log (K/T) Vs 1000/T plots for the corrosion of CS in the presence and absence of 2PC2AP in 1.0M HCl.

The values of activation energy and thermodynamic parameters in the absence and presence of imines are given in the Table 2.6. On analyzing the results, it was clear that the activation energy of metal dissolution increased with the concentration of heterocyclic imines. This indicated that resistance of metal disintegration was increased with the inhibitor concentration. The resultant positive enthalpy values point towards the fact that the corrosion process is endothermic and increasing the reluctance for the dissolution of metal with an

increase in concentration. Both the activation energy and enthalpy of corrosion increased continuously with inhibitor concentration for all imines.

On comparing the values of E_a and ΔH^* it is evident that these values are high in the presence of imines especially at higher concentration of 1.0mM. The increase in the E_a values and the endothermicity of corrosion with the concentration of imines definitely supports the argument that the imines strongly adsorbed on the surface of the metal specimen.

From the Table 2.6, the values of ΔS^* also increased with inhibitor concentration whereas in the case of blank and low imine concentrations entropy of activation was comparatively small, which suggests that there is a decrease in disorder for activated complex in the rate determining step.

Electrochemical studies

Electrochemical investigations employed during the study are EIS measurements and potentiodynamic polarization analysis. Electrochemical studies were conducted using Ivium compactstat-e electrochemical system, with three electrode cell assembly, in which saturated calomel electrode (SCE) was the reference electrode, platinum electrode as counter electrode and carbon steel specimen having $1cm^2$ exposed area was the working electrode. From EIS and potentiodynamic polarization studies, charge transfer resistance (R_{ct}) and corrosion current density (I_{corr}) were measured respectively and these parameters were related to corrosion inhibition efficiency of the compounds. Along with percentage of inhibition efficiency, the type of inhibition, whether anodic, cathodic or both are also derived.

Electrochemical impedance spectroscopy (EIS) studies

The corrosion behaviour of carbon steel in 1.0M HCl in the presence and absence of heterocyclic imines has been studied using EIS measurements. Nyquist plots and corresponding Bode plots of carbon steel in varying concentrations of seven pyridine based imine compounds in 1.0M HCl are depicted in the Figures from 2.27 to 2.33. From the plots, a marked difference in the impedance response of metal specimens was observed in the presence and absence of imines. Due to roughness or non homogeneous nature of the metal surface the semicircles exhibited slight irregularities[92-95]. Randles equivalent circuit was used to found the impedance parameters such as double layer capacitance C_{dl}, solution resistance R_S and charge transfer resistance R_{ct}[96,97]. The charge transfer resistance R_{ct} is a measure of electron transfer across the exposed area of the metal surface, which is inversely proportional to the rate of corrosion[98]. Impedance parameters of CS in the absence and presence of imine compounds were given in the Table 2.7. The corrosion inhibition efficiency of the imines mainly depends on the value of charge transfer resistance R_{ct}, which can be calculated using the equation

$$\eta_{EIS}\% = \frac{R_{ct} - R'_{ct}}{R_{ct}} \times 100$$

where R_{ct} and R'_{ct} are the charge transfer resistances of working electrode with and without inhibitor respectively.

On verifying the data in Table 2.7, it was clear that the charge transfer values (R_{ct}) were increased with increasing concentration of imine which may be due to the increased adsorption of imine inhibitor on the surface of metal.

Table 2.7 Electrochemical impedance parameters of CS in the presence and absence of heterocyclic imines of pyridine carbaldehyde in 1.0M HCl

Imines	Conc (mM)	C_{dl} (μFcm^{-2})	R_{ct} (Ωcm^2)	η_{EIS} (%)
	0	90.5	22.7	-
	0.2	90.5	22.8	29.75
2PCOX	0.4	79.9	32.4	72.80
	0.6	67.9	83.7	76.27
	0.8	57.7	95.9	79.44
	1.0	56.4	110.7	79.84
	0.2	84.6	125.1	81.81
3PCOX	0.4	83.4	147.3	84.55
	0.6	66.2	153.4	85.16
	0.8	63.6	265.9	91.44
	1.0	62.1	381.7	94.04
	0.2	87.4	42.2	46.08
	0.4	80.6	77.2	70.50
2PC4ABA	0.6	69.3	82.6	72.44
	0.8	68.1	123.2	81.53
	1.0	64.5	209.0	89.11
	0.2	70.9	95.4	76.13
	0.4	60.7	95.9	76.27
2PC3ABA	0.6	61.7	125.0	81.80
	0.8	57.7	198.2	88.52
	1.0	57.7	237.0	90.39
	0.2	83.4	132.0	82.76
	0.4	67.8	150.6	84.89
2PC2ABA	0.6	62.8	204.9	87.14
	0.8	53.0	315.9	92.80
	1.0	45.0	390.5	94.17
	0.2	82.5	84.75	73.14
	0.4	56.2	115.8	80.35
3PC3ABA	0.6	59.5	118.2	80.74
	0.8	57.4	143.3	84.12
	1.0	55.6	265.0	91.41
	0.2	94.5	149.3	84.76
	0.4	80.5	163.4	86.07
2PC2AP	0.6	75.9	246.8	90.78
	0.8	68.3	314.7	92.77
	1.0	50.2	319.6	92.88

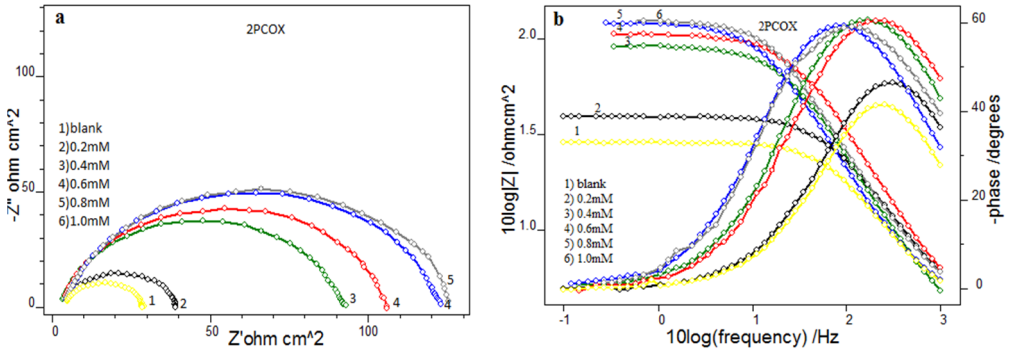

Figure 2.27 a) Nyquist plots and **b)** Bode plots of CS in the presence and absence of 2PCOX in 1.0M HCl

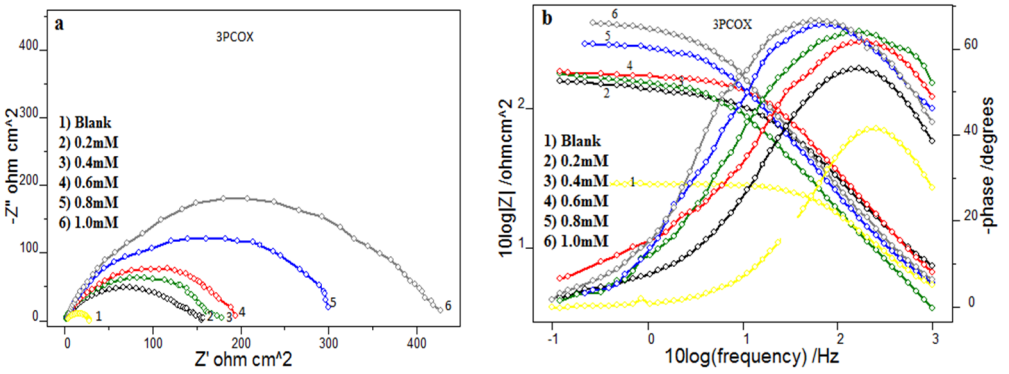

Figure 2.28 a) Nyquist plots and **b)** Bode plots of CS in the presence and absence of 3PCOX in 1.0M HCl

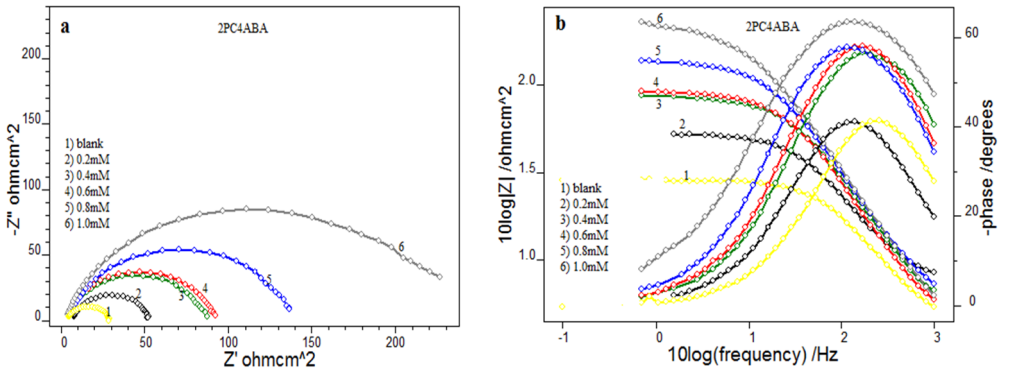

Figure 2.29 a) Nyquist plots and **b)** Bode plots of CS in the presence and absence of 2PC4ABA in 1.0 HCl

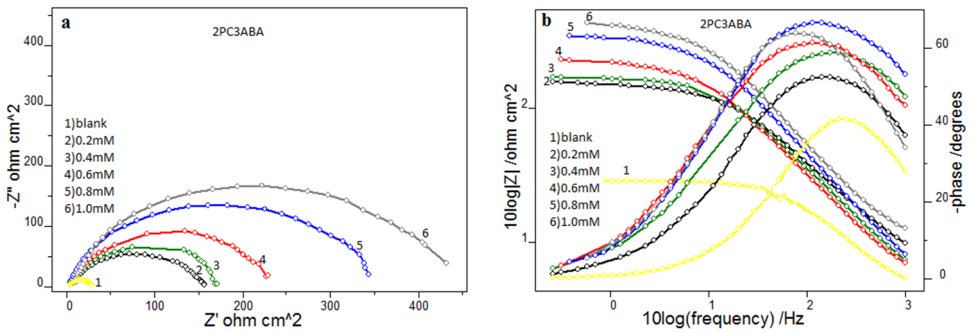

Figure 2.30 a) Nyquist plots and **b)** Bode plots of CS in the presence and absence of 2PC3ABA in 1.0M HCl

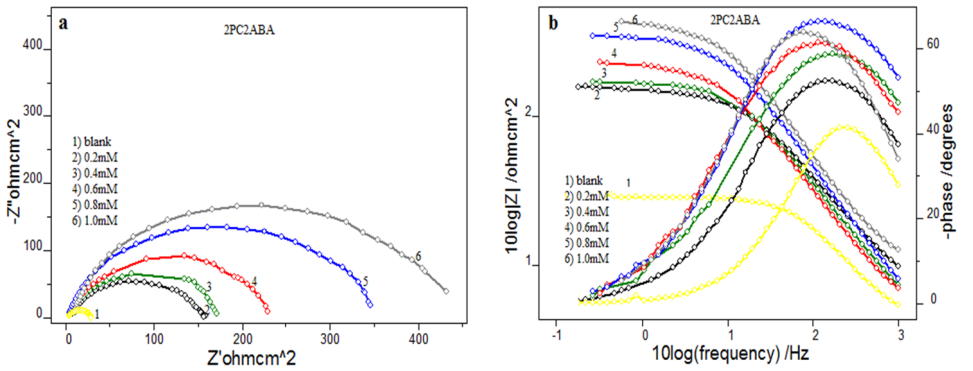

Figure 2.31 a) Nyquist plots and **b)** Bode plots of CS in the presence and absence of 2PC2ABA in 1.0M HCl

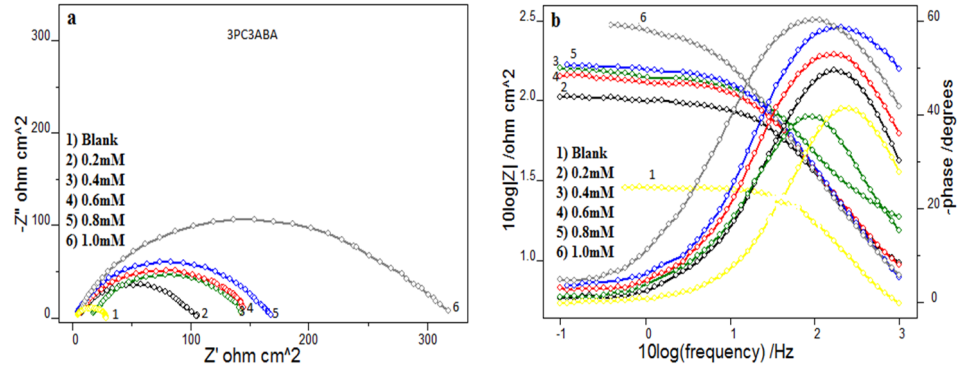

Figure 2.32 a) Nyquist plots and **b)** Bode plots of CS in the presence and absence of 3PC3ABA in 1.0M HCl

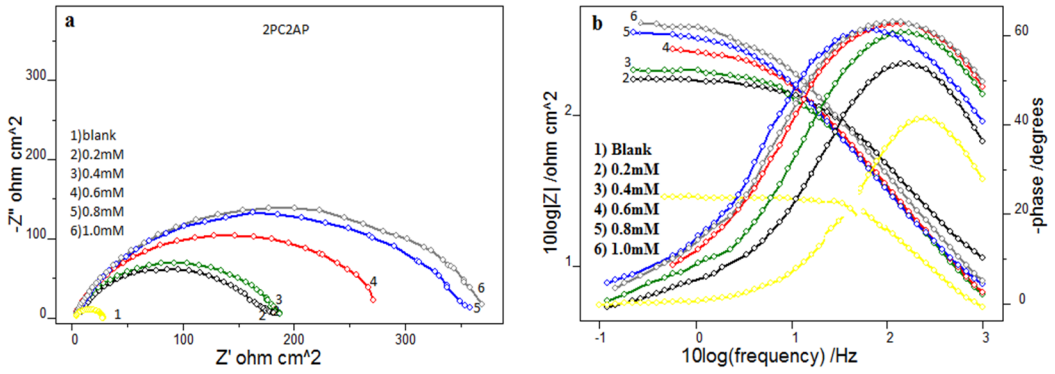

Figure 2.33 a) Nyquist plots and **b)** Bode plots of CS in the presence and absence of 2PC2AP in 1.0M HCl

The decrease in capacitance values C_{dl} with respect to inhibitor concentration can be attributed to the decrease in local dielectric constant and/or increase in the thickness of the electrical double layer. This emphasized the action of inhibitor molecules by adsorption at the metal–solution interface[99]. The percentage of inhibition (η_{EIS}%) for all imines showed a regular increase with increasing imine concentration.

From the analysis of impedance data, the majority of the compounds showed >90% of corrosion inhibition efficiency. All the imines acted as a good corrosion inhibitors in 1.0M HCl. The compounds 2PC2ABA and 3PCOX showed high corrosion inhibition efficiency i.e. 94% at 1.0mM concentration. The other compounds except 2PCOX exhibited comparable efficiency at higher concentration. This result was in good agreement with data observed in gravimetric analysis. The oxime 2PCOX showed low inhibition efficiency of 79% at maximum concentration 1.0mM. The low inhibition efficiency may be due to the presences of intramolecular H-bond, and hence weak adsorption of the oxime took place on the metal surface. The compounds 3PCOX, 2PC2ABA and

2PC2AP showed good inhibition efficiency (>80%) at minimum concentration 0.2mM. The 3-aminobenzoic acid derivatives of pyridine compounds showed low efficiency (76%) at lower concentration when compared to that of others. The compounds 2PC4ABA and 2PCOX displayed 46% and 29% of efficiency respectively at minimum concentration 0.2mM. The comparison of the inhibition efficiency of the imines is given in the Figure 2.35.

Impedance behaviour can be well explained by pure electric models that could verify and enable to calculate numerical values corresponding to the physical and chemical properties of electrochemical system under examination[100]. The simple equivalent circuit[101], that fit to many electrochemical system is composed of a double layer capacitance, R_s and R_{ct}. To reduce the effects due to surface irregularities of metal, constant phase element (CPE) is introduced into the circuit instead of a pure double layer capacitance which gives more accurate fit as shown in the Figure 2.34.

The impedance of CPE can be expressed as $Z_{CPE} = \frac{1}{Y_0 \ (j\omega)^n}$

where Y_0 is the magnitude of CPE, n is the exponent (phase shift), ω is the angular frequency and j is the imaginary unit. CPE may be resistance, capacitance and inductance depending upon the values of n[102]. In all experiments the observed value of n ranges between 0.8 and 1.0, suggesting the capacitive response of CPE.

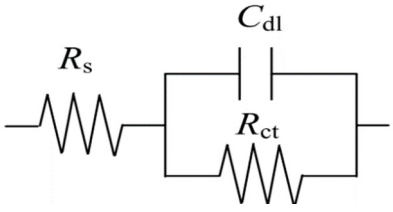

Figure 2.34 Equivalent circuit fitted for EIS

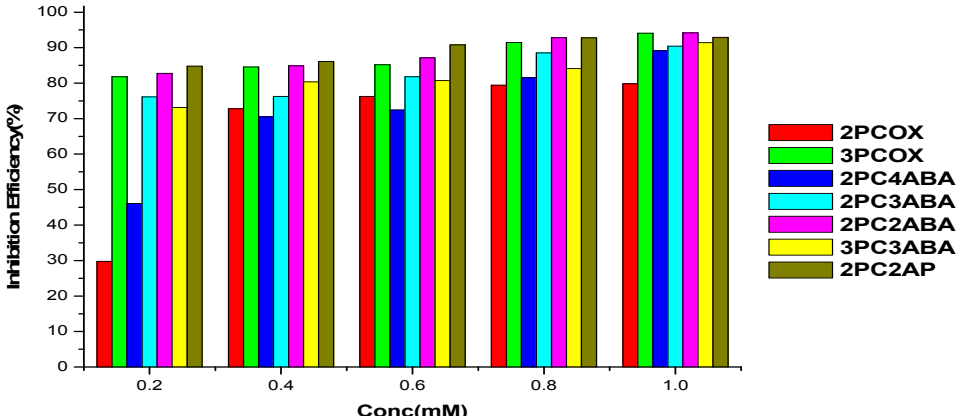

Figure 2.35 Variation of corrosion inhibition efficiencies (η_{EIS}%) of heterocyclic imines of pyridine carbaldehyde on CS in 1.0M HCl

Potentiodynamic polarization studies

Potentiodynamic polarization studies on CS specimens were conducted in HCl medium in the presence and absence of heterocyclic imines derived from pyridine carbaldehyde. The potentiodynamic polarization studies consist of Tafel polarization and linear polarization analysis. Potential scan range for the working electrode was selected between +250mV to -250mV and a sweep rate of 1.0mV/sec was maintained throughout the experiment with the help of Ivium compactsat-e electrochemical system. In the Figures 2.36 to 2.42, the linear polarization plots and Tafel plots for CS specimens in the presence and absence of imines in acidic medium are exhibited. Polarization parameters like corrosion current densities (I_{corr}), corrosion potential (E_{corr}), cathodic Tafel slope (b_c), anodic Tafel slope (b_a) and polarization resistance (R_p) of CS specimens in HCl medium containing various heterocyclic imines are provided in the Table 2.8.

From the Table 2.8, it is observed that there is prominent decrease in the corrosion current density (I_{corr}) of CS, in the presence of all heterocyclic imines

when compared to the I_{corr} of the CS specimen in the absence of imine (blank). The corrosion inhibition efficacy of the imines on CS gradually increased with the rise in concentration. On close examination of the Table 2.8 it is quite clear that the imines 2PC2ABA and 3PCOX displayed higher inhibitive action on CS surface when compared to the others according to Tafel polarization studies. Linear polarization analysis also supports this observation. The inhibition efficiency of the imines follows the order 2PCOX < 2PC4ABA < 2PC3ABA < 3PC3ABA < 2PC2AP < 3PCOX < 2PC2ABA. This trend is in good agreement with the observations found in gravimetric corrosion studies and EIS measurements. On analyzing the Tafel and linear polarization curves, it is quite evident that the slopes of the Tafel lines varied considerably in the presence and absence of imines. If both Tafel lines showed so much deviation from the blank more or less equally, then that type of imines can be considered as mixed type inhibitor. If cathodic or anodic slopes of Tafel lines varied considerably from the slope of Tafel line of uninhibited solution, the inhibitor could be regarded as an cathodic or anodic type inhibitor [103,104].

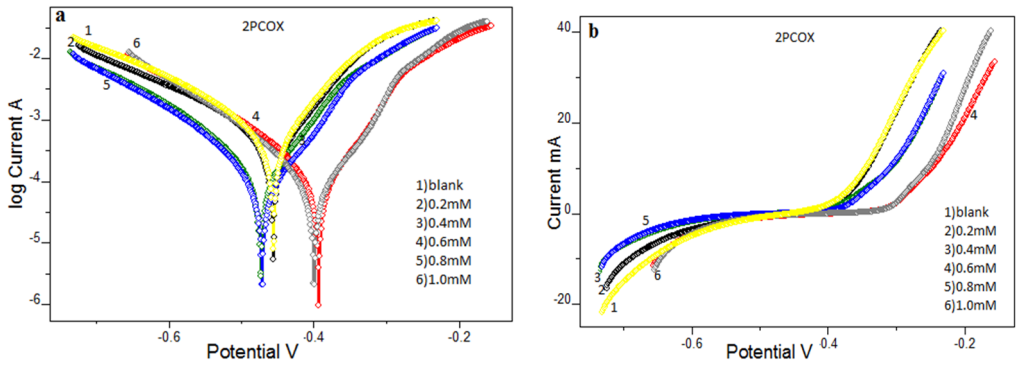

Figure 2.36 a) Tafel plots and **b)** Linear polarization plots of CS in the presence and absence of 2PCOX in 1.0M HCl.

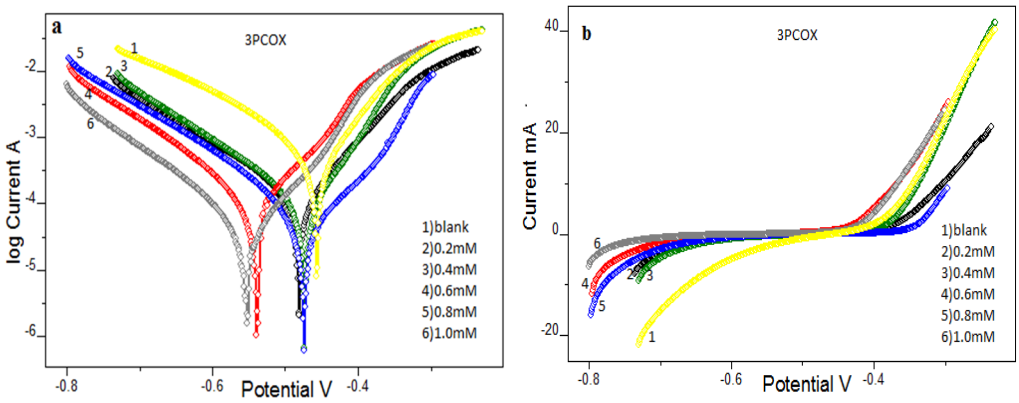

Figure 2.37 a) Tafel plots and **b)** Linear polarization plots of CS in the presence and absence of 3PCOX in 1.0M HCl.

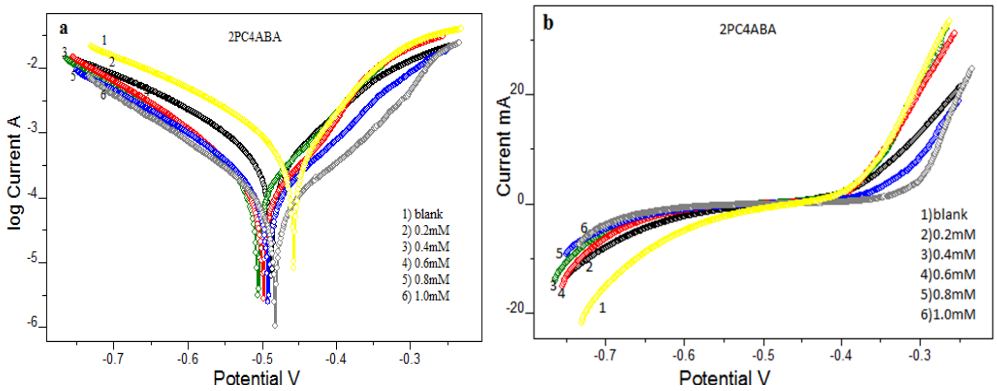

Figure 2.38 a) Tafel plots and **b)** Linear polarization plots of CS in the presence and absence of 2PC4ABAin 1.0M HCl

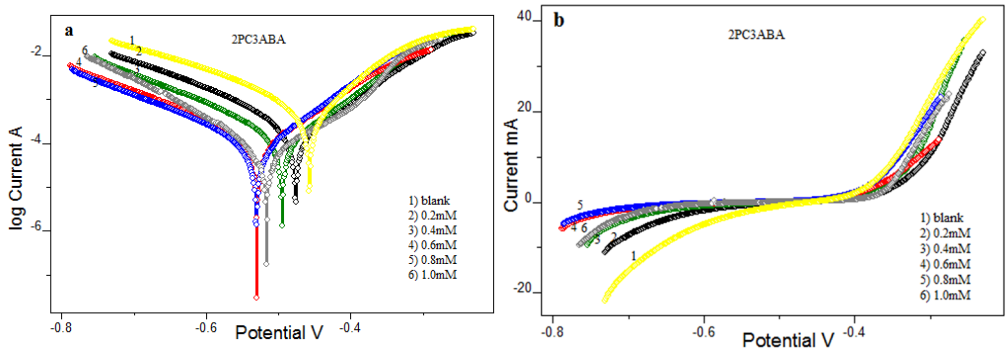

Figure 2.39 a) Tafel plots and **b)** Linear polarization plots of CS in the presence and absence of 2PC3ABA in 1.0M HCl.

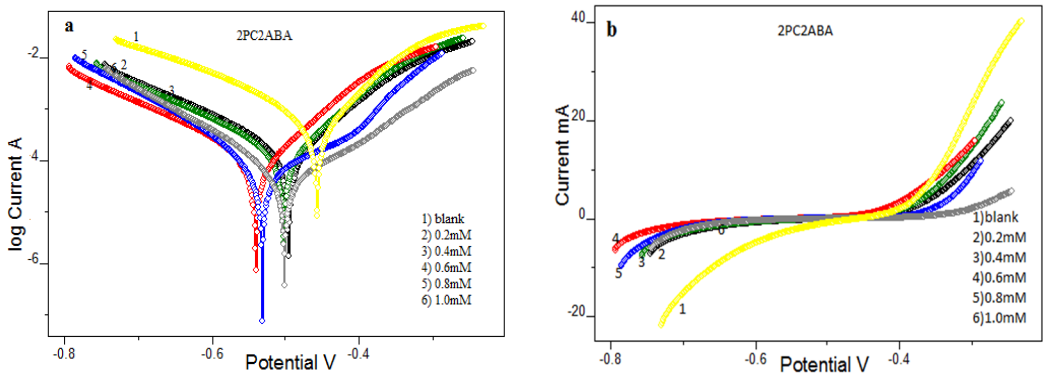

Figure 2.40 a) Tafel plots and **b)** Linear polarization plots of CS in the presence and absence of 2PC2ABA in 1.0M HCl.

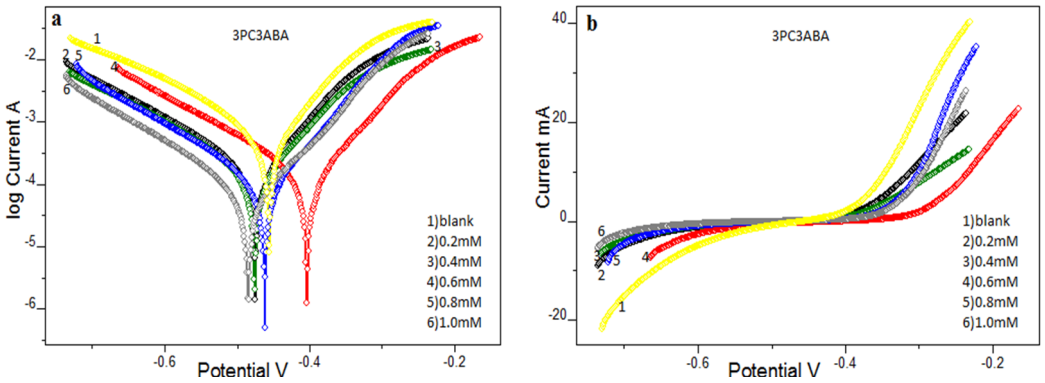

Figure 2.41 a) Tafel plots and **b)** Linear polarization plots of CS in the presence and absence of 3PC3ABA in 1.0M HCl.

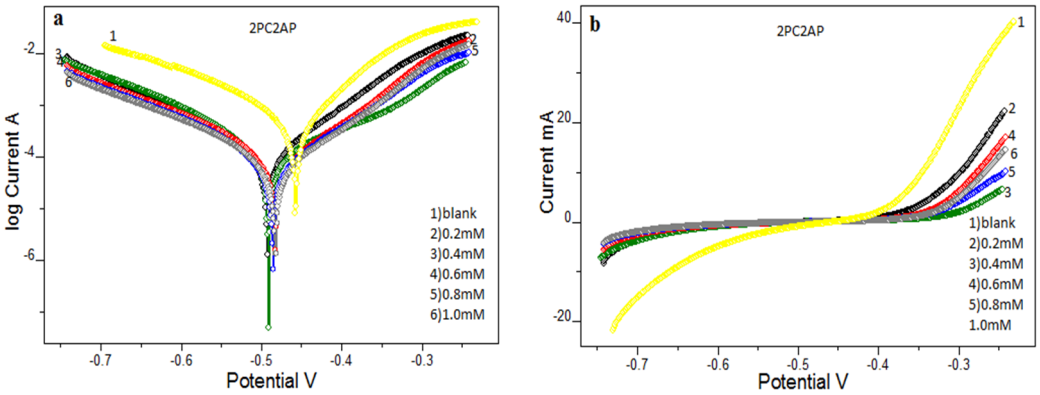

Figure 2.42 Tafel plots and **b)** Linear polarization plots of CS in the presence and absence of 2PC2AP in 1.0M HCl.

Table 2.8 Potentiodynamic polarization parameters of CS in the presence and absence of heterocyclic imines of pyridine carbaldehyde in 1.0M HCl

Imine	Tafel Data					Polarization Data		
	Conc (mM)	$-E_{corr}$ (mV/SCE)	I_{corr} ($\mu A/cm^2$)	b_a (mV/dec)	$-b_c$ (mV/dec)	η_{pol} (%)	R_p (ohm)	η_{Rp} (%)
	0	460	796	108	178	-	47.6	-
2PCOX	0.2	459	662	103	192	16.8	56.7	16.04
	0.4	478	248	103	145	68.8	165	71.15
	0.6	399	190	89	143	76.1	195	75.58
	0.8	461	152	82	140	80.9	224	78.75
	1.0	399	137	80	130	82.7	233	79.57
3PCOX	0.2	476	135	90	157	83.0	177.2	73.14
	0.4	479	127	78	140	84.0	213.0	77.65
	0.6	527	94	77	133	88.2	230.0	79.30
	0.8	442	56	73	148	92.9	417.0	88.28
	1.0	525	34	62	130	95.7	444.3	89.27
2PC4ABA	0.2	475	435	113	172	45.3	83.2	42.78
	0.4	485	171	81	144	78.5	166.4	71.39
	0.6	477	140	73	132	82.4	232.9	79.56
	0.8	470	128	90	146	83.9	254.0	81.25
	1.0	459	66	89	134	91.7	423.0	88.74
2PC3ABA	0.2	453	203	88	153	74.5	154.9	69.2
	0.4	474	127	81	153	84.0	245.9	80.64
	0.6	513	102	93	157	87.1	298.5	84.05
	0.8	515	84	83	156	89.4	345.2	86.21
	1.0	486	54	70	114	93.2	478.7	90.05
2PC2ABA	0.2	496	172	104	159	78.3	179.0	73.41
	0.4	500	152	95	158	80.9	194.0	75.46
	0.6	531	112	92	158	85.9	276.5	82.78
	0.8	487	43	84	126	94.6	406.6	88.29
	1.0	474	32	101	125	95.9	534.5	91.09
3PC3ABA	0.2	481	208	100	157	73.8	165.6	71.25
	0.4	482	177	108	156	77.7	175.0	72.80
	0.6	397	143	87	161	82.0	201	76.31
	0.8	449	91	73	149	88.5	278.9	82.93
	1.0	460	48	72	145	93.9	415	88.53
2PC2AP	0.2	477	123	91	149	84.5	200.5	76.26
	0.4	463	113	142	152	85.8	232.5	79.53
	0.6	454	87	84	167	89.0	287.6	83.45
	0.8	459	77	94	165	90.3	345.0	86.20
	1.0	453	47	84	167	94.0	467	89.80

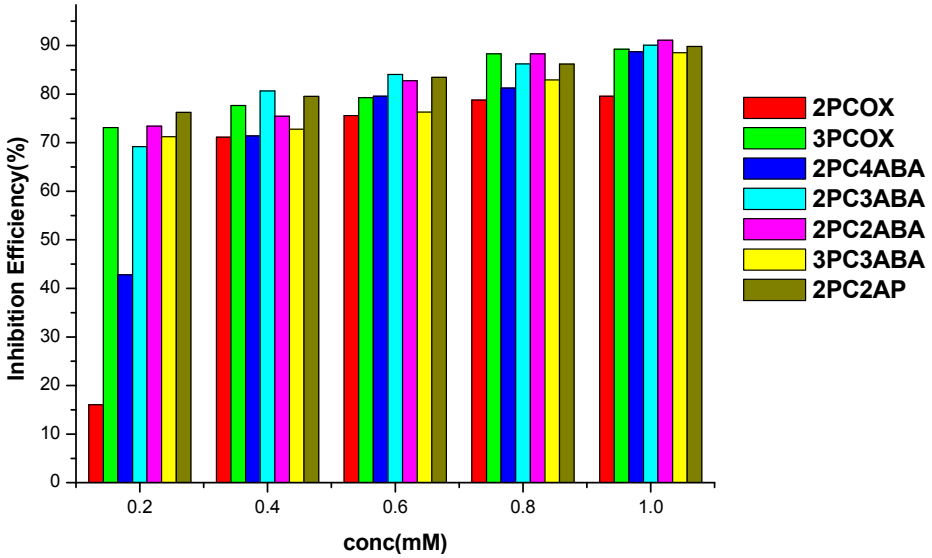

Figure 2.43 Variation of corrosion inhibition efficiencies (η_{Rp}%) of heterocyclic imines of pyridine carbaldehyde on CS in 1.0M HCl

In all cases, the cathodic slopes b_c and anodic slopes b_a of the Tafel curves were affected, and therefore it may be concluded that in general these heterocyclic imines acted as mixed type inhibitor in 1.0M HCl on CS surface. Furthermore, the E_{corr} values concerning the blank experiment did not alter considerably (>85) in all investigations. This behaviour also supplements the above argument. However, on close examination of Tafel slopes it can be understandable that 2PC4ABA and 2PC3ABA were behaving as more anodic type. Imines 2PCOX, 3PCOX, 2PC2ABA and 3PC3ABA are distinctly mixed type while the inhibitor 2PC2AP is prominently anodic in nature.

Electrochemical noise studies

Electrochemical noise (ECN) measurements were performed using a three-electrode cell system, which consists of two carbon steel electrodes of 1cm^2 area used as working electrode and counter electrode and SCE as reference

electrode. All ECN analyses were performed for a period of 1200 sec using Ivium compactstat-e-electrochemical system controlled by Iviumsoft software.

The noise current corresponding to the metal dipped in the HCl solution in the presence and absence of imines was represented in the Figure 2.44. From the Figure it was evident that the noise current of the metal have very low value in the presence imines, which implies that investigated imine compounds possess appreciable inhibition efficiency.

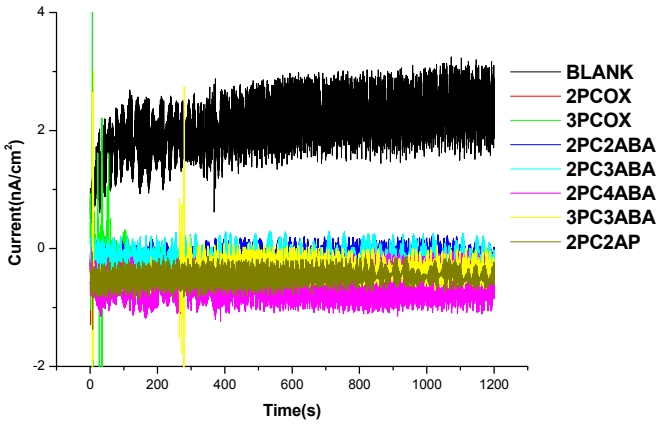

Figure 2.44 Noise current for CS in the presence and absence of heterocyclic imines of pyridine carbaldehyde (1.0mM) in 1.0M HCl

Pitting index value is the measurement of resisting capability of system against pitting corrosion. On analyzing the pitting index curves depicted in the Figure 2.46, it was understood that the amplitude of pitting index curves corresponding to the imine containing acid solution is higher than the metal specimen immersed in the acid solution in the absence of imines. For blank specimen the pitting index value was 0.05, while all the imines showed higher pitting index value. The higher pitting index value showed by 3PCOX that is 0.25.

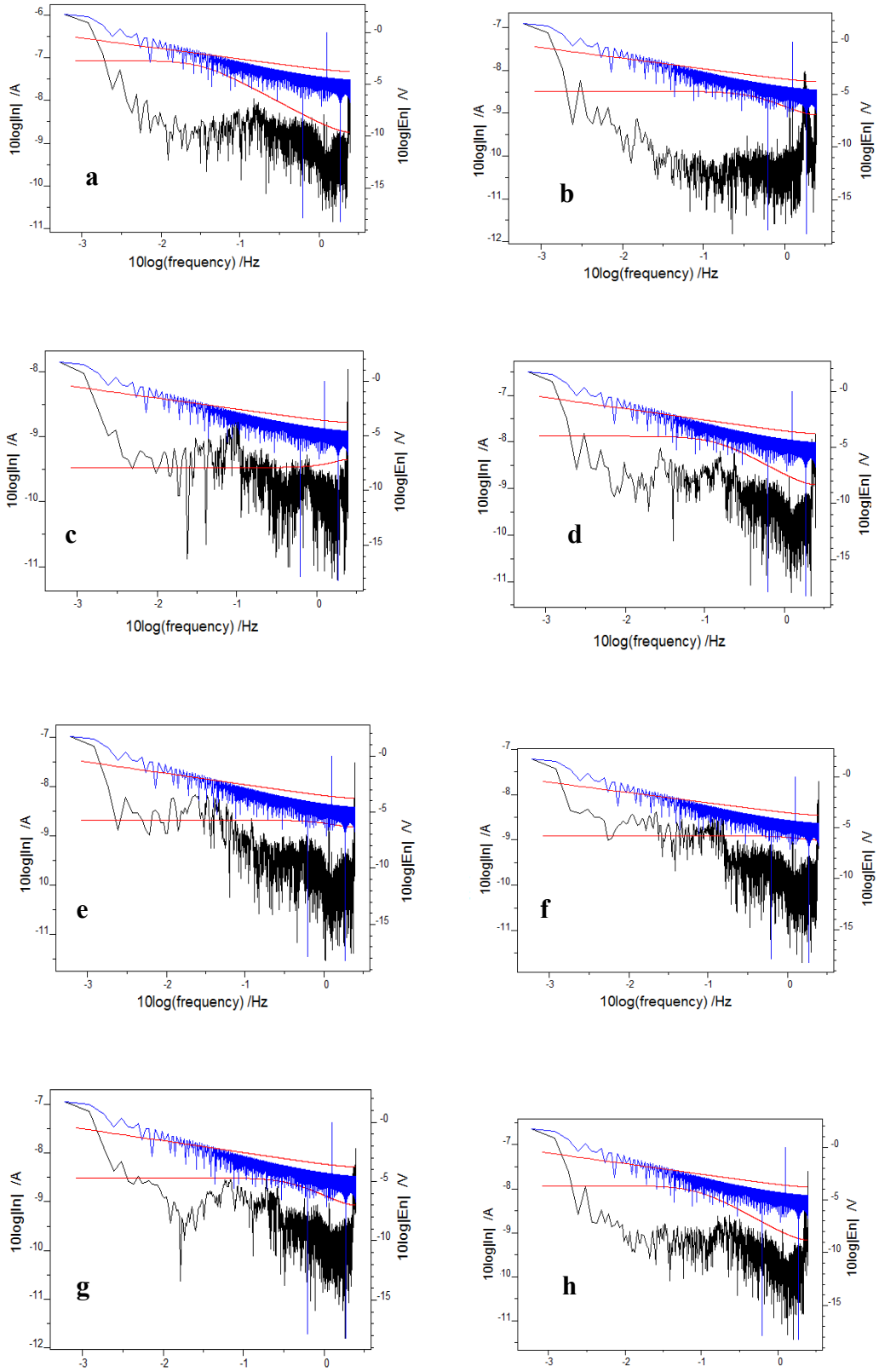

Figure 2.45 PSD curves of CS in **a**) blank **b**) 2PCOX **c**) 3PCOX **d**) 2PC4ABA **e**) 2PC3ABA **f**) 2PC2ABA **g**) 3PC3ABA **h**) 2PC2AP

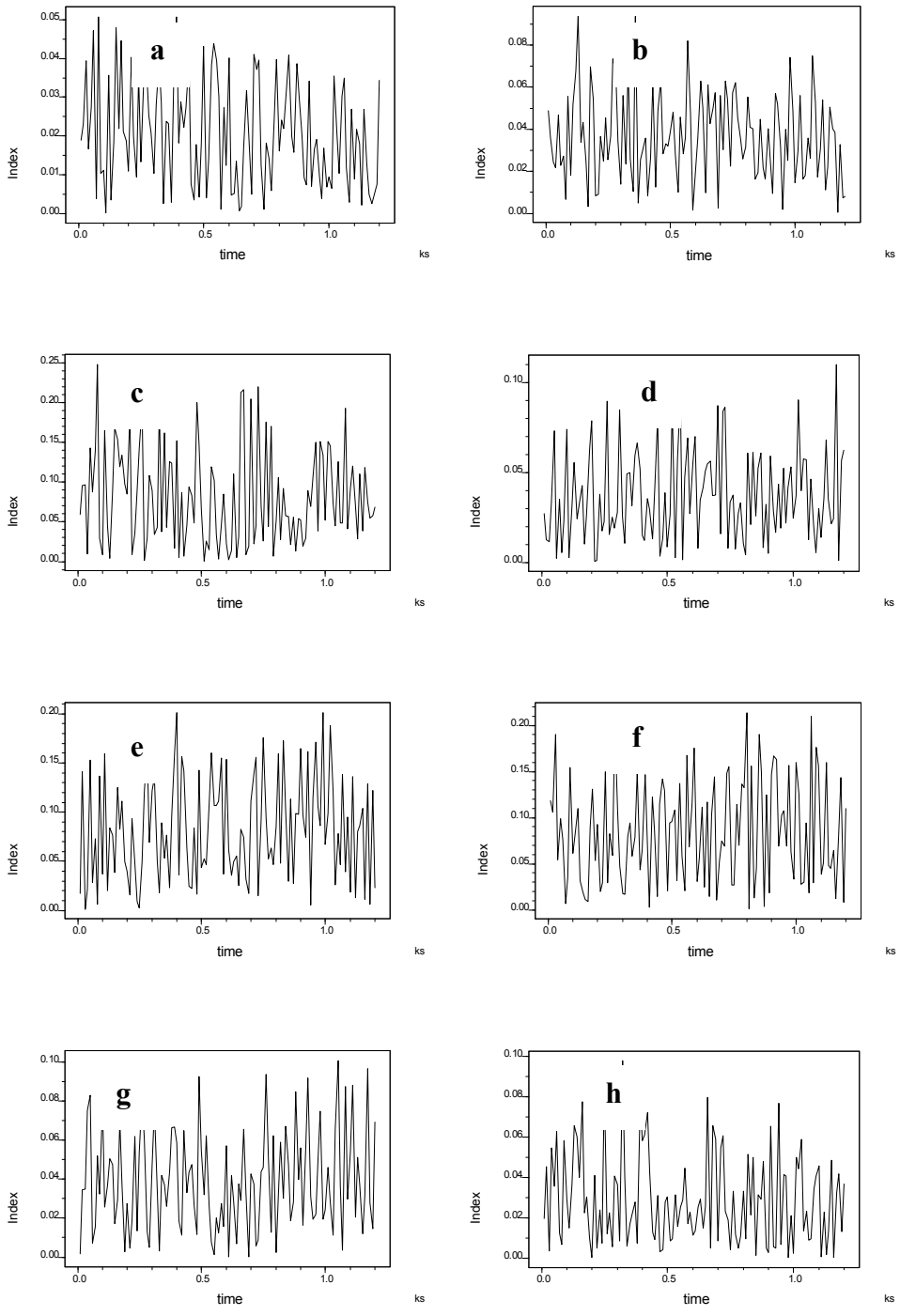

Figure 2.46 Pitting index curves of CS in **a**) blank **b**) 2PCOX **c**) 3PCOX **d**) 2PC4ABA **e**) 2PC3ABA **f**) 2PC2ABA **g**) 3PC3ABA **h**) 2PC2AP

PSD (Power Spectral Density) plots of systems were obtained by the frequency domain analysis of noise measurement, which is demonstrated in the Figure 2.45. On close analysis of PSD plots, it was cleared that the values of noise currents were comparatively low for imine containing acid solutions at all frequencies, than compared to blank, which implies that the prevention of localized corrosion on CS surface in the presence of imines.

The red lines shown in the FFT spectrum of various CS specimens depicts MEM curves. The slope of PSD plots also gives the information that the response of inhibiting molecules on the metal surface. In the presence of imines, the variation in the slope of PSD curve was observed; it indicated that the metal dissolution process was low in presence of imines.

Quantum mechanical studies

The corrosion inhibition response of organic molecules can be correlated with the energy of frontier molecular orbitals. The donor-acceptor interaction (HSAB concept) between the filled molecular orbitals of the inhibitor molecules and the vacant orbitals of Fe atoms on the surface are very important in the prevention of metal dissolution. The high value of E_{HOMO}, the lowest value of E_{LUMO} and energy difference between HOMO and LUMO (E_{LUMO}-E_{HOMO}, ΔE) are the important quantum mechanical parameters which facilitate the strong binding of the molecules on the metal surface. Optimization geometry of molecules and quantum mechanical calculations were performed by DFT method using GAMMESS software. A combination of Beck's three parameter exchange functional and Lee–Yang–Parr nonlocal correlation functional (B3LYP) was

employed in DFT calculations. Estimated quantum mechanical parameters like E_{HOMO}, E_{LUMO}, and ΔE for heterocyclic derivatives are provided in the Table 2.9. The optimized geometry of the molecules is represented in Figure from 2.47 to 2.53. Approximate HSAB parameters like electro negativity (χ) and chemical hardness (η) of the molecules are evaluated by the following equations and is reported in the Table 2.9

$\chi \approx -1/2\ (E_{HOMO} + E_{LUMO})$ $\eta \approx 1/2\ (E_{HOMO} - E_{LUMO})$ $\Delta N = \frac{\chi_{Fe} - \chi_{inhib}}{2(\eta_{Fe} + \eta_{inhib})}$

Table 2.9 Quantum mechanical parameters of heterocyclic imines of pyridine carbaldehyde on CS in 1.0M HCl

Imine	E_{HOMO} (eV)	E_{LUMO} (eV)	ΔE (eV)	χ	η	ΔN
2PCOX	-4.1633	1.1429	5.3062	1.5102	2.6531	1.0346
3PCOX	-4.3810	1.0340	5.4150	1.6735	2.7075	0.9836
2PC4ABA	-4.0270	0.6802	4.7072	1.6734	2.3536	1.1315
2PC3ABA	-3.4830	0.3537	3.8367	1.5646	1.9183	1.4166
2PC2ABA	-3.8900	0.5986	4.4886	1.6457	2.2443	1.1928
3PC3ABA	-4.1089	0.3809	4.4898	1.8640	2.2449	1.1439
2PC2AP	-2.8299	0.6258	3.4557	1.1020	1.7278	1.7067

The E_{HOMO} values of 2PC2AP, 2PC2ABA, 2PC3ABA were considerably higher than that of other compounds. The energy separation between HOMO and LUMO was appreciably lower for these compounds, which indicated that these imines were finer inhibitors. The HOMO and LUMO of these imines are represented in the Figures 2.54 to 2.67. This result indicated that the energy required to provide electrons from HOMO of the compound to the vacant orbitals of Fe is low. The number of electrons transferred (ΔN) from donor to acceptor molecules can also be found out. As an approximation, the chemical hardness of

Fe metal is assumed as zero, and the approximate electronegativity of bulk Fe is taken as 7eV, equation given below gives the approximate quantity of electron transferred from the inhibitor molecule to the Fe atoms. The number of electrons transferred from the inhibitor to the acceptor atom is higher for these three compounds mentioned above, which implies that these molecules make a strong coordinate type interaction with the metal atoms.

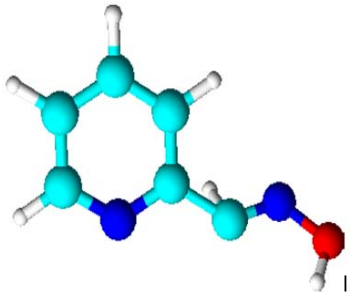

Figure 2.47 Optimized geometry of 2PCOX

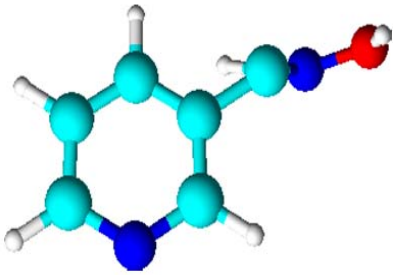

Figure 2.48 Optimized geometry of 3PCOX

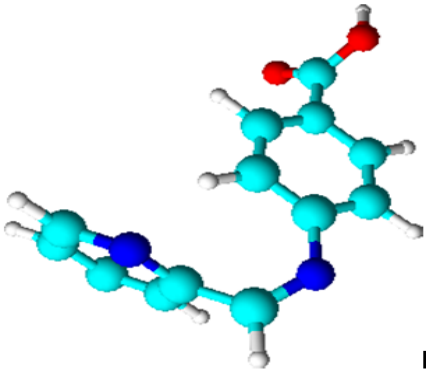

Figure 2.49 Optimized geometry of 2PC4ABA

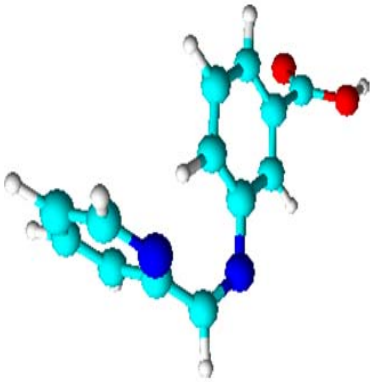

Figure 2.50 Optimized geometry of 2PC3ABA

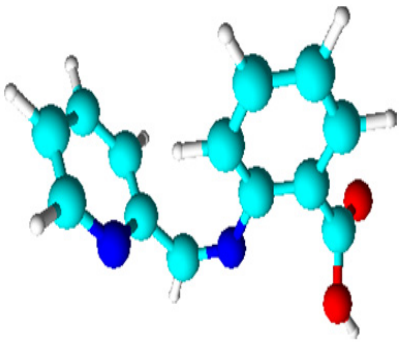

Figure 2.51 Optimized geometry of 2PC2ABA

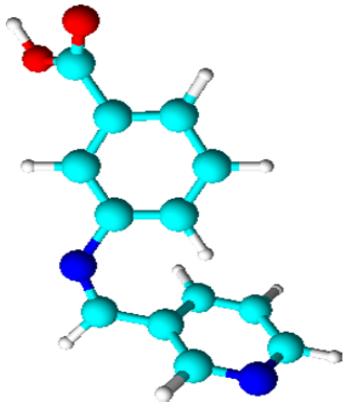

Figure 2.52 Optimized geometry of 3PC3ABA

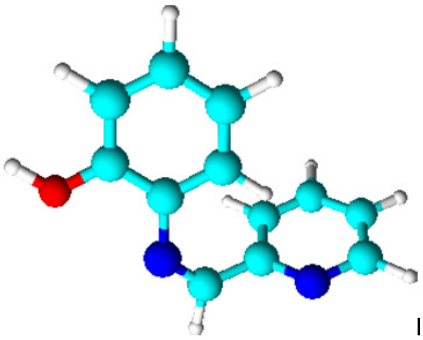

Figure 2.53 Optimized geometry of 2PC2AP

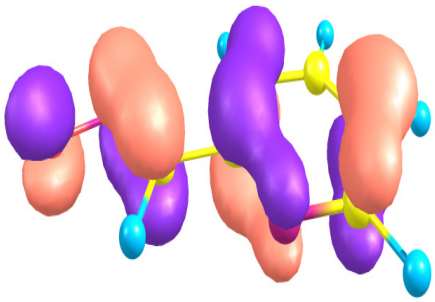

Figure 2.54 HOMO of 2PCOX

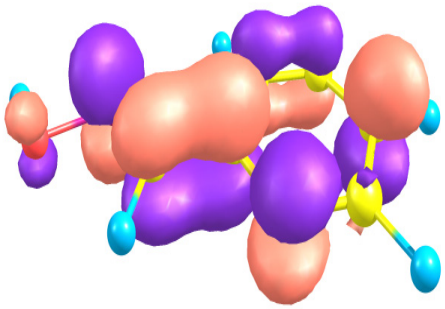

Figure 2.55 LUMO of 2PCOX

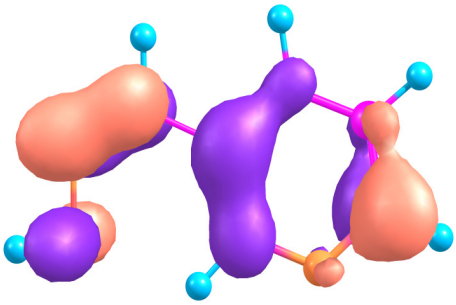

Figure 2.56 HOMO of 3PCOX

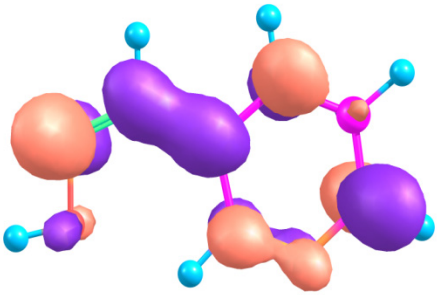

Figure 2.57 LUMO of 3PCOX

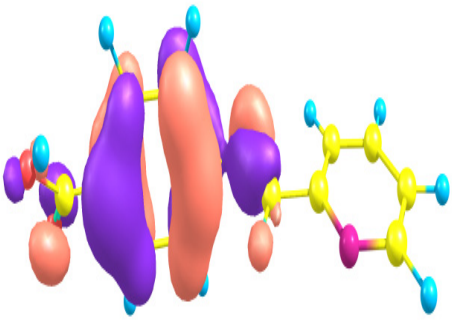

Figure 2.58 HOMO of 2PC4ABA

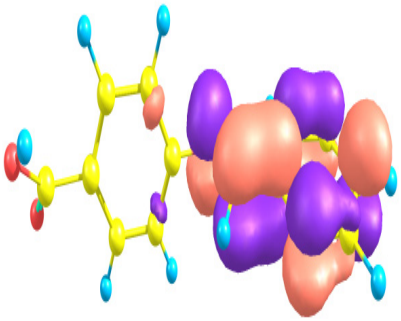

Figure 2.59 LUMO of 2PC4ABA

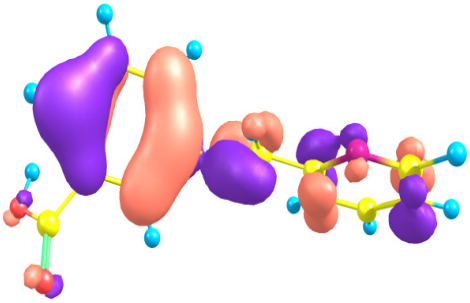

Figure 2.60 HOMO of 2PC3ABA

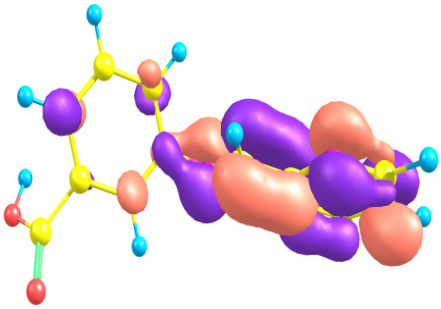

Figure 2.61 LUMO of 2PC3ABA

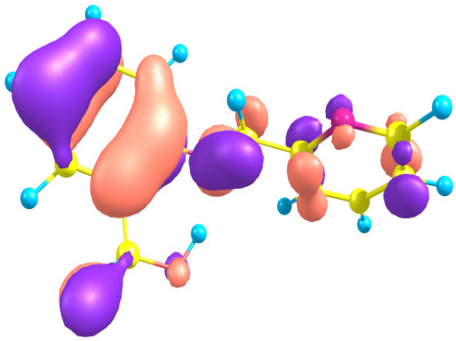

Figure 2.62 HOMO of 2PC2ABA

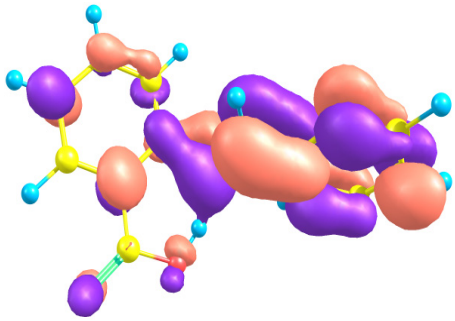

Figure 2.63 LUMO of 2PC2ABA

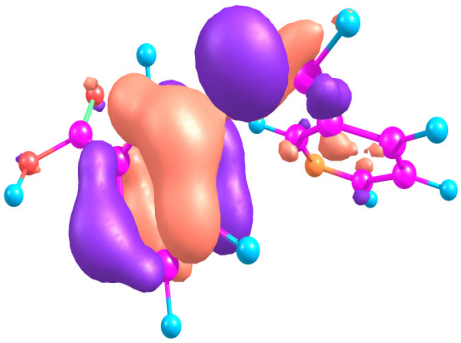

Figure 2.64 HOMO of 3PC3ABA

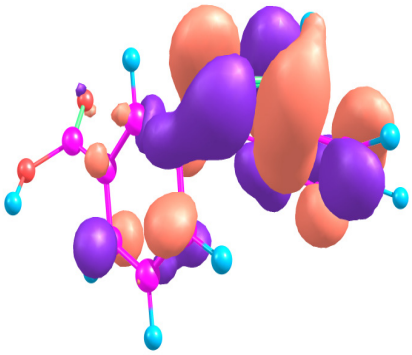

Figure 2.65 LUMO of 3PC3ABA

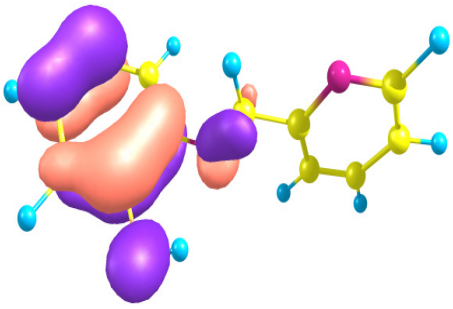

Figure 2.66 HOMO of 2PC2AP

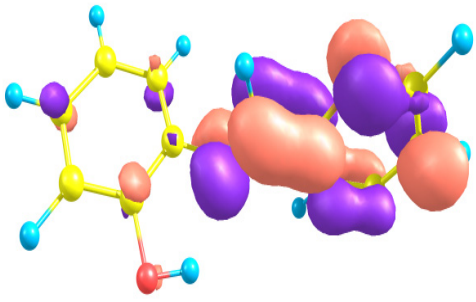

Figure 2.67 LUMO of 2PC2AP

Surface morphological studies

The mechanism of inhibition of heterocyclic imines on CS surface was determined by surface morphological studies which were conducted by taking SEM images of carbon steel specimens[105,106]. Figures 2.68 a, b and c show the SEM images of bare CS surface, CS specimen in 1.0M HCl and CS specimen in 1.0M HCl containing 2PC2ABA with 1.0mM concentration. From the Figure 2.68 (b), it was established that the metal surface was highly corroded in blank HCl solution. On close examination of the Figure 2.68(c), it was evident that the metal surface was clearer as bare in the presence of the imine 2PC2ABA, which is responsible for the formation of a protective film through adsorption on the metal surface and thereby reducing the rate of corrosion.

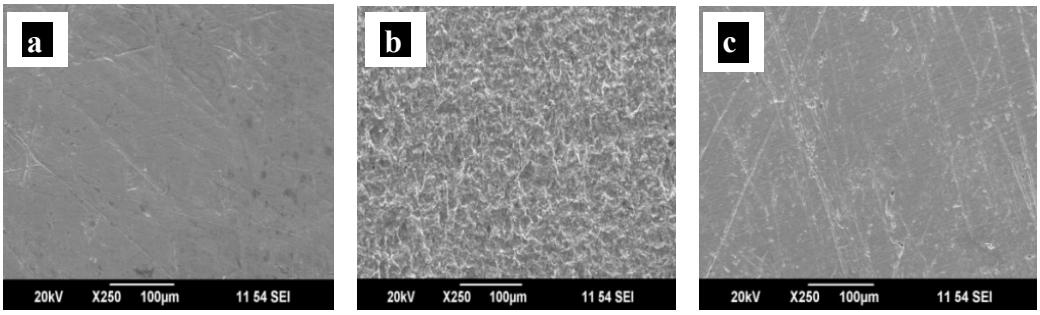

Figure 2.68 SEM images of **a)** bare metal **b)** metal immersed in 1.0M HCl **c)** metal immersed in 1.0M HCl containing 1.0mM 2PC2ABA

SECTION II

CORROSION INHIBITION STUDIES OF HETEROCYCLIC IMINES DERIVED FROM 3-FORMYLINDOLE CARBALDEHYDE ON CARBON STEEL IN 1.0M HCl

As discussed in the previous chapters, the corrosion response of the CS specimens was investigated in 1.0M HCl medium in the presence and absence of the heterocyclic imines derived from 3-formylindole carbaldehyde such as, 3-formylindole phenylhydrazone (3FIPH), 3-formylindole semicarbazone (3FISC), 3-formylindole thiosemicarbazone (3FITSC) and 3-formylindole-1,2-diaminocyclohexane (3FIDACH) by conventional gravimetric studies, surface morphological studies, quantum mechanical studies, EIS measurements and potentiodynamic polarization studies.

Weight loss studies

The four imine compounds were screened for their corrosion inhibition efficiency on CS in HCl medium using weight loss measurements. The solutions of the different inhibitor concentrations were treated with CS metal specimens for 24h and the gravimetric studies were conducted. The rate of corrosion was determined from the weight loss of the metal specimens after 24h. In the case of the blank specimen, the rate of corrosion in 1.0 M HCl, was 9.19 mmy^{-1}. The variation of corrosion rate of CS specimens with respect to varied imines concentration is displayed in the Table 2.10 and Figure 2.69

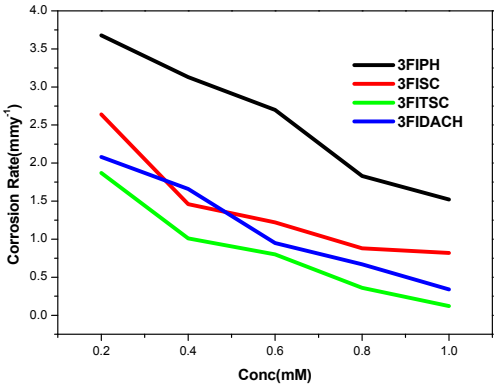

Figure 2.69 Variation of corrosion rate of heterocyclic imines of 3-formylindole carbaldehyde on CS in 1.0M HCl.

Table 2.10 Corrosion rate of CS in the presence and absence of heterocylcic imines of 3-formylindole carbaldehyde in 1.0M HCl

Conc	Corrosion rate (mmy^{-1})			
(mM)	3FIPH	3FISC	3FITSC	3FIDACH
0	9.19	9.19	9.19	9.19
0.2	3.68	2.64	1.87	2.08
0.4	3.13	1.46	1.01	1.66
0.6	2.70	1.22	0.80	0.95
0.8	1.83	0.88	0.36	0.67
1.0	1.52	0.82	0.12	0.34

From the Figure 2.69, it is able to understand that the rate of corrosion of CS considerably decreased with the concentration of the imines. A gradual decrease in the corrosion rate of CS was noticed in the presence of all imines in HCl. The variation of corrosion inhibition of imines with concentration is given in the Table 2.11. The corrosion inhibition efficacy of imines 3FITSC, 3FIDACH and 3FISC on CS at 1.0 mM concentration was >90%. Data in the Figure 2.70 and the Table 2.11, obviously established that the corrosion inhibition efficiency of the three imines 3FITSC, 3FIDACH and 3FISC were significantly higher than that of 3FIPH and such correlations were also seen at another concentrations too. The enhanced inhibition efficiency of 3FITSC can be explained by the presence

of highly polarizable sulphur atom in the molecule. 3FIDACH molecule has the presence of electron rich indole ring and two azomethine linkage. The enhanced efficiency of this molecule is due to the donation of electron cloud from azomethine group and aromatic rings to the vacant d-orbitals of Fe. Even though phenyl ring was absent in the amino part of the molecule, 3FITSC showed 98.65% inhibition efficiency as per the gravimetric method in HCl. This is definitely due to the presence of sulphur atom in the molecule. The highly poalarizable lone pair present on the sulphur atom act as a soft base, which can donate electrons to the vacant orbitals of Fe atoms (which can be considered as soft acid). According to Pearson's concept, soft bases strongly interact with soft acids. This soft-soft interaction is thus possible between 3FITSC and the Fe atoms, which may be responsible for the higher inhibition efficiency.

Table 2.11 Inhibition efficiencies of heterocyclic imines of 3-formylindole carbaldehyde on CS in 1.0M HCl

Conc	Inhibition efficiency (%)			
(mM)	3FIPH	3FISC	3FITSC	3FIDACH
0.2	59.93	71.28	79.58	77.41
0.4	65.91	84.16	89.02	81.91
0.6	70.60	86.76	91.30	89.61
0.8	80.07	90.38	96.07	92.62
1.0	83.44	91.02	98.65	96.21

It is obvious from the table and figure that the rate of corrosion of CS in the presence of both 3FITSC and 3FISC have similar trend i.e., rate of corrosion gradually decreased with the imine concentration. The reason for the similar response is due to the structural similarity of the molecules. The only difference in

the structures of 3FITSC and 3FISC is that the former contains a sulphur atom in the molecule, while the 3FISC contains oxygen atom instead of sulphur. 3FITSC and 3FISC showed efficiency of 98% and 91% respectively in 1.0M HCl at maximum concentration 1.0mM.

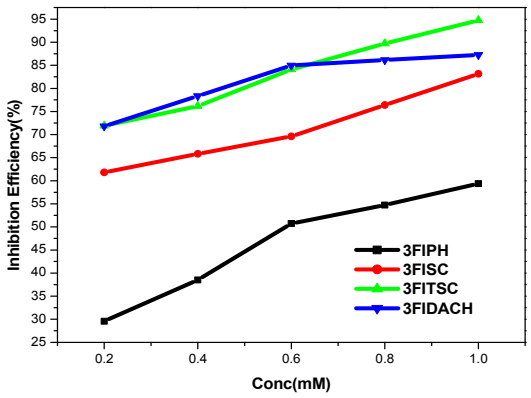

Figure 2.70 Variation of inhibition efficiencies (ηw%) of heterocyclic imines of 3-formylindole carbaldehyde on CS in 1.0M HCl

In the case of 3FIPH and 3FIDACH, the highly delocalized electron clouds of the benzene ring interact with the metal surface thoroughly and this prevent the metallic dissolution appreciably. 3FIPH have the indole moiety along with one phenyl ring of amino part, but it did not show the expected efficiency. This may be due to the considerable deviation of the molecules from planarity. The maximum inhibition efficiency of 3FIPH was 83%. When we compare the structures of 3FIDACH with others, it contains two indole moieties and two azomethine linkages. The planarity of the twoindole rings and the overall coplanarity of 3FIDACH helped the firm attachment of the molecule on the CS surface, thereby preventing the corrosion effectively. At 1.0mM concentration 3FIDACH showed 96% inhibition efficiency in 1.0M HCl.

Comparison between the inhibition efficiency of imines and its parent amines

Gravimetric analysis of steel specimens was also conducted in 1.0M HCl in the presence of parent amines in order to compare the inhibition efficiency with imines. The results are tabulated and graphically represented in the Table 2.12 and Figure 2.71 respectively, which displays the comparative analysis of corrosion inhibition values of imines and their parent amines.

Table 2.12 Corrosion inhibition efficiencies of heterocyclic imines of 3-formylindole carbaldehyde and their parent amines on CS in 1.0M HCl

Conc (mM)	Inhibition efficiency (%)							
	PH	3FIPH	SC	3FISC	TSC	3FITSC	DACH	3FIDACH
0.2	8.4	59.93	-16	71.28	2.5	79.58	-20	77.41
0.6	12.7	70.60	-3.4	86.76	10.4	91.30	-12.4	89.61
1.0	24.5	83.44	8.0	91.02	16.3	98.65	2.5	96.21

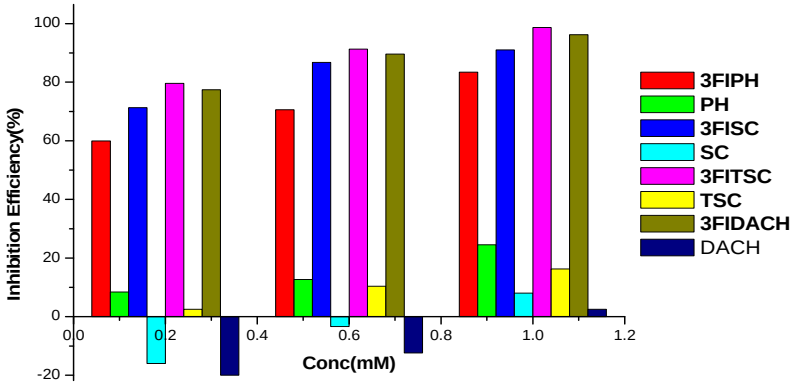

Figure 2.71 Comparison of corrosion inhibition efficiencies of heterocyclic imines of 3-formylindole carbaldehyde and their parent amines on CS in 1.0M HCl

From the data it is evident that the imines exhibited remarkable inhibition efficiencies in comparison with the inhibition efficiency of corresponding parent amines. This substantiates the significance of the azomethine (C=N) moiety exists

in the imines which involve in the inhibition mechanism of corrosion on the metal surface.

The parent amines which subjected to the gravimetric analysis were phenyl hydrazine hydrochloride (PH), semicarbazide (SC), thiosemicarbazide (TSC), and 1,2-diaminocyclohexane (DACH). TSC and PH showed slight positive values for corrosion inhibition. But the SC and DACH exhibited negative corrosion inhibition efficiency. This indicates that the parent amines act as corrosion accelerators in the aggressive medium.

Adsorption studies

The inhibition mechanism of heterocyclic imines is mainly explained by the adsorption process and their adsorption parameters can be determined by the selection of the best fit isotherm model with the assistance of correlation coefficient (R^2). Figures 2.72 to 2.75 represent the adsorption isotherms for the studied imines 3FIPH, 3FISC, 3FITSC and 3FIDACH in 1.0M HCl.

Table 2.13 Adsorption isotherms and the regression coefficient of heterocyclic imines of 3-formylindole carbaldehyde on CS in 1.0M HCl

	Regression coefficient (R^2)			
Isotherm	3FIPH	3FISC	3FITSC	3FIDACH
Langmiur	0.935	0.998	0.998	0.999
Freundlich	0.470	0.924	0.934	0.865
Temkin	0.521	0.982	0.986	0.939
Frumkin	0.010	0.496	0.509	0.360
El-Awady	0.508	0.917	0.856	0.932
Flory-Huggin	0.330	0.892	0.833	0.913

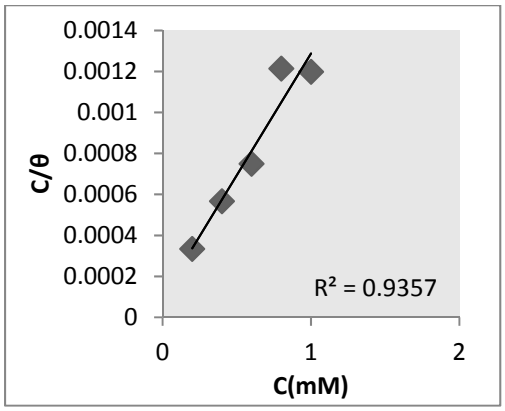

Figure 2.72 Langmuir isotherm for 3FIPH on CS in 1.0M HCl

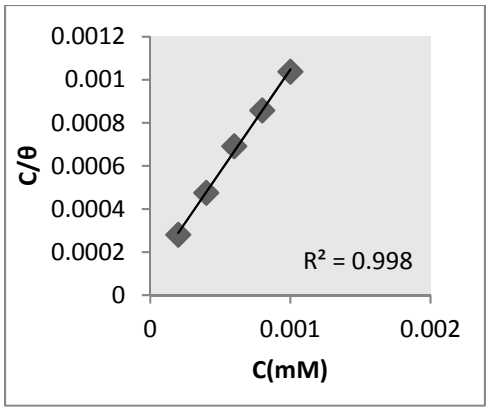

Figure 2.73 Langmuir isotherm for 3FISC on CS in 1.0M HCl

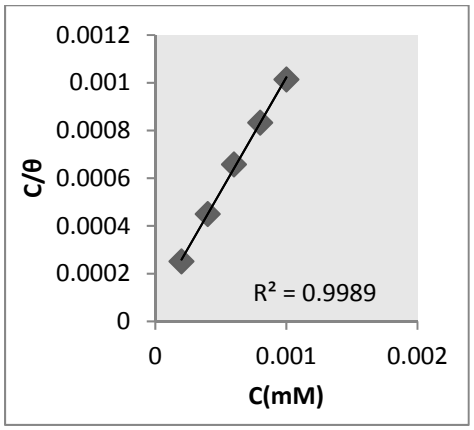

Figure 2.74 Langmuir isotherm for 3FITSC on CS in 1.0M HCl

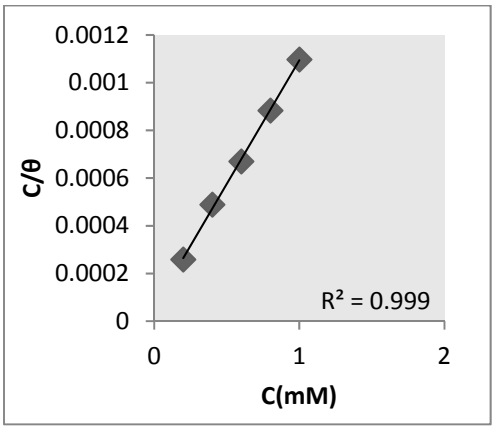

Figure 2.75 Langmuir isotherm for 3FIDACH on CS in 1.0M HCl

Table 2.14 Adsorption parameters of heterocyclic imines of 3-formylindole carbaldehyde on CS in 1.0M HCl

Adsorption parameter	3FIPH	3FISC	3FITSC	3FIDACH
K_{ads}	10064	10041	16244	17376
ΔG^0_{ads} (kJ/mol)	-33.12	-33.11	-34.05	-34.48

The adsorption behaviour of all imines can be explained by Langmuir isotherm. The regression coefficient and adsorption isotherms of various imines on CS are given in the Table 2.13. From Table 2.14 it is clear that 3FITSC and

3FIDACH has comparatively high K_{ads}, value than the other imines. So it is easy to assume that both compounds were adsorbed more efficiently on CS surface than others. The ΔG^0_{ads} for all imines denotes negative values which show the spontaneity of the process. In the present study, the ΔG^0_{ads} values of all imines were between -33kJmol^{-1} to -35kJmol^{-1} pointing out the fact that the adsorption process involves both physisorption and chemisorption.

Electrochemical studies

The electrochemical analysis including impedance studies and Tafel polarization studies is quick, accurate and reliable procedure to predict the corrosion inhibition capacity of molecules. The analysis was conducted using four indole based imine compounds such as 3FIPH, 3FISC, 3FITSC and 3FIDACH on CS in 1.0M HCl. The Ivium compactstat-e electrochemical system was employed for conducting the experiments.

Electrochemical impedance spectroscopy (EIS) studies

Nyquist plots and the combined Bode-impedance plots of the four imines, 3FIPH, 3FISC, 3FITSC and 3FIDACH are given in the Figures 2.76-2.79. Nyquist plots exhibited slightly depressed semi circles which had some irregularities in the low frequency regions. These irregularities were occurred due to the roughness of the metal surface. The analysis of each Nyquist plots of imines was done by using the most suitable equivalent circuit which contains two resistances and one capacitance. The parameters obtained from EIS analysis were R_s, R_{ct} and C_{dl}. Among these parameters in the equivalent circuit, it was found that solution resistance (R_s) was not varying with the concentration of inhibitor

during the analysis. Table 2.15 shows the impedance parameters such as charge transfer resistance, double layer capacitance and the corrosion inhibition efficiency of various imines on CS specimens, derived from EIS measurements.

Table 2.15 Electrochemical impedance parameters of CS in the presence and absence of heterocyclic imines of 3-formylindole carbaldehyde in 1.0M HCl

Imines	Conc (mM)	C_{dl} ($\mu F\ cm^{-2}$)	R_{ct} (Ωcm^2)	η_{EIS} (%)
	0.0	90.5	22.7	-
	0.2	75.3	45.3	49.80
3FIPH	0.4	65.2	50.1	54.53
	0.6	62.7	54.9	58.59
	0.8	42.3	138.4	83.55
	1.0	39.9	158.5	85.64
	0.2	59.2	69.4	67.18
3FISC	0.4	58.3	126.7	82.03
	0.6	48.3	173.8	86.90
	0.8	42.4	365.4	93.77
	1.0	30.0	383.2	94.06
	0.2	58.4	69.3	80.37
	0.4	41.7	163.3	86.06
3FITSC	0.6	33.2	242.5	90.61
	0.8	39.0	265.2	91.41
	1.0	44.0	576.3	96.05
	0.2	51.2	147.1	84.51
	0.4	41.1	249.4	90.87
3FIDACH	0.6	40.7	268.2	91.51
	0.8	39.1	302.3	92.47
	1.0	33.2	458.1	95.03

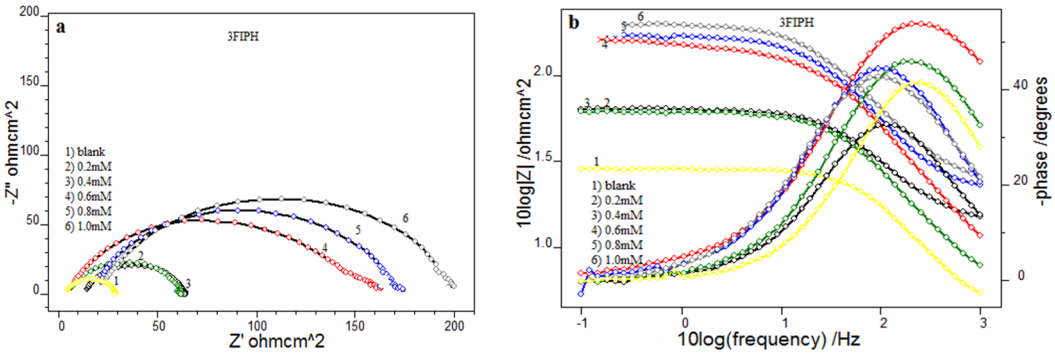

Figure 2.76 a) Nyquist plots and **b)** Bode plots of CS in the presence and absence of 3FIPH in 1.0M HCl

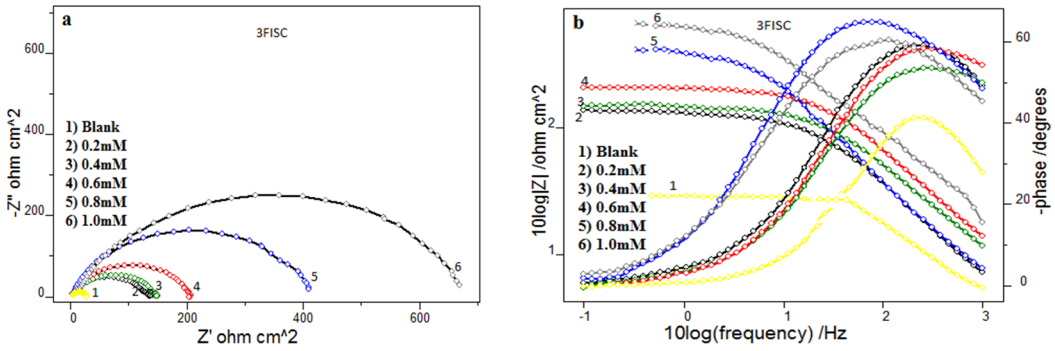

Figure 2.77 a) Nyquist plots and **b)** Bode plots of CS in the presence and absence of 3FISC in 1.0M HCl

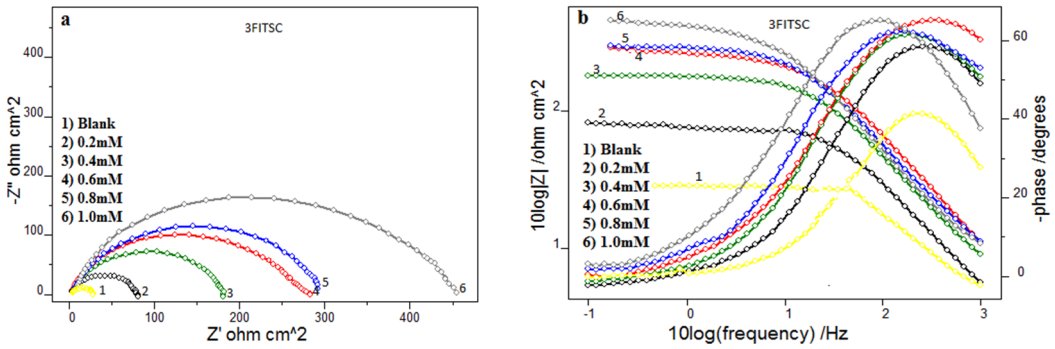

Figure 2.78 a) Nyquist plots and **b)** Bode plots of CS in the presence and absence of 3FITSC in 1.0M HCl

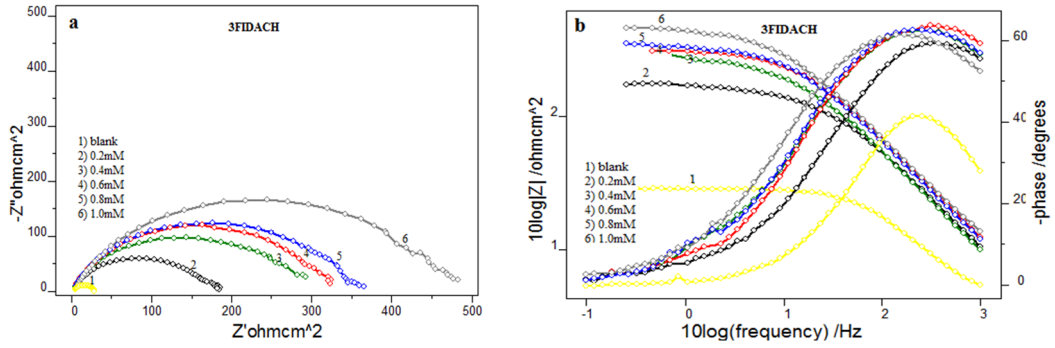

Figure 2.79 a) Nyquist plots and **b)** Bode plots of CS in the presence and absence of 3FIDACH in 1.0M HCl

Impedance parameter, charge transfer resistance (R_{ct}) of each imine increased considerably with the concentration of the inhibitor. This shows that all the heterocyclic imine molecules effectively hinder the charge transfer process of corrosion, and thus mitigate the metal dissolution appreciably in the aggressive medium. In all measurements, it can be seen that the double layer capacitance values were found to decrease with increasing concentration of imines, because of the enhanced adsorption of the inhibitor molecules on the metal specimen with concentration.

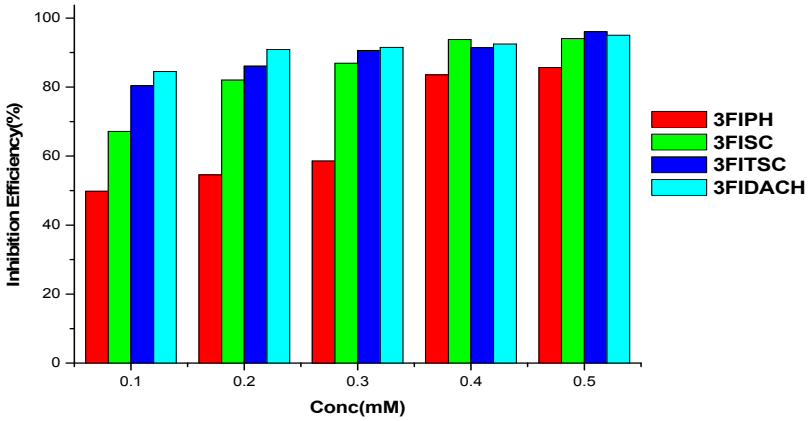

Figure 2.80 Variation of corrosion inhibition efficiencies (η_{EIS}%) of heterocyclic imines of 3-formylindole carbaldehyde on CS in 1.0M HCl

On critical analysis of the data, it is obvious that the three imine derivatives namely 3FITSC, 3FIDACH and 3FISC have comparable inhibition efficiencies at all concentrations. Maximum percentage of corrosion inhibition efficiency was shown by the imine 3FITSC in 1.0M HCl medium. Even at low concentrations, this molecule displayed better inhibition efficiency on CS. It showed inhibition efficiency 80% at low concentration of 0.2mM. This value gradually increased with the inhibitor concentration and reached 96% at 1.0mM.

Presence of aromatic ring of indole moiety, azomethine linkage, N-atom present on indole moiety and highly polarizing sulphur atom on amino part are responsible for the potential corrosion inhibition efficiency. Like this, the imine 3FIDACH also showed 95% efficiency. Presence of two azomethine linkage and aromatic rings (indole ring), caused the enhanced delocalization of π electron cloud in the molecule, which will definitely favour the interaction of the molecule on the metal surface. The results achieved from the gravimetric studies were also in good agreement with the EIS measurements. 3FISC molecule also exhibited good corrosion inhibition efficiency, but slightly less than that of 3FIDACH as obtained by EIS studies. It had a significant role in reducing the rate of corrosion of CS appreciably in HCl medium. The maximum efficiency noted for this molecule at 1.0mM concentration was of 94%.

The imine 3FIPH also displayed good corrosion inhibition efficiency especially at higher concentrations (Figure 2.80) but it showed less efficiency when compared to the efficiency of 3FISC as per EIS studies. Even though the molecule having aromatic rings, and azomethine groups, it showed low efficiency, may be due to the lack of planarity in the structure.

Potentiodynamic polarization studies

To emphasize the corrosion inhibition capacity of the imines derived from 3-formylindole on carbon steel and to propose the electrochemical site of interaction, potentiodynamic polarization studies were done with the help of three electrode system. Carbon steel with an exposed area of $1cm^2$ was used as the

working electrode. Linear polarization and Tafel polarization studies were performed using Ivium electrochemical system.

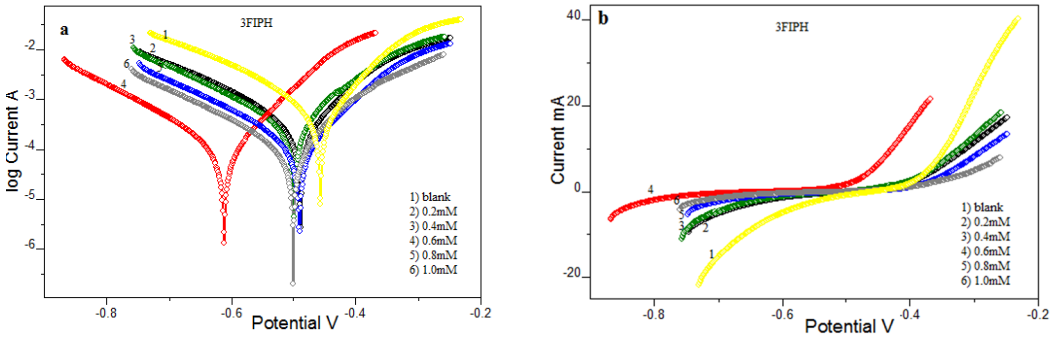

Figure 2.81 a) Tafel plots and **b)** Linear polarization plots of CS in the presence and absence of 3FIPH in 1.0M HCl

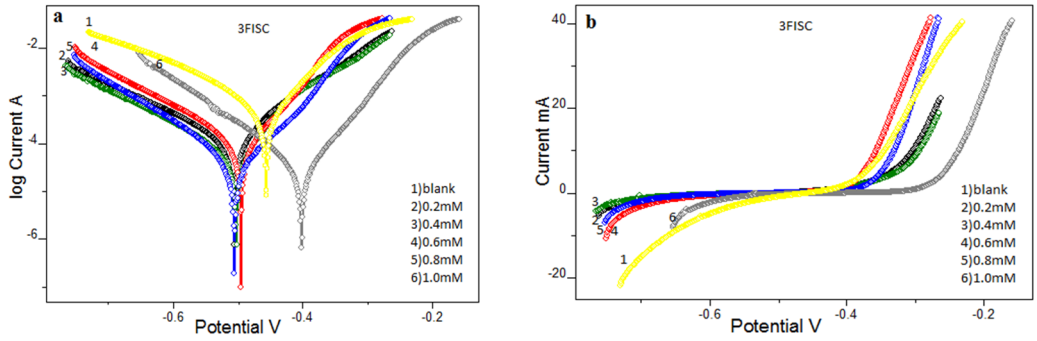

Figure 2.82 a) Tafel plots and **b)** Linear polarization plots of CS in the presence and absence of 3FISC in 1.0M HCl

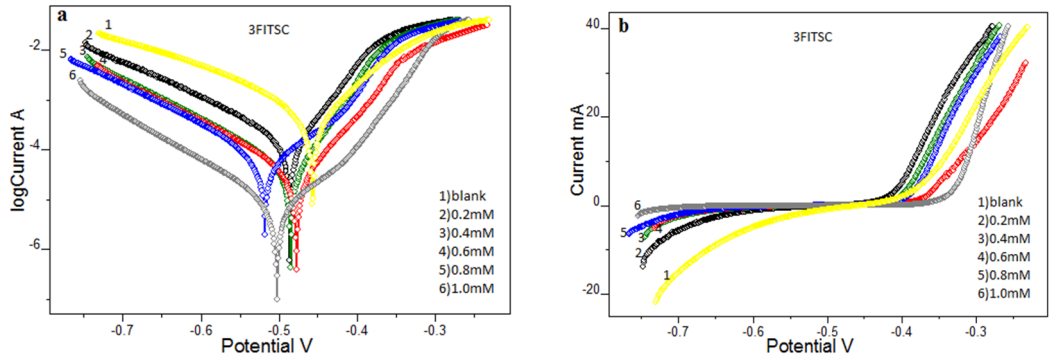

Figure 2.83 a) Tafel plots and **b)** Linear polarization plots of CS in the presence and absence of 3FITSC in 1.0M HCl

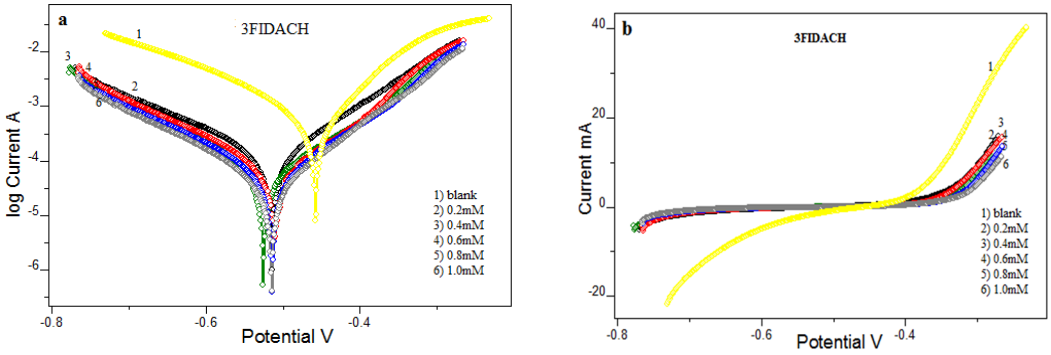

Figure 2.84 a) Tafel plots and **b)** Linear polarization plots of CS in the presence and absence of 3FIDACH in 1.0M HCl

Polarization resistance and corrosion current density were calculated from each analysis and inhibition efficiency was determined. Figures 2.81 to 2.84 represent the Tafel plots and polarization curves of the four imines derived from 3-formylindole carbaldehyde. All the Tafel plots of imines were exhibited the considerable difference from the Tafel plots of the uninhibited solution. Table 2.16 shows the Tafel data and linear polarization data obtained by the potentiodynamic polarization studies. On close observation of the data it is unambigius that the corrosion current densities of CS specimens decreased significantly with the concentration of the imines. It was the fact that these imines hinder the metal dissolution process appreciably either by intervening in the anodic or cathodic process of corrosion or both. Studies revealed that all the imines showed good corrosion inhibition efficiency on CS in 1.0M HCl solution. The imine 3FITSC showed excellent inhibition on the corroding metal. The results obtained by the potentiodynamic polarization studies were agreed with that of impedance studies.

Table 2.16 Potentiodynamic polarization parameters of CS in the presence and absence of heterocyclic imines of 3-formylindole carbaldehyde in 1.0M HCl

Imine	Tafel Data					Polarization Data		
	Conc (mM)	$-E_{corr}$ (mV/SCE)	I_{corr} ($\mu A/cm^2$)	b_a (mV/dec)	$-b_c$ (mV/dec)	η_{pol} (%)	R_p (ohm)	η_{Rp} (%)
	0	460	796	108	178	-	47.6	-
3FIPH	0.2	498	368	126	171	53.7	95.8	67.16
	0.4	510	323	123	162	59.4	87.6	64.09
	0.6	489	286	88	165	64.1	90.9	65.39
	0.8	522	134	136	165	83.2	272.2	88.43
	1.0	604	100	87	150	87.4	276.0	88.60
3FISC	0.2	519	139	119	162	82.5	210.6	77.40
	0.4	533	100	121	149	87.4	201.3	76.35
	0.6	482	97	65	143	87.8	361.7	86.84
	0.8	475	74	57	104	90.7	528.3	90.98
	1.0	395	65	61	122	91.8	554.1	91.41
3FITSC	0.2	534	134	110	137	83.2	128.6	62.99
	0.4	527	108	85	123	86.4	414.0	88.50
	0.6	479	41	67	126	94.9	606.1	92.15
	0.8	480	38	52	126	95.2	674.2	92.93
	1.0	467	4.15	47	112	99.5	2576.0	98.15
3FIDACH	0.2	504	112	108	174	85.9	244.2	87.12
	0.4	503	52	104	146	93.5	383.7	91.80
	0.6	480	50	79	158	93.7	443.9	92.91
	0.8	499	48	104	154	93.9	559.0	94.37
	1.0	504	38	99	148	95.2	718.8	95.62

A comparison of the inhibition efficiencies of all imines were done and portrayed in Figure 2.85. It is clear from the figure that, in all concentrations the imines 3FITSC displayed good corrosion inhibition efficiency. A highest inhibition efficiency was observed at a concentration of 1.0mM was 99%. Presence of aromatic ring, azomethine group and sulphur atom in the molecule, helped the imine to a make a strong interaction with the metal surface. The involvement of the benzenoid ring in the corrosion prevention process can further

be justified by demonstrating the inhibition efficiency of 3FIDACH molecule. 3FIDACH molecule showed the higher corrosion inhibition efficiency value very close to 3FITSC in HCl medium, due to the presence of two indole rings as well as two azomethine linkages. The other two imines 3FISC and 3FIPH also displayed good corrosion inhibition efficiency on CS surface, but it is well clear that 3FISC showed higher efficiency at all concentrations than 3FIPH even if it bear aromatic ring on the amino part. 3FIPH molecule did not exhibit an expected level of corrosion inhibition, on CS surface. A maximum inhibition efficiency 88% was shown by this molecule at 1.0mM concentration. Results of the linear polarization analysis showed good agreement with Tafel analysis in all investigations.

The potentiodynamic polarization studies can be employed for predicting the nature of the corrosion inhibitor. On analyzing the data presented in Table 2.16, it can be ensured that most of the imines appreciably changed the slope of the Tafel lines, while comparing the Tafel lines of uninhibited solution. If both the slopes of Tafel lines were affected considerably, the inhibitor molecule can be regarded as a mixed type one. Alternatively, if the anodic or cathodic slopes alter from the slope of the uninhibited solution, the inhibitor can be considered as anodic or cathodic type. In the present investigation, the two imines namely 3FISC and 3FIDACH affect the anodic and cathodic slopes in a uniform fashion and therefore these molecules can be regarded as mixed type inhibitors. On examining the Tafel slopes of the imines 3FIPH and 3FITSC it was evident that the cathodic slopes almost remain undisturbed during the polarization analysis,

suggesting that they were mainly acting on the anodic sites and thus reduced the rate of anodic process of corrosion considerably. Thus these imines were believed to act as anodic inhibitors.

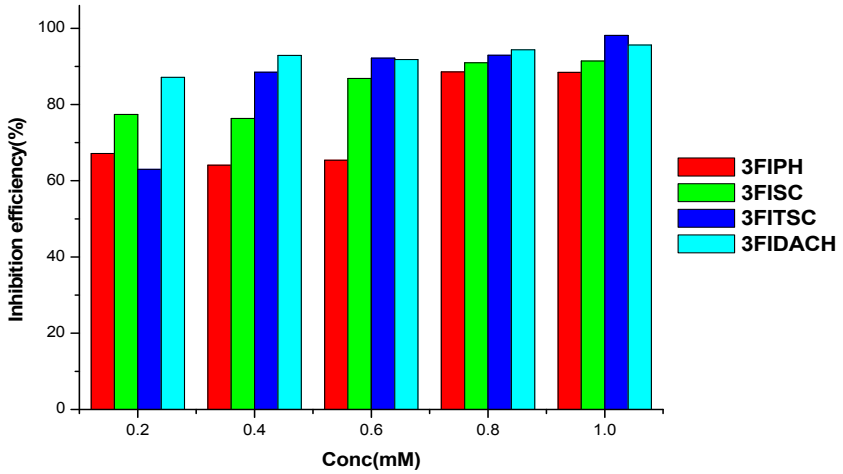

Figure 2.85 Variation of corrosion inhibition efficiencies (η_{Rp}%) of heterocyclic imines of 3-formylindole carbaldehyde on CS in 1.0M HCl

Electrochemical noise studies

Electrochemical noise (ECN) measurements were conducted using a three-electrode cell system. All ECN analyses were performed for a period of 1200 sec using Ivium compactstat-e-electrochemical system controlled by Iviumsoft software.

The noise current corresponding to the metal dipped in the HCl solution in the presence and absence of imines of 3-formylindole carbaldehyde was represented in the Figure 2.86. From the Figure it was evident that the noise current of the metal have very low value in the presence imines, which implies that investigated imine compounds possess appreciable inhibition efficiency.

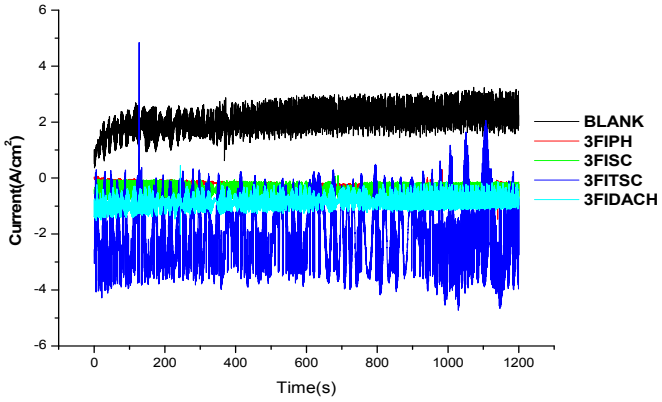

Figure 2.86 Noise current for CS in the presence and absence of heterocyclic imines of 3-formylindole carbaldehyde (1.0mM) in 1.0M HCl

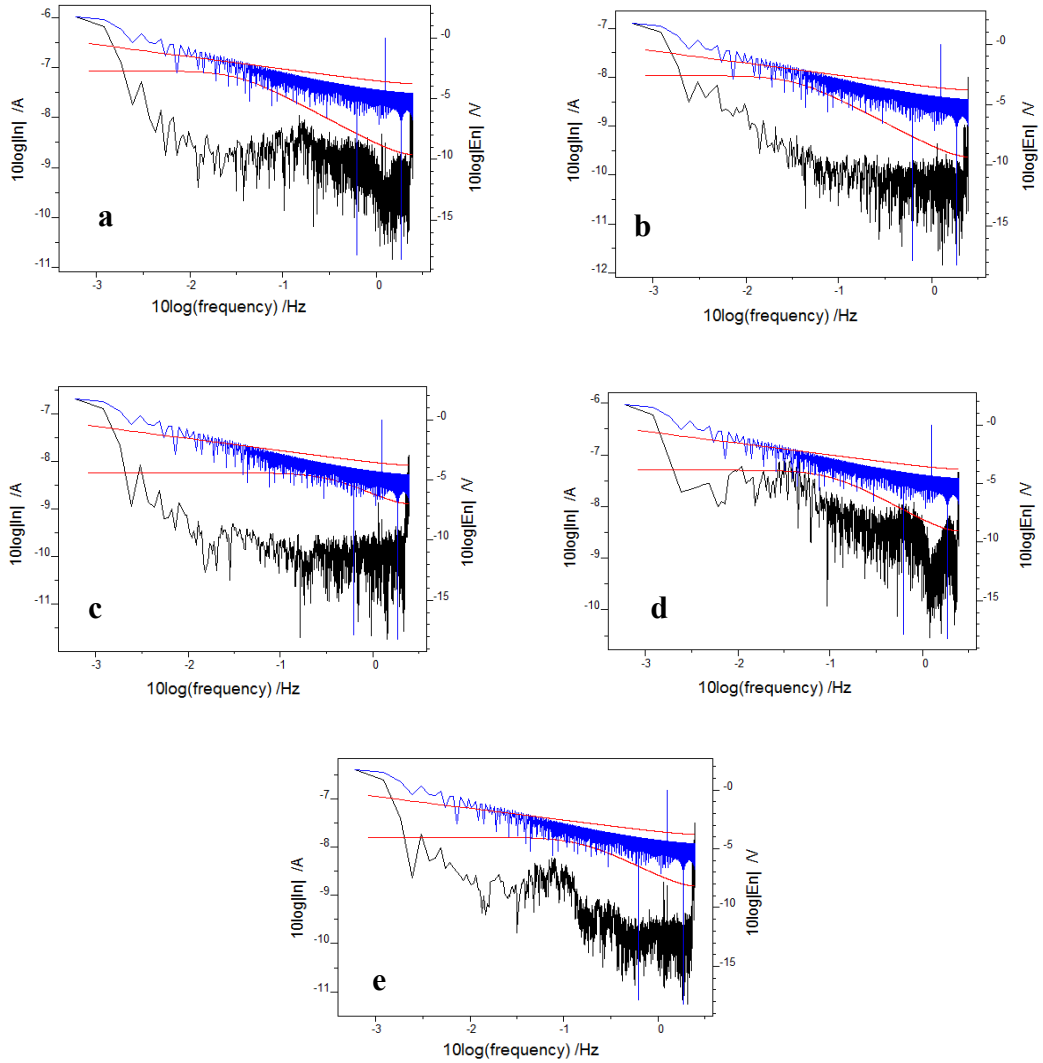

Figure 2.87 PSD curves of CS in **a**) blank **b**) 3FIPH **c**) 3FISC **d**) 3FITSC **e**) 3FIDACH

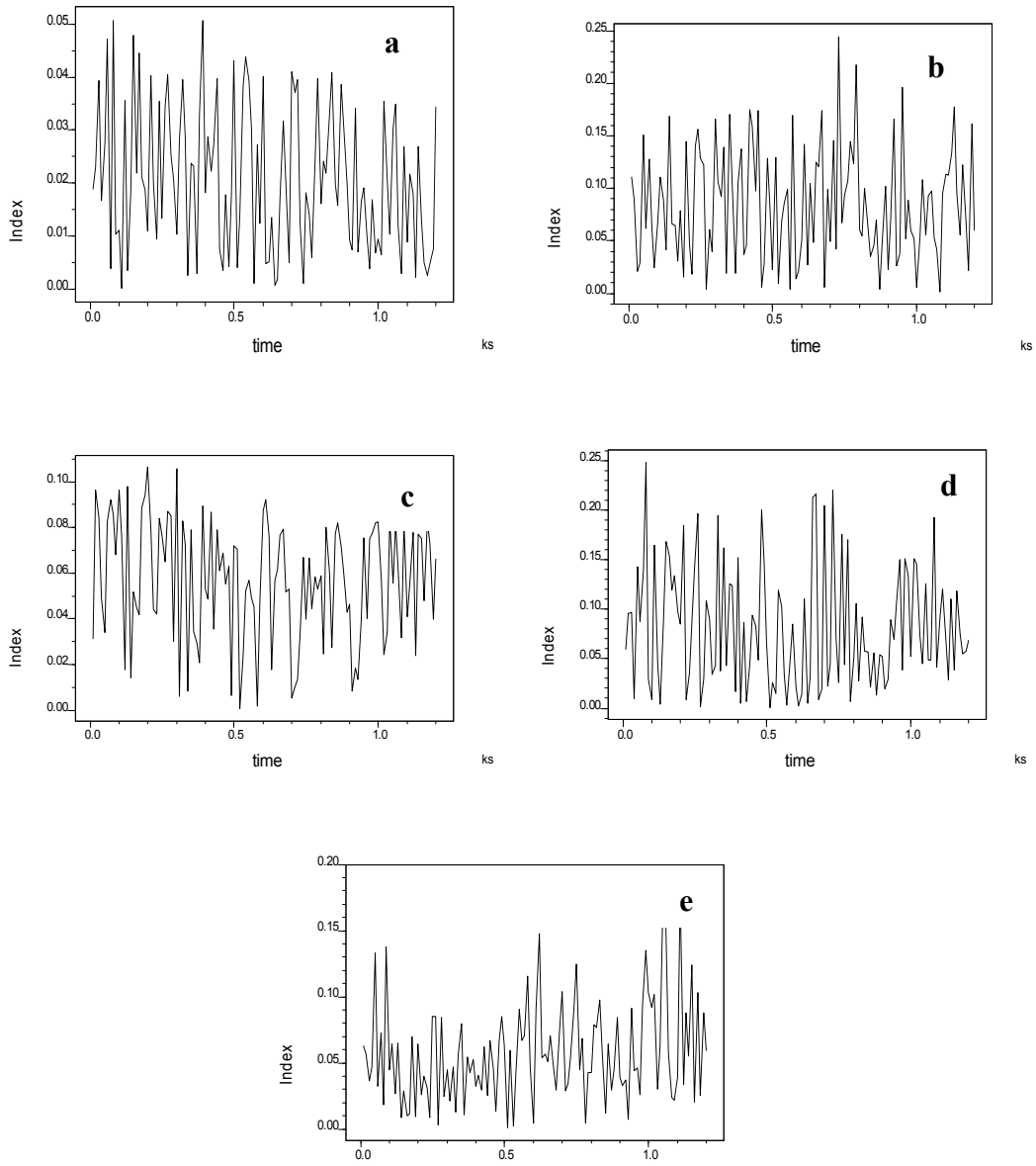

Figure 2.88 Pitting index curves of CS in **a**) blank **b**) 3FIPH **c**) 3FISC **d**) 3FITSC **e**) 3FIDACH

Pitting index value is the measurement of resisting capability of system against pitting corrosion. On analyzing the pitting index curves depicted in the Figure 2.88, it was understood that the amplitude of pitting index curves corresponding to the imine containing acid solution system was higher than the metal specimen immersed in the acid solution in the absence of imines. The high

value of pitting index was observed for the imines 3FIPH and 3FITSC as compared to the others which indicated that both imines prevent the pitting corrosion appreciably than others.

PSD (Power Spectral Density) plots of systems were obtained by the frequency domain analysis of noise measurement, which is demonstrated in the Figure 2.87. On close analysis of PSD plots, it was cleared that the values of noise current were comparatively low for imine containing acid solutions at all frequencies, which implies that the prevention of localized corrosion on CS surface in the presence of imines.

Quantum mechanical studies

The corrosion inhibition efficacy of various inhibitors can be correlated with the Frontier molecular orbital energies. The HSAB concept (donor-acceptor interaction) between the vacant orbitals of Fe atoms and the filled molecular orbitals of the inhibitor compounds has an important role in the prevention mechanism of metal disintegration. The lowest $E_{\mathrm{LUMO}} - E_{\mathrm{HOMO}}$ (ΔE) value of inhibitors is the essential quantum mechanical parameter which helps them to bind on the metal surface strongly. Quantum mechanical evaluations were carried out using DFT method by GAMMESS software. Calculated quantum mechanical parameters like E_{HOMO}, E_{LUMO}, ΔE, electronegativity (χ), hardness (η) and number of transferred electrons (ΔN) for the investigated inhibitors are tabulated in the Table 2.17 and optimized geometry of the imines are represented in the Figures 2.89 to 2.92. The calculations were conducted using following equations,

$\chi \approx -1/2\ (E_{\mathrm{HOMO}} + E_{\mathrm{LUMO}})$ $\quad \eta \approx 1/2\ (E_{\mathrm{HOMO}} - E_{\mathrm{LUMO}})$ $\quad \Delta N = \frac{\chi_{Fe} - \chi_{inhib}}{2(\eta_{Fe} + \eta_{inhib})}$

Table 2.17 Quantum mechanical parameters of heterocyclic imines of 3-formylindole carbaldehyde on CS in 1.0M HCl

Imine	E_{HOMO} (eV)	E_{LUMO} (eV)	ΔE (eV)	χ	η	ΔN
3FIPH	-3.047	1.632	4.680	0.7075	2.3402	1.344
3FISC	-2.857	2.041	4.820	0.9085	2.4105	1.264
3FITSC	-2.857	1.578	4.576	1.2050	2.2880	1.266
3FIDACH	-3.427	1.823	5.250	0.8080	2.6240	1.181

The ΔE between HOMO and LUMO was comparably low for 3FITSC, which implied that 3FITSC had predominant inhibition efficiency. These data indicated that the energy required to move electrons from HOMO of 3FITSC to the vacant orbitals of Fe was very low. The ΔN from donor to acceptors was also evaluated from these quantum mechanical parameters which provide the information about interaction with the metal atoms.

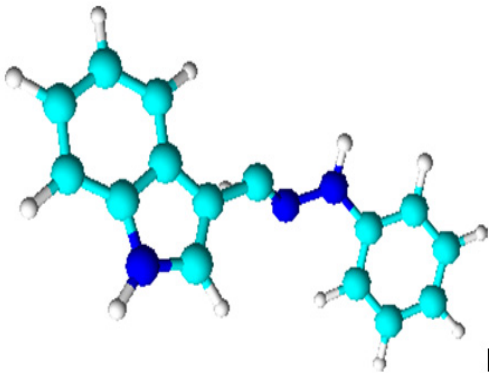

Figure 2.89 Optimized geometry of 3FIPH

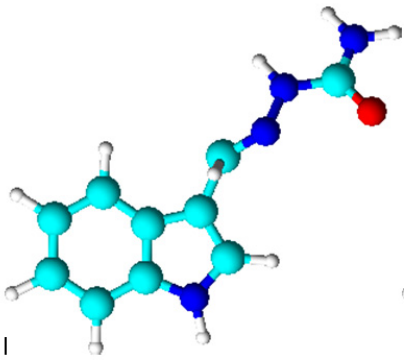

Figure 2.90 Optimized geometry of 3FISC

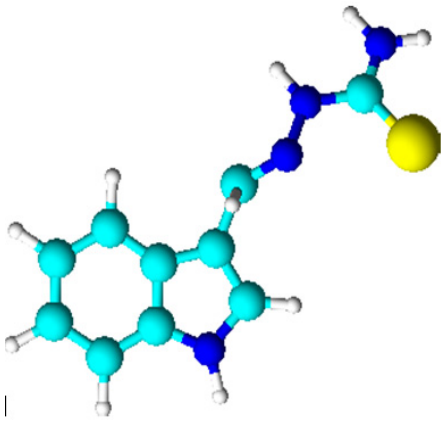

Figure 2.91 Optimized geometry of 3FITSC

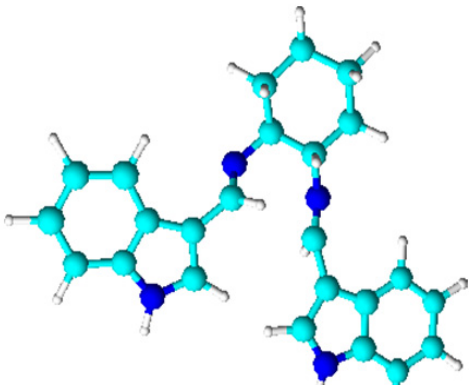

Figure 2.92 Optimized geometry of 3FIDACH

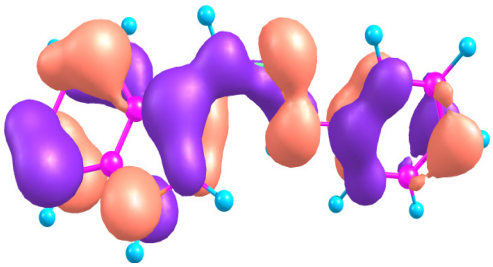

Figure 2.93 HOMO of 3FIPH

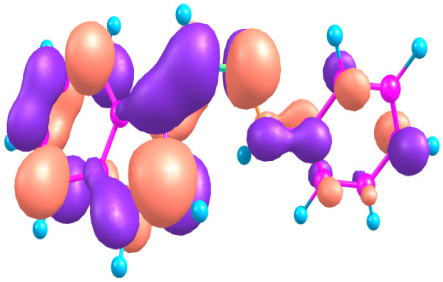

Figure 2.94 LUMO of 3FIPH

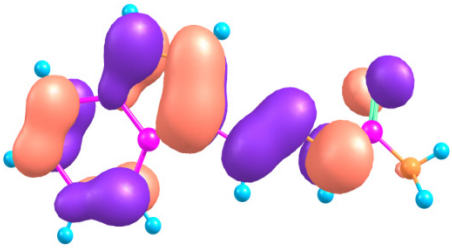

Figure 2.95 HOMO of 3FISC

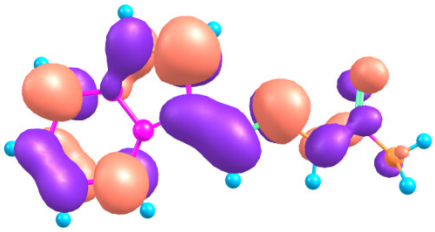

Figure 2.96 LUMO of 3FISC

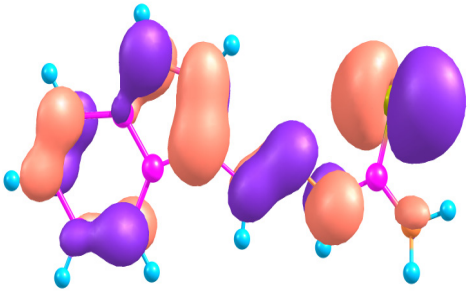

Figure 2.97 HOMO of 3FITSC

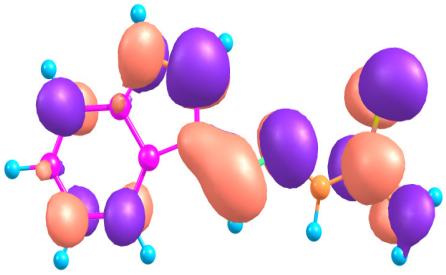

Figure 2.98 LUMO of 3FITSC

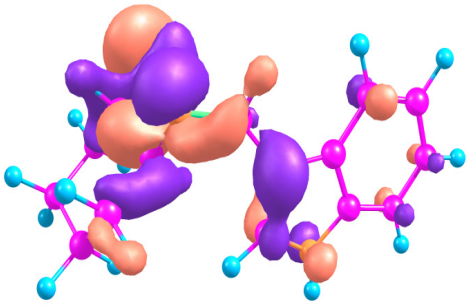

Figure 2.99 HOMO of 3FIDACH

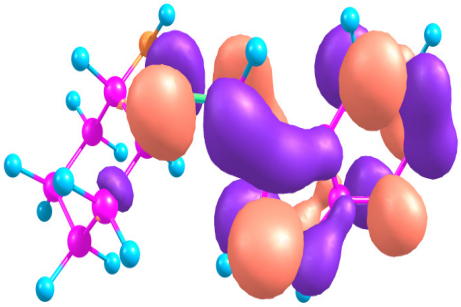

Figure 2.100 LUMO of 3FIDACH

Surface morphological studies

The morphological studies were conducted to verify the inhibition mechanism of investigated imine compounds on the CS surface, by using SEM images of steel surfaces. Figure 2.101 a, b and c represents the SEM images of bare sample, metal immersed in 1.0M HCl, and metal immersed in 1.0M HCl containing 1.0mM 3FITSC. On close examination of figures it was evident that the CS surface was highly corroded in blank HCl solution. Small cracks and pits on the bare metal surface which was generated by the surface polishing were totally disappeared due to the occurrence of severe corrosion, when the metal specimen was dipped in acid solution without inhibitors. The comparison of figures revealed that the surface damaging was appreciably decreased in the

presence of 3FITSC, and the corrosion tendency was considerably suppressed due to the formation of a protective film of 3FITSC through adsorption.

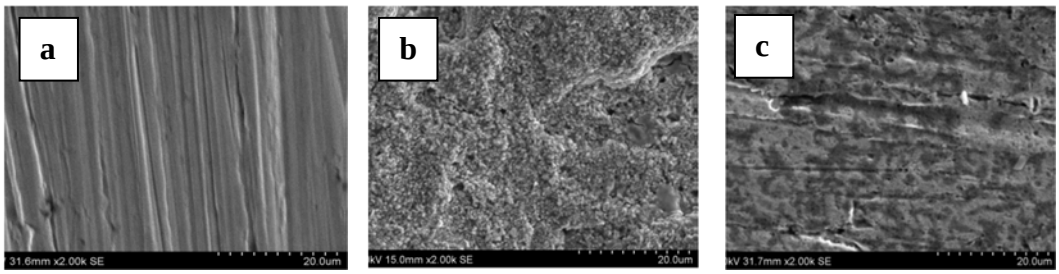

Figure 2.101 SEM images of **a)** bare metal **b)** metal immersed in 1.0M HCl **c)** metal immersed in 1.0M HCl containing 1.0mM 3FITSC

CHAPTER 4

CORROSION INHIBITION STUDIES OF HETEROCYCLIC IMINES ON CARBON STEEL IN 0.5M H_2SO_4

The corrosion inhibition nature of the imines namely pyridine-2-carbaldehyde oxime (2PCOX), pyridine-3-carbaldehyde oxime (3PCOX), pyridine-2-carbaldehyde-4-aminobenzoic acid (2PC4ABA), pyridine-2-carbaldehyde-3-aminobenzoic acid (2PC3ABA), pyridine-2-carbaldehyde-2-aminobenzoic acid (2PC2ABA), pyridine-3-carbaldehyde-3-aminobenzoic acid (3PC3ABA), pyridine-2-carbaldehyde-2-aminophenol (2PC2AP), 3-formylindole phenylhydrazone (3FIPH), 3-formylindole semicarbazone (3FISC), 3-formylindole thiosemicarbazone (3FITSC) and 3-formylindole-1,2-diaminocyclohexane (3FIDACH) were resolved on carbon steel in 0.5M H_2SO_4 by means of weight loss studies, electrochemical impedance and potentiodynamic polarization studies. Adsorption studies were used to verify the mechanism of corrosion. The SEM analysis was also examined to determine the surface behaviour of metal.

This chapter is divided into two sections; in which section I handle with corrosion inhibition studies of heterocyclic imines derived from pyridine carbaldehyde and section II narrates the corrosion inhibition studies of imines derived from 3-formylindole carbaldehyde in 0.5M H_2SO_4 medium on carbon steel.

SECTION I

CORROSION INHIBITION STUDIES OF HETEROCYCLIC IMINES DERIVED FROM PYRIDINE CARBALDEHYDE ON CARBON STEEL IN 0.5M H_2SO_4

The corrosion inhibition performance of seven heterocyclic imines derived from pyridine carbaldehyde such as 2PCOX, 3PCOX, 2PC4ABA, 2PC3ABA, 2PC2ABA, 3PC3ABA and 2PC2AP were studied in 0.5M H_2SO_4 by weight loss studies, electrochemical impedance spectroscopy and potentiodynamic polarization analysis using the inhibitor imine solutions of concentration range 0.2mM-1.0mM.

Weight loss studies

The weight loss studies of CS were conducted by immersing the metal specimens of 1cm^2 area in 0.5M H_2SO_4 for 24h in the presence and absence of imines and analyzed them to get an idea about the effect of imines on corrosion inhibition. The corrosion rate of CS in mmy^{-1} and percentage of inhibition efficiency in the presence and absence of imines were represented in the Table 2.18 and 2.19 respectively. The plots were given in the Figure 2.102 and 2.103 respectively.

From the Table 2.19 it is clear that all the studied imines behaved as potential corrosion inhibitors on CS in 0.5M H_2SO_4 and the efficiency of inhibition increased with increasing concentration of imines. The imine 2PC2ABA showed marked inhibition efficiency at all concentrations and exhibited a maximum efficiency 97% at 1.0mM concentration. 2PC2AP, 3PC3ABA and 3PCOX also exhibited very good corrosion inhibition efficiency

89%, 84%, and 80% respectively at 1.0mM concentration. 2PC3ABA and 2PC4ABA exhibited relatively poor efficiency in H_2SO_4 medium and 2PCOX showed only 31% efficiency at 1.0mM concentration. The inhibition efficiency analysis of imines follows the order 2PCOX < 2PC3ABA < 2PC4ABA < 3PCOX < 3PC3ABA < 2PC2AP< 2PC2ABA. At all concentrations, all imines except 2PC2ABA and 2PC2AP showed comparatively low corrosion inhibition efficiency in H_2SO_4 than in HCl medium.

Table 2.18 Corrosion rate of CS in the presence and absence of heterocylcic imines of pyridine carbaldehyde in 0.5M H_2SO_4

Conc (mM)	Corrosion rate (mmy^{-1})						
	2PCOX	**3PCOX**	**2PC4ABA**	**2PC3ABA**	**2PC2ABA**	**3PC3ABA**	**2PC2AP**
0	27.08	27.08	27.08	27.08	27.08	27.08	27.08
0.2	25.39	11.67	16.06	11.78	3.02	10.24	4.22
0.4	22.90	8.36	12.44	10.23	2.56	7.36	3.82
0.6	20.38	7.23	8.15	8.43	1.14	5.84	3.31
0.8	19.13	5.80	6.84	7.75	0.91	5.23	3.05
1.0	18.53	5.249	5.87	6.63	0.75	4.19	2.79

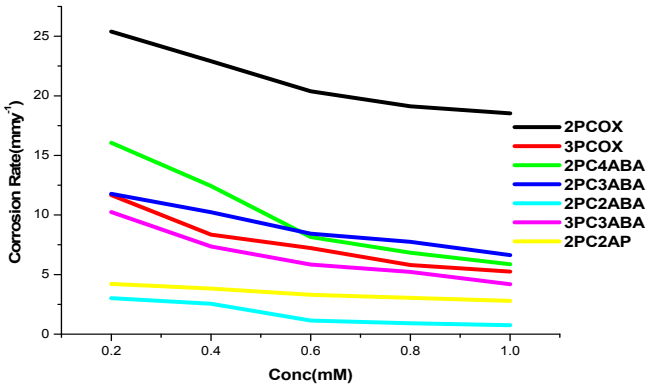

Figure 2.102 Variation of corrosion rate of heterocyclic imines of pyridine carbaldehyde on CS in 0.5M H_2SO_4

Table 2.19 Corrosion inhibition efficiencies of heterocyclic imines of pyridine carbaldehyde on CS in 0.5M H_2SO_4

Conc (mM)	Inhibition efficiency (%)						
	2PCOX	**3PCOX**	**2PC4ABA**	**2PC3ABA**	**2PC2ABA**	**3PC3ABA**	**2PC2AP**
0.2	6.26	56.90	40.69	56.49	88.84	62.19	84.42
0.4	15.45	69.10	54.06	62.22	90.54	72.82	85.89
0.6	24.73	73.30	69.90	68.87	95.79	78.43	87.78
0.8	29.38	78.57	74.74	71.38	96.64	80.69	88.74
1.0	31.57	80.61	78.32	75.52	97.23	84.52	89.69

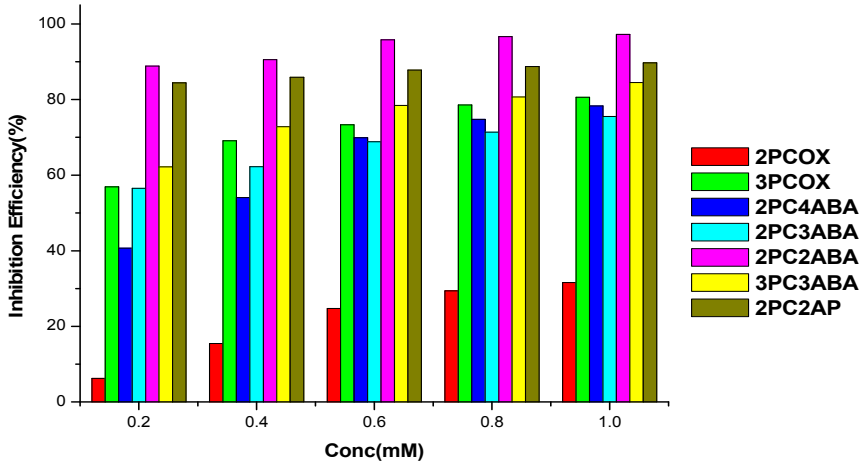

Figure 2.103 Variation of inhibition efficiencies (ηw%) of heterocyclic imines of pyridine carbaldehyde on CS in 0.5M H_2SO_4

Adsorption studies

The corrosion inhibition mechanism of imines can be established by adsorption process and the resultant modifications formed on the metal surface can be explained by plotting adsorption isotherms. The adsorption parameters are calculated by selecting most suitable isotherm assisted by the regression coefficient (R^2). The values of regression coefficient of different adsorption

isotherms tried are given in the Table 2.20. The imines 3PCOX, 2PC3ABA, 2PC4BA, 3PC3ABA and 2PC2AP satisfied Langmuir adsorption isotherm and the remaining two imines 2PCOX and 2PC4ABA obeyed Temkin and El-Awardy adsorption isotherm respectively. The calculated adsorption parameters are given in the Table 2.21 and the adsorption isotherms are represented in the Figures 2.104 to 2.110.

Table 2.20 Adsorption isotherms and the regression coefficients of heterocyclic imines of pyridine carbaldehyde on CS in 0.5M H_2SO_4

Isotherm	Regression coefficient (R^2)						
	2PCOX	3PCOX	2PC4ABA	2PC3ABA	2PC2AABA	3PC3ABA	2PC2AP
Langmiur	0.001	0.999	0.329	0.996	0.999	0.999	0.999
Freundlich	0.941	0.911	0.923	0.975	0.887	0.743	0.98
Temkin	0.988	0.991	0.98	0.980	0.916	0.905	0.977
Frumkin	0.985	0.994	0.329	0.892	0.073	0.911	0.947
El-Awady	0.978	0.994	0.981	0.97	0.907	0.992	0.964
Flory-Huggin	0.023	0.989	0.946	0.947	0.895	0.987	0.959

Table 2.21 Adsorption parameters of heterocyclic imines of pyridine carbaldehyde on CS in 0.5M H_2SO_4

Adsorption Parameter	2PCOX	3PCOX	2PC4ABA	2PC3ABA	2PC2ABA	3PC3ABA	2PC2AP
K_{ads}	28.78	7142	3915	7299	31152	8849	43497
ΔG^0_{ads} (kJ/mol)	-18.46	-32.26	-30.75	-32.31	-35.94	-32.79	-36.78

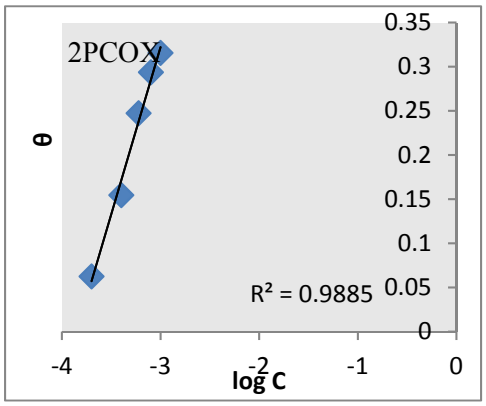

Figure 2.104 Temkin isotherm for 2PCOX on CS in 0.5M H_2SO_4

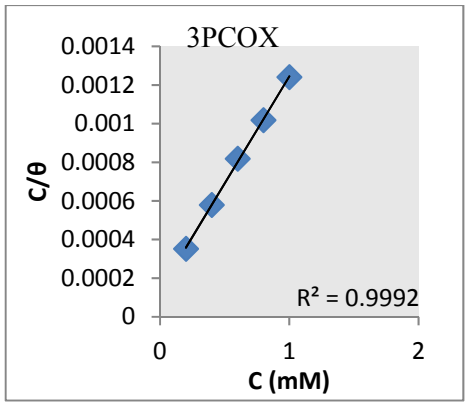

Figure 2.105 Langmuir isotherm for 3PCOX on CS in 0.5M H_2SO_4

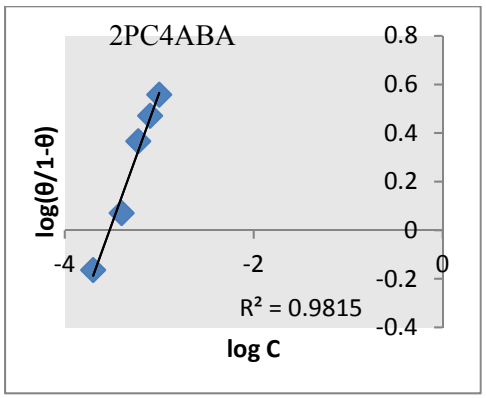

Figure 2.106 El-Awady isotherm for 2PC4ABA on CS in 0.5M H_2SO_4

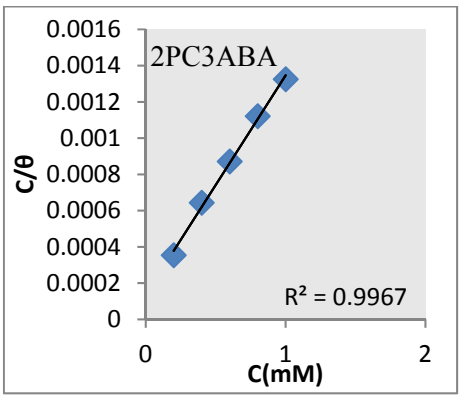

Figure 2.107 Langmuir isotherm for 2PC3ABA on CS in 0.5M H_2SO_4

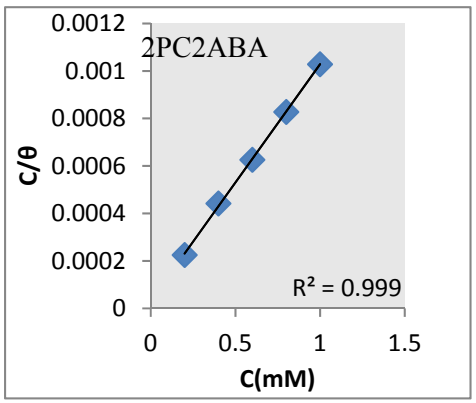

Figure 2.108 Langmuir isotherm for 2PC2ABA on CS in 0.5M H_2SO_4

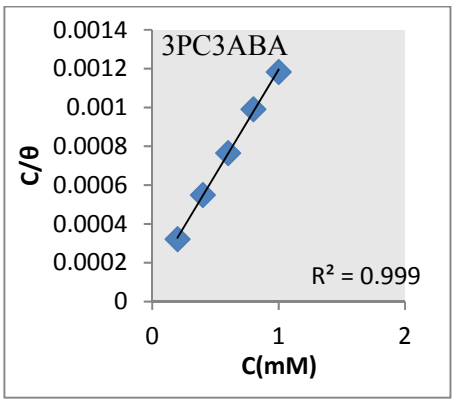

Figure 2.109 Langmuir isotherm for 3PC3ABA on CS in 0.5M H_2SO_4

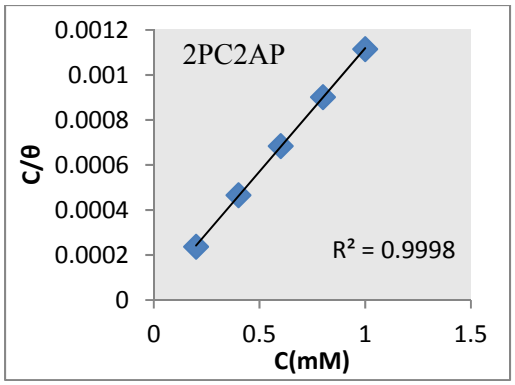

Figure 2.110 Langmuir isotherm for 2PC2AP on CS in 0.5M H_2SO_4

The imines 2PC2AP and 2PC2ABA possess high K_{ads} value compared to the other imines suggesting that they adsorbed so effectively on the surface of CS and formed an effective protective layer on the surface of metal. The free energy of adsorption value of 2PC2AP and 2PC2ABA were -36.78 $kJmol^{-1}$ and -35.94 $kJmol^{-1}$ respectively. All the imines had negative value of free energy that denotes the spontaneous adsorption process shown by the molecule. The ΔG^0_{ads} for 2PCOX was -18.46 $kJmol^{-1}$ that indicated the adsorption of this imine was mainly electrostatic in nature; the K_{ads} value for this imine was very low, for the week interaction occurred on the CS surface by the imine. All the other remaining imines showed the interaction on the metal surfaces by both physisorption and chemisorptions. It can be concluded that generally all studied imines effectively hindered the dissolution of metal by providing a protection barrier on the surface of metal.

Electrochemical studies

The electrochemical corrosion investigations on imine derivatives of pyridine carbaldehyde were carried out using a three electrode assembly, in which calomel electrode, platinum electrode and metal specimen CS having area 1cm^2 were used as reference electrode, counter electrode and working electrode respectively. The electrochemical investigations including electrochemical impedance and potentiodynamic polarization studies were conducted by Ivium compactstat-e-electrochemical system.

Electrochemical impedance spectroscopy (EIS) studies

Electrochemical impedance studies were conducted in the frequency ranging from 1KHz to 100mHz with amplitude of 10mV as excitation signals. The constant potential (OCP) was maintained throughout the experiment. The different concentrations of imines were prepared for performing electrochemical impedance studies on CS in 0.5M H_2SO_4. The Nyquist and Bode plots obtained from EIS studies of seven imine compounds displayed in the Figures 2.111 to 2.117 and the data from the plots such as charge transfer resistance (R_{ct}) and double layer capacitance (C_{dl}) are depicted in the Table 2.22. The inhibition efficiency was calculated using following equation.

$$\eta_{EIS}\% = \frac{R_{ct} - R'_{ct}}{R_{ct}} \times 100$$

where R_{ct} and R'_{ct} are the charge transfer resistances of working electrode with and without inhibitor respectively. Impedance parameters calculated implies that the compounds which reduce the transfer of charge/ dissolution of metal can

Table 2.22 Electrochemical impedance parameters of CS in the presence and absence of heterocyclic imines of pyridine carbaldehyde in 0.5M H_2SO_4

Imines	Conc (mM)	C_{dl} ($\mu F\ cm^{-2}$)	R_{ct} (Ωcm^2)	η_{EIS} (%)
	0	73.4	12.52	-
2PCOX	0.2	95.6	13.21	5.22
	0.4	93.6	13.92	10.06
	0.6	81.3	15.74	20.46
	0.8	76.1	15.87	21.11
	1.0	75.5	18.75	33.23
3PCOX	0.2	73.2	22.91	45.35
	0.4	63.3	32.34	61.29
	0.6	61.2	38.75	67.69
	0.8	45.5	44.88	72.10
	1.0	47.4	48.87	74.38
2PC4ABA	0.2	84.2	18.88	33.69
	0.4	83.5	23.59	46.93
	0.6	88.6	24.72	49.35
	0.8	76.4	25.10	50.12
	1.0	74.4	25.21	50.34
2PC3ABA	0.2	88.4	37.73	66.82
	0.4	79.5	39.44	68.26
	0.6	73.0	46.64	73.16
	0.8	71.4	50.14	75.03
	1.0	51.9	55.98	77.63
2PC2ABA	0.2	71.3	149.7	91.64
	0.4	59.5	167.9	92.54
	0.6	54.2	271.8	95.39
	0.8	54.1	283.4	95.58
	1.0	52.3	362.5	96.55
3PC3ABA	0.2	90.2	25.52	50.94
	0.4	85.9	47.26	73.51
	0.6	77.6	49.06	74.48
	0.8	52.3	52.51	76.16
	1.0	45.1	56.35	77.78
2PC2AP	0.2	95.2	138.4	90.95
	0.4	63.4	144.7	91.35
	0.6	55.5	199.3	93.72
	0.8	41.2	217.4	94.24
	1.0	39.1	221.2	94.34

effectively prevent the metal corrosion. Generally organic inhibitors displayed relatively poor corrosion inhibition efficiency in H_2SO_4 medium, and it was already confirmed by many researchers. On analyzing the data in Table 2.22 the imines 2PC2ABA and 2PC2AP showed above 90% inhibition efficiency at all concentrations and a maximum efficiency of 96% and 94% respectively were exhibited at 1.0mM concentration whereas 2PC3ABA, 3PC3ABA and 3PCOX showed only moderate inhibition efficiency at higher concentration.

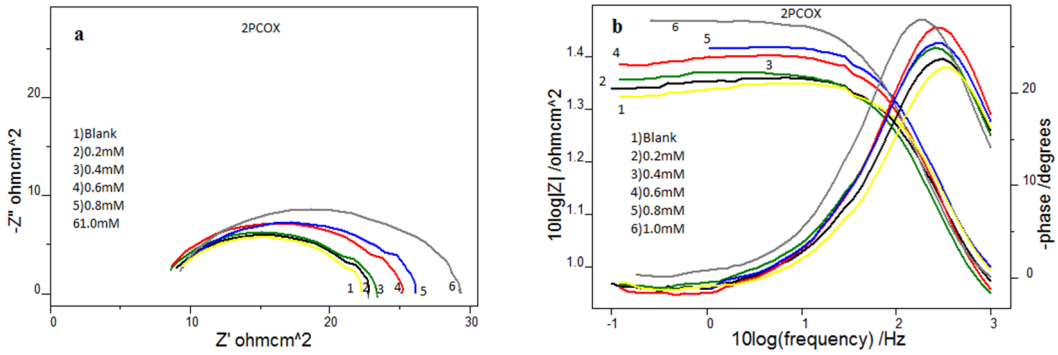

Figure 2.111 a) Nyquist plots and **b)** Bode plots of CS in the presence and absence of 2PCOX in 0.5M H_2SO_4

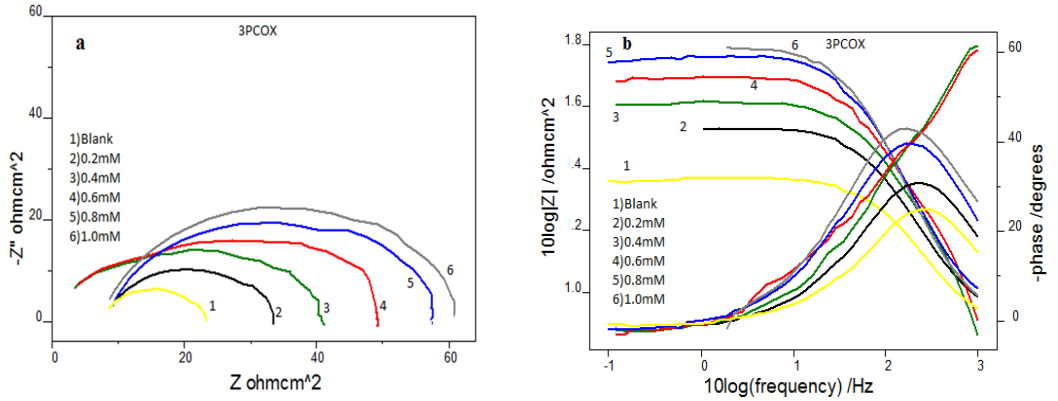

Figure 2.112 a) Nyquist plots and **b)** Bode plots of CS in the presence and absence of 3PCOX in 0.5M H_2SO_4

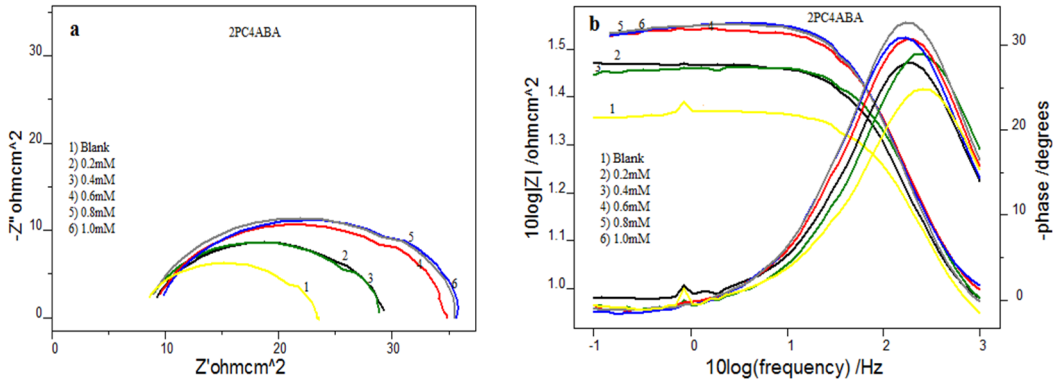

Figure 2.113 a) Nyquist plots and **b)** Bode plots of CS in the presence and absence of 2PC4ABA in 0.5M H_2SO_4

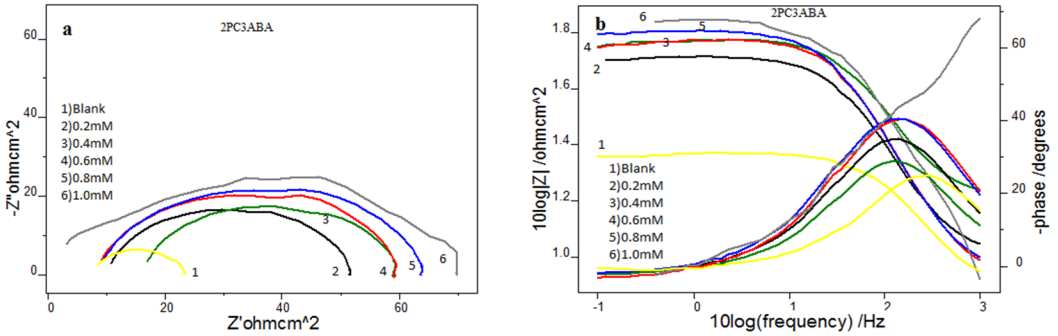

Figure 2.114 a) Nyquist plots and **b)** Bode plots of CS in the presence and absence of 2PC3ABA in 0.5M H_2SO_4

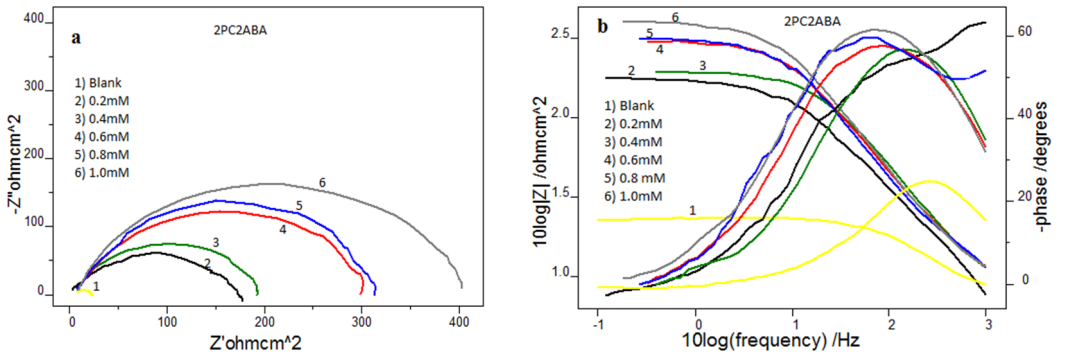

Figure 2.115 a) Nyquist plots and **b)** Bode plots of CS in the presence and absence of 2PC2ABA in 0.5M H_2SO_4.

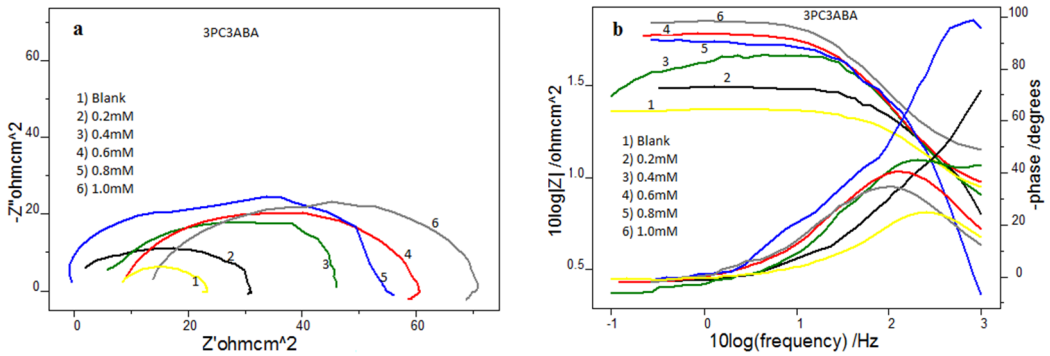

Figure 2.116 a) Nyquist plots and **b)** Bode plots of CS in the presence and absence of 3PC3ABA in 0.5M H_2SO_4

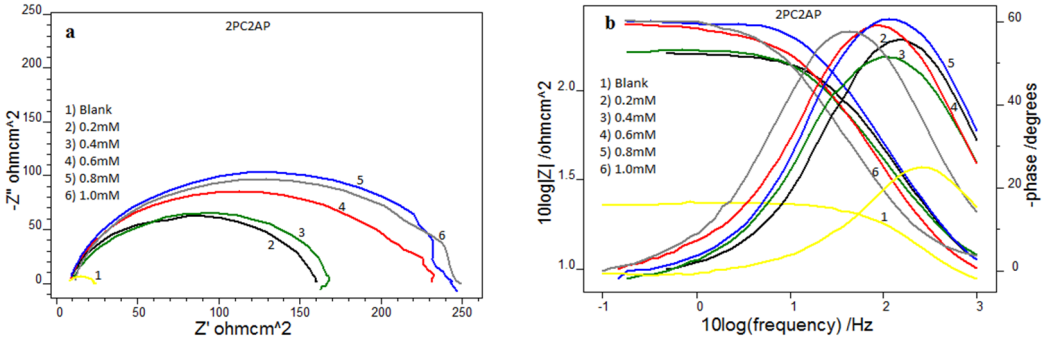

Figure 2.117 a) Nyquist plots and **b)** Bode plots of CS in the presence and absence of 2PC2AP in 0.5M H_2SO_4.

On comparing with other imines, 2PCOX acted as a poor corrosion inhibitor and attained efficiency of 33% only at maximum concentration 1.0mM. The comparisons of the inhibition efficiencies of imines on CS in 0.5M H_2SO_4 was represented in the Figure 2.118.The results obtained from the EIS studies revealed that the inhibition efficiency of imines on CS in 0.5M H_2SO_4 was comparatively higher than the gravimetric studies. This trend can be explained by the fact that the electrochemical analysis is a quick corrosion monitoring technique whereas in gravimetric analysis the compounds have a tendency to hydrolyze into parent amine by the prolonged treatment (24h) in acid.

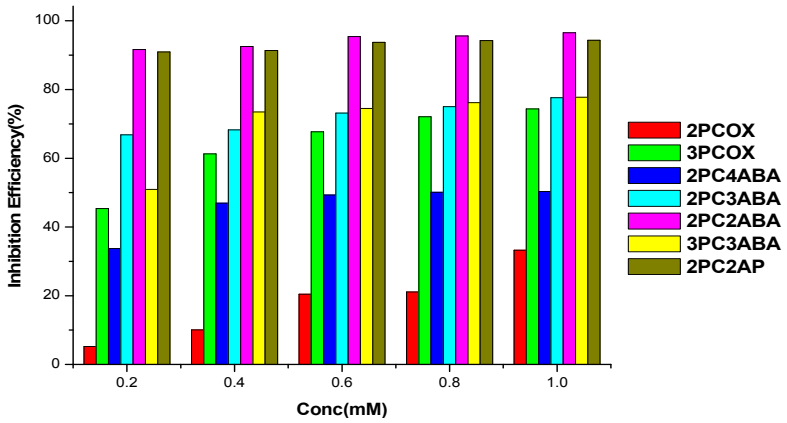

Figure 2.118 Variation of corrosion inhibition efficiencies ($\eta_{EIS}\%$) of heterocyclic imines of pyridine carbaldehyde on CS in 0.5M H_2SO_4.

Potentiodynamic polarization studies

The polarization study of imines on CS was conducted by Tafel extrapolation and linear polarization technique. The inhibition efficiency was calculated using corrosion current density (I_{corr}) and polarization resistance (R_p) by following relations.

$$\eta_{pol}\% = \frac{I_{corr} - I\prime_{corr}}{I_{corr}} \times 100 \qquad \eta_{Rp}\% = \frac{R\prime p - Rp}{R\prime p} \times 100$$

where I_{corr} and I'_{corr} are the corrosion current density of the expressed area of the working electrode in the absence and presence of inhibitor. The polarization plots were obtained in the electrode potential range of -250 to +250 mV vs equilibrium potential at a sweep rate of 1mV/sec. R'_p and R_p are the polarization resistances in the presence and absence of inhibitor respectively. The polarization data of imines was depicted in the Table 2.23. The Figures 2.119 to 2.125 represent the Tafel and linear polarization plots of the seven imine compounds on CS in 0.5M H_2SO_4.

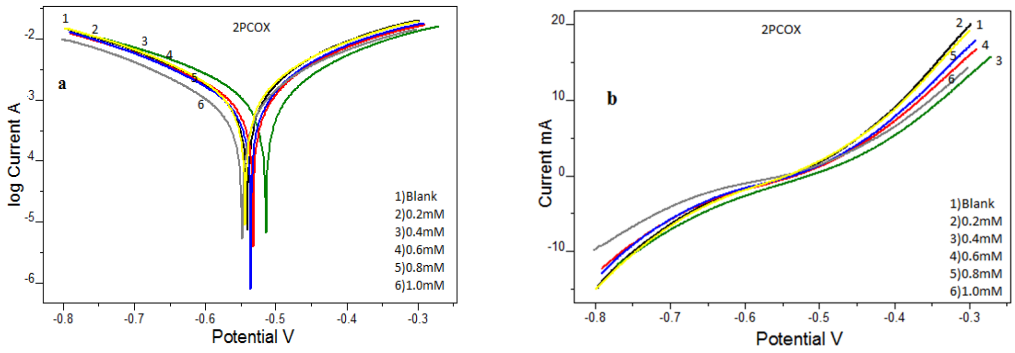

Figure 2.119 a) Tafel plots and **b)** Linear polarization plots of CS in the presence and absence of 2PCOX in 0.5M H_2SO_4.

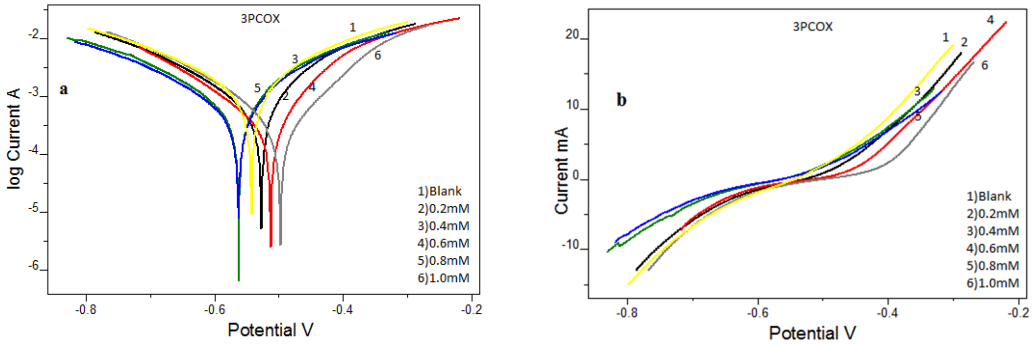

Figure 2.120 a) Tafel plots and **b)** Linear polarization plots of CS in the presence and absence of 3PCOX in 0.5M H_2SO_4.

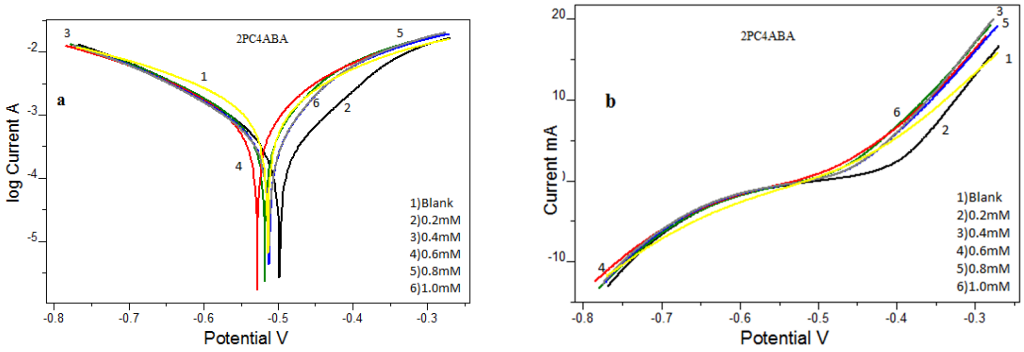

Figure 2.121 a) Tafel plots and **b)** Linear polarization plots of CS in the presence and absence of 2PC4ABA in 0.5M H_2SO_4.

Table 2.23 Potentiodynamic polarization parameters of CS in the presence and absence of heterocyclic imines of pyridine carbaldehyde in 0.5M H_2SO_4

Imine	Tafel Data					Polarization Data		
	Conc (mM)	$-E_{corr}$ (mV/SCE)	I_{corr} ($\mu A/cm^2$)	b_a (mV/dec)	$-b_c$ (mV/dec)	η_{pol} (%)	Rp (ohm)	η_{Rp} (%)
	0	559	1488	209	217		26.0	
2PCOX	0.2	563	1422	206	210	4.4	28.2	7.92
	0.4	522	1327	206	240	10.8	31.4	17.07
	0.6	556	1252	209	215	15.8	30.9	15.70
	0.8	562	1232	206	206	17.2	32.4	19.51
	1.0	572	930	207	199	37.5	42.9	39.29
3PCOX	0.2	561	1030	198	184	30.7	42.6	38.84
	0.4	582	890	196	201	40.1	46.9	44.57
	0.6	577	829	218	139	44.2	73.7	64.68
	0.8	586	695	194	196	53.2	51.2	49.14
	1.0	485	400	110	173	73.1	81.3	67.96
2PC4ABA	0.2	549	1070	193	172	28.0	38.9	33.00
	0.4	546	1030	185	144	30.7	43.4	40.01
	0.6	546	960	187	132	35.4	45.7	43.04
	0.8	546	840	177	146	43.5	55.9	53.38
	1.0	542	780	165	134	47.5	57.1	54.38
2PC3ABA	0.2	515	619	194	156	44.5	77.1	66.22
	0.4	581	776	195	175	47.8	63.9	59.28
	0.6	571	711	177	174	52.2	61.1	57.39
	0.8	550	670	177	157	54.9	71.4	63.54
	1.0	552	609	188	181	59.0	72.6	64.14
2PC2ABA	0.2	607	635	211	128	57.3	163.0	84.02
	0.4	574	484	194	134	67.4	145.8	82.14
	0.6	507	284	170	116	80.9	157.8	83.50
	0.8	557	258	150	125	82.6	332.0	92.16
	1.0	486	92	78	138	93.8	249.3	89.55
3PC3ABA	0.2	550	1050	197	200	29.4	38.9	33.04
	0.4	562	720	177	167	51.6	66.4	60.77
	0.6	564	670	180	158	54.9	97.2	73.20
	0.8	551	610	180	161	59.0	79.7	67.33
	1.0	558	260	107	143	82.5	154.4	83.13
2PC2AP	0.2	575	489	184	132	56.2	196.2	86.73
	0.4	582	583	206	137	60.8	148.0	82.41
	0.6	588	502	194	128	66.2	227.4	88.55
	0.8	551	377	164	144	74.6	173.4	84.98
	1.0	572	198	137	134	86.6	267.9	90.27

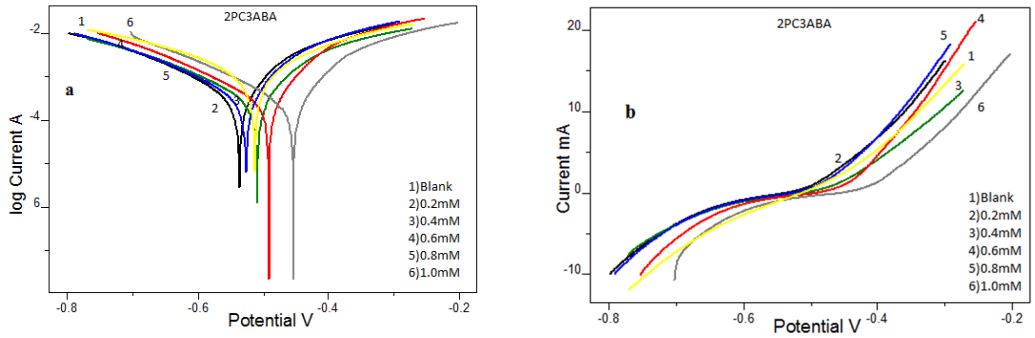

Figure 2.122 a) Tafel plots and **b)** Linear polarization plots of CS in the presence and absence of 2PC3ABA in 0.5M H_2SO_4.

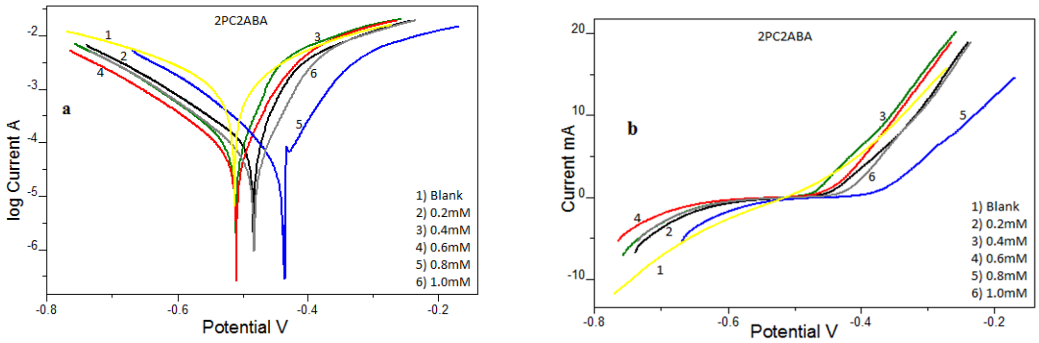

Figure 2.123 a) Tafel plots and **b)** Linear polarization plots of CS in the presence and absence of 2PC2ABA in 0.5M H_2SO_4.

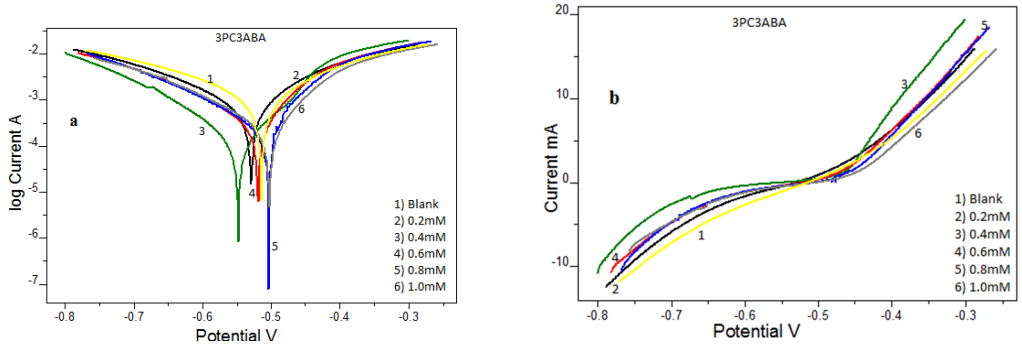

Figure 2.124 a) Tafel plots and **b)** Linear polarization plots of CS in the presence and absence of 3PC3ABA in 0.5M H_2SO_4.

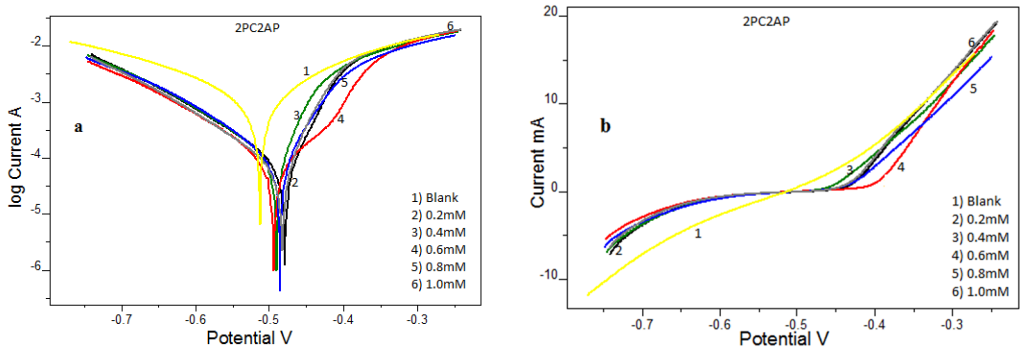

Figure 2.125 Tafel plots and **b)** Linear polarization plots of CS in the presence and absence of 2PC2AP in 0.5M H_2SO_4.

From the table it was easily understood that the corrosion current density (I_{corr}) decreased with increasing concentration of imines. The imine 2PC2ABA displayed the low corrosion current density as compared to other imines and a maximum efficiency 93% was achieved at 1.0mM concentration. The imines 3PC3ABA and 2PC2AP showed better efficiency of 82.5% and 86% respectively and 2PC2ABA and 2PC2AP showed comparable inhibition efficiency at lower concentration.

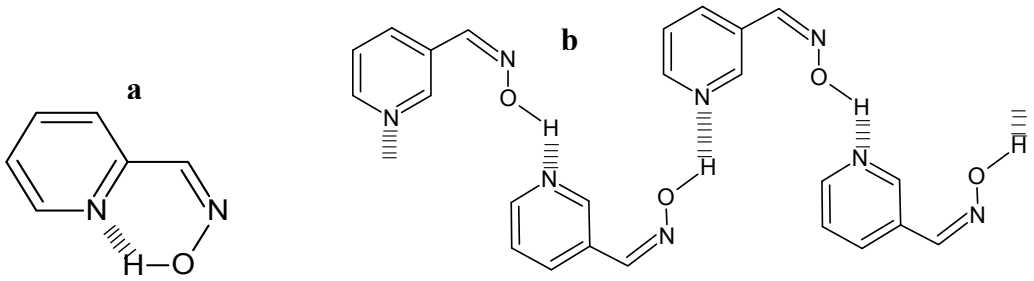

Figure 2.126 a) Intramolecular H-bond in 2PCOX **b**) intermolecular H-bond in 3PCOX

On comparing the efficiency of oximes, the 3PCOX showed better efficiency than 2PCOX and showed 73% efficiency at maximum concentration 1.0mM, while 2PCOX showed only 37%. It can be attributed by the presence of

intramolecular H-bonding in 2PCOX depicted in the Figure 2.126 and it was well explained in the previous chapter.

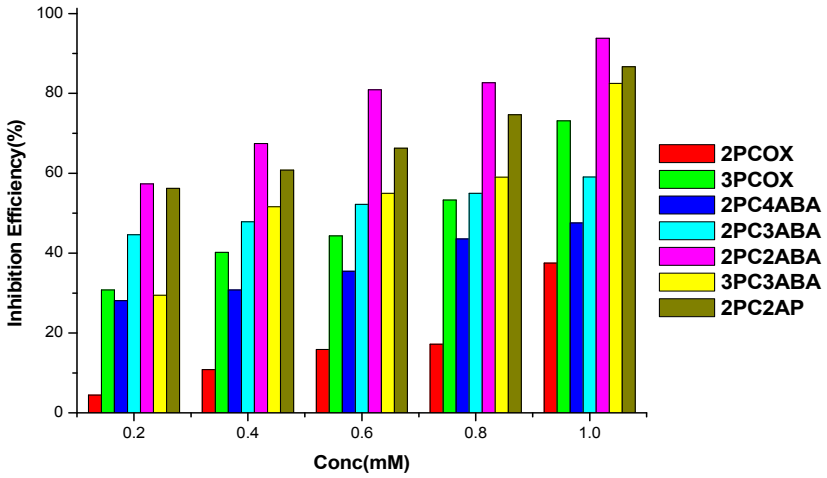

Figure 2.127 Variation of corrosion inhibition efficiencies (η_{pol}%) of heterocyclic imines of pyridine carbaldehyde on CS in 0.5M H_2SO_4

The slope analysis of Tafel lines revealed that for 2PCOX, the anodic slopes were not changed appreciably which confirmed the cathodic inhibitor nature of the imine. All other imines displayed considerable variation in both anodic and cathodic slopes suggesting that these imines act as mixed type inhibitors. The corrosion inhibition efficiency observed for imines follows the order 2PC2ABA> 2PC2AP> 3PC3ABA> 3PCOX> 2PC3ABA> 2PC4ABA> 2PCOX. The comparison of inhibition efficiencies of these seven imines is displayed in the Figure 2.127.

Surface morphological studies

The mechanism of inhibition of investigated imines on CS surface was confirmed by surface morphological studies which were performed by taking SEM images of steel surfaces. From the analysis of the SEM images 2.128 a) bare

sample b) metal immersed in 0.5M H_2SO_4 c) metal immersed in 0.5M H_2SO_4 containing 1.0mM 2PC2AP. It was evident that the carbon steel surface was highly damaged by corrosion in blank H_2SO_4 solution. In the absence of imine 2PC2AP, the corrosion leads to the disappearance of cracks and pits formed by the surface polishing on the bare metal surface. On close examination of the figures it was established that the surface was clearer as bare in the presence of imine, which confirmed the suppression of corrosion tendency of CS by the formation of a protective film of imine inhibitor through adsorption on the surface.

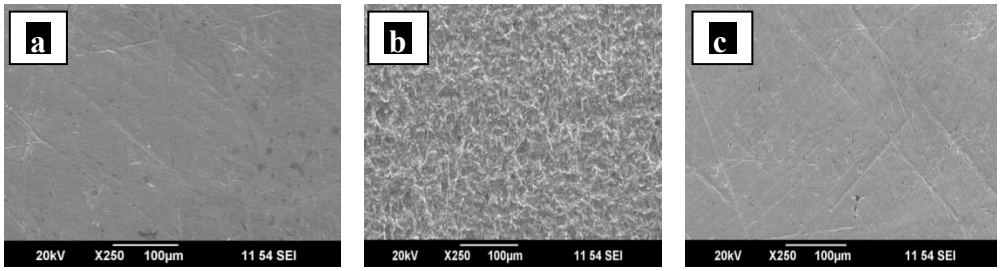

Figure 2.128 SEM images of **a)** bare metal **b)** metal immersed in 0.5M H_2SO_4 **c)** metal immersed in 0.5M H_2SO_4 containing 1.0mM 2PC2AP

SECTION II

CORROSION INHIBITION STUDIES OF HETEROCYCLIC IMINES DERIVED FROM 3-FORMYLINDOLE CARBALDEHYDE ON CARBON STEEL IN 0.5M H_2SO_4

The detailed study of corrosion inhibition capacity of imines derivatives of 3-formylindole carbaldehyde namely 3FIPH, 3FISC, 3FITSC and 3FIDACH on carbon steel in 0.5M H_2SO_4 are well presented in this section. Different methods such as weight loss measurements, adsorption studies, electrochemical methods like electrochemical impedance measurements and potentiodynamic polarization studies were employed for the investigations on anticorrosion activity of imines.

Weight loss studies

The weight loss studies of CS were conducted by immersing the metal specimens of $1cm^2$ area in 0.5M H_2SO_4 for 24h in the presence and absence of imines and analyzed them to get an idea about the effect of imines on corrosion inhibition. The corrosion rate of CS in mmy^{-1} and percentage of inhibition efficiency in the presence and absence of imines were represented in the Table 2.24 and 2.25 respectively. Similarly the rate of corrosion and percentage of inhibition efficiencies are graphically represented in the Figures 2.129 and 2.130 respectively.

From the Tables and Figures it is quite evident that the corrosion rate of CS decreased considerably in the presence of all the four imines and showed a gradual increase in the inhibition efficiency with increased imine concentration. A prominent decrease in the corrosion rate was noticed for 3FIDACH and

3FITSC and they showed the corrosion rate of 3.45mmy^{-1} and 1.42mmy^{-1} respectively at 1.0mM concentration.

Table 2.24 Corrosion rate of CS in the presence and absence of heterocylcic imines of 3-formylindole carbaldehyde in 0.5M H_2SO_4

Conc (mM)	Corrosion rate (mmy^{-1})			
	3FIPH	3FISC	3FITSC	3FIDACH
0	27.08	27.08	27.08	27.08
0.2	19.07	10.34	7.61	7.63
0.4	16.65	9.26	6.45	5.86
0.6	13.34	8.23	4.30	4.07
0.8	12.26	6.39	2.78	3.76
1.0	11.00	4.56	1.42	3.45

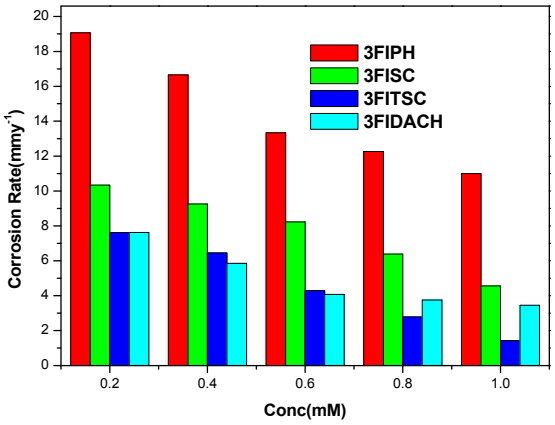

Figure 2.129 Variation of corrosion rate of heterocyclic imines of 3-formylindole carbaldehyde on CS in 0.5M H_2SO_4

The analysis of corrosion inhibition efficiency tabulated in the Table 2.26 revealed that all the imines displayed above 80% efficiency at 1.0mM concentration and in which 3FITSC achieved the highest inhibition efficiency 94.74%. In addition to the presence of nitrogen atom and the highly delocalized л electrons present on the aromatic ring, the enhanced efficiency of 3FITSC can be attributed to the presence of highly polarizable sulphur atom. The imines

3FISC and 3FIDACH also showed high corrosion inhibition efficiency of 83.17% and 87.24% respectively at maximum concentration. Even at lower concentration (0.2mM) 3FITSC and 3FIDACH showed fair inhibition efficiency of 71% while 3FISC exhibited relatively moderate efficiency 61.81% in the same concentration. Among these four imines, 3FIPH was found to possess comparatively weak inhibition efficiency even at 1.0mM concentration (59.37%). Comparison of inhibition efficiencies of imines on CS in 0.5M H_2SO_4 is represented in the Figure 2.130.

Table 2.25 Inhibition efficiencies of heterocyclic imines of 3-formylindole carbaldehyde on CS in 0.5M H_2SO_4

Conc (mM)	Inhibition efficiency (%)			
	3FIPH	3FISC	3FITSC	3FIDACH
0.2	29.58	61.81	71.90	71.81
0.4	38.52	65.82	76.18	78.35
0.6	50.74	69.61	84.11	84.96
0.8	54.73	76.39	89.72	86.13
1.0	59.37	83.17	94.74	87.24

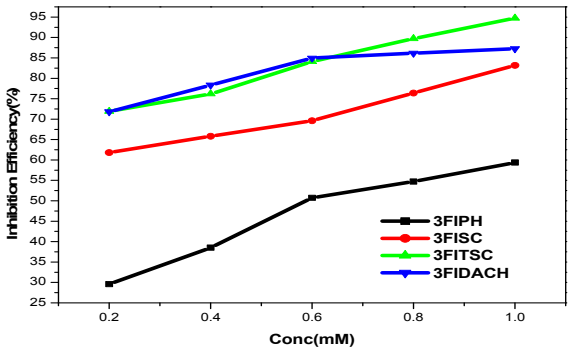

Figure 2.130 Variation of inhibition efficiencies (η_w%) of heterocyclic imines of 3-formylindole carbaldehyde on CS in 0.5M H_2SO_4

Adsorption studies

The mechanism of interaction of the imines on CS was verified by means of adsorption isotherms. The best fit isotherm model was selected and represented in the Table 2.26 by the evaluation of regression coefficient. The isotherm satisfied the imines were exhibited in the Figures 2.131 to 2.134. The Langmuir adsorption isotherm was suitable for the imines 3FISC and 3FITSC while 3FIPH and 3FIDACH were followed El-awady adsorption isotherm. The imine 3FIPH displayed poor corrosion inhibition efficiency on CS, exhibited low value of adsorption equilibrium constants and displayed low free energy of adsorption (Table 2.27).

Table 2.26 Adsorption isotherms and regression coefficients of heterocyclic imines of 3-formylindole carbaldehyde on CS in 0.5M H_2SO_4

	Regression coefficient (R^2)			
Isotherm	3FIPH	3FISC	3FITSC	3FIDACH
Langmiur	0.871	0.984	0.993	0.878
Freundlich	0.955	0.980	0.992	0.878
Temkin	0.978	0.873	0.936	0.970
Frumkin	0.655	0.258	0.242	0.805
El-Awady	0.982	0.827	0.856	0.973
Flory-Huggin	0.937	0.736	0.786	0.964

Table 2.27 Adsorption parameters of heterocyclic imines of 3-formylindole carbaldehyde on CS in 0.5M H_2SO_4

Adsorption parmeter	3FIPH	3FISC	3FITSC	3FIDACH
K_{ads}	1607	6711	8620	20741
ΔG^0_{ads} (kJ/mol)	-28.53	-32.1	-32.73	-34.93

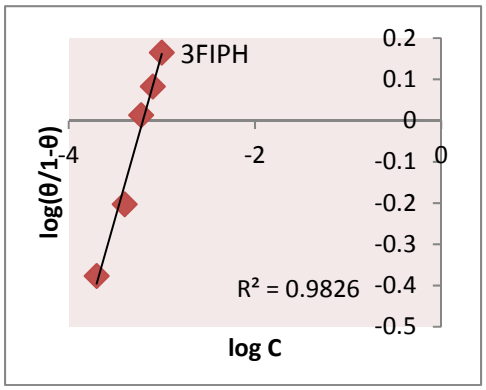

Figure 2.131 El-Awady isotherm for 3FIPH on CS in 0.5M H_2SO_4

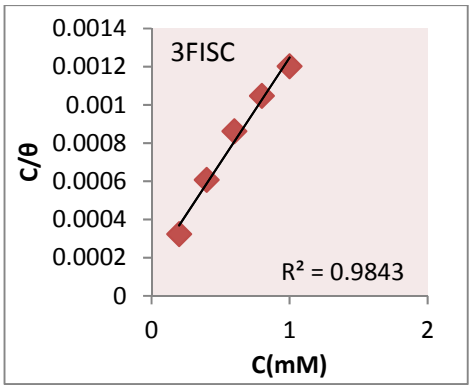

Figure 2.132 Langmuir isotherm for 3FISC on CS in 0.5M H_2SO_4

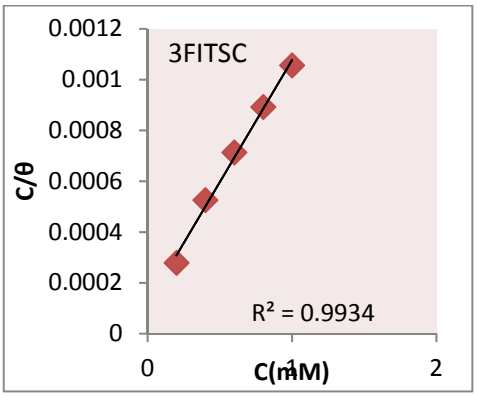

Figure 2.133 Langmuir isotherm for 3FITSC on CS in 0.5M H_2SO_4

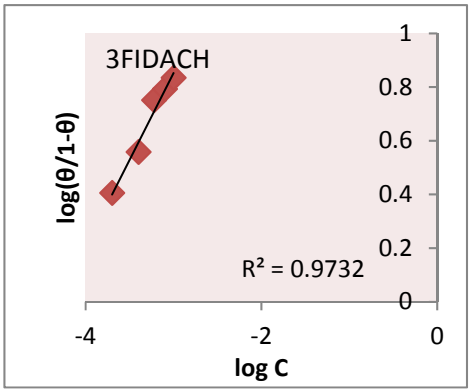

Figure 2.134 El-Awady isotherm for 3FIDACH on CS in 0.5M H_2SO_4

From the Table 2.27 it is evident that the free energy for all the four imine molecules lies between -28.53kJmol^{-1} and -34.93kJmol^{-1}, indicating the involvement of both physisorption and chemisorptions process during the monolayer formation of inhibitor on the CS surface. The negative value for ΔG^0_{ads}, indicated the spontaneity of the reaction. The imine 3FIPH displayed very low value of adsorption equilibrium constant, which establishes the possibility of multilayer adsorption of the molecule on the surface of metal. The imines 3FISC,

3FITSC and 3FIDACH exhibited high values of K_{ads} and ΔG^0_{ads} implied that monolayer of the protective molecules formed on the surface mainly through chemical interaction. Even if the rate of corrosion of CS in sulphuric acid was very high, these molecules are capable for making a good protection barrier against the dissolution of Fe atoms.

Electrochemical studies

The electrochemical analysis including impedance studies and Tafel polarization studies is quick, accurate and reliable procedure to predict the corrosion inhibition capacity of molecules. The analysis was conducted using four indole based imine derivatives such as 3FIPH, 3FISC, 3FITSC and 3FIDACH on CS in 0.5M H_2SO_4. The Ivium compactstat-e-electrochemical system was employed for conducting the experiments. In the three electrode assembly, saturated calomel electrode (SCE) was used as the reference electrode. Platinum electrode having $1cm^2$ area was taken as counter electrode. Metal specimens with an exposed area of $1cm^2$ in acidic solution were used as the working electrode.

Electrochemical impedance spectroscopy (EIS) studies

In the electrochemical impedance study, the working area of the metal specimens was exposed to the electrolyte for 1 hour prior to recording the measurement. Constant potential (OCP) was maintained in all measurements and a frequency range of 1KHz to 100mHz with amplitude of 10 mV as excitation signal was employed. The percentage of inhibitions from impedance measurements were calculated by the following expression

$$\eta_{EIS}\,\% = \frac{R_{ct} - R'_{ct}}{R_{ct}}\ X100$$

where R_{ct} and R'_{ct} are the charge transfer resistances of working electrode with and without inhibitor respectively.

From the analysis of Nyquist plots and Bode plots (Figures 2.135 to 2.138) for CS specimens, it was evident that the impedance response of metal specimens showed a marked difference in the presence and absence of the imines. The slight irregularities observed in the semicircles may be attributed to the roughness or non homogeneous nature of the metal surface. The Randles equivalent circuit that fit to many electrochemical system is composed of a double layer capacitance, R_s and R_{ct}. To reduce the effects due to surface irregularities of metal, constant phase element (CPE) is introduced into the circuit instead of a pure double layer capacitance which gives more accurate fit.

The EIS parameters such as R_{ct} and CPE and the calculated values of percentage of inhibition efficiency (η_{EIS}%) of imines for CS specimens are listed in the Table 2.28. It was evident from the data that R_{ct} values were increased with increasing inhibitor concentration. The value of R_{ct} is a measure of electron transfer across the exposed area of the metal surface and it is inversely proportional to the rate of corrosion. Decrease in capacitance values C_{dl} with inhibitor concentration can be attributed to the decrease in local dielectric constant and increase in the thickness of the electrical double layer. This emphasized the action of inhibitor molecules at the metal–solution interface by adsorption. The percentage of inhibition (η_{EIS}%) showed a regular increase with increase in inhibitor concentration.

Table 2.28 Electrochemical impedance parameters of CS in the presence and absence of heterocyclic imines of 3-formylindole carbaldehyde in 0.5M H_2SO_4

Imines	Conc (mM)	C_{dl} ($\mu F\ cm^{-2}$)	R_{ct} (Ωcm^2)	η_{EIS} (%)
	0	73	12.52	-
	0.2	84	18.8	33.65
3FIPH	0.4	80	19.5	36.06
	0.6	72	19.8	36.80
	0.8	71	20.9	40.27
	1.0	68	26.9	53.58
	0.2	58	56.9	77.99
3FISC	0.4	48	65.0	80.74
	0.6	38	87.6	85.72
	0.8	42	90.0	86.09
	1.0	26	190.1	93.41
	0.2	73	63.2	80.20
	0.4	60	92.3	86.44
3FITSC	0.6	29	437.5	97.14
	0.8	25	616.9	97.97
	1.0	25	855.3	98.54
	0.2	34	220.8	94.33
	0.4	28	384.2	96.74
3FIDACH	0.6	30	465.1	97.31
	0.8	24	526.6	97.62
	1.0	24	720.4	98.26

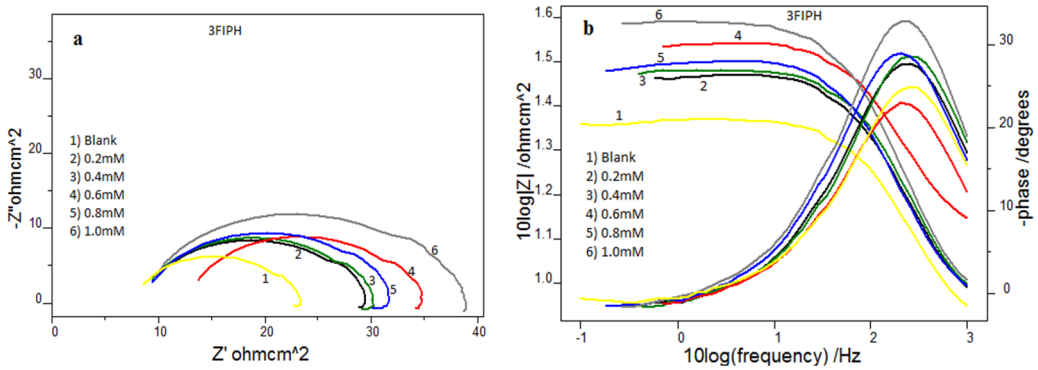

Figure 2.135 a) Nyquist plots and **b)** Bode plots of CS in the presence and absence of 3FIPH in 0.5M H_2SO_4

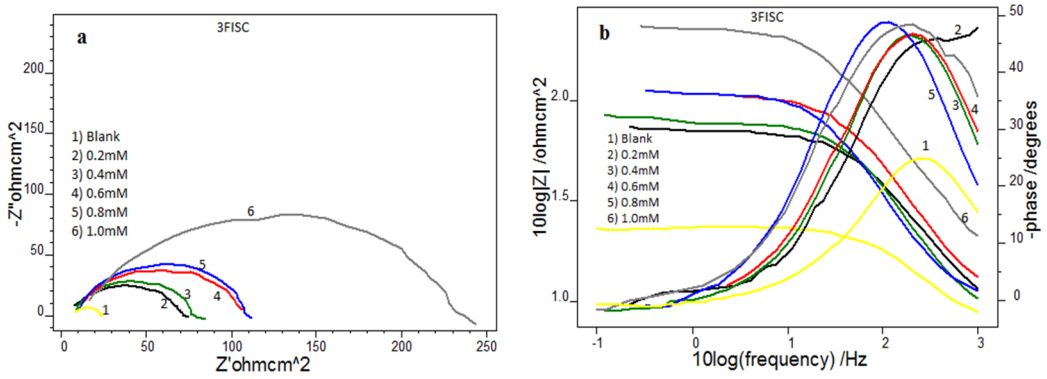

Figure 2.136 a) Nyquist plots and **b)** Bode plots of CS in the presence and absence of 3FISC in 0.5M H_2SO_4

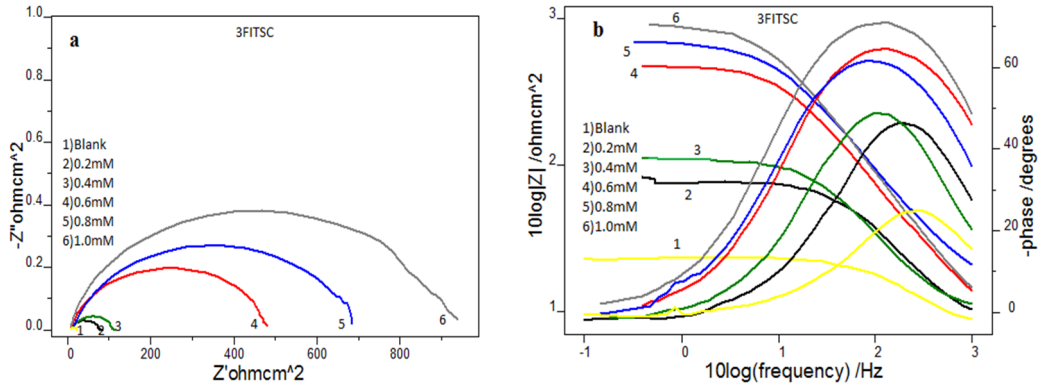

Figure 2.137 a) Nyquist plots and **b)** Bode plots of CS in the presence and absence of 3FITSC in 0.5M H_2SO_4

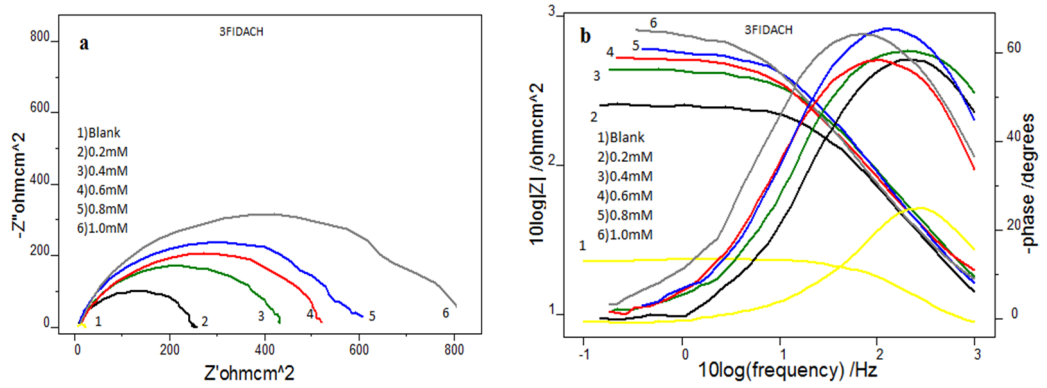

Figure 2.138 a) Nyquist plots and **b)** Bode plots of CS in the presence and absence of 3FIDACH in 0.5M H_2SO_4

From the EIS studies, it was evident that the imines as 3FISC, 3FITSC and 3FIDACH acted as potential corrosion inhibitor in 0.5M H_2SO_4. Both 3FITSC and 3FIDACH exhibited 98% and 3FISC showed 93% inhibition efficiency. The imine 3FITSC contained azomethine linkage along with highly polarizable S atom, which increases the electron availability on that molecule, which may be the reason for the increased corrosion inhibition efficiency. 3FIDACH showed 94% of inhibition efficiency even at lower concentration. The enhanced efficiency of this molecule was related to the structure that it contained two azomethine linkage and two indole moiety which were coplanar, and hence provide increased availability of the electrons on the ring for interaction with metal surface. The interaction of 3FIDACH on CS surface in 0.5M H_2SO_4 depicted in the Figure 2.139.

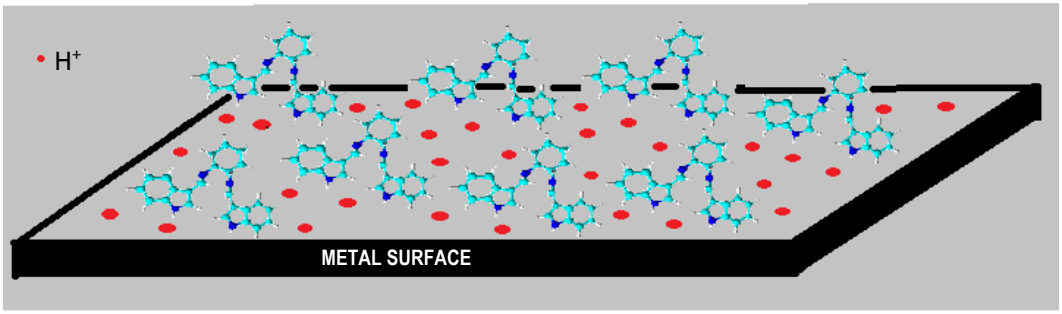

Figure 2.139 Interaction of 3FIDACH on CS surface in 0.5M H_2SO_4

The molecules 3FITSC and 3FISC exhibited 80% and 77% of inhibition efficiency at minimum concentration while 3FIPH possess low efficiency of 53% in H_2SO_4. Even though 3FIPH molecule contains phenyl ring, it displayed low inhibition efficiency, may be due to the lack of coplanarity and hydrolysis of the molecule in H_2SO_4 medium. For all the investigated imines corrosion inhibition

efficiencies increases appreciably with the concentration and it is given in the Table 2. 29. At the highest concentration of 1.0mM, η_{EIS}% of imines follows the order 3FIPH< 3FISC <3FIDACH <3FITSC.

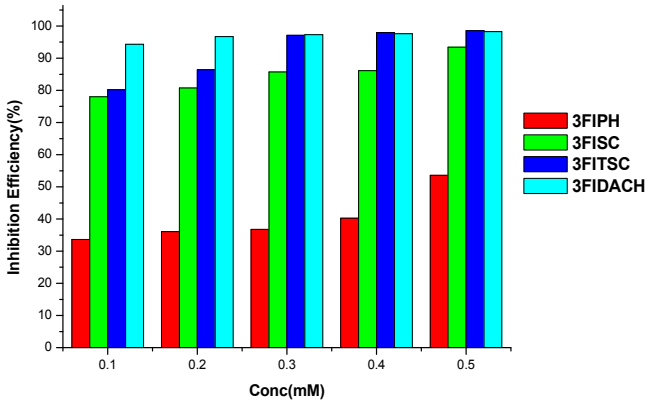

Figure 2.140 Variation of corrosion inhibition efficiencies (η_{EIS}%) of heterocyclic imines of 3-formylindole carbaldehyde on CS in 0.5M H_2SO_4

Potentiodynamic polarization studies

Electrochemical polarization studies of CS specimens in 0.5M sulphuric acid in the presence and absence of imines were performed by recording anodic and cathodic potentiodynamic polarization curves. Polarization plots were obtained in the electrode potential range -250 to +250 mV vs equilibrium potential at a sweep rate of 1mV/sec. The percentage of inhibition efficiency (η_{pol}%) was assessed from the measured I_{corr} values using the following relation :

$$\eta_{pol}\,\% = \frac{I_{corr} - I'_{corr}}{I_{corr}}\ X100$$

where I_{corr} and I'_{corr} are the corrosion current densities of the exposed area of the working electrode in the absence and presence of inhibitor.

From the slope analysis of the linear polarization curves in the vicinity of corrosion potential of blank and different concentrations of the inhibitor, the values of polarization resistance (R_p) were obtained. From the evaluated polarization resistance, the inhibition efficiency was calculated using the relationship

$$\eta_{Rp}\% = \frac{R'p - Rp}{R'p} \times 100$$

where R'_p and R_p are the polarization resistances in the presence and absence of inhibitor respectively. Tafel polarization and linear polarization curves of the imines are represented in the Figures 2.141 to 2.144. The Table 2.29 provides the data of polarization parameters such as anodic slope, cathodic slope, corrosion potential and corrosion current density of imines.

On analyzing the data, it can easily understand that corrosion current density of CS specimens was decreased gradually in the presence of imines. The decrease in corrosion current density of CS specimens indicated the reduction of corrosion rate. The imines effectively reduced the dissolution of metal and hence acted as potential corrosion inhibitor. The compounds 3FITSC and 3FIDACH exhibited above 90% efficiency at all concentrations except the minimum concentration (0.2mM) and achieved a maximum efficiency of 98% and 96% respectively in 0.5M H_2SO_4 at 1.0mM concentration. The efficiency of 3FIPH was much lower than other imines in all the measurements. Heteroatoms, aromatic rings and azomethine linkage present in the molecule cause to enhance the corrosion inhibition power of these imines, compared to the imines derived from pyridine derivatives in sulphuric acid medium. On examining the Tafel

slopes, all the four imines affect the anodic and cathodic sites of corrosion and can be called as mixed corrosion inhibitor.

Table 2.29 Potentiodynamic polarization parameters of CS in the presence and absence of heterocyclic imines of 3-formylindole carbaldehyde in 0.5M H_2SO_4

Imine	Tafel data					Polarization data		
	Conc (mM)	$-E_{corr}$ (mV/SCE)	I_{corr} ($\mu A/cm^2$)	b_a (mv/dec)	$-b_c$ (mv/dec)	η_{pol} (%)	R_p (ohm)	η_{Rp} (%)
3FIPH	0.0	559	1488	209	217	-	26.04	-
	0.2	579	1043	201	177	29.91	36.6	28.85
	0.4	570	1031	198	179	30.71	39.59	34.23
	0.6	572	1004	199	177	32.53	39.89	34.72
	0.8	577	901	216	186	39.45	44.51	41.48
	1.0	576	693	183	152	53.43	77.39	66.35
3FISC	0.2	602	545	186	160	63.37	68.4	61.93
	0.4	525	543	169	165	63.51	83.32	68.74
	0.6	524	470	172	162	68.41	95.02	72.59
	0.8	597	360	182	143	75.81	95.03	72.60
	1.0	522	280	150	154	81.18	247	89.46
3FITSC	0.2	623	466	216	146	68.68	102.8	74.67
	0.4	567	146	130	121	90.19	418.1	93.77
	0.6	519	31	70	132	97.92	591.1	95.59
	0.8	535	27	136	132	98.19	1236.0	97.89
	1.0	511	16	65	122	98.92	976.5	97.33
3FIDACH	0.2	540	460	184	143	69.09	229.9	88.67
	0.4	533	172	161	111	88.44	917.8	97.16
	0.6	559	99	108	134	93.35	641.1	95.94
	0.8	435	60	79	137	95.97	682.1	96.18
	1.0	497	45	76	142	96.98	587.4	95.57

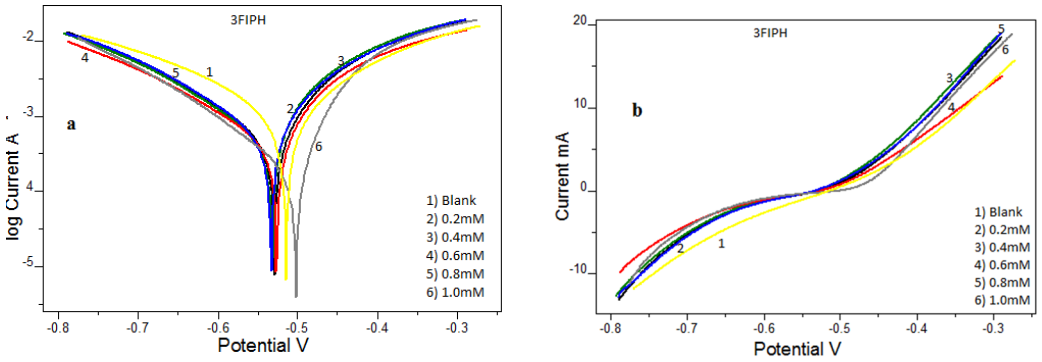

Figure 2.141 a) Tafel plots and **b**) Linear polarization plots of CS in the presence and absence of 3FIPH in 0.5M H_2SO_4

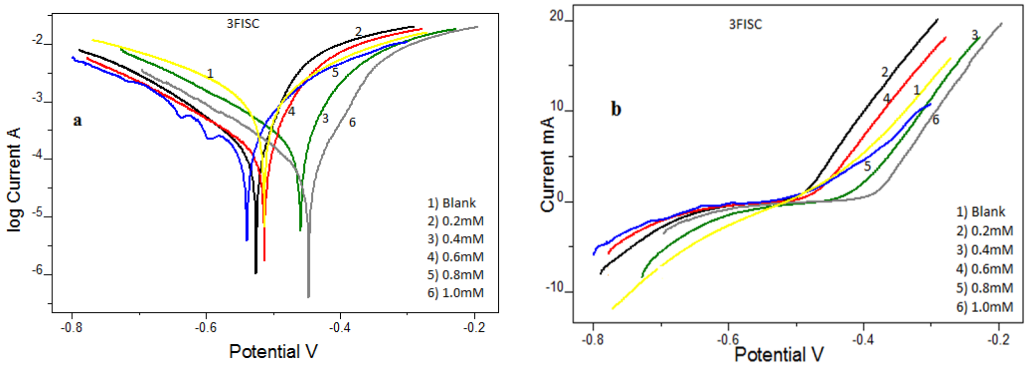

Figure 2.142 a) Tafel plots and **b)** Linear polarization plots of CS in the presence and absence of 3FISC in 0.5M H_2SO_4

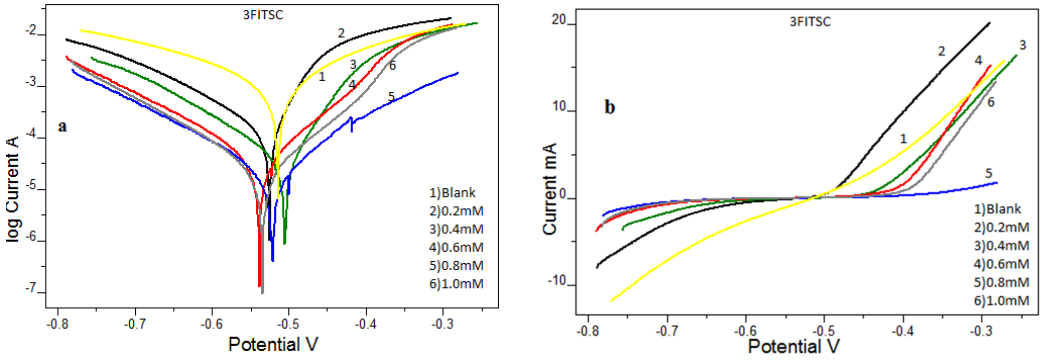

Figure 2.143 a) Tafel plots and **b)** Linear polarization plots of CS in the presence and absence of 3FITSC in 0.5M H_2SO_4

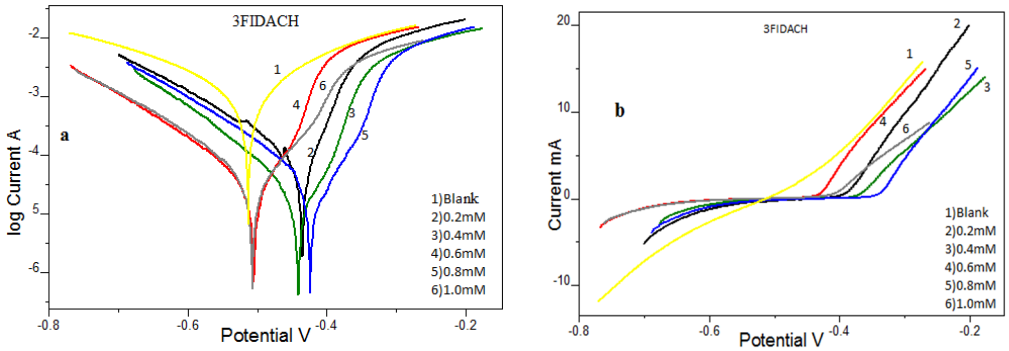

Figure 2.144 a) Tafel plots and **b)** Linear polarization plots of CS in the presence and absence of 3FIDACH in 0.5M H_2SO_4

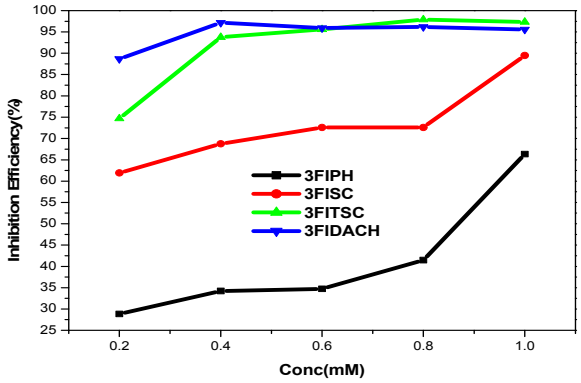

Figure 2.145 Variation of corrosion inhibition efficiencies (η_{Rp}%) of heterocyclic imines of 3-formylindole carbaldehyde on CS in 0.5M H_2SO_4

Surface morphological studies

SEM images of CS surface were taken to verify the mechanism of corrosion inhibition. Bare metal surface contains some irregularities, which may be due to the surface polishing, which is obvious in the scanning micrograph. The CS surface dipped in the acid solution was highly damaged by corrosion in the absence of imine 3FITSC. On comparing the SEM images (Figure 2.146) of a) bare sample b) metal immersed 0.5M H_2SO_4 and c) metal immersed in 0.5M H_2SO_4 containing 1.0mM 3FITSC, it can be revealed that the CS surface was less

corroded in the presence of imine 3FITSC, due to the formation of protective film through adsorption.

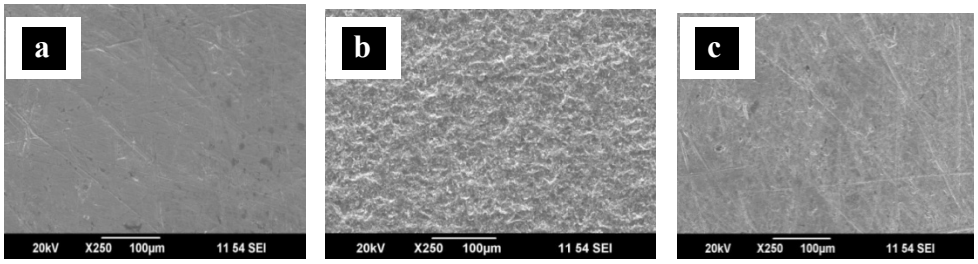

Figure 2.146 SEM images of **a)** bare metal **b)** metal immersed in 0.5M H_2SO_4 **c)** metal immersed in 0.5M H_2SO_4 containing 1.0mM 3FITSC

CHAPTER 5

CORROSION INHIBITION STUDIES OF HETEROCYCLIC IMINES ON COPPER IN 0.1M HNO_3

The methodology applied for monitoring the corrosion inhibition efficiencies on copper in 0.1M HNO_3 using the imines, pyridine-2-carbaldehyde oxime (2PCOX), pyridine-3-carbaldehyde oxime (3PCOX), pyridine-2-carbaldehyde-4-aminobenzoic acid (2PC4ABA), pyridine-2-carbaldehyde-3-aminobenzoic acid (2PC3ABA), pyridine-2-carbaldehyde-2-aminobenzoic acid (2PC2ABA), pyridine-3-carbaldehyde-3-aminobenzoic acid (3PC3ABA), pyridine-2-carbaldehyde-2-aminophenol (2PC2AP), 3-formylindole phenyl hydrazone (3FIPH), 3-formylindole semicarbazone (3FISC), 3-formylindole thiosemicarbazone (3FITSC), 3-formylindole-1,2-diaminocyclohexane (3FIDACH) comprises of electrochemical impedance and potentiodynamic polarization studies. The quantum mechanical studies were conducted to correlate the theoretical and experimental data. The adsorption and surface morphological analysis were also implemented to confirm the corrosion inhibition mechanism.

This chapter is divided into two sections; in which corrosion inhibition investigations of heterocyclic imines derived from pyridine carbaldehyde were explained in section I. Response of copper corrosion towards the application of imines derived from 3-formylindole carbaldehyde were investigated in detail and presented in section II.

SECTION I

CORROSION INHIBITION STUDIES OF HETEROCYCLIC IMINES DERIVED FROM PYRIDINE CARBALDEHYDE ON COPPER IN 0.1M HNO_3

The corrosion inhibition efficiency of imines derived from pyridine carbaldehyde was investigated on copper in 0.1M HNO_3 medium. Electrochemical impedance spectroscopy, potentiodynamic polarization analysis, quantum mechanical studies and surface morphological investigations were used along with adsorption studies for the evaluation and verification of the mechanism of corrosion inhibition on copper in nitric acid medium. As metallic copper deterioration was relatively weak, compared to carbon steel, emphasis was given to electrochemical investigations rather than gravimetric analysis to monitor the anticorrosive property of the synthesized imines.

Electrochemical studies

Electrochemical studies were conducted using Ivium compactstat-e electrochemical system, with three electrode cell assembly, in which saturated calomel electrode (SCE) was the reference electrode, platinum electrode as counter electrode and copper specimen having $1cm^2$ exposed area was the working electrode. From EIS and potentiodynamic polarization studies, charge transfer resistance (R_{ct}) and corrosion current density (I_{corr}) were measured respectively and these parameters were related to corrosion inhibition efficiency of the compounds.

Electrochemical impedance spectroscopy (EIS) studies

The electrochemical studies were conducted using Ivium compactstat-e-electrochemical system which consists of a three electrode system, in which reference electrode and counter electrode were saturated calomel electrode and platinum electrode respectively and copper metal specimen having 1cm^2 area was used as the working electrode. The impedance measurement was done after one hour of exposure time of the metal specimen in nitric acid solution. The EIS experiments were conducted in the absence and presence of imines at varying concentrations. The impedance parameters such as charge transfer resistance (R_{ct}), solution resistance (R_s), double layer capacitance (C_{dl}) and the calculated values of percentage of inhibition efficiency (η_{EIS}%) on copper specimens are listed in the Table 2.30. The Nyquist plots and combined impedance - Bode plots of copper specimens treated are given in Figures 2.147 to 2.153.

The impedance nature of metal specimen in the absence and presence of pyridine carbaldehyde imines varied considerably. The slight irregularities in the plots attributed to the non-homogeneity on the metal surface. It is reported that pure electric circuit models can be used for studying the impedance behavior. Equivalent circuit, composed of solution resistance R_s, charge transfer resistance R_{ct}, and double layer capacitance C_{dl}, gives an accurate fit to the impedance behaviour, in which a constant phase element (CPE) was maintained in the circuit for balancing the irregularity arising due to the non-homogeneity of the metal surface throughout the experiment. The equivalent circuit diagram was shown in the Figure 2.3 in the previous chapter.

The impedance of CPE can be expressed as

$$Z_{CPE} = 1/Y_0 (jw)^n$$

where Y_0 is the magnitude of CPE, n is the exponent (phase shift), ω is the angular frequency and j is the imaginary unit.

The CPE may be resistance, capacitance and inductance depending upon the values of n. In the present course of studies, the values of n ranges between 0.8 to 1.0. Using the values of charge transfer resistance, the corrosion inhibition efficiencies of the heterocyclic derivatives can be derived by employing the equation.

$$\eta_{EIS}\,\% = \frac{R_{ct} - R'_{ct}}{R_{ct}}\,X100$$

where R_{ct} and R'_{ct} are the charge transfer resistance of the electrode with and without inhibitor respectively.

From the observed values in the table, it is evident that as the concentration of imine increases the charge transfer resistance (R_{ct}) values (which is inversely proportional to corrosion rate) also increases. The magnitude of R_{ct} value is an indication of the prevention of charge transfer during the process of corrosion, which controls the metallic dissolution, when the metal is in contact with acid solution. The C_{dl} values decreased with increase in concentration of heterocyclic imines which indicates the lowering of local dielectric constant or increase in the thickness of electrical double layer with the inhibitor concentration. This effect is attributed to the adsorption of organic molecules on the metal surface.

Table 2.30 shows the inhibition efficiency of imines derived from pyridine-carbaldehyde. The maximum inhibition efficiency was 97.3% for 2PC2ABA, 91.2% for 2PC3ABA, 85.5% for 2PC4ABA, 89% for 3PC3ABA, 91.9% for 2PC2AP, 90% for 3PCOX and 26.4%for 2PCOX, at 1.0mM concentration.

From the Figure 2.155, it is also clear that 2PC2ABA shows relatively higher inhibition efficiency, when compared the other imine inhibitors under study. The compounds derived from pyridine carbaldehyde show inhibition efficiency in the order 2PC2ABA> 2PC2AP > 2PC3ABA>3PCOX >3PC3ABA >2PC4ABA>2PCOX.

Among the seven inhibitors, 2PC2ABA and 2PC2AP showed very good corrosion inhibition efficiency even at the lower concentration 0.2mM and 2PCOX showed low inhibition efficiency at all concentrations compared to other compounds. At concentrations 0.2mM, 0.4mM and 0.6mM, 2PCOX showed negative inhibition efficiency or corrosion accelerating behavior and increases the rate of corrosion by metal dissolution. This may be due to the strong tendency of 2PCOX molecules to make co-ordinate bond with Cu^{2+} ion.

On analyzing the results, the imines 3PCOX and 3PC3ABA derived from pyridine-3-carbaldehyde had comparable inhibition efficiency at higher concentration 1.0mM. Both 3PCOX and 3PC3ABA showed maximum inhibition efficiency around 90% at 1.0mM concentration. At lower concentration 0.2mM these imines exhibited the inhibition efficiency 53% and 26% respectively.

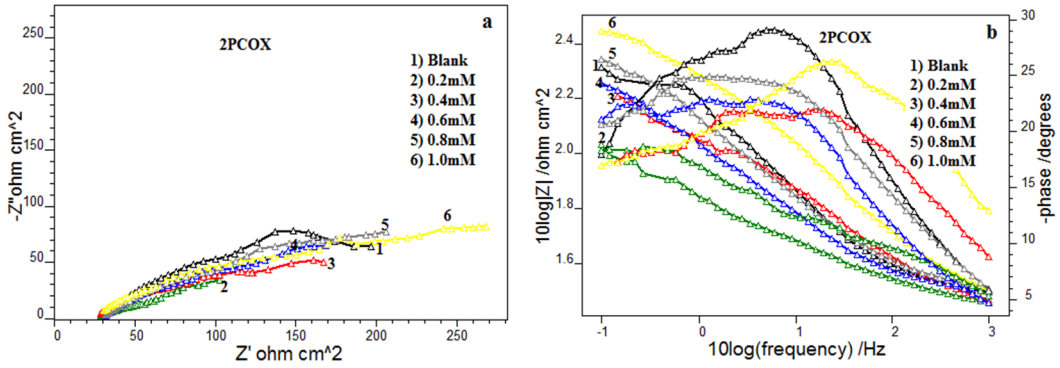

Figure 2.147 a) Nyquist plots and **b)** Bode plots of Cu in the presence and absence of 2PCOX in 0.1M HNO_3

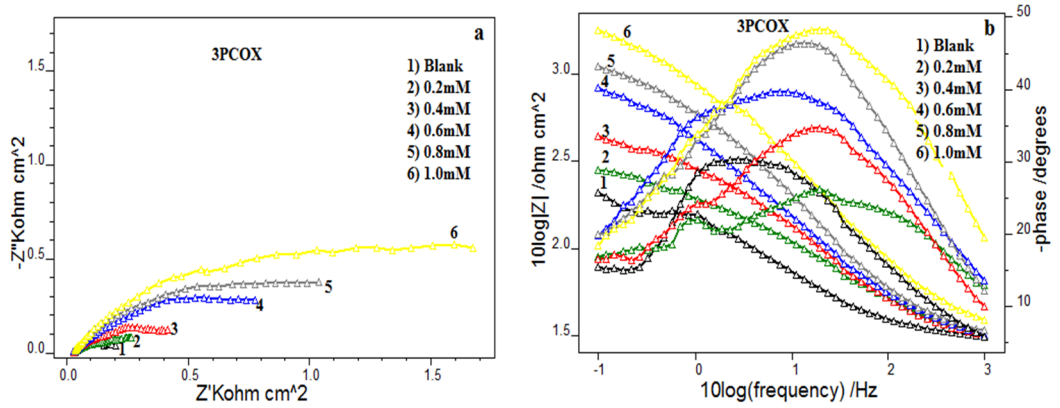

Figure 2.148 a) Nyquist plots and **b)** Bode plots of Cu in the presence and absence of 3PCOX in 0.1M HNO_3

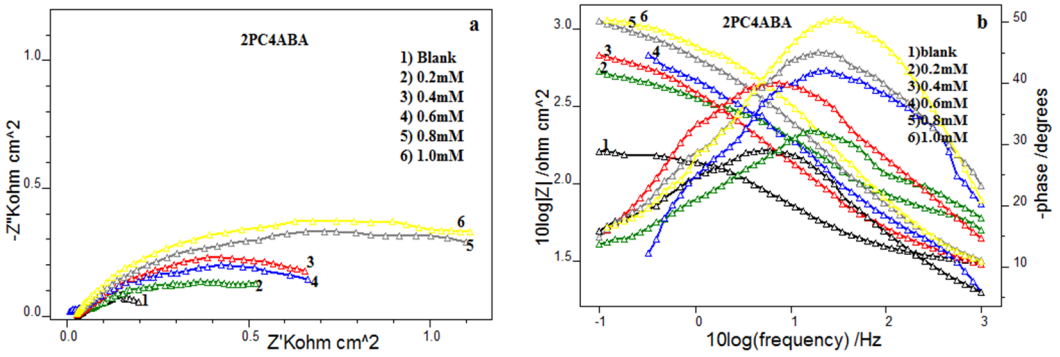

Figure 2.149 a) Nyquist plots and **b)** Bode plots of Cu in the presence and absence of 2PC4ABA in 0.1M HNO_3

Table 2.30 Electrochemical impedance parameters of copper in the presence and absence of heterocyclic imines of pyridine carbaldehyde in 0.1M HNO_3

Imines	Conc (mM)	C_{dl} (μFcm^{-2})	R_{ct} (Ωcm^2)	η_{EIS} (%)
	0	745	135.9	-
	0.2	3716	55.3	-145.8
2PCOX	0.4	2095	114.9	-18.3
	0.6	1545	121.9	-11.5
	0.8	1439	155.9	12.8
	1.0	535	186.6	26.4
	0.2	2018	294.6	53.9
3PCOX	0.4	334	307.6	55.8
	0.6	385	672.2	79.8
	0.8	235	879.8	84.6
	1.0	157	1379.0	90.1
	0.2	341	350.8	61.3
	0.4	315	545.9	75.1
2PC4ABA	0.6	212	735.9	81.5
	0.8	166	856.4	84.1
	1.0	110	939.7	85.5
	0.2	744	188.6	27.9
	0.4	585	417.4	67.4
2PC3ABA	0.6	170	480.2	71.7
	0.8	114	1334.0	89.8
	1.0	99	1545.5	91.2
	0.2	112	2147.2	93.6
	0.4	76	3578.4	96.2
2PC2ABA	0.6	70	3844.5	96.4
	0.8	67	3862.3	96.4
	1.0	66	5147.6	97.3
	0.2	652	184.2	26.2
	0.4	730	237.6	42.8
3PC3ABA	0.6	545	369.8	63.3
	0.8	421	660.2	79.4
	1.0	156	1313.0	89.6
	0.2	380	724.7	81.2
	0.4	234	1014.1	86.6
2PC2AP	0.6	218	1259.7	89.2
	0.8	139	1392.4	90.2
	1.0	90	1668.4	91.9

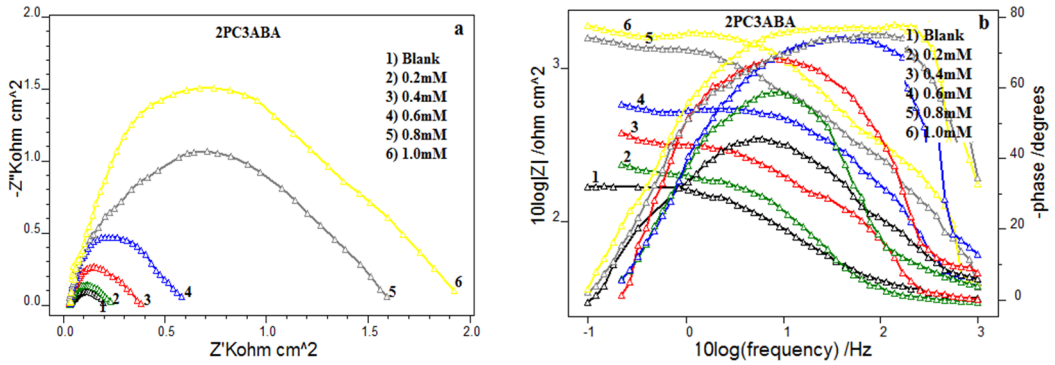

Figure 2.150 a) Nyquist plots and **b)** Bode plots of Cu in the presence and absence of 2PC3ABA in 0.1M HNO_3

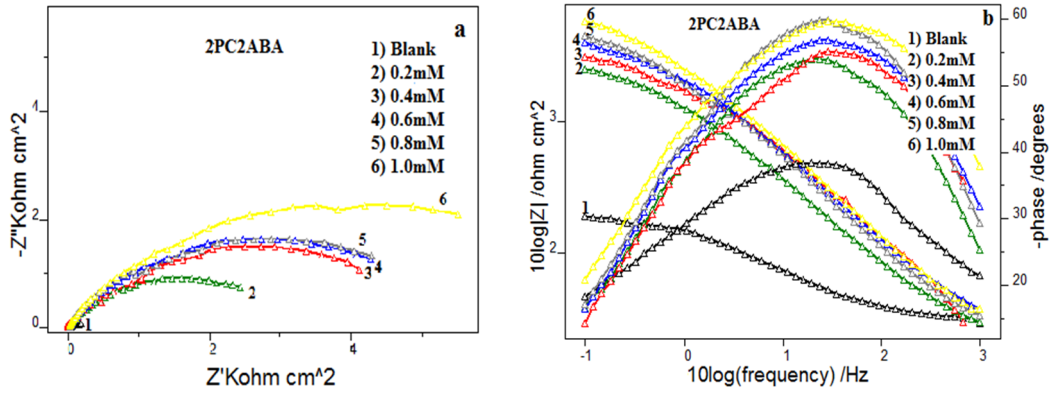

Figure 2.151 a) Nyquist plots and **b)** Bode plots of Cu in the presence and absence of 2PC2ABA in 0.1M HNO_3

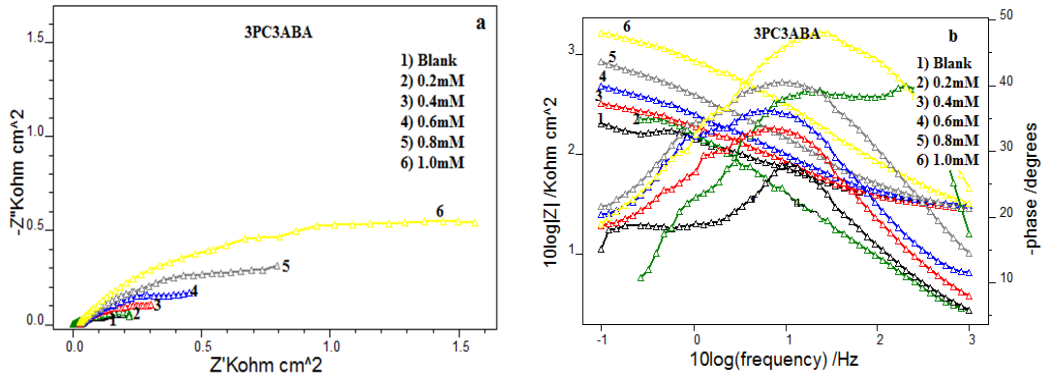

Figure 2.152 a) Nyquist plots and **b)** Bode plots of Cu in the presence and absence of 3PC3ABA in 0.1M HNO_3

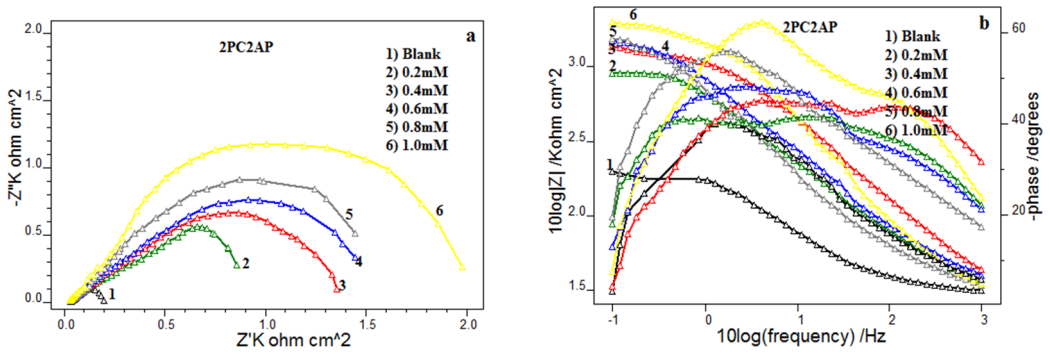

Figure 2.153 a) Nyquist plots and **b)** Bode plots of Cu in the presence and absence of 2PC2AP in 0.1M HNO_3

Among pyridine based imines, 2PC2ABA and 2PC2AP exhibited marked corrosion inhibition efficiency at all the concentrations, when compared to other imines. The increased efficiency may be due to the possibility of formation of inter molecular H-bond among themselves, thereby facilitating the effective formation of a protective layer on the surface of metal by the H-bonded imine compounds.

Considering the amino benzoic acid derivatives of pyridine, even if they had similarity in their structure, they exhibited difference in their corrosion inhibition efficiency. The 2PC2ABA exhibited greater than 90% efficiency at all concentrations compared to other amino benzoic acid derivatives. 2PC3ABA and 3PC3ABA showed comparable efficiency around 90% at maximum concentration of 1.0mM. 2PC4ABA showed slight lower efficiency than others.

The evaluated corrosion inhibition efficiency of 2PCOX was always less than 3PCOX at all varying concentrations. This lower corrosion inhibition efficiency of 2PCOX when compared to that of 3PCOX can be attributed to their hydrogen bonding nature. When the structures of these molecules are examined,

there exists a possibility for the formation of hydrogen bonds as in the Figure 2.154.

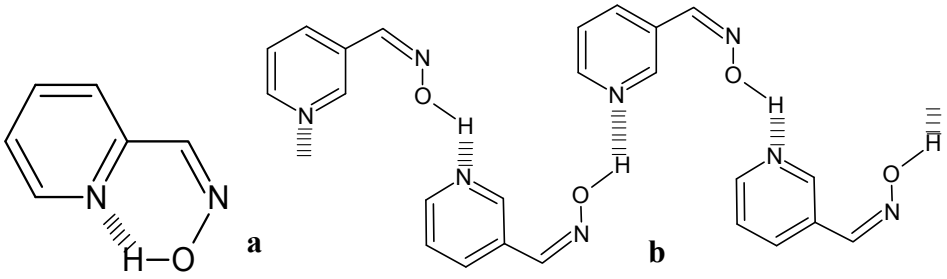

Figure 2.154 H-bond present in **a**) 2PCOX and **b**) 3PCOX

2PCOX prefer to make intra molecular hydrogen bonds while 3PCOX molecules largely aggregate by inter molecular hydrogen bonds. It is well known that the surface interaction by the molecules on the metal is the main factor responsible for the mitigation of the rate of corrosion. If 2PCOX form intra molecular hydrogen bonds, it can be assumed that the molecules interact the metal surface independently i.e., there is no molecular interaction between the adsorbed molecules which gives the protons an ample opportunity to attack on the metal surface. Considering the intermolecular hydrogen bond in 3PCOX molecules, the molecules aggregated to each other forms molecular layers and gets adsorbed on the copper surface appreciably. The exposed area of the metal towards the corroding medium will be significantly reduced due to this phenomenon resulting in the lowering of the rate of corrosion and increased corrosion inhibition efficiency.

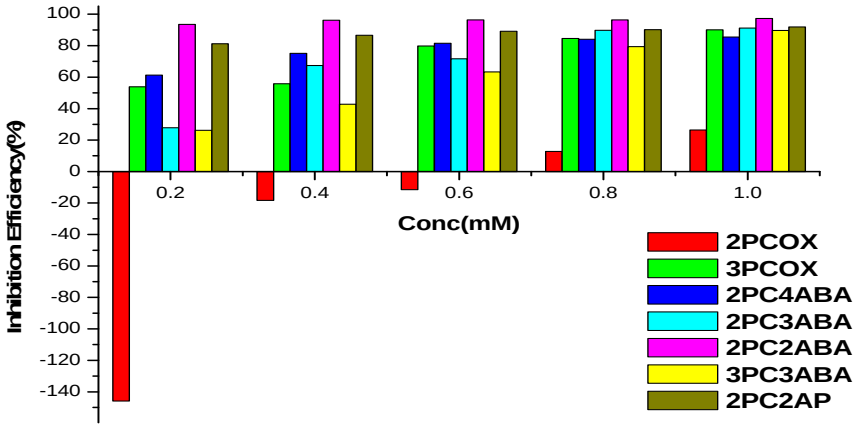

Figure.2.155 Variation of corrosion inhibition efficiencies (η_{EIS}%) of heterocyclic imines of pyridine carbaldehyde on Cu in 0.1M HNO_3

Adsorption studies

It is well known that most of organic molecules prevent the acid corrosion by adsorbing them on the metal surface which makes the study of adsorption by these molecules very important to reveal the mechanism of corrosion inhibition.

Table 2.31 Adsorption isotherms and the regression coefficients of heterocyclic imines of pyridine carbaldehyde on copper in 0.1M HNO_3

Isotherm	Regression coefficient (R^2)					
	3PCOX	2PC4ABA	2PC3ABA	2PC2ABA	3PC3ABA	2PC2AP
Langmiur	0.944	0.999	0.780	0.999	0.919	0.999
Freundlich	0.904	0.840	0.846	0.755	0.988	0.898
Temkin	0.870	0.968	0.953	0.887	0.967	0.988
Frumkin	0.625	0.981	0.934	0.940	0.900	0.990
El-Awady	0.868	0.990	0.960	0.905	0.941	0.995
Flory-Huggin	0.705	0.985	0.572	0.901	0.818	0.993

The mechanism of corrosion prevention was studied by plotting various adsorption isotherms with the help of correlation coefficient (R^2). Best fit adsorption isotherm was selected based on the correlation coefficient which is closely equal to unity. In the present study, the isotherms considered are Langmuir, Freundlich, Frumkin, Temkin, Flory-Huggin and El-Awady adsorption isotherms. Table 2.31 contains the adsorption isotherm models and their correlation coefficients for pyridine carbaldehyde derivatives on copper in 0.1M HNO_3. The parameters such as adsorption equilibrium constant K_{ads} and free energy of adsorption ΔG^0_{ads} (Table 2.32) can be evaluated using best fit adsorption isotherm. The free energy of adsorption can be calculated by the equation.

$$\Delta G^0_{ads} = -RT\ln(55.5K_{ads})$$

where 55.5 is the molar concentration of water, R is the universal gas constant and T is the temperature in Kelvin. Negative value of ΔG^0_{ads} shows the spontaneity of the reaction. The values of ΔG^0_{ads} up to -20kJmol^{-1} implies that the interaction between the inhibitor molecules and metal is physisorption and if ΔG^0_{ads}value is more negative than -40kJmol^{-1}, indicates the chemisorption process. Sometimes the ΔG^0_{ads} values lies between -20kJmol^{-1} and -40kJmol^{-1}, which means that the interaction between the compound and metal surface involves both physisorptions and chemisorptions. The adsorption isotherms are represented in the figures 2.156 to 2.161.

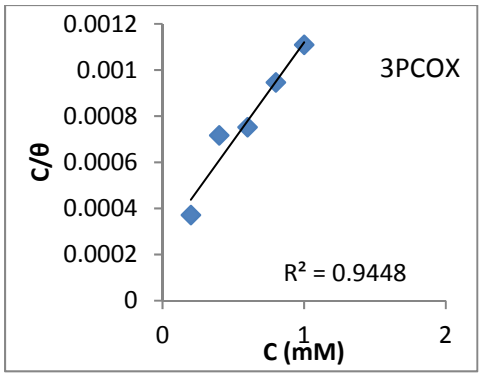

Figure 2.156 Langmuir isotherm for 3PCOX on Cu in 0.1M HNO_3

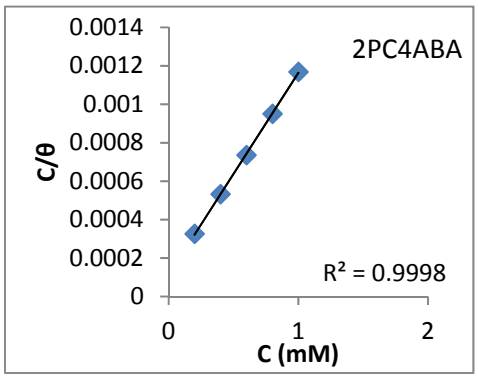

Figure 2.157 Langmuir isotherm for 2PC4ABA on Cu in 0.1M HNO_3

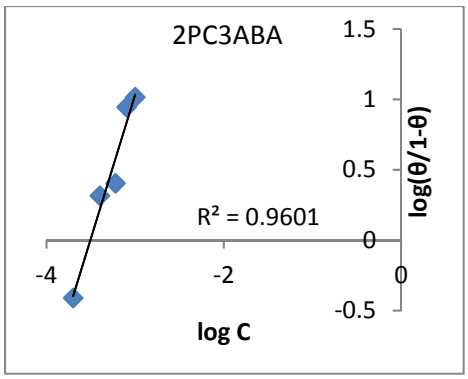

Figure 2.158 El-Awady isotherm for 2PC3ABA on Cu in 0.1M HNO_3

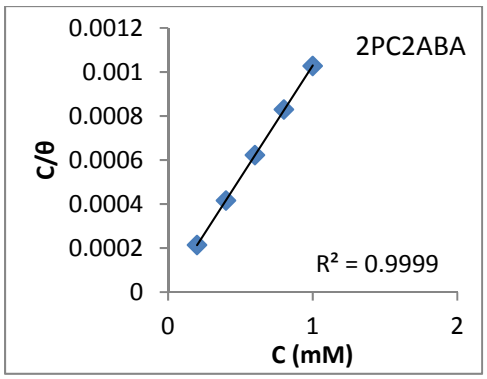

Figure 2.159 Langmuir isotherm for 2PC2ABA on Cu in 0.1M HNO_3

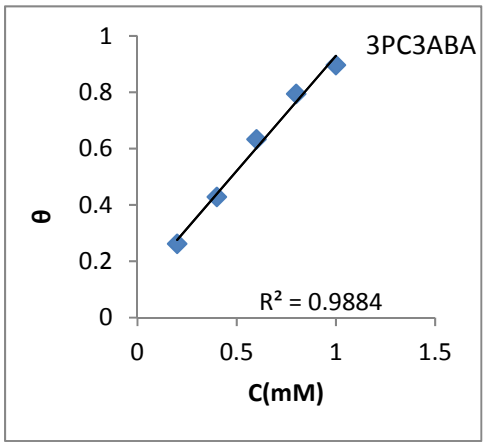

Figure 2.160 Freundlich isotherm for 3PC3ABA on Cu in 0.1M HNO_3

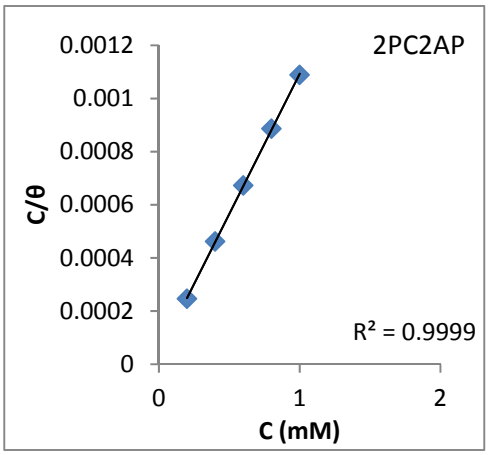

Figure 2.161 Langmuir isotherm for 2PC2AP on Cu in 0.1M HNO_3

The compounds derived from pyridine carbaldehyde 2PC2ABA, 2PC4ABA, 2PC2AP and 3PCOX obeyed Langmuir adsorption isotherm. The compounds such as 2PCMABA satisfactorily obeyed El-Awady adsorption isotherm and 3PC3ABA Freundlich adsorption isotherm. The heterocyclic oxime 2PCOX was having very weak interaction on surface of the metal. For lower concentration of 2PCOX showed negative inhibition efficiency indicating corrosion antagonistic behavior. The dissolution of copper metal to metal ion can be observed when it was dipped in 0.1MHNO_3 containing 2PCOX at lower concentration and hence not possible to plot any adsorption isotherms for 2PCOX molecule. In other words 2PCOX molecules do not get adsorbed on the Cu metal surface in HNO_3 medium. All the molecules except 2PCOX mainly adsorbed through both physisorption and chemisorptions on the copper surface.

Table 2.32 Adsorption parameters of heterocyclic imines of pyridine carbaldehyde on copper in 0.1M HNO_3

Adsorption Parameter	2PCOX	3PCOX	2PC4ABA	2PC3ABA	2PC2ABA	3PC3ABA	2PC2AP
K_{ads}	-	3745	8928	3199	1,11,111	817	26315
ΔG^0_{ads} (kJ/mol)	-	-30.64	-32.82	-30.0	-39.13	-26.83	-35.52

The adsorption parameters calculated using the isotherms are provided in Table 2.32. From the table it is clear that the free energy values are negative which shows the spontaneity of the reaction and ranges from -26kJ/mol to -39kJ/mol, which is an indication of both physisorption and chemisorption

involved in the process. The compounds 2PC2ABA and 2PC2AP were showing strong interaction on surface of metal and had the free energy of -39.13 and -35.52kJ/mol respectively. It is unambiguous that the interaction of 2PC2ABA on Cu metal surface in 0.1M HNO_3 is mainly chemical in nature. On comparing the adsorption parameters of 3PC3ABA and 3PCOX, it can be seen that, the later has strong interactions on the surface of metal than the former.

Potentiodynamic polarization studies

Potentiodynamic polarization studies were conducted using Ivium-compactstat-e electrochemical work station. The working electrode was scanned between a potential range of -250mV to +250mV at a sweep rate of 1mV/sec. The polarization analysis includes Tafel polarization as well as linear polarization studies. The parameters such as corrosion current densities (I_{corr}), corrosion potential (E_{corr}), cathodic Tafel slope (b_c), anodic Tafel slope (b_a) and polarization resistance (R_p) were measured from the polarization curves. Figures 2.162 to 2.168 represent the Tafel plots and polarization curves of copper in the presence and absence of heterocyclic derivatives.

The Tafel data and linear polarization data obtained by potentiodynamic polarization studies of copper in the presence and absence of seven imine derivatives of pyridine-carbaldehyde are given in the Table 2.33. Results clearly envisage the corrosion inhibition efficiency increased with increase in concentration of the inhibitor and the corrosion current density decreased with increase in concentration.

The corrosion inhibition efficiency was inversely proportional to corrosion current density. In this study 2PC2ABA showed high inhibition efficiency (96%) at concentration at 1.0mM concentration. This is in good agreement with electrochemical impedance spectroscopic study. And therefore it is concluded that the inhibitor molecules get adsorbed on the metal surface, thereby reducing the dissolution of metal considerably. The inhibition efficiency of 2PC3ABA and 3PC3ABA displayed 89% at maximum concentration and the imines 2PC2AP and 2PC4ABA exhibited slight lower efficiency compared to the above discussed ones at higher concentration. Here also the inhibitor 2PCOX showed very low corrosion inhibition efficiency at all concentrations.

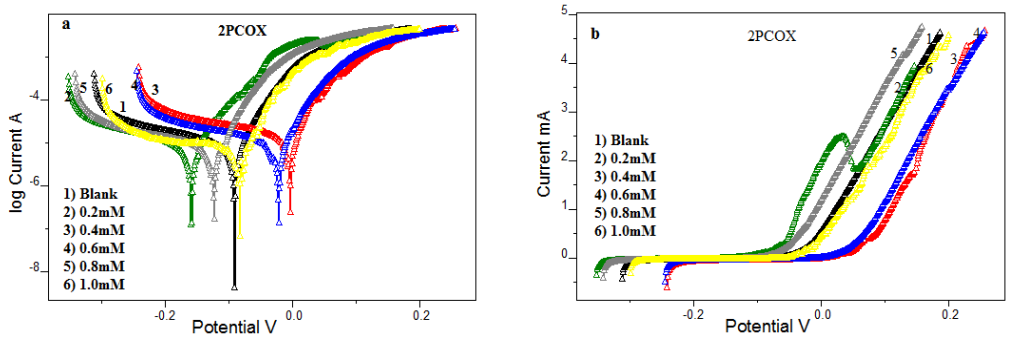

Figure 2.162 Tafel plots and **b)** Linear polarization plots of Cu in the presence and absence of 2PCOX in 0.1M HNO_3

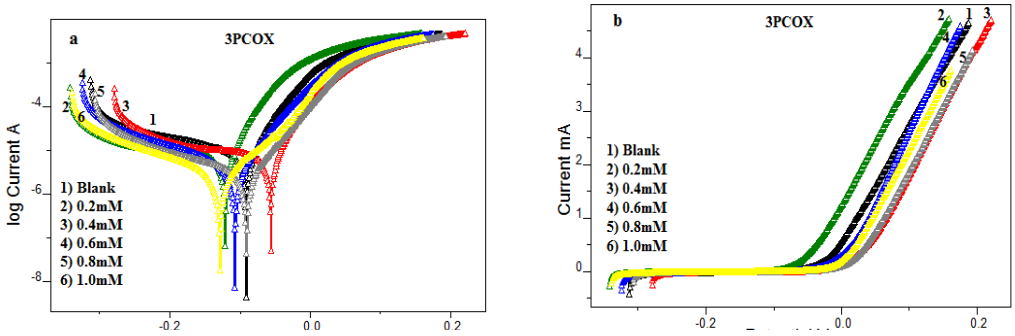

Figure 2.163 Tafel plots and **b)** Linear polarization plots of Cu in the presence and absence of 3PCOX in 0.1M HNO_3

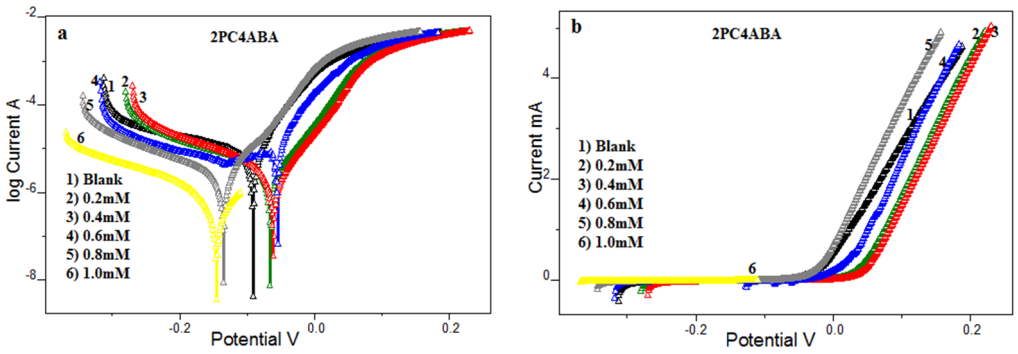

Figure 2.164 Tafel plots and **b)** Linear polarization plots of Cu in the presence and absence of 2PC4ABA in 0.1M HNO_3

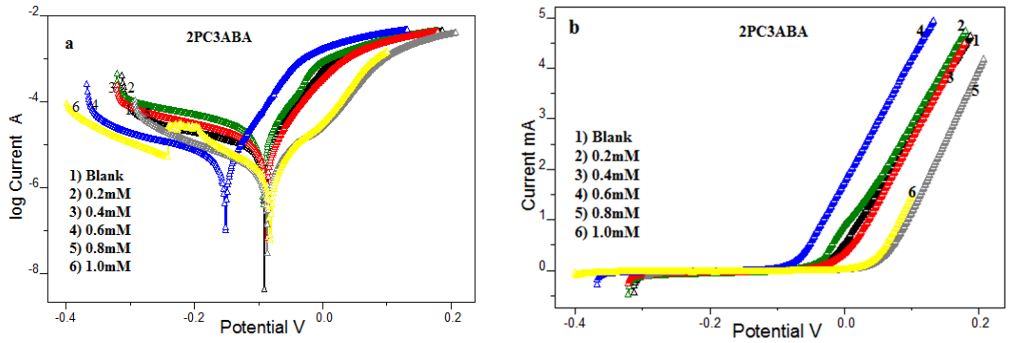

Figure 2.165 Tafel plots and **b)** Linear polarization plots of Cu in the presence and absence of 2PC3ABA in 0.1M HNO_3

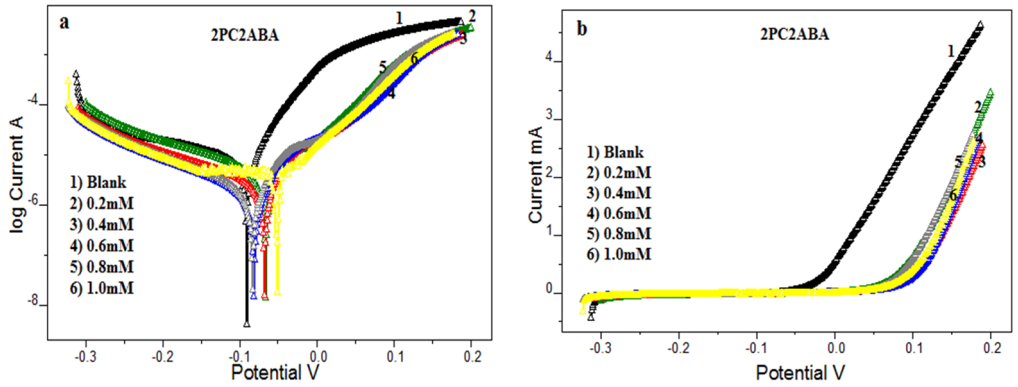

Figure 2.166 Tafel plots and **b)** Linear polarization plots of Cu in the presence and absence of 2PC2ABA in 0.1M HNO_3

Table 2.33 Potentiodynamic polarization parameters of copper in the presence and absence of heterocyclic imines of pyridine carbaldehyde in 0.1M HNO_3

Imines	Tafel data					Polarization data		
	Conc (mM)	$-E_{corr}$ (mV/SCE)	I_{corr} ($\mu A/cm^2$)	b_a (mv/dec)	$-b_c$ (mv/dec)	η_{pol} (%)	R_p (ohm)	η_{Rp} (%)
	0	240	27	168	309		1758	
2PCOX	0.2	339	52.7	214	283	-95.1	952	-84.6
	0.4	100	37.7	134	370	-39.6	1355	-29.7
	0.6	158	26.2	159	340	2.96	1681	-4.58
	0.8	274	23.2	163	321	14.0	1948	9.75
	1.0	271	18.7	178	372	30.7	2537	30.7
3PCOX	0.2	313	18.4	173	399	31.85	2456	28.42
	0.4	191	14.8	143	299	45.18	3214	45.30
	0.6	160	8.2	100	198	69.62	4454	60.53
	0.8	145	4.8	94	196	82.04	6321	72.19
	1.0	125	2.6	69	182	90.19	9645	81.78
2PC4ABA	0.2	128	7.3	100	204	72.85	5830	69.84
	0.4	111	6.8	95	91	74.78	6651	73.56
	0.6	159	6.4	99	245	76.29	7254	73.76
	0.8	183	4.5	88	172	83.14	9473	81.44
	1.0	118	3.9	41	215	85.25	11378	84.54
2PC3ABA	0.2	236	25.1	202	215	7.04	1914	8.15
	0.4	166	17.0	128	295	37.03	2578	31.80
	0.6	286	11.4	147	269	57.78	3428	48.72
	0.8	80	5.8	68	177	78.51	6500	72.95
	1.0	120	2.7	78	154	89.81	9170	80.82
2PC2ABA	0.2	49	3.8	68	211	85.81	8045	78.14
	0.4	54	2.1	72	195	92.03	12347	85.76
	0.6	79	1.6	82	172	93.82	15890	88.93
	0.8	63	1.4	63	163	94.81	16560	89.38
	1.0	67	1.0	65	150	96.25	18472	90.48
3PC3ABA	0.2	248	21.0	163	313	22.2	2076	15.3
	0.4	300	16.2	147	320	40.0	2595	32.2
	0.6	267	14.9	129	327	44.9	3032	42.0
	0.8	182	11.9	89	286	55.7	3219	45.3
	1.0	196	2.7	70	187	89.7	6453	72.7
2PC2AP	0.2	51	12.2	78	287	54.81	3876	54.64
	0.4	14	7.5	77	222	72.07	5677	69.03
	0.6	68	6.3	80	240	76.63	5955	70.48
	0.8	64	4.5	71	238	83.15	8235	78.15
	1.0	63	3.5	72	231	86.81	9677	83.83

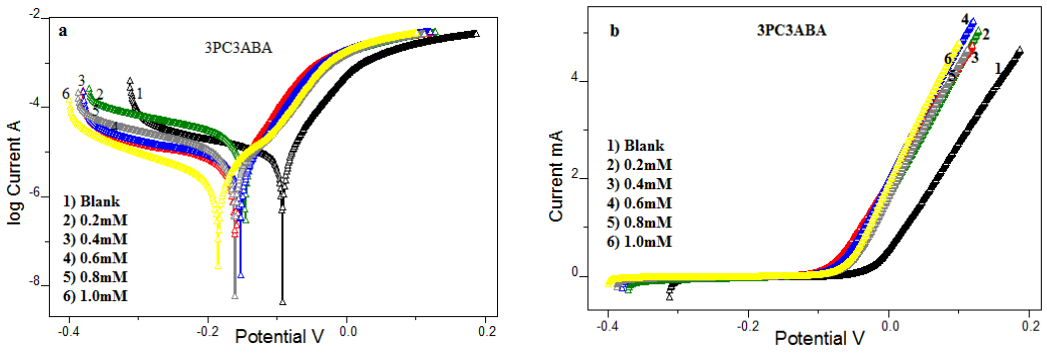

Figure 2.167 Tafel plots and **b)** Linear polarization plots of Cu in the presence and absence of 3PC3ABA in 0.1M HNO_3

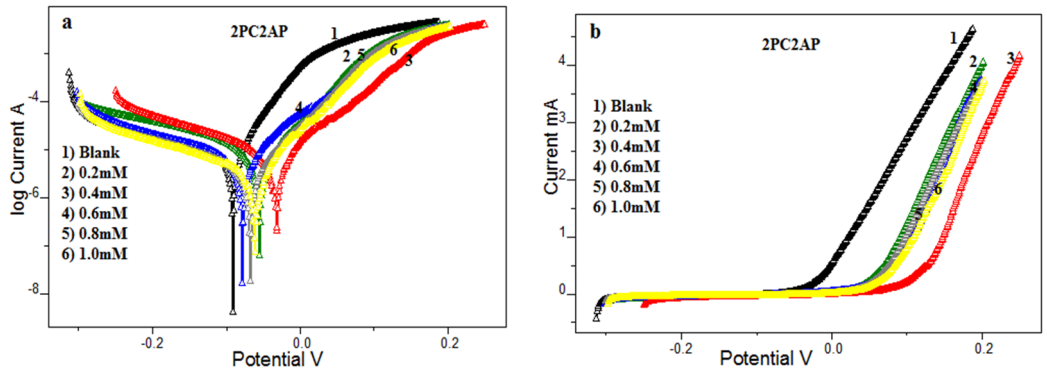

Figure 2.168 Tafel plots and **b)** Linear polarization plots of Cu in the presence and absence of 2PC2AP in 0.1M HNO_3

In the case of 2PC4ABA and 2PCOX, the cathodic slopes and anodic slopes varied considerably suggesting that these molecules are acting as cathodic and anodic inhibitors and thus can be regarded as mixed type inhibitors. Since the heterocyclic compound 2PC2AP only showed anodic shift of Tafel lines, appreciably, it can be assumed that this compound mainly affects the anodic process of corrosion ie, they inhibit the metal dissolution process by preventing the oxidation of Cu atoms mainly at anode.

In Tafel polarization study 3PCOX and 3PC3ABA exhibited comparable inhibition efficiency and a maximum inhibition efficiency about 90% was

obtained at 1.0mM concentration. As in both cases the anodic and cathodic slope varied considerably, it is evident that 3PCOX and 3PC3ABA also act as mixed type inhibitors. The values of polarization resistance were in good agreement with Tafel polarization values of both compounds.

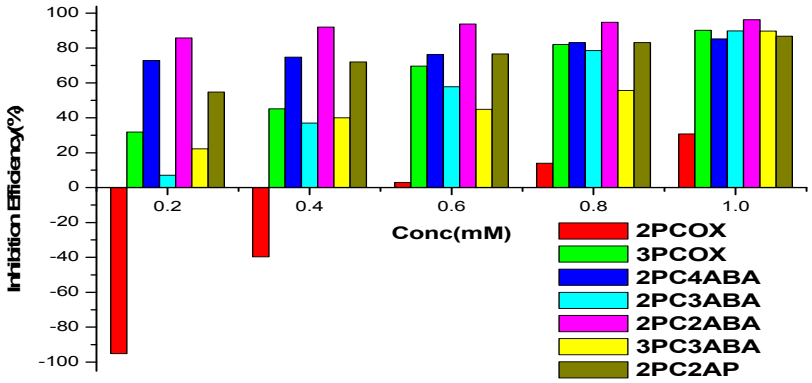

Figure 2.169 Variation of corrosion inhibition efficiencies (η_{pol}%) of heterocyclic imines of pyridine carbaldehyde on copper in 0.1M HNO_3

If one examines the structure of imines, many potential sites of inhibitor–metal interaction can be recognized. The unshared pair of electrons present on two N atoms is of key importance in making coordinate bond with the metal. The π-electron cloud of the aromatic rings and the azomethine linkage also participate in the inhibition mechanism. Furthermore, the double bonds in the inhibitor molecule permit the back donation of metal d electrons to the π* orbital and this type of interaction cannot occur with amines

Quantum mechanical studies

The quantum mechanical studies offered a platform for the correlation of corrosion inhibition response of organic heterocyclic imines with the energy of frontier molecular orbitals. The donor-acceptor interaction (HSAB concept)

between the vacant orbitals of copper atoms and the filled molecular orbitals of the inhibitor molecules has a prominent role in the prevention of mechanism of metal corrosion. High value of E_{HOMO}, the low value of E_{LUMO} and energy difference between HOMO and LUMO E_{LUMO}-E_{HOMO} (ΔE), values of imines help the molecules to bind on the metal surface strongly. Geometry optimization of imines and quantum mechanical calculations were carried out using DFT method by GAMMESS software. A combination of Beck's three parameter exchange functional and Lee–Yang–Parr nonlocal correlation functional (B3LYP) was employed in DFT calculations. The quantum mechanical parameters like E_{HOMO}, E_{LUMO}, ΔE, electro negativity (χ), chemical hardness (η) of the molecules and number of electrons transferred (ΔN) for the studied heterocyclic imines are calculated in the Table 2.34.

The energy separation between HOMO and LUMO and the energy of LUMO were considerably lower for 2PC2ABA and 2PC2AP compared to other three pyridine-2-carbaldehyde derivatives, which indicate that 2PC2ABA and 2PC2AP are better inhibitors than others. These data implies that the energy required in rendering electrons from HOMO of 2PC2ABA and 2PC2AP to the vacant orbitals of Cu is low compared to other molecules. The E_{HOMO} value of 2PC2AP was appreciably higher than that of 2PC2ABA. The molecules such as 2PC3ABA and 2PC4ABA have comparable values for energies of HOMO and LUMO and energy separation between HOMO and LUMO. The compound 2PCOX has high value for energy difference between HOMO and LUMO, which justifies 2PCOX acting as a poor inhibitor compared to the other pyridine-2-

carbaldehyde derivatives. The (ΔN) from donor to acceptors are also calculated from these quantum mechanical parameters which provide the information about interaction with metal atoms. As an approximation, the chemical hardness of Cu metal and the approximate electro negativity of bulk Cu are assumed as zero and 4.48eV respectively.

$\chi \approx -1/2\ (E_{HOMO} + E_{LUMO})$ $\eta \approx 1/2\ (E_{HOMO} - E_{LUMO})$ $\Delta N = \frac{\chi_{Cu} - \chi_{inhib}}{2(\eta_{Cu} + \eta_{inhib})}$

Table 2.34 Quantum mechanical parameters of heterocyclic imines of pyridine carbaldehyde on copper in 0.1M HNO_3

Imines	E_{HOMO} (eV)	E_{LUMO} (eV)	ΔE (eV)	χ	η	ΔN
2PCOX	-4.163	1.1429	5.3062	1.5102	2.6531	0.5596
3PCOX	-4.381	1.0340	5.4150	1.6735	2.7075	0.5182
2PC4ABA	-4.027	0.6802	4.7072	1.6734	2.3536	0.5962
2PC3ABA	-3.483	0.3537	3.8367	1.56465	1.9183	0.7598
2PC2ABA	-3.89	0.5986	4.4886	1.6457	2.2443	0.6314
3PC3ABA	-4.108	0.3809	4.4898	1.8640	2.2449	0.5826
2PC2AP	-2.829	0.6258	3.4557	1.10202	1.7278	0.9774

The number of electrons transferred from the inhibitor to the acceptor atom is higher for 2PC2AP, and it is in the order of 2PC2AP> 2PC2ABA> 2PC4ABA> 2PC3ABA> 2PCOX. The large number of electrons transferred suggests that the molecule make a strong coordinate type interaction with the metal atoms.

Surface morphological Studies

To verify mechanism of corrosion inhibition, the SEM images of Cu surface were taken with and without the heterocyclic oxime derived from pyridine

carbaldehyde. From the analysis of the SEM images, Figure 2.170 (a) bare metal and (b) metal immersed in 0.1M HNO_3 are entirely different. Surface images of copper specimens in the presence of the heterocyclic oximes, Figure 2.170 (c) copper in presence of 3PCOX and (d) copper in presence of 2PCOX, are also showed difference in their textures. On close examination of the Figures 2.170 (c) and (d), it can be noticed that a thin protective layer of 3PCOX is attached on the copper surface thereby 3PCOX exhibited the enhanced inhibition efficiency than 2PCOX.

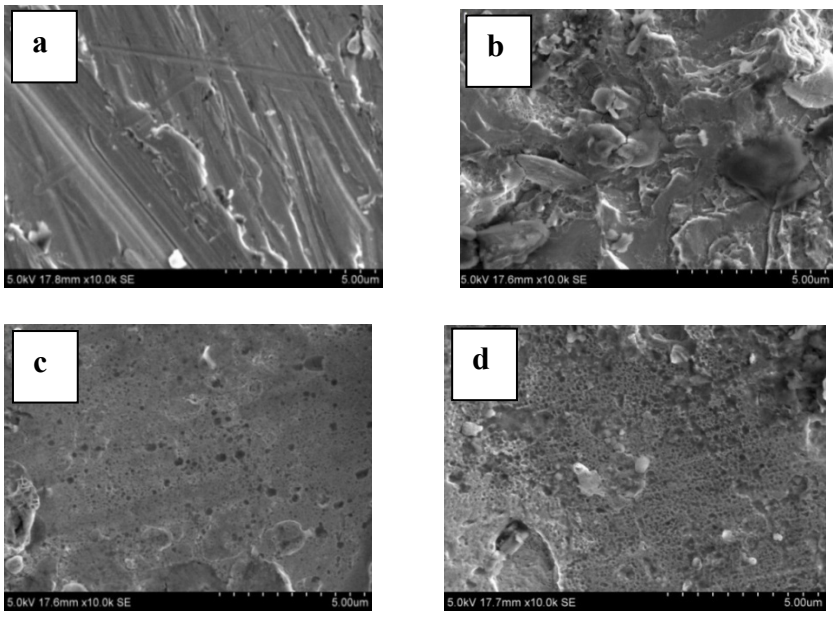

Figure 2.170 SEM images of **a**) bare metal **b**) Cu immersed in 0.1M HNO_3 **c**) Cu immersed in 0.1M HNO_3 containing 1.0mM 3PCOX **d**) Cu immersed in 0.1M HNO_3 containing 1.0mM 2PCOX

SECTION II

CORROSION INHIBITION STUDIES OF HETEROCYCLIC IMINES DERIVED FROM 3-FORMYLINDOLE CARBALDEHYDE ON COPPER IN 0.1M HNO_3

The corrosion inhibition behaviour of 3-formylindole carbaldehyde derivatives such as 3FIPH, 3FISC, 3FITSC and 3FIDACH on copper metal were well studied and explained in this section. Electrochemical impedance spectroscopy, potentiodynamic polarization, adsorption, surface morphology and quantum mechanical investigations were mainly adapted for the corrosion inhibition property analysis of the synthesized 3-formylindole carbaldehyde derivatives.

Electrochemical studies

The electrochemical analysis including impedance studies and Tafel polarization studies is quick, accurate and reliable procedure to predict the corrosion inhibition capacity of molecules. Electrochemical studies were conducted using Ivium compactstat-e-electrochemical system, with three electrode cell assembly, in which saturated calomel electrode (SCE) was the reference electrode, platinum electrode as counter electrode and copper specimen having 1cm^2 exposed area was the working electrode.

Electrochemical impedance spectroscopy (EIS) studies

The electrochemical impedance studies were conducted in 0.1M HNO_3 on copper by using heterocyclic derivatives such as 3FIPH, 3FISC, 3FITSC and 3FIDACH. The obtained Nyquist and Bode plots of imines were represented in

the Figures 2.171 to 2.174. The irregularities observed in the semicircle curve of the Nyquist plot can be explained due to the roughness of the metal surface. The suitable equivalent circuit corresponding to the study consists of solution resistance (R_S), charge transfer resistance (R_{ct}) and a double layer capacitance (C_{dl}). The impedance parameters such as solution resistance (R_S), charge transfer resistance (R_{ct}) and a double layer capacitance (C_{dl}) as well as the corrosion inhibition efficiency for four indole based imine compounds was depicted in the Table 2.35. The inhibition efficiency of compounds mainly depends on the values of charge transfer resistance.

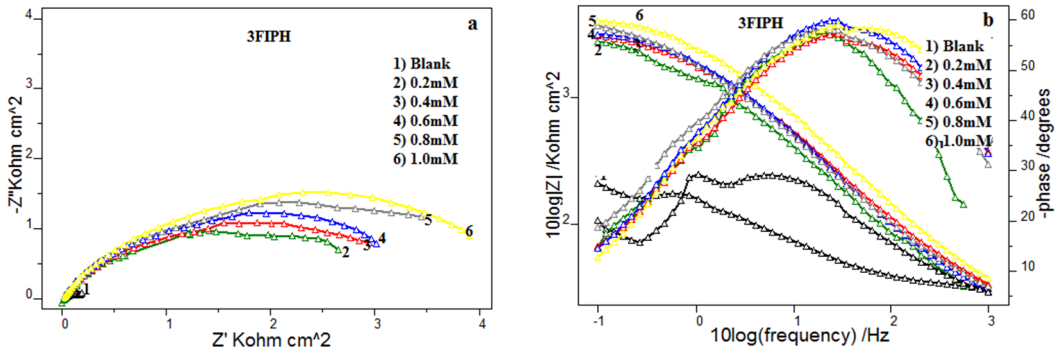

Figure 2.171 a) Nyquist plots and **b)** Bode plots of Cu in the presence and absence of 3FIPH in 0.1M HNO_3

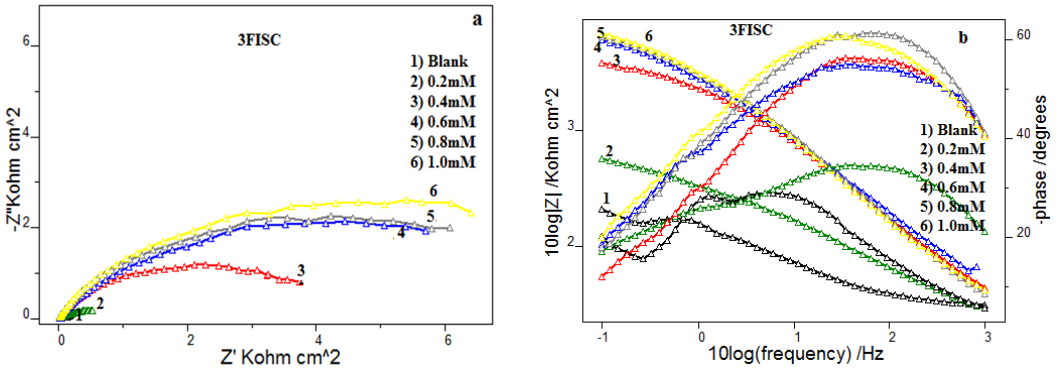

Figure 2.172 a) Nyquist plots and **b)** Bode plots of Cu in the presence and absence of 3FISC in 0.1M HNO_3

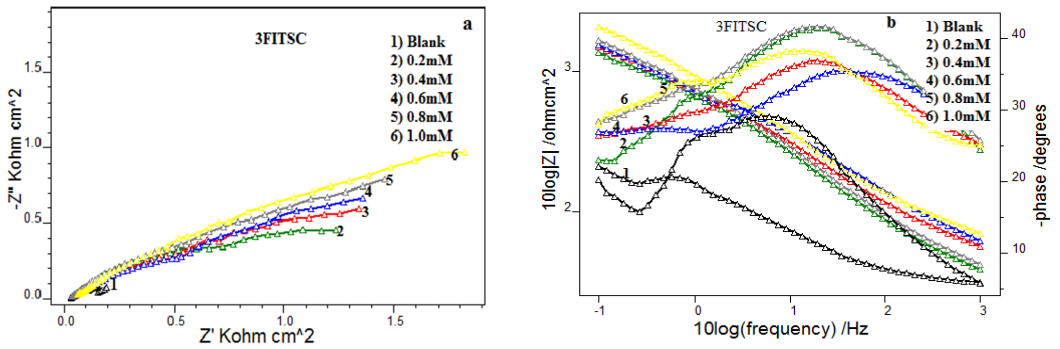

Figure 2.173 a) Nyquist plots and b) Bode plots of Cu in the presence and absence of 3FITSC in 0.1M HNO_3

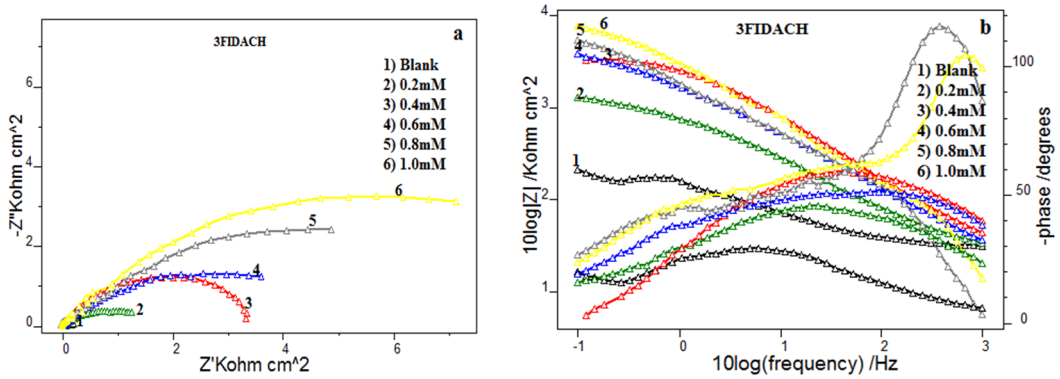

Figure 2.174 a) Nyquist plots **b)** Bode plots of Cu in the presence and absence of 3FIDACH in 0.1M HNO_3

From the analysis of the Table 2.35 it is established that the charge transfer resistance increased with increase in concentration of the imines as compared to the blank solution. The increase in the value of charge transfer resistance indicated that it can effectively prevent the conversion of metal to its corresponding ions and leads to decrease the rate of metal dissolution.

On analyzing the table all the investigated heterocyclic imines exhibited eminent corrosion inhibition efficiency at all concentrations. 3FIDACH showed 86% inhibition efficiency at minimum concentration 0.2mM and maximum inhibition efficiency 98% was achieved at 1.0mM concentration on copper in

0.1M HNO_3. The high interaction of 3FIDACH molecule on copper metal was explained by the presence of two azomethine linkage, aromatic ring systems (two indole ring), and the planarity of two indole ring in the molecule, the presence of heteroatom and delocalization of л electrons. The imines 3FIPH and 3FISC exhibited inhibition efficiency 96% and 97% at 1.0mM concentration respectively. In the case of 3FIPH above 90% efficiency was obtained at all concentration. The imine 3FITSC showed slight lower efficiency compared to other imines, and get the maximum efficiency was 92%.

Table 2.35 Electrochemical impedance parameters of copper in the presence and absence of heterocyclic imines of 3-formylindole carbaldehyde in 0.1M HNO_3

Imines	Conc (mM)	C_{dl} (μFcm^{-2})	R_{ct} (Ωcm^2)	η_{EIS} (%)
	0	745	135.9	-
	0.2	80	2212	93.86
	0.4	81	2577	94.73
3FIPH	0.6	66	2784	95.19
	0.8	68	3127	95.65
	1.0	48	3516	96.13
	0.2	395	405	66.48
	0.4	56	3041	95.53
3FISC	0.6	46	5021	97.29
	0.8	50	5390	97.48
	1.0	42	5910	97.70
	0.2	331	1032	86.83
	0.4	282	1151	88.19
3FITSC	0.6	279	1212	88.79
	0.8	246	1345	89.90
	1.0	244	1723	92.11
	0.2	146	998	86.39
	0.4	107	2985	95.45
3FIDACH	0.6	96	3127	95.65
	0.8	62	4976	97.26
	1.0	30	7100	98.09

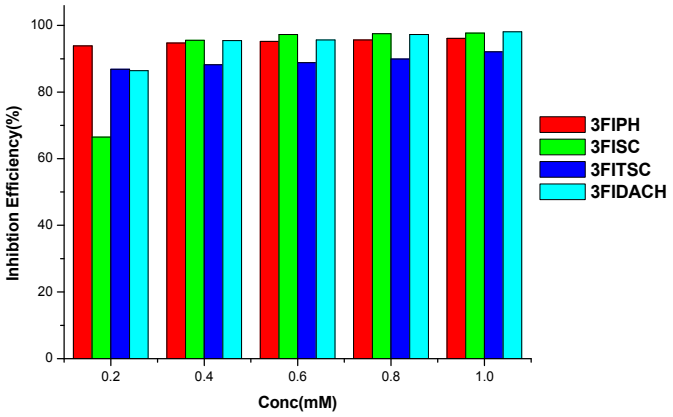

Figure 2.175 Variation of corrosion inhibition efficiencies (η_{EIS}%) of heterocyclic imines of 3-formylindole carbaldehyde on Cu in 1.0M HNO_3

Adsorption studies

The corrosion inhibition mechanism can be verified by checking different adsorption isotherms and most suitable one was selected with the help of regression coefficient (R^2). The regression coefficient and adsorption isotherms of various imines on Cu are given in the Table 2.36. Figures 2.176 to 2.179 represent the adsorption isotherms for the studied imines 3FIPH, 3FISC, 3FITSC and 3FIDACH in 0.1M HNO_3. All the four indole carbaldehyde derivatives 3FIPH, 3FISC, 3FITSC and 3FIDACH obeyed Langmuir adsorption isotherm on copper in 0.1M HNO_3.

The free energy of adsorption for all the four imines lies between -33 to -39 kJ/mol, which gives the information that the molecules was adsorbed on the metal surface through physisorption and chemisorption. The large negative value, very close to -40kJ/mol indicated that the molecules were chemically adsorbed on the metal surface, which was considered as very strong interaction. The negative

sign of free energy showed the spontaneity of the reaction. The molecules prevent the dissolution of metal by forming protective layer on the surface the metal.

Table 2.36 Adsorption isotherms and the regression coefficients of heterocyclic imines of 3-formylindole carbaldehyde on copper in 0.1M HNO_3

Isotherm	Regression coefficient (R^2)			
	3FIPH	3FISC	3FITSC	3FIDACH
Langmuir	1.000	0.989	0.999	0.999
Freundlich	0.981	0.492	0.954	0.718
Temkin	0.981	0.697	0.858	0.877
Frumkin	0.910	0.96	0.927	0.323
El-Awady	0.960	0.661	0.805	0.954
Flory-Huggin	0.958	0.476	0.787	0.946

Table 2.37 Adsorption parameters of heterocyclic imines of 3-formylindole carbaldehyde on copper in 0.1M HNO_3

Adsorption parameter	3FIPH	3FISC	3FITSC	3FIDACH
K_{ads}	1,24,224	13,125	43,572	33,178
ΔG^0_{ads} (kJ/mol)	-39.40	-33.78	-36.78	-36.10

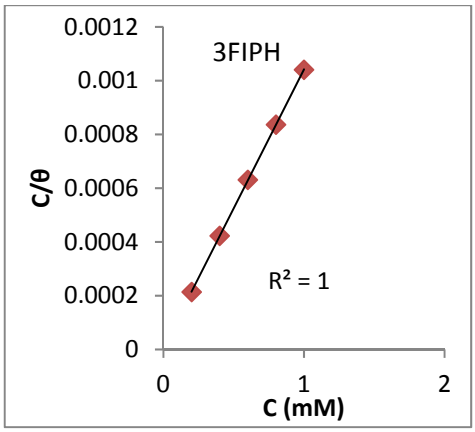

Figure 2.176 Langmuir isotherm for 3FIPH on Cu in 0.1M HNO_3

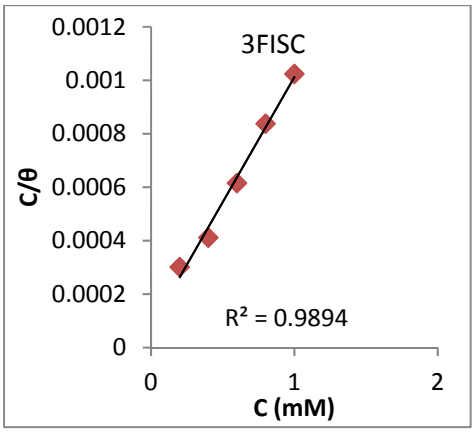

Figure 2.177 Langmuir isotherm for 3FISC on Cu in 0.1M HNO_3

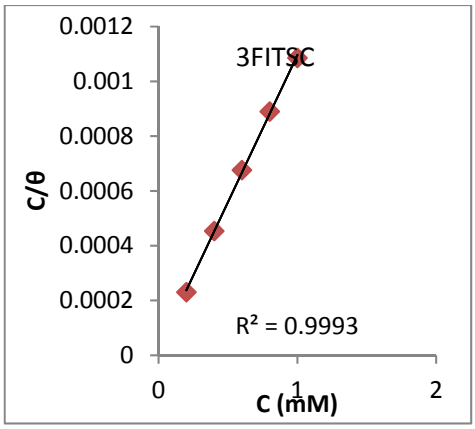

Figure 2.178 Langmuir isotherm for 3FITSC on Cu in 0.1M HNO_3

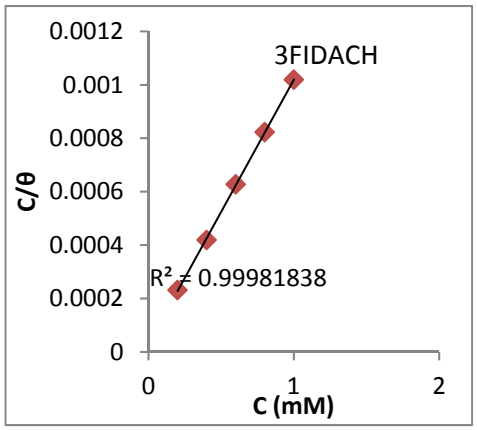

Figure 2.179 Langmuir isotherm for 3FIDACH on Cu in 0.1M HNO_3

Potentiodynamic polarization studies

The potentiodynamic polarization studies were conducted by using three electrode assemblies to confirm the inhibitory action of indole derivatives on copper. Here the saturated calomel electrode was used as reference electrode, platinum was used as counter electrode and the copper metal was used as working electrode. The corrosion current density and polarization resistance were calculated from Tafel polarization and linear polarization studies respectively. The parameters such as corrosion current density and polarization resistance were lead to inhibition efficiency calculation.

Tafel polarization parameters and linear polarization parameters are given in the Table 2.38. On examining the data, it was clear that there was a relation lies between corrosion current density and inhibition efficiency of the molecule, when the concentration of the imines increased the corrosion inhibition efficiency was also increased. The interaction of molecules on either anodic site or cathodic site or both can resist the conversion of metal to its ion, and there by corrosion current

density was decreased. The Tafel plots and linear polarization plots of 3-formylindole carbaldehyde derivatives are given in the Figures 2.180 to 2.183. The Tafel plots of compounds showed marked difference from the Tafel plot of the blank.

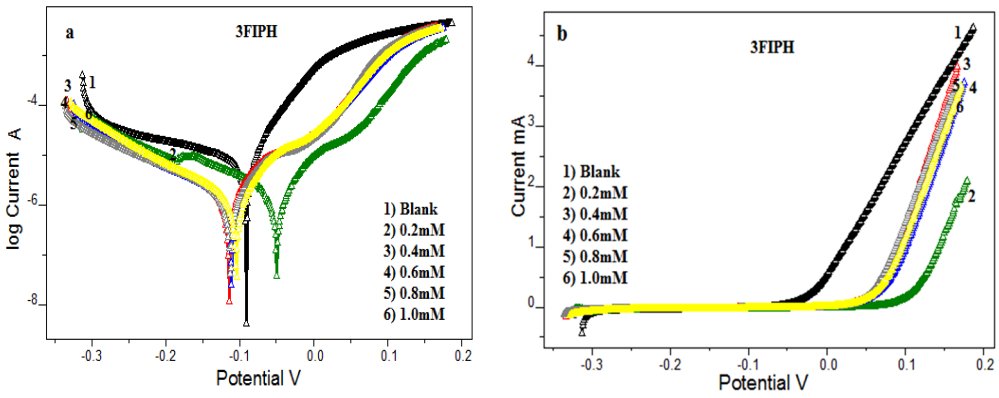

Figure 2.180 a) Tafel plots and **b)** Linear polarization plots of Cu in the presence and absence of 3FIPH in 0.1M HNO_3

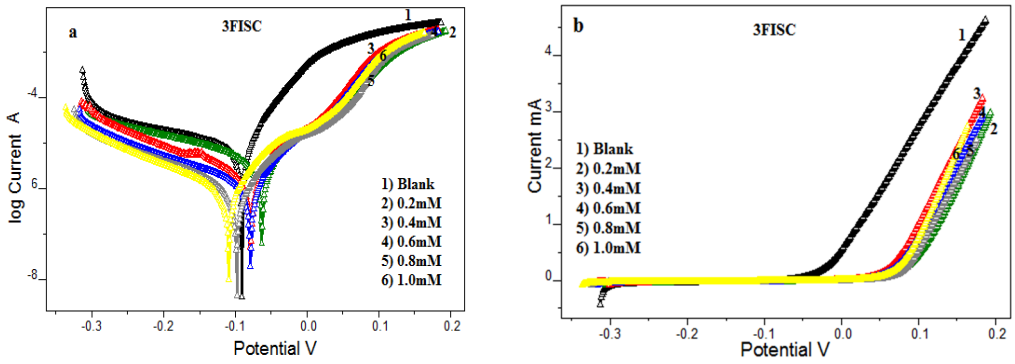

Figure 2.181 a) Tafel plots and **b)** Linear polarization plots of Cu in the presence and absence of 3FISC in 0.1M HNO_3

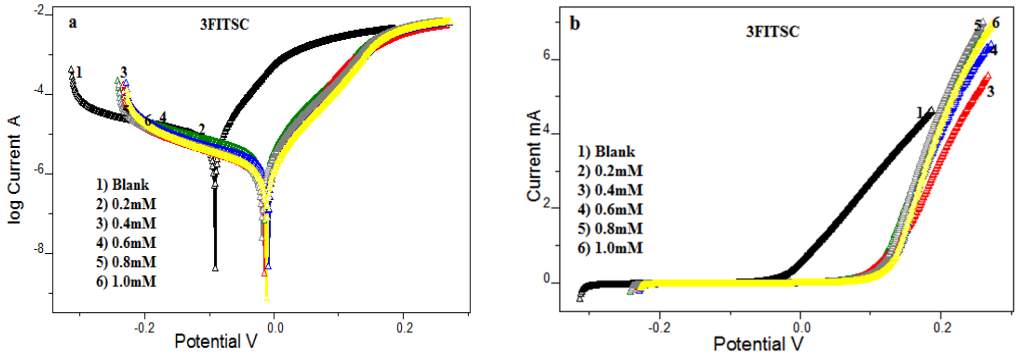

Figure 2.182 a) Tafel plots and **b)** Linear polarization plots of Cu in the presence and absence of 3FITSC in 0.1M HNO_3

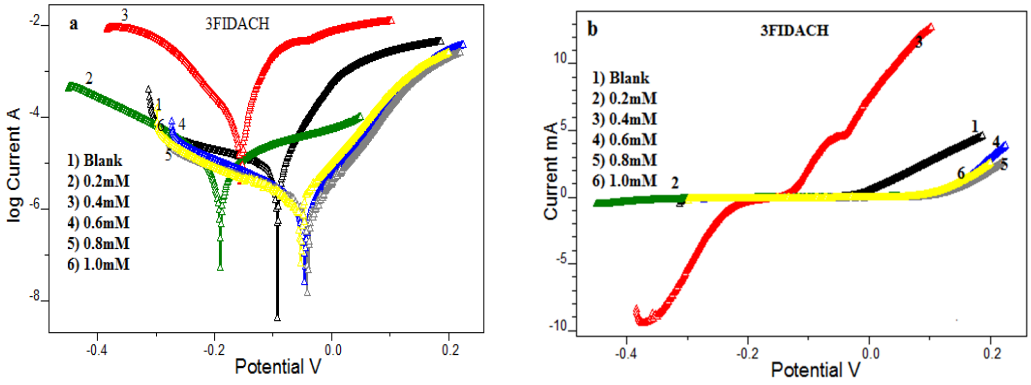

Figure 2.183 a) Tafel plots and **b)** Linear polarization plots of Cu in the presence and absence of 3FIDACH in 0.1M HNO_3

On analyzing the table it was revealed that all the imines exhibited very good corrosion inhibition efficiency at all concentrations. In Tafel polarization studies all the imines displayed around 96% efficiency at maximum concentration 1.0mM. At lower concentration also the indole based imines showed appreciable inhibition efficiency. On verifying the slopes of the imines, it was noticed that the anodic slopes of the molecules 3FIPH, 3FISC and 3FITSC do not undergo much variation which indicates the interaction of these imines mainly at cathodic site. Thus 3FIPH, 3FISC and 3FITSC molecule can be called as cathodic inhibitor. In

the case of 3FIDACH both the cathodic and anodic Tafel lines undergo considerable variations, which means this molecule acted as mixed type inhibitor.

Table 2.38 Potentiodynamic polarization parameters of copper in the presence and absence of heterocyclic imines of 3-formylindole carbaldehyde in 0.1M HNO_3

Imine	Tafel Data						Polarization data	
	Conc (mM)	$-E_{corr}$ (mV/SCE)	I_{corr} ($\mu A/cm^2$)	b_a (mv/dec)	$-b_c$ (mv/dec)	η_{pol} (%)	R_p (ohm)	η_{Rp} (%)
3FIPH	0	240	27.0	168	309	-	1758	-
	0.2	19.7	2.35	64	264	91.3	20776	91.5
	0.4	82.9	1.10	59	148	96.1	22884	92.3
	0.6	90.7	1.06	64	141	96.3	23564	92.5
	0.8	74.3	0.94	54	155	96.5	24362	92.7
	1.0	89.4	0.88	61	122	96.7	25786	93.1
3FISC	0.2	319	3.98	65	283	91.3	8567	79.4
	0.4	63.4	1.29	57	161	96.0	20567	91.4
	0.6	63.5	1.01	57	183	96.3	25345	93.0
	0.8	74.5	0.92	66	182	96.5	26742	93.4
	1.0	97.3	0.75	69	152	96.7	28990	93.9
3FITSC	0.2	36.1	3.71	70	225	86.2	7284	75.9
	0.4	77.9	2.72	86	180	89.9	11000	84.0
	0.6	35.1	2.20	68	186	91.9	12431	85.9
	0.8	36.2	1.84	64	186	93.1	16788	89.5
	1.0	27.1	1.42	62	172	94.7	20435	91.4
3FIDACH	0.2	187	4.4	294	157	83.7	6785	74.1
	0.4	221	3.6	260	116	86.7	8342	78.9
	0.6	135	1.6	66	190	94.1	12890	86.4
	0.8	304	1.2	62	209	95.3	18967	90.7
	1.0	67	1.0	66	190	96.1	24567	92.8

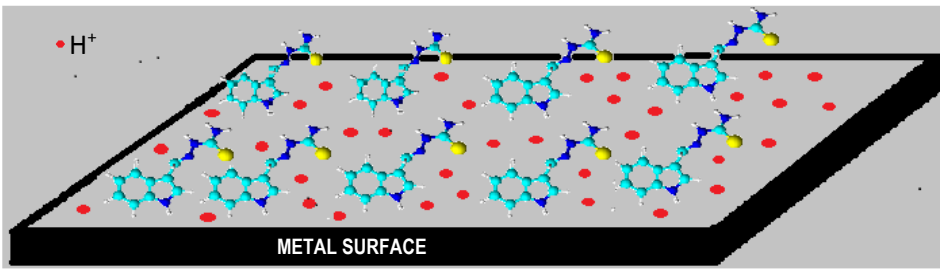

Figure 2.184 Interaction of 3FITSC on Cu surface

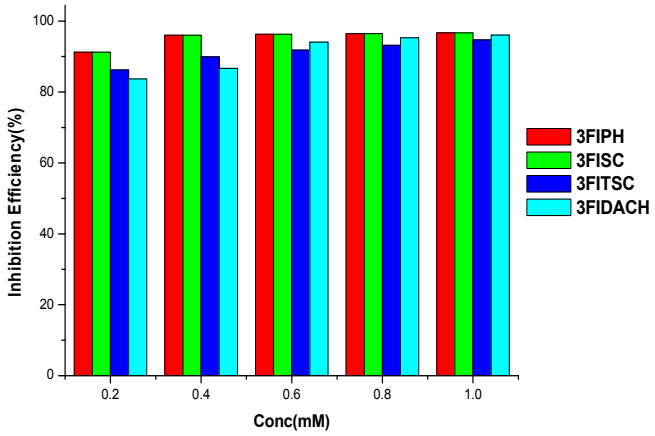

Figure 2.185 Variation of corrosion inhibition efficiencies (η_{pol}%) of heterocyclic imines of 3-formylindole carbaldehyde on Cu in 1.0M HNO_3

Quantum mechanical studies

The corrosion inhibition behaviour of heterocyclic organic molecules can be studied by examining the frontier molecular orbital energy levels that is E_{HOMO} and E_{LUMO}. According to HSAB concept, the donor-acceptor type interaction was possible between vacant d orbitals of the metal atoms and filled molecular orbitals of organic molecules. The quantum mechanical calculations were done by using GAMMESS software and method adopted was DFT. For strong interaction between organic molecules and the metal surface, E_{HOMO} value should be large and the difference between E_{HOMO} and E_{LUMO} should be low. The quantum mechanical parameters such as E_{HOMO}, E_{LUMO} and ΔE for four indole derivatives are depicted in the Table 2.39. The HSAB parameters like chemical hardness (η) and electronegativity (χ) of the organic molecules were calculated by the following equations.

$\chi \approx -1/2\ (E_{HOMO} + E_{LUMO})$ $\quad \eta \approx 1/2\ (E_{HOMO} - E_{LUMO})$ $\quad \Delta N = \frac{\chi_{Cu} - \chi_{inhib}}{2(\eta_{Cu} + \eta_{inhib})}$

Table 2.39 Quantum mechanical parameters of heterocyclic imines of 3-formylindole carbaldehyde on copper in 0.1M HNO_3

Imine	E_{HOMO} (eV)	E_{LUMO} (eV)	ΔE (eV)	χ	η	ΔN
3FIPH	-3.047	1.633	4.679	0.707	2.339	0.751
3FISC	-2.857	2.040	4.897	0.408	2.449	0.831
3FITSC	-2.857	1.578	4.435	0.639	2.218	0.866
3FIDACH	-3.265	1.578	4.843	0.844	2.422	0.751

According to quantum mechanical study the electronic behavior of the imines derived from 3-formylindole are more or less identical. As evident from the Table 2.39, that the quantum mechanical parameters of these imines are comparable due to this similar electronic behavior and they displayed close similarity between their corrosion inhibition parameters.

Surface morphological studies

SEM images of copper specimens are shown in the Figures 2.186 such as (a) copper metal specimen that is bare metal, (b) Cu treated with 0.1M HNO_3 for 24h (blank) and (c) Cu treated with 1.0mM 3FITSC in 0.1M HNO_3 solution.

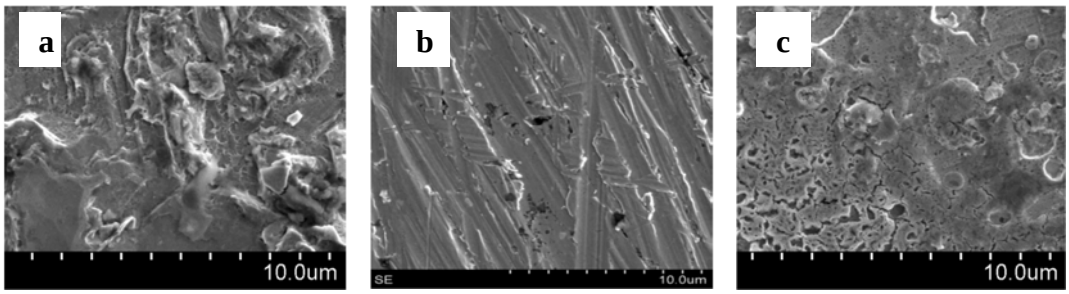

Figure 2.186 SEM images of **a**) bare metal **b**) Cu immersed in 0.1M HNO_3 **c**) Cu immersed in 0.1M HNO_3 containing 1.0mM 3FITSC

The surface morphological studies revealed the mechanism of interaction of indole derivatives on the surface of copper. Due to surface polishing the bare metal has some irregularities. In the presence of 3FITSC, the compound form a protective layer on the surface of the metal that reduced the metal dissolution compared to the copper in blank solution, which was evident from the SEM images.

SUMMARY

The corrosion inhibition efficiency of newly synthesized heterocyclic imines such as pyridine-2-carbaldehyde oxime (2PCOX), pyridine-3-carbaldehyde oxime (3PCOX), pyridine-2-carbaldehyde-4-aminobenzoic acid (2PC4ABA), pyridine-2-carbaldehyde-3-aminobenzoic acid (2PC3ABA), pyridine-2-carbaldehyde-2-aminobenzoic acid (2PC2ABA), pyridine-3-carbaldehyde-3-aminobenzoic acid (3PC3ABA), pyridine-2-carbaldehyde-2-aminophenol (2PC2AP), 3-formylindole phenylhydrazone (3FIPH), 3-formylindole semicarbazone (3FISC), 3-formylindole thiosemicarbazone (3FITSC), 3-formylindole-1,2-diaminocyclohexane (3FIDACH) on carbon steel (in 1.0M HCl and 0.5M H_2SO_4) and copper in (0.1M HNO_3) were conducted using gravimetric corrosion inhibition studies and electrochemical corrosion monitoring methods such as electrochemical impedance spectroscopy (EIS) and potentiodynamic polarization studies. Majority of the imines behaved as good corrosion inhibitors on carbon steel and copper in acidic media. The mechanism of corrosion inhibition of the heterocyclic imines was verified by adsorption studies and confirmed by surface morphological analysis.

The seven imines which are derived from pyridine carbaldehyde showed good corrosion inhibition efficiencies on CS in 1.0M HCl. The imines 2PC2ABA, 2PC2AP and 3PCOX showed higher inhibition efficiency than others in hydrochloric acid solution. The enhanced efficiency of the imines 2PC2ABA and 2PC2AP was due to the presence of aromatic ring system in the molecule and in the case of 3PCOX intermolecular hydrogen bond formation accountable for the

inhibition efficiency. The four imines 3PCOX, 2PC2ABA, 3PC3ABA and 2PC2AP followed Langmuir adsorption isotherm on CS surface. The imines 2PCOX, 2PC4ABA obeyed El-Awady and 2PC3ABA followed Temkin adsorption isotherm. The effect of temperature on the corrosion studies of CS in 1.0M HCl in the presence and absence of these imines and surface morphological studies revealed that these molecules make a protective barrier on CS surface and thus prevent the metallic dissolution appreciably. Results obtained from the ac impedance studies and polarization analyses were comparable with the gravimetric studies. Polarization studies revealed that the imines 2PC4ABA and 2PC3ABA were behaving as more anodic type inhibitor, the imine 2PCOX, 3PCOX, 2PC2ABA and 3PC3ABA were distinctly mixed type and 2PC2AP was prominently anodic in nature.

The heterocyclic imines derived from 3-formylindole carbaldehyde namely 3FIPH, 3FISC, 3FITSC and 3FIDACH showed excellent inhibition efficiency in 1.0M HCl on CS at maximum concentration 1.0mM. The 3FITSC and 3FIDACH showed above 95% inhibition efficiency at maximum concentration 1.0mM. The presence of electron density on the aromatic ring systems and highly polarizable sulphur atom are responsible by which the molecules 3FIDACH and 3FITSC showed very good corrosion inhibition efficiency. From the adsorption studies all the four imines obeyed Langmuir adsorption isotherm. The values of adsorption parameters suggested that adsorption process was spontaneous and the interaction between the metal and inhibitor molecules involves both electrostatic-adsorption and chemisorptions. In

the electrochemical impedance studies the corrosion inhibition efficiencies of imines followed the order 3FITSC>3FIDACH>3FISC>3FIPH. The potentiodynamic polarization studies suggested that the inhibitors 3FISC and 3FIDACH acted as mixed type inhibitors where as 3FIPH and 3FITSC mainly acted on anodic site so they believed to act as anodic inhibitor.

In sulphuric acid medium, the corrosion inhibition capacities of imines 2PC2ABA and 2PC2AP was very noticeable. The imines 3PC3ABA and 3PCOX displayed fair inhibition efficiency. The imine 2PC2ABA showed 97% inhibition efficiency at 1.0mM concentration in 0.5M H_2SO_4. The imines 3PCOX, 2PC3ABA, 2PC2ABA, 3PC3ABA and 2PC2AP satisfied Langmuir adsorption isotherm. The imines 2PCOX and 2PC4ABA obeyed Temkin and El-Awady adsorption isotherm respectively. The values of free energy of adsorption of all imines except 2PCOX suggested that the adsorption involved both physisorption and chemisorptions. The EIS and polarization studies were also conducted to check the corrosion inhibition response of these molecules for a period of 1hour. These results also were in good agreement with each other.

The heterocyclic imines 3FISC, 3FITSC and 3FIDACH showed good corrosion inhibition efficiency on CS in 0.5M H_2SO_4. A maximum of 94% efficiency was achieved by 3FITSC at a concentration 1.0mM. The imines 3FISC and 3FITSC followed Langmuir adsorption isotherm, while the imines 3FIPH and 3FIDACH followed El-Awady adsorption isotherm. The results of electrochemical corrosion studies and weight loss studies were comparable for these imines in H_2SO_4 medium. Potentiodynamic polarization studies established

that the imines affect the anodic and cathodic sites of corrosion and these imines acted as mixed type corrosion inhibitor.

In nitric acid medium the copper corrosion was studied in the presence and absence of imines derived from pyridine carbaldehyde. According to EIS studies the imines 2PC2ABA, 2PC2AP, 3PCOX and 2PC3ABA exhibited above 90% inhibition efficiency at 1.0mM concentration. The oxime 2PCOX showed metal dissolution property at lower concentrations; because of this enhanced corrosion behaviour 2PCOX did not obey any adsorption isotherm. The other imines such as 3PCOX, 2PC4ABA, 2PC2ABA and 2PC2AP followed Langmuir adsorption isotherm. The 2PC3ABA and 3PC3ABA obeyed the El-Awady and Freundlich isotherm respectively. The values of adsorption parameters indicated that all imines except 2PCOX showed strong interaction on the metal surface by forming a protective monolayer on the surface of metal. The polarization studies also revealed that the imines other than 2PC2AP showed variations in the cathodic and anodic Tafel lines considerably and they acted as mixed type inhibitor. The imine 2PC2AP showed anodic shift of Tafel lines appreciably, thus it can be assumed that this imine mainly affect anodic process of corrosion.

All the four imines 3FIPH, 3FISC, 3FITSC and 3FIDACH showed excellent corrosion inhibition efficiency in 0.1M HNO_3 on copper. The four imines exhibited greater than 90% inhibition efficiency at maximum concentration 1.0 mM in nitric acid medium. At lower concentrations also they showed good corrosion inhibition efficiency. On comparing with HCl and H_2SO_4 medium the imine 3FIPH showed good corrosion inhibition on copper in nitric

acid. This may arise due to the strong interaction of the imine 3FIPH with copper metal. The enhanced corrosion inhibition efficiency of 3FIDACH due to the presence of 2 aromatic rings and two azomethine linkage and the presence of highly polarizable sulphur atom was responsible for the efficiency of 3FITSC. All the four imines obeyed Langmuir adsorption isotherm .The adsorption parameters indicated that the imines were adsorbed on the metal surface through physisorption and chemisorption. From polarization data, 3FIPH, 3FISC and 3FITSC molecules acted as cathodic inhibitor, while 3FIDACH acted as mixed type inhibiter.

The surface morphological study and the electrochemical noise measurement were also conducted to verify the mechanism of corrosion and also inhibition capacity of imines against metal dissolution. From the pitting index curve, in the presence of heterocyclic imines the pitting corrosion is decreased compared to blank.

The quantum mechanical studies offered a platform for the correlation of corrosion inhibition response of these molecules with the energy of frontier molecular orbitals. High value of E_{HOMO}, the lowest value of E_{LUMO} and energy difference between HOMO and LUMO E_{LUMO}-E_{HOMO} (ΔE) are the important quantum mechanical parameters which facilitate the strong binding of the molecules on the metal surface. The imines showed good corrosion inhibition efficiency, which was satisfied the above conditions. The parameters like electro negativity (χ) and chemical hardness (η) of the molecules in solution phase were also evaluated by DFT method using GAMMESS software.

REFERENCES

1. V. Cicek, B. Al-Numan, *Corrosion Chemistry*, Scrivener publishing USA, Wiley, (2011).
2. W. V. Baeckmann, W. Schvenk, W. Prinz, *Handbook of Cathodic Corrosion Protection,* Gulf Professional Publishing: Burlington, 3rd Edition, (1997) 1-26.
3. G. Koch, J. Varney, N. Thompson, O. Moghissi, M. Gould, J. Payer, *International Measures of Prevention Applications and Economics of Corrosion Technologies Study,* NACE International: Houston, Texas, USA, (2016).
4. S. Scheiner, C. Hellmich, *Corrosion Science,* 49 (2007) 319-346.
5. R. W. Revie, H. H. Uhlig, *Corrosion and Corrosion Control: An Introduction to Corrosion Science and Engineering*, Wiley, 4th edition, (2008).
6. P. Kritzer, *Journal of Supercritical Fluids,* 29 (2004) 1-29.
7. J. R. Davis, *Corrosion: Understanding the Basics*. ASM International, 1st edition, (2000).
8. L. S. V. Delinder, A. deS. Brasunas, *Corrosion Basics: An Introduction*. National Association of Corrosion Engineers, 1st edition, (1984).
9. A. V. Levy, *Solid Particle Erosion and Erosion-corrosion of Materials*. ASM International, United states, (1995).
10. A. Philip, P. E. Schweitzer, *Encyclopedia of Corrosion Technology*, CRC Press, Taylor and Francis group, 2nd edition, (2004).

11. Z. S. Smialowska, *Pitting Corrosion of Metals*, National Association of Corrosion Engineers, 1st edition, (1986).
12. A. Conde, J. de Damborenea, *Corrosion Science,* 42 (2000) 1363-1377.
13. T. Marlaud, B. Malki, C. Henon, A. Deschamps, B. Baroux, *Corrosion Science,* 53 (2011) 3139-3149.
14. Guillaumin, V.; Mankowski, G., *Corrosion Science*, 41 (1998) 421-438.
15. Parvathavarthini, N.; Dayal, R. K., *Corrosion Reviews*, 27 (2009) 113-146.
16. L. David, Litak, G. Bela, *Environmental Engineers Hand book*, CRC Press, (1997) .
17. S. Mahajan, *Encyclopedia of Materials: Science and Technology*, Elsevier: Oxford, 1st edition (2001).
18. Y. Y. Qian, Y. X. Li, S. Jungwirth, N. Seely, Y. D. Fang, X. M. Shi, *International Journal of Electrochemical Science,* 10 (2015) 10756-10780.
19. M. Goyal, S. Kumar, I. Bahadur, C. Verma, E. E. Ebenso, *Journal of Molecular Liquids,* 256 (2018) 565-573.
20. G. H. Cartledge, *Corrosion,* 18 (1962) 316-322.
21. M. Pourbaix, *Corrosion Science,* 14 (1974) 25-82.
22. N. Khalil, *Electrochimica Acta,* 48 (2003) 2635-2640.
23. B. E. A. Rani, B. B. J. Basu, *International Journal of Corrosion,* 2012 (2012) 1-16.
24. F. M. Donahue, K. Nobe, *Journal of Electrochemical Society,* 112 (1965) 886-891.

25. B. E. Brycki, I. H. Kowalczyk, A. Szulc, O. Kaczerewska, M. Pakiet, *Organic Corrosion Inhibitors:* In *Corrosion Inhibitors, Principles and Recent Applications*, Intech Open (2017).
26. J. Aljourani, K. Raeissi, M. A. Golozar, *Corrosion Science,* 51 (2009) 1836-1843.
27. H. M. A. El-Lateef, *Corrosion Science,* 92 (2015) 104-117.
28. M. G. Hosseini, A. Ehteshamzadeh, T. Shahrabi, *Electrochimica Acta,* 52 (2007) 3680-3685.
29. E. E. Elemike, H. U. Nwankwo, D. C. Onwudiwe, E. C. Hosten, *Journal of Molecular Structure,* 1141 (2017) 12-22.
30. E. E. Elemike, H. U. Nwankwo, D. C. Onwudiwe, E. C. Hosten, *Journal of Molecular Structure,* 1147 (2017) 252-265.
31. E. A. Badr, M. A. Bedair, S. M. Shaban, *Materials Chemistry and Physics,* 219 (2018) 444-460.
32. A. Dutta, S. K. Saha, P. Banerjee, A. K. Patra, D. Sukul, *RSC Advances,* 6 (2016) 74833-74844.
33. M. Behpour, S. M. Ghoreishi, N. Soltani, M. Salavati-Niasari, M. Hamadanian, A. Gandomi, *Corrosion Science,* 50 (2008) 2172-2181.
34. H. Keleş, D. M. Emir, M. Keles, *Corrosion Science,* 101 (2015) 19-31.
35. S. Vikneshvaran, S. Velmathi, *Journal of Nanoscience and Nanotechnology* 19 (2019) 4458-4464.
36. A. Yurt, A. Balaban, S. U. Kandemir, G. Bereket, B. Erk, *Materials Chemistry and Physics,* 85 (2004) 420-426.

37. M. A. Amin, S. S. A. El-Rehim, E. E. F. El-Sherbini, R. S. Bayoumi, *Electrochimica Acta,* 52 (2007) 3588-3600.

38. O. Olivares, N. V. Likhanova, B. Gomez, J. Navarrete, M. E. Llanos-Serrano, E. Arce, J. M. Hallen, *Applied Surface Science,* 252 (2006) 2894-2909.

39. E. Machnikova, K. H. Whitmire, N. Hackerman, *Electrochimica Acta,* 53 (2008) 6024-6032.

40. O. Benali, L. Larabi, M. Traisnel, L. Gengembre, Y. Harek, *Applied Surface Science,* 253 (2007) 6130-6139.

41. M. Tourabi, K. Nohair, M. Traisnel, C. Jama, F. Bentiss, *Corrosion Science,* 75 (2013) 123-133.

42. M. Abdallah, E. A. Helal, A. S. Fouda, *Corrosion Science, 48* (2006) 1639-1654.

43. M. Cubillos, M. Sancy, J. Pavez, E. Vargas, R. Urzua, J. H. Roman, B. Tribollet, J. H. Zagal, M. A. Páez, *Electrochimica Acta,* 55 (2010) 2782-2792.

44. C. Ogretir, B. Mihci, G. Bereket, *Journal of Molecular Structure: THEOCHEM,* 488 (1999) 223-231.

45. M. Lashgari, M. R. Arshadi, M. Biglar, *Chemical Engineering Communications,* 197 (2010) 1303-1314.

46. K. F. Khaled, M. A. Amin, N. A. Al-Mobarak, *Journal of Applied Electrochemistry,* 40 (2010) 601-613.

47. G. Karthik, M. Sundaravadivelu, *Egyptian Journal of Petroleum,* 25 (2016) 481-493.

48. Zarrouk, B. Hammouti, H. Zarrok, M. Bouachrine, K. Khaled, S. Al-Deyab, *International Journal of Electrochemical Science,* 7 (2012) 89-105.
49. A. A. Nasser, V. R. Giri, S. Karthikeyan, K. Srinivasan, R. Karthikeyan, *Der Chemica Sinica,* 3 (2012) 402-412.
50. P. F. Khan, V. Shanthi, R. K. Babu, S. Muralidharan, R. C. Barik, *Journal of Environmental Chemical Engineering,* 3 (2015) 10-19.
51. E. M. Sherif, S. M. Park, *Electrochimica Acta,* 51 (2006) 6556-6562.
52. M. A. Elmorsi, A. M. Hassanein, *Corrosion Science,* 41 (1999) 2337-2352.
53. V. P. Raphael, J. T. Kakkassery, S. K. Shanmughan, S. Varghese, *International Journal of Metals,* 2016 (2016) 1-8.
54 ASTM G31-72, Standard Practice for Laboratory Immersion Corrosion Testing of Metals, ASTM International, West Conshohocken, PA, (2004)
55. P. E. P. A. Schweitzer, *Fundamentals of Corrosion: Mechanisms, Causes, and Preventative Methods*, CRC press, Taylor & Francis (2009).
56. K. Y. Foo, B. H. Hameed, *Chemical Engineering Journal,* 156 (2010) 2-10.
57. X. Li, S. Deng, H. Fu, T. Li, *Electrochimica Acta,* 54 (2009) 4089-4098.
58. E. Khamis, *Corrosion,* 46 (1990) 476-484.
59. S. S. A. El-Rehim, M. A. M. Ibrahim, K. F. Khaled, *Journal of Applied Electrochemistry,29* (1999) 593-599.
60. E. McCafferty, *Introduction to Corrosion Science,* Springer, (2010).
61. M. Bouklah, N. Benchat, B. Hammouti, A. Aouniti, S. Kertit, *Materials Letters,* 60 (2006) 1901-1905.

62. H. H. Uhling, R. W. Revie, *Corrosion and Corrosion Control*, John Wiley & Sons: New York, (1985).

63. J. M. McIntyre, H. Q. Pham, *Progress in Organic Coatings,* 27 (1996) 201-207.

64. U. Rammelt, G. Reinhard, *Progress in Organic Coatings,* 21 (1992) 205-226.

65. H. Nyquist, *The Bell System Technical Journal,* 11 (1932) 126-147.

66. A. Raman, P. Labine, *Reviews on Corrosion Inhibitor Science and Technology, NACE, Houston TX ,* (1996).

67. G. E. Badea, A. Caraban, M. Sebesan, S. Dzitac, P. Cret, A. Setel, *Journal of Sustainable Energy*, 1(1) (2010) 1-4.

68. R. G. Kelly, J. R. Scully, D. Shoesmith, R. G. Buchheit, *Electrochemical Techniques in Corrosion Science and Engineering*, CRC Press Taylor and Francis Group, 1st edition (2002).

69. A. J. Bard, L. R. Faulkner, *Electrochemical Methods: Fundamentals and Applications*, Wiley, 2nd edition, (2000).

70. G. T. Burstein, *Corrosion Science,* 47 (2005) 2858-2870.

71. F. Mansfeld, *Corrosion,* 37 (1981) 301-307.

72. B. M. Mistry, S. K. Sahoo, D. H. Kim, S. Jauhari, *Surface and Interface Analysis,* 47 (2015) 706-718.

73. Y. K. Agrawal, J. D. Talati, M. D. Shah, M. N. Desai, N. K. Shah, *Corrosion Science,* 46 (2004) 633-651.

74. G. K. Gomma, M. H. Wahdan, *Materials Chemistry & Physics,* 39 (1995) 209-213.

75. H. Ashassi-Sorkhabi, B. Shaabani, D. Seifzadeh, *Electrochimica Acta,* 50 (2005) 3446-3452.

76. M. Hosseini, S. F. L.Mertens, M. Ghorbani, M. R. Arshadi, *Materials Chemistry & Physics,* 78 (2003) 800-808.

77. M. Behpour, S. M. Ghoreishi, N. Soltani, M. Salavati-Niasari, *Corrosion Science,* 51 (2009) 1073-1082.

78. J. Smulko, K. Darowicki, A. Zieliński, *Electrochemistry Communications,* 4 (2002) 388-391.

79. V. S. Sastri, J. R. Perumareddi, *Corrosion*, 53 (1997) 617-622.

80. W. H. Ailor, *Handbook of Corrosion Testing and Evaluation*, John Wiley & Sons: New York, (1971).

81. R. M. Issa, M. K. Awad, F. M. Atlam, *Applied Surface Science*, 255(5) (2008) 2433-2441.

82. R. G. Pearson, *Inorganic Chemistry*, 27 (1988) 734-740.

83. S. Xia, M. Qiu, L. Yu, F. Liu, H. Zhao, *Corrosion Science*, 50(7) (2008) 2021-2029.

84. Q. Qu, Z. Hao, S. Jiang, L. Li, W. Bai, *Materials and Corrosion*, 59(11) (2008) 883-888.

85. F. Bentiss, M. Traisnel, M. Lagrenee, *Corrosion Science*, 42(1) (2000) 127-146.

86. D. P. Schweinsberg, G. A. George, A. K. Nanayakkara, D. A. Steinert, *Corrosion Science,* 28(1) (1988) 33-42.

87. H. Shokry, M. Yuasa, I. Sekine, R.M. Issa, H.Y El-baradie, G. K. Gomma, *Corrosion Science*, 40(12) (1998) 2173-2186

88. A. K. Singh, M. A. Quraishi, *Journal of Applied Electrochem*istry, 40(7) (2010) 1293-1306.

89. E. Cano, J. L. Polo, A. La Iglesia, J. M. Bastidas, *Adsorption*, 10(3) (2004) 219-225.

90. F. Bentiss, M. Lebrini, M. Lagrenée, *Corrosion Sci*ence, 47(12) (2005) 2915-2935.

91. A. Fouda, A. Hussein, *Journal of the Korean Chemical Society*, 56 (2) (2012) 264-274.

92. H. H. Hassan, E. Abdelghani, M. A. Amin, *Electrochimica Acta*, 52(22) (2007) 6359-6366.

93. M. S. Abdel-Aal, M.S. Morad*, British Corrosion Journal*, 36(4) (2001) 253-260.

94. P. Bommersbach, C. A. Dumont, J.P. Millet, B. Normand, *Electrochimica Acta*, 51(6) (2005) 1076-1084.

95. M. H. Hussin, M. J. Kassim, *International Journal of Electrochemical Science*, 6 (2011) 1396-1414.

96. M. El Azhar, B. Mernari, M. Traisnel, F. Bentiss, M. Lagrenee, *Corrosion Science*, 43(12) (2001) 2229-2238.

97. A.K. Satapathy, G. Gunasekaran, S. C. Sahoo, P. V. Kumar Amit, *Corrosion Science*, 51(12) (2009) 2848-2856.

98. I. L. Rosenfield, *Corrosion Inhibitors*, McGraw-Hill, New york, (1981).

99. M. MaCafferty, N. Hackerman, *Journal of Electrochemical Society*, 119 (1972) 146-154.

100. A. S. Priya, V.S. Muralidharam, A. Subramannia, *Corrosion*, 64 (2008) 541-552.

101. O. Lahodry-Sarc, F. Kapor, *Material Corrosion*, 53 (2002) 266-288.

102. A. K. Singh, S. K. Shukla, M. Singh, M.A. Quraishi, *Materials Chemistry and Physics*, 129(1-2) (2011) 68-76.

103. X. Li, S. Deng, H. Fu, *Corrosion Science*, 51(6) (2009) 1344-1355.

104. E. S. Ferreira, C. Giacomelli, F.C Giacomelli, A. Spinelli, *Materials Chemistry and Physics,* 83 (2004) 129-134.

105. F. El-Taib, A. S. Fouda, M. S. Radwan, *Materials Chemistry and Physics*, 125 (2011) 26-36

106. S. John, A. Joseph, *Materials Chemistry and Physics,* 133 (2012) 1083-1091